Studies on
Reactivity–Control of Copper Complexes
by Pyridylalkylamine Ligands

ピリジルアルキルアミン系配位子を用いた銅錯体の
反応制御に関する研究

理学研究科

物質分子系専攻

平成 **16** 年度

Takao Osako

(大迫　隆男**)**

Studies on
Reactivity–Control of Copper Complexes
by Pyridylalkylamine Ligands

January, 2005

Takao Osako

Department of Chemistry

Graduate School of Science

Osaka City University

Contents

General Introduction

Copper proteins that bind and/or activate molecular oxygen play essential roles in many biological systems. These copper proteins possess mononuclear, dinuclear, and multinuclear copper active sites and perform various biological functions including dioxygen transport, oxidation of substrates coupled with O_2-reduction, monooxygenation, dioxygenation, and disproportionation of superoxide ion (Scheme 1).[1-3] Recently, a great deal of information about the structure of the copper active centers have been provided by X-ray crystallographic and spectroscopic studies, revealing great diversities in the metal site nuclearities and coordinatinon geometries. It has been also demonstrated that the physicochemical properties and the various functions among the copper proteins depend on these structual differences.[1-3]

Scheme 1

Function of Copper Enzyme

- *O_2 Transport (Hemocyanin)*
- *Oxidase (Amine Oxidase, Galactose Oxidase, Catechol Oxidase, Laccase, etc.)*

$$O_2 + 2\,H^+ + 2\,e^- \longrightarrow H_2O_2$$

$$O_2 + 4\,H^+ + 4\,e^- \longrightarrow 2\,H_2O$$

- *Monooxygenase* (*Dopamine β-Monooxygenase, Peptidylglycine a-Amidating Monooxygenase, Tyrosinase, etc.*)

$$S + O_2 + 2\,H^+ + 2\,e^- \longrightarrow SO + H_2O$$

- *Dioxygenase (Quercetin 2,3-Dioxygenase)*

$$S + O_2 \longrightarrow SO_2$$

- *Superoxide Dismutase (Cu/Zn Superoxide Dismutase)*

$$2\,O_2^- \longrightarrow O_2 + O_2^{2-}$$

With the goal of clarifying dioxygen activation mechanism in copper proteins, synthetic modeling approaches have been widely performed by many researchers in order to understand how dioxygen interacts with the reduced sites of these copper proteins and what factors control the fate of the resulting intermediates. Dioxygen may be bound to a single metal ion following 1- or 2-electron reduction as either superoxide (O_2^-) or peroxide (O_2^{2-}), and can

coordinate in an "end-on" η^1 or a "side-on" η^2 fashion, and protonation of these products may also occur to yield a hydroperoxide species (Chart 1). Subsequent coordination of the bound oxygen ligand to a second copper ion can result in a number of bridging modes and the O–O bond may also be cleaved on coordination to the copper ion, resulting in complexes containing μ-oxo bridges derived from dioxygen (Chart 1). Further binding modes are potentially available in tri- and tetranuclear complexes (Chart 1).[4-9] These copper-dioxygen complexes supported by different types of ligands have been characterized by X-ray crystallographic and spectroscopic studies. However ligand effects on the formation process of these copper-dioxygen species as well as on copper-dioxygen reactivity have yet to be clarified in detail.

Chart 1

Mononuclear

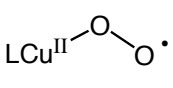

η^1–superoxo

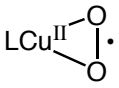

η^2–superoxo

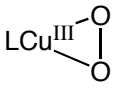

η^2–peroxo

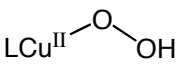

η^1–hydroperoxo

Dinuclear

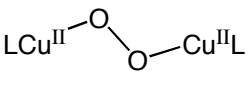

trans–μ–1,2–peroxo

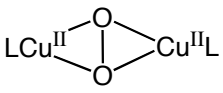

μ–η^2:η^2–peroxo

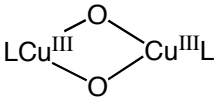

bis(μ–oxo)

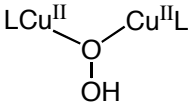

μ–1,1–hydroperoxo

Trinuclear

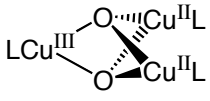

bis(μ_3–oxo)

Tetranuclear

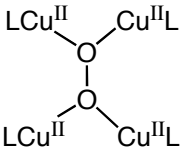

μ_4–peroxo

The (2-pyridyl)alkylamine ligands have been playing very important roles in the copper-dioxygen model chemistry.[6,7,9] One of the most widely utilized *tetradentate* ligands is TMPA [tris(2-pyridylmethyl)amine] (Chart 2),[10] which was applied for the synthesis of (*trans*-μ-1,2-peroxo)dicopper(II) complex (Chart 1), the first structurally characterized Cu_2/O_2 complex.[11] The bis[2-(2-pyridyl)ethyl]amine *tridentate* ligands (^{H}Pye2^{R}, see Chart 2) have been also widely utilized in copper(I)/dioxygen chemistry. In contrast to the case of TMPA tetradentate ligand system, bis[2-(2-pyridyl)ethyl]amine *tridentate* ligands predominantly

provide a (μ-η^2:η^2-peroxo)dicopper(II) complex (Chart 1) in the reaction of the corresponding copper(I) complexes and dioxygen.[7,12-15] In addition, Itoh and his coworkers have recently developed a series of [2-(2-pyridyl)ethyl]amine *didentate* ligands (^{H}Pye1$^{R,R'}$, see Chart 2) that allowed ones to assess the chemistry of not only (μ-η^2:η^2-peroxo)dicopper(II) complex but also bis(μ-oxo)dicopper(III) complex and mixed-valent bis(μ_3-oxo) trinuclear copper(II,II,III) complex (Chart 1).[16,17] However, effects of substituents and the alkyl linker chain length of ligands on copper-dioxygen reactivity have yet to be addressed in detail in the pyridylalkylamine ligand systems.

Chart 2

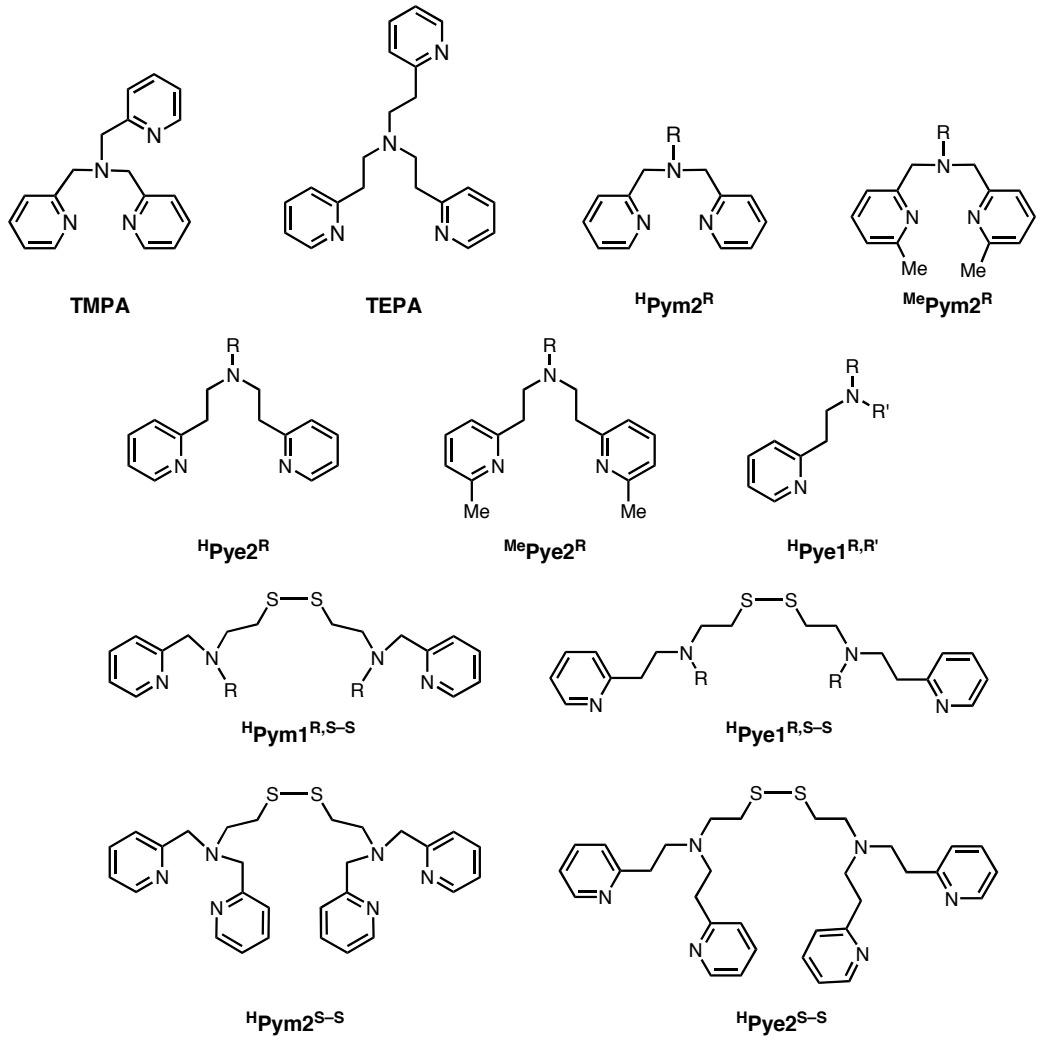

This study is intended to investigate dioxygen activation mechanism by copper(I) complexes in order to get insights into the catalytic mechasnim of copper enzymes. Ligand

effects on the structure, physicochemical properties, and reactivities of copper complexes and derived copper-dioxygen species have been systematically studied by using a series of pyridylalkylamine ligands (Chart 2). In addition, reactivity of dicopper-dioxygen complexes (Cu_2/O_2) supported by $^{H}Pye2^{R}$ and $^{H}Pye1^{R,R'}$ and dicopper-disulfide complexes (Cu_2/S_2) generated by using the disulfide ligands $^{H}Pym1^{R,S-S}$ and $^{H}Pye1^{R,S-S}$ toward external substrates such as phenol derivatives have been investigated in order to get insights into the enzymatic functions. Furthermore, carbon-halogen bond activation mechanism by copper(I) complexes have been also investigated to provide important mechanistic information about the initiation process of atom transfer radical polymerization (ATRP) reaction.[18]

In chapter 1, a low-temperature stopped-flow technique has been applied to study the reaction between copper(II) complexes of the 2-pyridylethylamine tridentate and tetradentate ligands ($^{H}Pye2^{R}$ and TEPA) and H_2O_2 in the presence of triethylamine. The study enabled ones to detect a mononuclear Cu^{II}-peroxo complex presumably having a η^2-binding mode for the first time. It has also been found that the ligand denticity (tridentate *vs*. tetradentate) and the steric effects of the *N*-alkyl substituents in the pyridylethylamine ligands drastically alter the reactivity of the initially formed Cu^{II}-hydroperoxo intermediates and following mononuclear Cu^{II}-peroxo intermediates. These results provide significantly important information about the dioxygen-activation mechanism at the mononuclear copper active sites in biological and industrial systems.

In chapter 2, ligand effects of a series of 2-pyridylalkylamine derivatives on the structure, physicochemical properties, and reactivity of the copper(I) complexes have been investigated to demonstrate that the structure and reactivities of copper(I) complexes toward O_2 are significantly affected by the alkyl linker chain length ($-CH_2-$ *vs*. $-CH_2CH_2-$) connecting the tertiary amine nitrogen and pyridine nucleus as well as by the methyl groups at the 6-position of pyridine nucleus. In addition, electronic and/or steric effects of the benzylic substituents of the ligand sidearm as well as the *p*-substituents of the phenyl group of the ligand sidearm have been also investigated in detail. These results provided important insights into how the structure, physicochemical properties, and reactivities of copper(I) complexes are modulated by the supporting ligands.

In chapter 3, the reaction of *p*-substituted benzyl halides and copper(I) complexes of series of (2-pyridyl)alkylamine ligands has been investigated in detail. In the case of tridentate ligand *N*,*N*-bis(2-pyridylmethyl)-2-phenylethylamine ($^{H}Pym2^{Phe}$) and tetradentate ligand tris(2-pyridylmethyl)amine (TMPA), the C–C coupling reaction of benzyl halides proceeded

smoothly to give the 1,2-diphenylethane derivatives and copper(II)-halide complex. A reaction mechanism involving a dinuclear copper(III)-halide organometallic intermediate is proposed, based on the kinetic results, including observed electronic effects of *p*-substituents and the rate-dependence on the bond dissociation energy of the carbon-halogen bond, as well as the ligand effects.

Finally in chapter 4, reactivities of dicopper-dioxygen complexes (Cu_2/O_2) and dicopper-disulfide complexes (Cu_2/S_2) toward external substrates such as phenol derivatives have been investigated in order to shed light on the catalytic mechanism of copper enzymes. It has been found that oxidation of phenols by a (μ-η^2:η^2-peroxo)dicopper(II) complex and a bis(μ-oxo)dicopper(III) complex proceeds efficiently to provide C–C coupling dimer of phenols and that the reactivity of the bis(μ-oxo)dicopper(III) complex is much higher than that of the (μ-η^2:η^2-peroxo)dicopper(II) complex. Detailed kinetic analysis has revealed that the oxidation proceeds via proton-coupled electron transfer (PCET). Furthermore, a novel C–S bond formation reaction has been found to take place, when a lithium phenolate was treated with a disulfide-bridged dicopper(I) complex or a bis(μ-thiolato)dicopper(II) complex under very mild conditions. The reaction has been suggested to proceed via a disulfide-bridged(μ-phenoxo)dicopper(I) complex as the common intermediate. Copper(II) complexes of the modified ligands containing a thioether group have also been isolated and structurally characterized as model compounds of galactose oxidase active site.

References

(1) Solomon, E. I.; Chen, P.; Metz, M.; Lee, S. K.; Palmer, A. E. *Angew. Chem. Int. Ed.* **2001**, *40*, 4570-4590.

(2) Klinman, J. P. *Chem. Rev.* **1996**, *96*, 2541-2561.

(3) Solomon, E. I.; Sundaram, U. M.; Machonkin, T. E. *Chem. Rev.* **1996**, *96*, 2563-2605.

(4) Mirica, L. M.; Ottenwaelder, X.; Stack, T. D. P. *Chem. Rev.* **2004**, *104*, 1013-1045.

(5) Lewis, E. A.; Tolman, W. B. *Chem. Rev.* **2004**, *104*, 1047-1076.

(6) Hatcher, L. Q.; Karlin, K. D. *J. Biol. Inorg. Chem.* **2004**, *9*, 669-683.

(7) Itoh, S.; Fukuzumi, S. *Bull. Chem. Soc. Jpn.* **2002**, *75*, 2081-2095.

(8) Suzuki, M.; Furutachi, H.; Okawa, H. *Coord. Chem. Rev.* **2000**, *200*, 105-129.

(9) Schindler, S. *Eur. J. Inorg. Chem.* **2000**, 2311-2326.

(10) The ligands used in this study are shown in Chart 2. TMPA and TEPA are well-known

tetradentate ligands consisting of three 2-pyridylmethyl and 2-(2-pyridyl)ethyl groups, respectively. The corresponding tridentate ligands are described as $^{H}Pym2^{R}$ and $^{H}Pye2^{R}$, where $^{H}Pym2$ and $^{H}Pye2$ denote bis(2-pyridylmethyl)amine and bis[2-(2-pyridyl)ethyl]amine, respectively, and R is an *N*-alkyl substituent. The corresponding tridentate ligands with 6-methylpyridine are indicated as $^{Me}Pym2^{R}$ and $^{Me}Pye2^{R}$, where the superscript 'Me' indicates the methyl group at the 6-position of pyridine nucleus. Then, the [2-(2-pyridyl)ethyl]amine didentate ligand is described as $^{H}Pye1^{R,R'}$, where R and R' denote the alkyl substituents of the tertiary amine nitrogen. The disulfide ligands are named similarly by adding superscript 'S-S' after the ligand abbreviations.

(11) Jacobson, R. R.; Tyeklar, Z.; Farooq, A.; Karlin, K. D.; Liu, S.; Zubieta, J. *J. Am. Chem. Soc.* **1988**, *110*, 3690-3692.

(12) Karlin, K. D.; Gultneh, Y.; Hutchinson, J. P.; Zubieta, J. *J. Am. Chem. Soc.* **1982**, *104*, 5240-5242.

(13) Itoh, S.; Kondo, T.; Komatsu, M.; Ohshiro, Y.; Li, C. M.; Kanehisa, N.; Kai, Y.; Fukuzumi, S. *J. Am. Chem. Soc.* **1995**, *117*, 4714-4715.

(14) Itoh, S.; Nakao, H.; Berreau, L. M.; Kondo, T.; Komatsu, M.; Fukuzumi, S. *J. Am. Chem. Soc.* **1998**, *120*, 2890-2899.

(15) Itoh, S.; Kumei, H.; Taki, M.; Nagatomo, S.; Kitagawa, T.; Fukuzumi, S. *J. Am. Chem. Soc.* **2001**, *123*, 6708-6709.

(16) Itoh, S.; Taki, M.; Nakao, H.; Holland, P. L.; Tolman, W. B.; Que, L.; Fukuzumi, S. *Angew. Chem. Int. Ed.* **2000**, *39*, 398-400.

(17) Taki, M.; Teramae, S.; Nagatomo, S.; Tachi, Y.; Kitagawa, T.; Itoh, S.; Fukuzumi, S. *J. Am. Chem. Soc.* **2002**, *124*, 6367-6377.

(18) Matyjaszewski, K.; Xia, J. H. *Chem. Rev.* **2001**, *101*, 2921-2990.

Chapter 1

Kinetic Studies on the Reactions of Copper(II) Complexes and H_2O_2

Abstract: Low-temperature stopped-flow studies have been performed on the reactions of copper(II) complexes supported by [2-(2-pyridyl)ethyl]amine tridentate and tetradentate ligands (^{H}Pye2$^{Phe\text{-}Ph}$, ^{H}Pye2$^{H–Phe}$, and TEPA) and hydrogen peroxide in the presence of triethylamine. It has been shown that the reactions of copper(II) complexes of ^{H}Pye2$^{Phe\text{-}Ph}$ and ^{H}Pye2$^{H–Phe}$ with H_2O_2 gave a mononuclear Cu^{II}–peroxo complex presumably having an η^2-binding mode that is generated from an initially formed Cu^{II}–hydroperoxo intermediate. The present result is the first example of direct detection of a mononuclear Cu^{II}–peroxo complex, providing important information about the reactive intermediates involved in biological and industrial oxidation processes.

Introduction

Mononuclear copper–active oxygen complexes are key reactive intermediates in many biological and catalytic oxidation processes.[1–4] Aliphatic hydroxylation by O_2 is accomplished at the mononuclear copper active sites in dopamine β-hydroxylase (DβH) and peptidylglycine α-amidating monooxygenase (PAM), and the oxidative modifications of tyrosine to TPQ (2,4,5-trihydroxyphenylalanine quinone) and LTQ (lysine tyrosylquinone) cofactors are performed with the aid of cupric ion in the active sites of copper-containing amine oxidases and lysyl oxidase, respectively.[4,5] In these reactions, mononuclear Cu^{II}–hydroperoxo and/or Cu^{II}–peroxo species have been invoked as the reactive intermediates that participate in the aliphatic and aromatic hydroxylation reactions.[4,5] In order to assess such intermediates, a great deal of efforts have been made to develop metastable mononuclear copper model compounds. Thus, the Cu^{II}–hydroperoxo complexes have been prepared by the reaction of copper(II) precursor and H_2O_2,[6–9] and mononuclear Cu^{II}–superoxo complexes both in the end-on (η^1-superoxo) and the side-on (η^2-superoxo) binding modes have been characterized in the reactions of copper(I) complexes and O_2 (see Chart 1).[10–13] Although these studies have provided profound insights into the structure and spectroscopic features of the hydroperoxo and superoxo complexes, no information is presently available about mononuclear Cu^{II}–peroxo species.

Chart 1

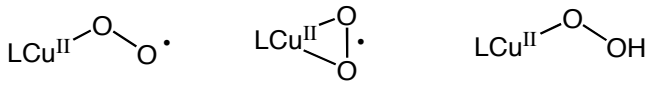

η^1–superoxo η^2–superoxo η^1–hydroperoxo

In this chapter, low-temperature stopped-flow studies have been performed on the reactions of copper(II) complexes supported by the tridentate ligands (^{H}Pye2$^{Phe\text{-}Ph}$ and ^{H}Pye2$^{H–Phe}$; Chart 2) with H_2O_2 to demonstrate that a mononuclear Cu^{II}–peroxo complex presumably having an η^2-binding mode is generated from an initially formed Cu^{II}–hydroperoxo intermediate.[14] The present result is the first example of direct detection of a mononuclear Cu^{II}–peroxo complex, providing important information about the reactive intermediates involved in the biological and industrial oxidation processes.

Chart 2

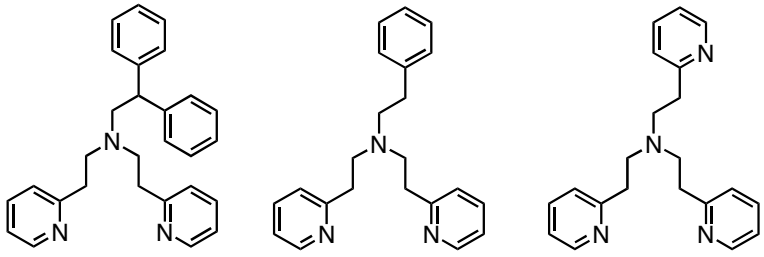

^{H}Pye2$^{Phe–Ph}$ **^{H}Pye2$^{H–Phe}$** **TEPA**

Experimental Section

General. All chemicals used in this study except the ligands and the complexes were commercial products of the highest available purity and were further purified by the standard methods, if necessary.[15] Synthetic procedures of ligands ^{H}Pye2$^{H–Phe}$ and TEPA (tris[2-(2-pyridyl)ethyl]amine) as well as the copper(II) complex of ^{H}Pye2$^{H–Phe}$ were reported previously.[16,17] FT-IR spectra were recorded with a Shimadzu FTIR-8200PC. UV-vis spectra were measured using a Hewlett Packard HP8453 diode array spectrophotometer with a Unisoku thermostated cell holder designed for low temperature measurements. Mass spectra were recorded with a JEOL JMS–700T Tandem MS station. ^{1}H-NMR spectra were recorded on a JEOL FT-NMR Lambda 300WB. ESR measurements were performed on a JEOL

JES-ME spectrometer at –150 °C. Elemental analysis was carried out on a Perkin-Elmer or a Fisons instruments EA1108 Elemental Analyzer.

Visible Resonance Raman Measurements. The 406.7 nm line of a Kr^+ laser (Model 2060 Spectra Physics) was used as the exciting source. Visible resonance Raman scattering was detected with a liquid nitrogen cooled CCD detector (Model LN/CCD-1340 x 400PB, Princeton Instruments) attached to a 1 m single polychlimator (Model MC-100DG, Ritsu Oyo Kogaku). The slit width and slit height were set to be 200 μm and 20 mm, respectively. The spectral slit width is 11.8 cm^{-1}. A wavenumber per one chennel is 1.3 cm^{-1}. The used laser power was 3.3 mW at the sample point. All measurements were carried out with a spinning cell (1000 rpm) at –80 ~ –100 ˚C. Raman shifts were calibrated with indene, toluene and CCl_4 and accuracy of the peak positions of the Raman bands was ±1 cm^{-1}.

Synthesis.

***N,N*-Bis[2-(2-pyridyl)ethyl]-2,2-diphenylethylamine (^{H}Pye2$^{Phe\text{-}Ph}$).** This compound was prepared by treating 2,2-diphenylethylamine (1.97 g, 10 mmol) and 2-vinylpyridine (5.25 g, 50 mmol) in refluxing CH_3OH (20 mL) containing acetic acid (3.01 g, 50 mmol) for 10 days. After removal of the solvent by evaporation, the resulting oily material was dissolved into H_2O (200 mL), and was extracted with $CHCl_3$ (200 mL x 3). After drying over anhydrous K_2CO_3, evaporation of the organic solvent gave yellow oily material, from which ^{H}Pye2$^{Phe\text{-}Ph}$ was isolated by SiO_2 column chromatographic treatment ($CHCl_3$-AcOEt) in 54 % yield (2.21 g); ^{1}H-NMR (300 MHz, $CDCl_3$) δ 2.76–2.96 (8 H, m, -CH_2CH_2Py), 3.16 (2H, d, J = 7.5 Hz, -CH_2CHPh_2), 4.09 (1H, t, J = 7.5 Hz, -CHPh_2), 6.76 (2H, d, J = 7.8 Hz, $H_{Py\text{-}5}$), 7.03–7.26 (12 H, m, C_6H_4 and $H_{Py\text{-}3}$), 7.43 (2 H, td, J = 1.8 and 7.8 Hz, $H_{Py\text{-}4}$), 8.50 (2 H, ddd, J = 0.9, 1.8 and 4.8 Hz, $H_{Py\text{-}6}$); FAB-HRMS (pos.), Calcd for $C_{28}H_{29}N_3$: m/z = 406.2283. Found: m/z = 406.2289.

[Cu^{II}(^{H}Pye2$^{Phe\text{-}Ph}$)(ClO$_4$)$_2$]•H$_2$O. Ligand ^{H}Pye2$^{Phe\text{-}Ph}$ (122.3 mg, 0.3 mmol) was treated with $Cu^{II}(ClO_4)_2$•$6H_2O$ (111.2 mg, 0.3 mmol) in CH_3OH (10 mL) for 30 min at room temperature. Addition of ether (200 mL) to the mixture gave blue solids that were isolated by decantation, washed with ether three times, and dried (83 % yield). Single crystals were obtained by vapor diffusion of ether into a CH_3OH solution of the complex. FT-IR (KBr): 1130, 1043, and 621 cm^{-1} (ClO_4^-); FAB-MS (pos.), m/z = 569.2 ($[M]^+$); Anal. for [Cu^{II}(^{H}Pye2$^{Phe\text{-}Ph}$)(ClO$_4$)$_2$]•H$_2$O. Calcd for $C_{28}H_{31}O_9N_3CuCl_2$: C, 48.88; H, 4.54; N, 6.11. Found: C, 48.72; H, 4.48; N, 6.06.

[Cu^{II}(TEPA)(ClO$_4$)]ClO$_4$. Ligand TEPA (332.5 mg, 1.0 mmol) was treated with $Cu^{II}(ClO_4)_2$•$6H_2O$ (370.5 mg, 1.0 mmol) in CH_3CN (10 mL) for 30 min at room temperature.

Addition of ether (200 mL) to the mixture gave a blue oily material that was isolated by decantation and re-dissolved into CH_3OH (10 mL). Addition of the CH_3OH solution into ether (200 mL) gave blue solids that were isolated by decantation, washed with ether three times, and dried (95 % yield). Single crystals were obtained by vapor diffusion of ether into a CH_3OH solution of the complex. FT-IR (KBr): 1143, 1081, and 625 cm^{-1} (ClO_4^-); FAB-MS (pos.), m/z = 494.07 ($[M]^+$); Anal. for $[Cu^{II}(TEPA)(ClO_4)](ClO_4)$. Calcd for $C_{21}H_{28}O_8N_4CuCl_2$: C, 39.98; H, 4.47; N, 8.88. Found: C, 40.18; H, 4.16; N, 8.87.

Caution! The perchlorate salts in this study are all potentially explosive and should be handled with care.

Kinetic Measurements. Kinetic measurements for the reaction of copper(II) complexes (0.2 mM) and H_2O_2 were performed by using a multi-scan double mixing stopped-flow spectrophotometer designed for low-temperature measurements (RSP-1000, Unisoku Co., Ltd.) in CH_3OH at –90 °C. The reaction of $[Cu^{II}(^{H}Pye2^{Phe\text{-}Ph})(ClO_4)_2]$ and H_2O_2 at the higher concentration (Figure 12) was followed as reported previously[17] by using a Hewlett Packard HP8453 diode array spectrophotometer with a Unisoku thermostated cell holder designed for low temperature measurements.

X–ray Structure Determination. Single crystals for X-ray structural analysis were obtained by vapor diffusion of ether into a MeOH solution of the complex. The single crystal was mounted on a glass-fiber. Data of X–ray diffraction were collected by a Rigaku RAXIS–RAPID imaging plate two–dimensional area detector using graphite–monochromated Mo$K\alpha$ radiation (λ = 0.71070 Å) to 2θ max of 55.0 °. All the crystallographic calculations were performed by using Crystal Structure software package of the Rigaku Corporation and Molecular Structure Corporation [Crystal Structure: Crystal Structure Analysis Package version 1.01, Rigaku Corp. and Molecular Structure Corp. (2000)]. The crystal structure was solved by the direct methods and refined by the full–matrix least squares using SIR-92. All non–hydrogen atoms and hydrogen atoms were refined anisotropically and isotropically, respectively. Summary of the X–ray crystallographic data and selected bond lengths and angles are given in Tables 1 and 2.

Results and Discussion

Synthesis and Structural Characterization of Copper(II) Complexes. Ligand $^{H}Pye2^{Phe-Ph}$ was prepared by Michael addition of 2,2-diphenylethylamine to 2-vinylpyridine in refluxing methanol under acidic conditions. The copper(II) complexes of $^{H}Pye2^{Phe-Ph}$ and TEPA were obtained by treating the ligands with an equimolar amount of $Cu^{II}(ClO_4)_2 \bullet 6H_2O$ in CH_3OH or CH_3CN. Ligands $^{H}Pye2^{H-Phe}$ and TEPA as well as the copper(II) complex of $^{H}Pye2^{H-Phe}$ were prepared by the reported methods.[16,17]

Crystal structures of $[Cu^{II}(^{H}Pye2^{Phe-Ph})(ClO_4)_2]$ and $[Cu^{II}(TEPA)(ClO_4)](ClO_4)$ have been determined as shown in Figure 1. The crystallographic data of the complexes are presented in Table 1, and their selected bond lengths and angles around the copper ion are summarized in Table 2.

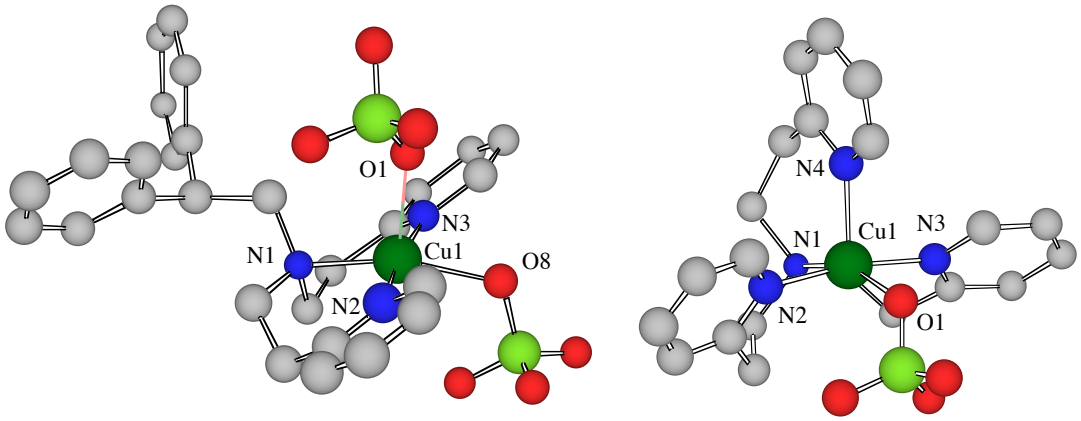

$[Cu^{II}(^{H}Pye2^{Phe-Ph})(ClO_4)_2]$ **$[Cu^{II}(TEPA)(ClO_4)](ClO_4)$**

Figure 1. Chem 3D views of the crystal structures of $[Cu^{II}(^{H}Pye2^{Phe-Ph})(ClO_4)_2]$ and $[Cu^{II}(TEPA)(ClO_4)](ClO_4)$. The non-coordinated counter anions and hydrogen atoms are omitted for clarity.

Copper(II) complex $[Cu^{II}(^{H}Pye2^{Phe-Ph})(ClO_4)_2]$ exhibits a distorted square-pyramidal geometry ($\tau = 0.20$) consisted of the tertiary amine, N(1), and the two pyridine nitrogen atoms of ligands, N(2) and N(3), and one of the perchlorate anions occupying the basal square plane and another perchlorate anion as the axial ligand (Figure 1, left). The crystal structure of $[Cu^{II}(^{H}Pye2^{Phe-Ph})(ClO_4)_2]$ is very close to that of the copper(II) complex of $^{H}Pye2^{H-Phe}$.[17a] $[Cu^{II}(TEPA)(ClO_4)](ClO_4)$ has a similar distorted square-pyramidal strucutre ($\tau = 0.17$), where the axial ligand is the third pyridine of TEPA instead of perchlorate anion (Figure 1 right).

Table 1. Summary of X-ray Crystallographic Data

	$[Cu^{II}(^{H}Pye2^{Phe-Ph})(ClO_4)_2]$	$[Cu^{II}(TEPA)(ClO_4)](ClO_4)$
empirical formula	$C_{28}H_{31}N_3O_9Cl_2Cu$	$C_{21}H_{24}N_4O_8Cl_2Cu$
formula weight	688.02	594.89
crystal system	monoclinic	monoclinic
space group	C2 (#5)	$P2_1/c$ (#14)
a, Å	13.9559(6)	14.1176(9)
b, Å	11.6086(6)	10.5506(7)
c, Å	18.811(1)	16.199(1)
β, deg	96.811(2)	91.886(3)
V, Å^3	3026.1(2)	2411.5(2)
Z	4	4
F(000)	1420.00	1220.00
D_{calc}, g/cm^3	1.510	1.638
T, °C	–115	–115
crystal size, mm	0.20 x 0.20 x 0.20	0.20 x 0.20 x 0.10
μ (MoKα), cm^{-1}	9.55	11.82
diffractometer	Rigaku RAXIS-RAPID	Rigaku RAXIS-RAPID
radiation	MoKα (0.71069 Å)	MoKα (0.71069 Å)
$2\theta_{max}$, deg	54.9	55.0
no. of reflns measd	13778	10865
no. of reflns obsd	2752 [$I > 1.0\sigma(I)$]	3873 [$I > 2.0\sigma(I)$]
no. of variables	418	349
R^a	0.060	0.064
$R_w{}^b$	0.071	0.102

[a] $R = \Sigma||F_o| - |F_c||/\Sigma|F_o|$. [b] $R_w = \{\Sigma w(|F_o| - |F_c|)^2/\Sigma wF_o{}^2\}^{1/2}$.

Table 2. Selected Bond Lengths (Å) and Angles (deg)

$[Cu^{II}(^{H}Pye2^{Phe-Ph})(ClO_4)_2]$

Cu(1)–O(1)	2.298(5)	Cu(1)–O(8)	2.099(5)
Cu(1)–N(1)	2.056(5)	Cu(1)–N(2)	1.982(6)
Cu(1)–N(3)	2.033(5)		
O(1)–Cu(1)–O(8)	93.2(2)	O(1)–Cu(1)–N(1)	105.6(2)
O(8)–Cu(1)–N(1)	160.4(2)	O(1)–Cu(1)–N(2)	93.2(2)
O(8)–Cu(1)–N(2)	87.9(2)	N(1)–Cu(1)–N(2)	96.5(2)
O(1)–Cu(1)–N(3)	86.5(2)	O(8)–Cu(1)-N(3)	85.8(2)
N(1)–Cu(1)–N(3)	89.7(2)	N(2)–Cu(1)–N(3)	173.7(2)

$[Cu^{II}(TEPA)(ClO_4)](ClO_4)$

Cu(1)–O(1)	2.172(3)	Cu(1)–N(1)	2.049(4)
Cu(1)–N(2)	2.022(4)	Cu(1)–N(3)	2.001(4)
Cu(1)–N(4)	2.143(4)		
O(1)–Cu(1)–N(1)	159.3(2)	O(1)–Cu(1)–N(2)	85.9(2)
N(1)–Cu(1)–N(2)	89.8(2)	O(1)–Cu(1)–N(3)	87.1(2)
N(1)–Cu(1)–N(3)	93.8(2)	N(2)–Cu(1)–N(3)	169.4(2)
O(1)–Cu(1)–N(4)	97.8(1)	N(1)–Cu(1)–N(4)	102.8(2)
N(2)–Cu(1)–N(4)	93.9(2)	N(3)–Cu(1)–N(4)	94.9(2)

Reaction of Copper(II) Complex and Hydrogen Peroxide. Reactions of the copper(II) complexes with H_2O_2 were studied using a multi-scan double mixing stopped-flow spectrophotometer at –90 °C in methanol. In Figure 2 is shown the spectral change for the first rapid process (t = 0 ~ 60 ms) of the reaction between copper(II) complex of the *tridentate* ligand ($^{H}Pye2^{Phe-Ph}$), $[Cu^{II}(^{H}Pye2^{Phe-Ph})(ClO_4)_2]$ (0.2 mM), and H_2O_2 (2.0 mM) in the presence of triethylamine (2.0 mM), where an absorption band at 360 nm (ε = 2,280 M^{-1} cm^{-1}) readily appeared [spectrum (a)]. The reaction obeys first-order kinetics as shown in the inset of Figure

2, and plot of the first-order rate constant $k_{obs(1)}$ against the hydrogen peroxide concentration, $[H_2O_2]$ = 2 ~ 10 mM, at a fixed concentration of triethylamine (2.0 mM) gave a Michaelis-Menten type saturation curve as shown in Figure 3. A similar saturation curve was obtained when the triethylamine concentration $[Et_3N]$ was increased from 2 mM to 10 mM at a fixed concentration of H_2O_2 (2.0 mM) (Figure 4). These kinetic results can be explained by the reaction sequences shown in Eqs. (1) and (2), where the counter anions (ClO_4^-) are omitted for simplicity.

$$H_2O_2 + Et_3N \underset{}{\overset{K_1}{\rightleftharpoons}} HO_2^- Et_3NH^+ \quad (1)$$

$$[LCu^{II}]^{2+} + HO_2^- Et_3NH^+ \xrightarrow{k_1} [LCu^{II}\text{–}OOH]^+ + Et_3NH^+ \quad (2)$$

(**A**)

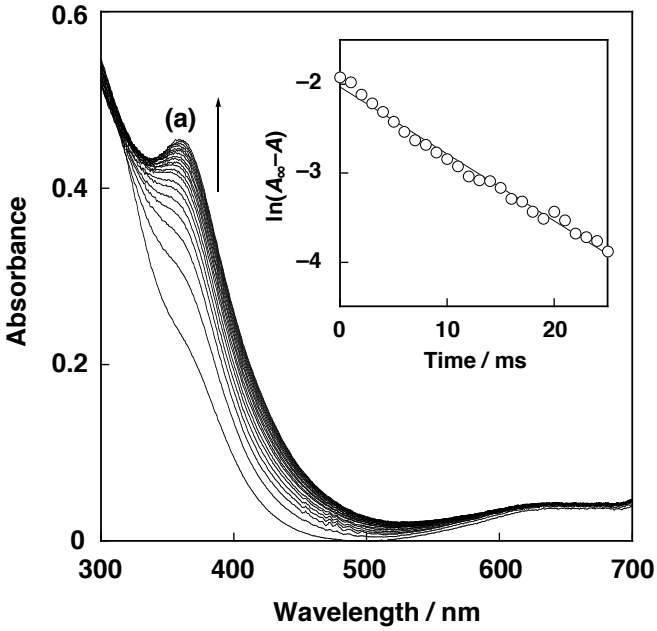

Figure 2. Spectral change for the first 60 ms of the reaction of $[Cu^{II}(^{H}Pye2^{Phe\text{-}Ph})(ClO_4)_2]$ (0.2 mM) with H_2O_2 (2.0 mM) in the presence of triethylamine (2.0 mM) in CH_3OH at –90°C. Inset: pseudo-first-order plot based on the absorption change at 360 nm.

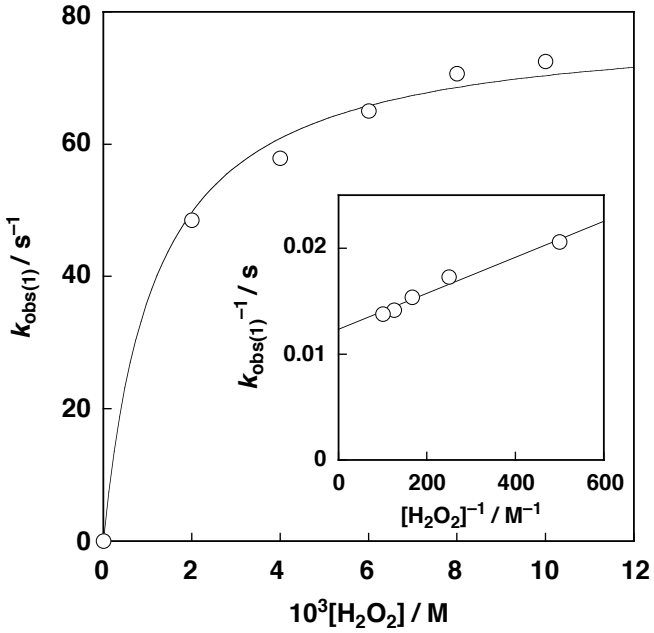

Figure 3. Plot of $k_{obs(1)}$ *vs*. $[H_2O_2]$ for the reaction of $[Cu^{II}(^{H}Pye2^{Phe\text{-}Ph})(ClO_4)_2]$ (0.2 mM) in the presence of triethylamine (2.0 mM) in MeOH at –90˚C. Inset: plot of $k_{obs(1)}^{-1}$ *vs*. $[H_2O_2]^{-1}$.

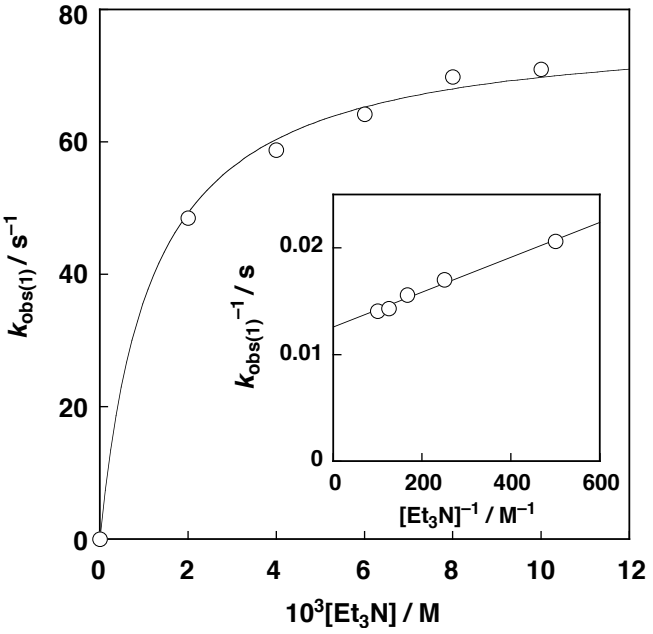

Figure 4. Plot of $k_{obs(1)}$ *vs*. $[Et_3N]$ for the reaction of $[Cu^{II}(^{H}Pye2^{Phe\text{-}Ph})(ClO_4)_2]$ (0.2 mM) in the presence of hydrogen peroxide (2.0 mM) in MeOH at –90˚C. Inset: plot of $k_{obs(1)}^{-1}$ *vs*. $[Et_3N]^{-1}$.

Under the reaction conditions mentioned above, the kinetic equation can be drawn as $k_{obs(1)} = (k_1K_1[H_2O_2][Et_3N])/(K_1[H_2O_2] + 1)$ in the presence of the excess amount of H_2O_2 (for Figure 3) and as $k_{obs(1)} = (k_1K_1[H_2O_2][Et_3N])/(K_1[Et_3N] + 1)$ in the presence of the excess amount of Et_3N (for Figure 4). Double reciprocal plots in both cases gave straight lines as shown in the insets of the respective figures (Figures 3 and 4), from which the acid-base equilibrium constant K_1 and the rate constant k_1 have been determined as 7.2 (± 0.5) x 10^2 M^{-1} and 4.1 (± 0.3) x 10^4 M^{-1} s^{-1} (from Figure 3) and 7.7 (± 0.4) x 10^2 M^{-1} and 4.0 (± 0.3) x 10^4 M^{-1} s^{-1} (from Figure 4), respectively. The good agreement in the K_1 and k_1 values determined independently from the rate dependence on $[H_2O_2]$ and $[Et_3N]$ strongly support the accuracy of the proposed mechanism shown in Eqs. (1) and (2).

The reaction of copper(II) complex supported by the *tetradentate* ligand (TEPA), $[Cu^{II}(TEPA)(ClO_4)](ClO_4)$, with H_2O_2 under the same experimental conditions also gave an intermediate exhibiting a similar absorption spectrum (λ_{max} = 332 nm, ε = 4,240 M^{-1} cm^{-1}, Figure 5). The kinetic behavior of this reaction was also the same to that of the former reaction

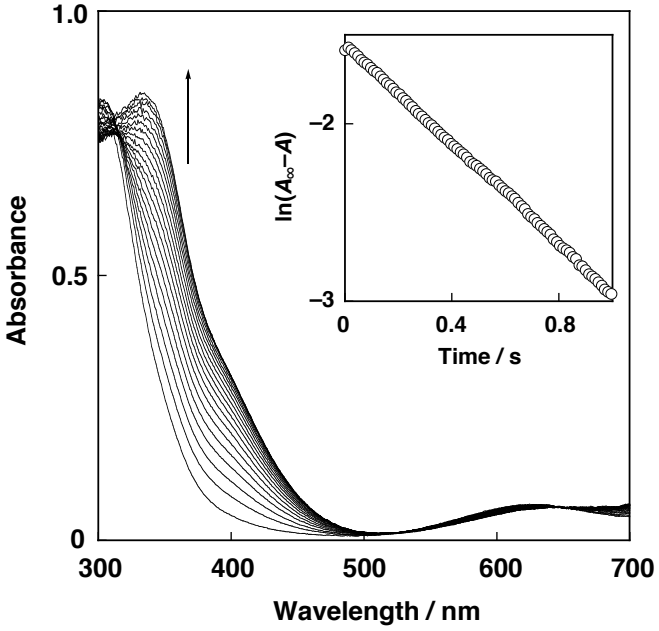

Figure 5. Spectral change for the first 1.2 s of the reaction of $[Cu^{II}(TEPA)(ClO_4)](ClO_4)$ (0.2 mM) with H_2O_2 (4.0 mM) in the presence of triethylamine (2.0 mM) in MeOH at –90°C. Inset: pseudo-first-order plot based on the absorption change at 401 nm.

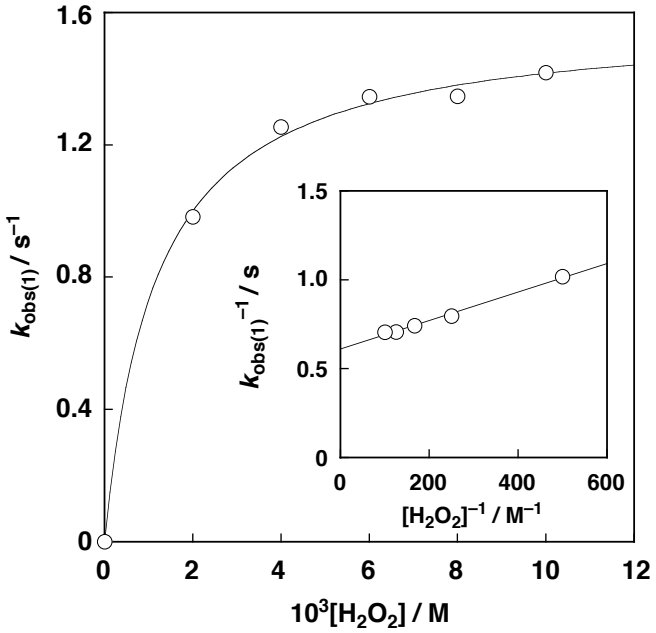

Figure 6. Plot of $k_{obs(1)}$ *vs*. $[H_2O_2]$ for the reaction of $[Cu^{II}(TEPA)(ClO_4)](ClO_4)$ (0.2 mM) in the presence of triethylamine (2.0 mM) in MeOH at –90˚C. Inset: plot of $k_{obs(1)}^{-1}$ *vs*. $[H_2O_2]^{-1}$.

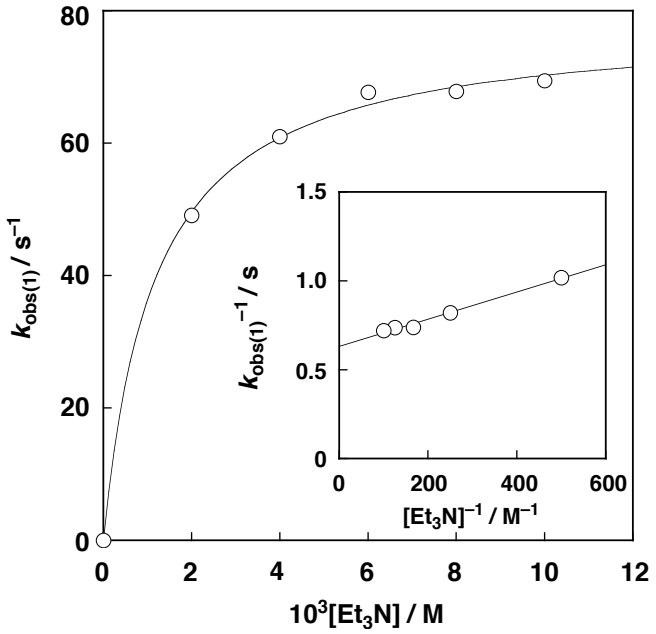

Figure 7. Plot of $k_{obs(1)}$ *vs*. $[Et_3N]$ for the reaction of $[Cu^{II}(TEPA)(ClO_4)](ClO_4)$ (0.2 mM) in the presence of hydrogen peroxide (2.0 mM) in MeOH at –90˚C. Inset: plot of $k_{obs(1)}^{-1}$ *vs*. $[Et_3N]^{-1}$.

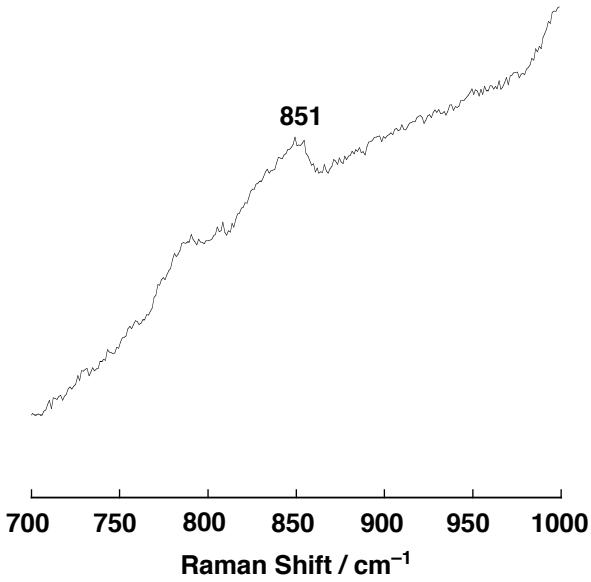

Figure 8. Resonance Raman spectrum of $[Cu^{II}(TEPA)(^{16}O_2H)]^+$ obtained with an excitation wavelength of 406.7 nm in MeOH at –80°C.

as shown in Figures 6 and 7 (K_1 = 7.6 (± 0.4) x 10^2 M^{-1} and k_1 = 8.2 (± 0.4) x 10^2 M^{-1} s^{-1} from Figure 6 and K_1 = 8.3 (± 0.4) x 10^2 M^{-1} and k_1 = 7.9 (± 0.4) x 10^2 M^{-1} s^{-1} from Figure 7). Moreover, the λ_{max} and their ε values in the UV-vis as well as the resonance Raman band at 851 cm^{-1} (Figure 8)[18] of the intermediate are fairly close to those of the reported mononuclear Cu^{II}–hydroperoxo complexes supported by other tetradentate pyridine ligands.[7–9] All the spectroscopic features as well as the good agreement in the K_1 values between the TEPA and the $^{H}Pye2^{Phe\text{-}Ph}$ ligand systems (K_1 = 7.2 ~ 7.9 x 10^2 M^{-1}) indicate that the initially formed intermediates both in the tridentate and tetradentate ligand systems involve an η^1-OOH group as shown in Eq. (2). Notably, fate of the Cu^{II}–hydroperoxo intermediate of *tridentate* ligand $^{H}Pye2^{Phe\text{-}Ph}$ was totally different from that of the TEPA-complex. Namely, the hydroperoxo intermediate (**A**) supported by the *tetradentate* ligand TEPA was converted into the corresponding copper(I) complex, $[Cu^{I}(TEPA)]^+$ ($k_{obs(2)}$ = 0.19 ± 0.1 s^{-1}),[19] whereas the hydroperoxo species supported by the *tridentate* ligand ($^{H}Pye2^{Phe\text{-}Ph}$) readily gave a mononuclear Cu^{II}–peroxo intermediate (**B**) as demonstrated below.

Thus, the Cu^{II}–OOH intermediate (**A**) with $^{H}Pye2^{Phe\text{-}Ph}$ further reacted in the next step (t = 100 ms ~ 1.5 s) to give a spectral change shown in Figure 9, where the absorption band around

360 nm due to **A** [spectrum (a)] further increased obeying first-order kinetics to give spectrum (b) with λ_{max} = 366 nm (ε = 3,110 M^{-1} cm^{-1}).

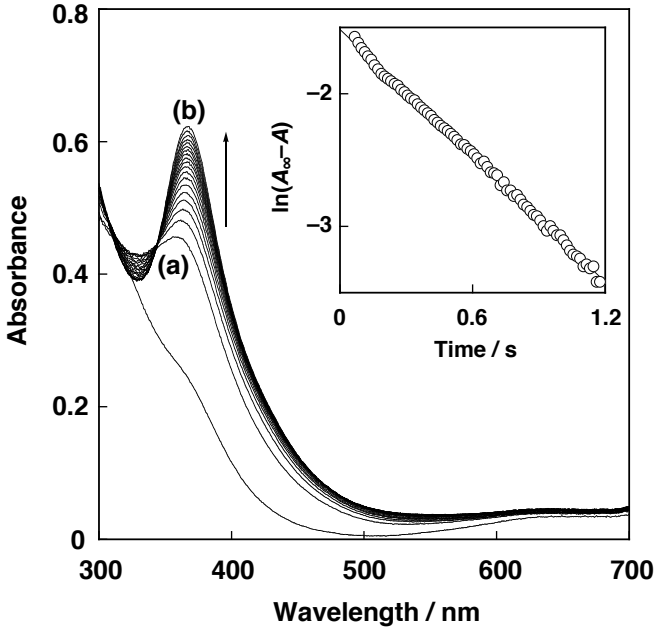

Figure 9. Spectral change for the reaction of $[Cu^{II}(^{H}Pye2^{Phe\text{-}Ph})(ClO_4)_2]$ (0.2 mM) with H_2O_2 (2.0 mM) in the presence of triethylamine (2.0 mM) in CH_3OH at –90°C from t = 0.1 – 1.5 s. Inset: pseudo-first-order plot based on the absorption change at 366 nm.

The observed first-order rate constant $k_{obs(2)}$ = 1.6 (± 0.1) s^{-1} of this process was independent both on $[H_2O_2]$ and $[Et_3N]$ (Figures 10a and 10b), indicating that the second process involves an intramolecular reaction of the mononuclear hydroperoxo intermediate (**A**). The peak position of the final spectrum (b) in Figure 9 resembles that of the reported (μ-η^2:η^2-peroxo)dicopper(II) complexes, but the absorption intensity (ε) is significantly smaller than that of the reported dinuclear copper(II) peroxo complexes.[17,20] Furthermore, an ESR spectrum of a copper(II) complex with a $d_{x^2-y^2}$ ground state [spectrum (b) in Figure 11], which is different from that of the starting copper(II) complex [spectrum (a) in Figure 11], was obtained in the early stage of the reaction. In addition, a similar absorption spectrum was obtained in the reaction of $[Cu^{II}(^{H}Pye2^{H-Phe})(ClO_4)_2]$ with H_2O_2 under the same experimental conditions (λ_{max} = 362 nm, ε = 4,880 M^{-1} cm^{-1}), although the Cu^{II}–OOH intermediate of $^{H}Pye2^{H-Phe}$ was too reactive to be detected. Based on these results together with the totally

different reaction patterns of the Cu^{II}–OOH intermediate (**A**) between the *tridentate* and *tetradentate* ligand systems, it has been tentatively assigned the second intermediate observed in Figure 9 is a mononuclear Cu^{II}–peroxo complex (**B**) having a η^2-binding mode as indicated in Eq. (3).

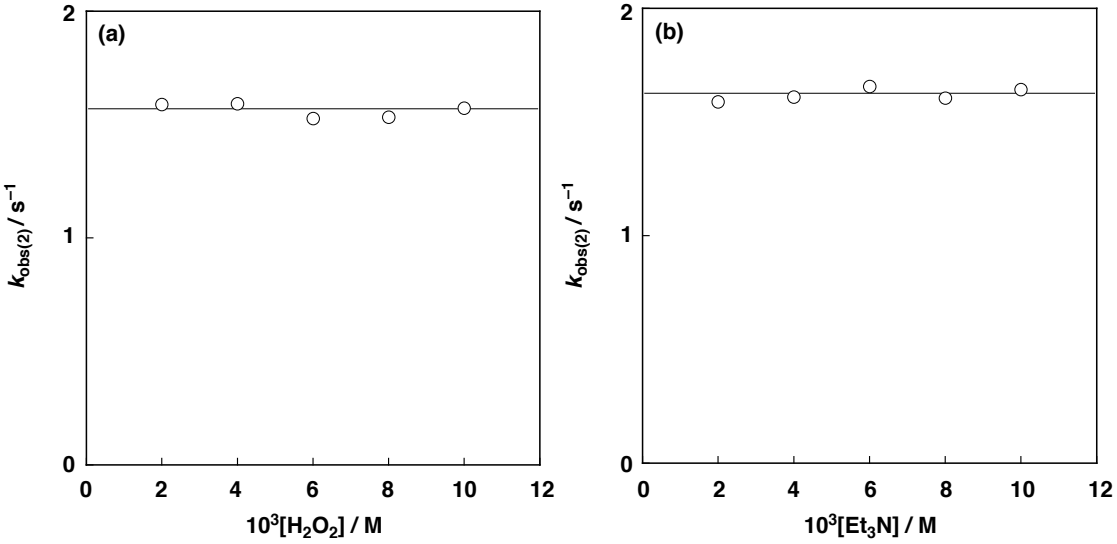

Figure 10. (a) Plot of $k_{obs(2)}$ *vs*. $[H_2O_2]$ for the reaction of $[Cu^{II}(^{H}Pye2^{Phe\text{-}Ph})(ClO_4)_2]$ (0.2 mM) in the presence of triethylamine (2.0 mM) in MeOH at –90°C (b) Plot of $k_{obs(2)}$ *vs*. $[Et_3N]$ for the reaction of $[Cu^{II}(^{H}Pye2^{Phe\text{-}Ph})(ClO_4)_2]$ (0.2 mM) in the presence of triethylamine (2.0 mM) in MeOH at –90°C.

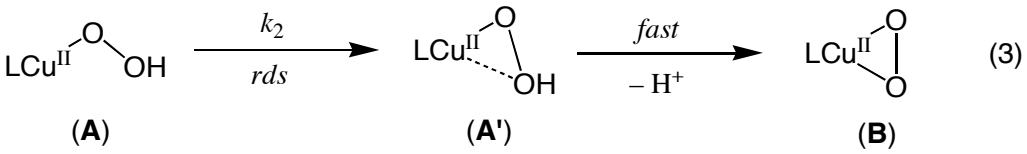

The lack of rate-dependence on $[Et_3N]$ in the $k_{obs(2)}$ process (Figure 10b) may suggest that the internal rearrangement of the ligand framework from the η^1-hydroperoxo (**A**) to an η^2-hydroperoxo (**A'**) [side-on type hydroperoxo, shown in Eq. (3)] is rate-determining, while the following deprotonation from **A'** to give **B** is much faster. The higher reactivity of the

hydroperoxo intermediate (**A**) of ligand ^{H}Pye2$^{H–Phe}$ as compared to that of ^{H}Pye2^{Phe-Ph} can be attributed to the different steric bulkiness of the *N*-alkyl substituents (-CH_2CHPh_2 in ^{H}Pye2^{Phe-Ph}

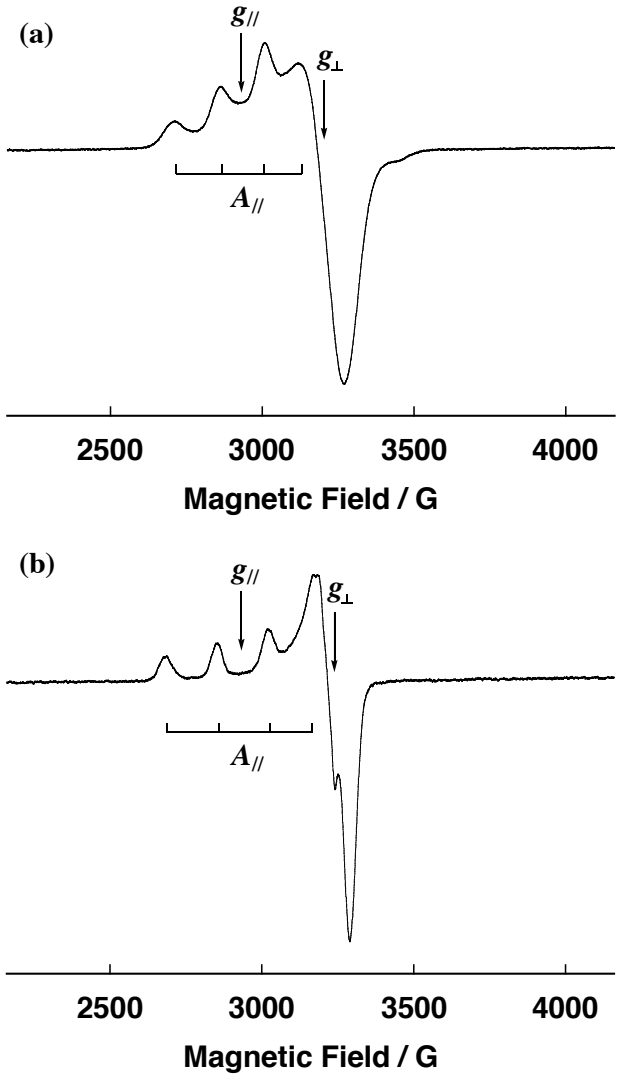

Figure 11. (a) ESR spectrum of [Cu^{II}(^{H}Pye2^{Phe-Ph})$(ClO_4)_2$] (starting material) (2.0 x 10^{-3} M) in acetone at –150°C. ESR parameters $g_{//} = 2.251$, $g_{\perp} = 2.062$, $A_{//} = 157.5$ G. (b) ESR spectrum of the intermediate generated in the reaction of [Cu^{II}(^{H}Pye2^{Phe-Ph})$(ClO_4)_2$] (2.0 x 10^{-3} M) and H_2O_2 (2.0 x 10^{-3} M) in the presence of Et_3N (2.0 x 10^{-3} M) in acetone at –150°C. ESR parameters $g_{//} = 2.238$, $g_{\perp} = 2.044$, $A_{//} = 168.4$ G.

vs. -CH_2CH_2Ph in ^{H}Pye2$^{H–Phe}$). Namely, the larger *N*-alkyl group (-CH_2CHPh_2) in ^{H}Pye2^{Phe-Ph} may retard the rearrangement of the monodentate η^1-hydroperoxo ligand in **A** to the bidentate η^2-hydroperoxo ligand in **A'**, stabilizing the hydroperoxo intermediate **A** in the ^{H}Pye2^{Phe-Ph} complex as compared to the ^{H}Pye2$^{H–Phe}$ system. Furthermore, this process is completely prohibited in the case of the *tetradentate* ligand system (TEPA), since there is no extra coordination site available for formation of the side-on (hydro)peroxo intermediate(s). Thus, the kinetic results as well as the ligand effects of ^{H}Pye2$^{H–Phe}$ and TEPA are all consistent with formation of the proposed side-on peroxo intermediate (**B**).

The mononuclear Cu^{II}–peroxo intermediate (**B**) was further converted into a (μ-η^2:η^2-peroxo)dicopper(II) complex (**C**) at a *higher concentration* of the copper complex. Thus, the reaction of [Cu^{II}(^{H}Pye2^{Phe-Ph})(ClO_4)$_2$] (2.0 mM) with H_2O_2 (2.0 mM) in the presence of triethylamine (2.0 mM) in methanol at –90 °C gave a spectral change shown in Figure 12, where the spectrum of the mononuclear copper(II)–peroxo intermediate (**B**) immediately appeared [spectrum (b) in Figure 12] and then the characteristic absorption band at 366 nm (ε = 11,460 M^{-1} cm^{-1}) together with a small band at 540 nm (ε = 800 M^{-1} cm^{-1}) gradually developed [spectrum (c)]. The final spectrum is nearly the same to that of the previously reported (μ-η^2:η^2-peroxo)dicopper(II) complex supported by ^{H}Pye2$^{H–Phe}$,[17] and the resulting solution was ESR-silent. Furthermore, the resonance Raman spectrum of the product exhibits Raman bands at 741 cm^{-1} and 281 cm^{-1} the former of which shifted to 700 cm^{-1} when $H_2{}^{16}O_2$ is substituted to $H_2{}^{18}O_2$ (Figure 13).[21] The formation of the (μ–η^2:η^2-peroxo)dicopper(II) complex obeys the second-order kinetics (k_3 = 2.6 (± 0.1) x 10^2 M^{-1} s^{-1}), demonstrating that this reaction is a bimolecular process with respect to the copper(II) complex.

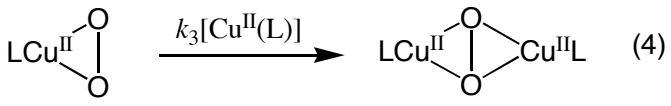

(**B**) (**C**) (4)

In summary, the low-temperature stopped-flow technique has been applied to study the reactions between copper(II) complexes of the tridentate and tetradentate pyridylethylamine ligands and H_2O_2, enabling ones to detect a mononuclear Cu^{II}–peroxo complex presumably having a η^2-binding mode. It has also been found that the ligand denticity (tridentate *vs*. tetradentate) and the steric effects of the *N*-alkyl substituents in the pyridylethylamine

derivatives drastically alter the reactivity of the initially formed Cu^{II}–hydroperoxo intermediates. These results provide significantly important information about the dioxygen-activation mechanism in biological and industrial systems.

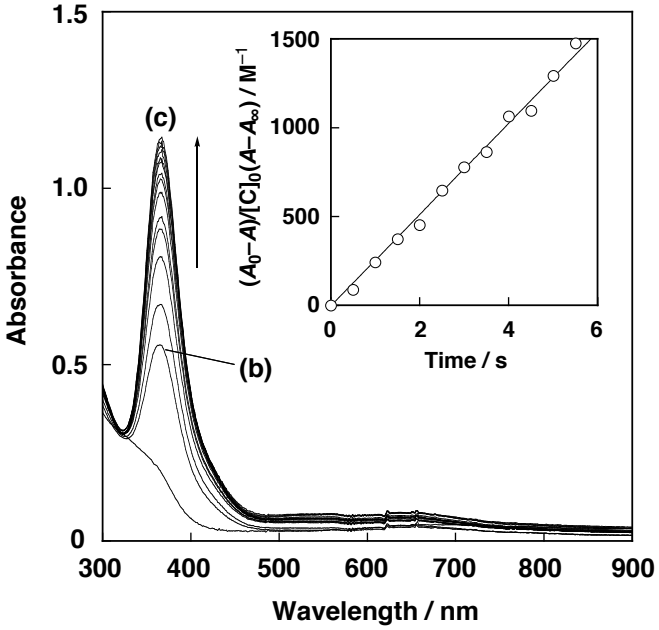

Figure 12. Spectral change for the reaction of $[Cu^{II}(^{H}Pye2^{Phe\text{-}Ph})(ClO_4)_2]$ (2.0 mM) with H_2O_2 (2.0 mM) in the presence of triethylamine (2.0 mM) in CH_3OH at –90˚C. Inset: second-order plot based on the absorption at 366 nm.

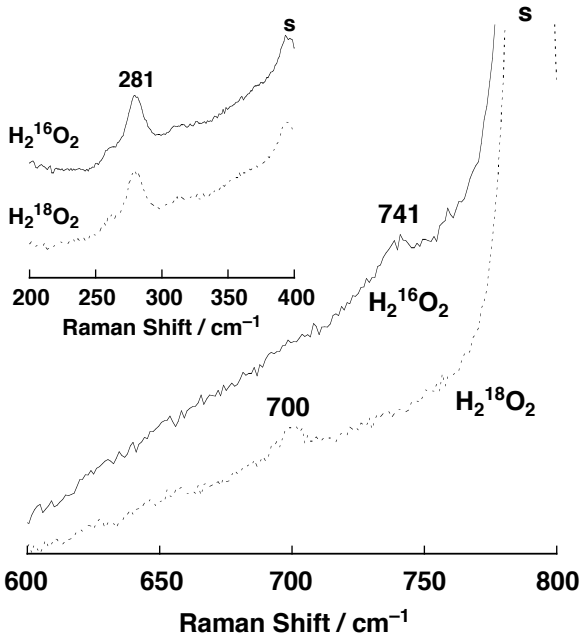

Figure 13. Resonance Raman spectrum of $[Cu^{II}_2(^{H}Pye2^{Phe\text{-}Ph})_2(\mu\text{-}^{16}O_2)]^{2+}$ (solid line) and $[Cu^{II}_2(^{H}Pye2^{Phe\text{-}Ph})_2(\mu\text{-}^{16}O_2)]^{2+}$ (dashed line) obtained with an excitation wavelength of 406.7 nm in MeOH at –80°C: "s" denotes a solvent absorption band. Inset: resonance Raman spectra of 200 – 400 cm^{-1} region.

References

(1) Blackman, A. G.; Tolman, W. B. in *Metal-Oxo and Metal-Peroxo Species in Catalytic Oxidations* (Ed.: Meunier, B.), Springer, Berlin, **2000**, pp 179-211.

(2) Schindler, S. *Eur. J. Inorg. Chem.* **2000**, 2311-2326.

(3) Solomon, E. I.; Sundaram, U. M.; Machonkin, T. E. *Chem. Rev.* **1996**, *96*, 2563-2605.

(4) Klinman, J. P. *Chem. Rev.* **1996**, *96*, 2541-2561.

(5) Okeley, N. M.; van der Donk, W. A. *Chem. Biol.* **2000**, *7*, R159-R171.

(6) Chen, P.; Fujisawa, K.; Solomon, E. I. *J. Am. Chem. Soc.* **2000**, 122, 10177-10193.

(7) Wada, A.; Harata, M.; Hasegawa, K.; Jitsukawa, K.; Masuda, H.; Mukai, M.; Kitagawa, T.; Einaga, H. *Angew. Chem.* **1998**, *110*, 874-875; *Angew. Chem. Int. Ed.* **1998**, *37*, 798-799.

(8) Kodera, M.; Kita, T.; Miura, I.; Nakayama, N.; Kawata, T.; Kano, K.; Hirota, S. *J. Am. Chem. Soc.* **2001**, *123*, 7715-7716.

(9) Ohtsu, H.; Itoh, S.; Nagatomo, S.; Kitagawa, T.; Ogo, S.; Watanabe, Y.; Fukuzumi, S. *Inorg. Chem.* **2001**, *40*, 3200-3207.

(10) Fujisawa, K.; Tanaka, M.; Moro-oka, Y.; Kitajima, N. *J. Am. Chem. Soc.* **1994**, *116*, 12079-12080.

(11) Spencer, D. J. E.; Aboelella, N. W.; Reynolds, A. M.; Holland, P. L.; Tolman, W. B. *J. Am. Chem. Soc.* **2002**, *124*, 2108-2109.

(12) Karlin, K. D.; Wei, N.; Jung, B.; Kaderli, S.; Niklaus, P.; Zuberbühler, A. D. *J. Am. Chem. Soc.* **1993**, *115*, 9506-9514.

(13) Lee, D.-H.; Wei, N.; Murthy, N. N.; Tyeklár, Z.; Karlin, K. D.; Kaderli, S.; Jung, B.; Zuberbühler, A. D. *J. Am. Chem. Soc.* **1995**, *117*, 12498-12513.

(14) The low temperature stopped-flow technique has been well documented to be a useful tool for the detection of unstable copper-dioxygen intermediates; (a) Halfen, J. A.; Mahapatra, S.; Wilkinson, E. C.; Kaderli, S.; Young, V. G., Jr.; Que, L., Jr.; Zuberbühler, A. D.; Tolman, W. B. *Science* **1996**, *271*, 1397-1400. (b) Karlin, K. D.; Kaderli, S.;

Zuberbühler, A. D. *Acc. Chem. Res.* **1997**, *30*, 139-147. (c) Weitzer, M.; Schatz, M.; Hampel, F.; Heinemann, F. W.; Schindler, S. *J. Chem. Soc., Dalton Trans.* **2002**, 686-694.

(15) Armarego, W. L. F.; Perrin, D. D. *Purification of Laboratory Chemicals,* 4th ed.; Pergamon Press: Elmsford, NY, 1996.

(16) Karlin, K. D.; Sherman, S. E. *Inorg. Chim. Acta.* **1982**, *65*, L39-L40.

(17) (a) Itoh, S.; Kondo, T.; Komatsu, M.; Ohshiro, Y.; Li, C.; Kanehisa, N.; Kai, Y.; Fukuzumi, S. *J. Am. Chem. Soc.* **1995**, *117*, 4714-4715. (b) Itoh, S.; Nakao, H.; Berreau, L. M.; Kondo, T.; Komatsu, M.; Fukuzumi, S. *J. Am. Chem. Soc.* **1998**, *120*, 2890-2899.

(18) Because of low intensity of the Raman band of the ^{18}O-derivative, the amount of the isotope shift could not be determined accurately. Although the Raman evidence for the (η^1-hydroperoxo)copper(II) species is not as strong as in earlier instances,[6–9] the structural similarity of this molecule to others in the series[9] and great similarities of the UV-vis and the ^{16}O-Raman data to those of the other (η^1-hydroperoxo)copper(II) complexes[6–9] are strong enough arguments for the presence of the hydroperoxo intermediate.

(19) The UV-vis and ESI-MS of the final solution were exactly the same to those of the authentic sample of [Cu^{I}(TEPA)](ClO_4). Although mechanism of the reaction has yet to be investigated in detail, rate-determining O–O bond homolysis of the hydroperoxo copper(II) intermediate of TEPA may be involved in the formation of [Cu^{I}(TEPA)]$^+$ product.

(20) Kitajima, N.; Fujisawa, K.; Moro-oka, Y. *J. Am. Chem. Soc.* **1989**, *111*, 8975-8976.

(21) The isotope insensitive Raman band at 281 cm^{-1} has recently been assigned to an A_g "accordion" mode of the Cu_2O_2 peroxo core involving predominantly Cu–Cu motion; Henson, M. J.; Mahadevan, V.; Stack, T. D. P.; Solomon, E. I. *Inorg. Chem.* **2001**, *40*, 5068-5069.

Chapter 2

Ligand Effects on the Structures, Physicochemical Properties, and Reactivities of Copper(I) Complexes

Abstract: Ligand effects on the structures, physicochemical properties, and reactivities of copper(I) complexes supported by pyridylalkylamine tridentate ligands have been investigated to demostrate that the small perturbations induced by the methyl substitution at 6-position of pyridine nucleus and by changing the alkyl linker chain length between the tertiary amine nitrogen and the pyridine nucleus (ethylene and methylene) lead to drastic effects on the structures and reactivities of the complexes. Crystal structures of the copper(I) complexes $\mathbf{2}^{\mathbf{R}}$ supported by bis[2-(2-pyridyl)ethyl]amine ligands ^{H}Pye2^{R} have been solved to demonstrate that all the copper(I) complexes form an η^2-copper-arene interaction (d-π interaction) at the phenyl ring of the ligand sidearm. Existence of the copper-arene interaction in a non-polar organic solvent such as CH_2Cl_2 has also been demonstrated by the observation of an intense MLCT band around 290 nm, and the magnitude of interaction is evaluated by the detailed analysis of the ^{1}H- and ^{13}C-NMR spectra and the redox potentials ($E_{1/2}$) of the copper ion as well as the ligand exchange reaction between the phenyl ring and CH_3CN as an external ligand. The copper(I) complexes $\mathbf{2}^{\mathbf{X–Phe}}$ reacted with O_2 at –80 °C in CH_2Cl_2 to give the corresponding (μ-η^2:η^2-peroxo)dicopper(II) complexes, the formation rates (k_{obs}) of which were significantly retarded by the stronger d-π interaction, while complexes $\mathbf{2}^{\mathbf{Phe–Me}}$ and $\mathbf{2}^{\mathbf{Phe–Ph}}$ exhibiting the strongest d-π interaction showed virtually no reactivity toward O_2 under the same experimental conditions. On the other hand, complex $\mathbf{1}^{\mathbf{Phe}}$•$CH_3CN$ suppoted by ^{Me}Pye2^{Phe} possessing the methyl substituents at 6-position of ^{H}Pye2^{R} has a distorted tetrahedral geometry, which consists of three nitrogen atoms of the ligand and one nitrogen atom of the bound CH_3CN. Steric repulsion between the 6-methyl group on the pyridine nucleus of ^{Me}Pye2^{Phe} and the metal ion of the complex prevents the cuprous complex from adaptation to a three-coordinate geometry which must have a shorter Cu–N(pyridine) distance (~1.88 Å). Thus, the four-coordinate $\mathbf{1}^{\mathbf{Phe}}$•$CH_3CN$ complex with a longer Cu–N bond (1.98~2.13 Å) becomes favorable, resulting in rather strong binding of CH_3CN to the metal ion. Thus, the reactivity of the copper(I) complexes of ^{Me}Pye2^{Phe} toward dioxygen is almost lost, showing sharp contrast to the high reactivity of the copper(I) complex supported by a similar tridentate ligand ^{H}Pye2$^{H–Phe}$. In contrast with the copper(I) complexes of bis[2-(2-pyridyl)ethyl]amine

ligand systems, copper(I) complex $\mathbf{4}^{\mathbf{Phe}}$ supported by bis(2-pyridylmethyl)amine ligand $^{H}Pym2^{Phe}$ possesses a trigonal pyramidal geometry in which a d-π interaction with an η^1-binding mode exists between the metal ion and one of the ortho-carbons of the phenyl ring of the ligand sidearm (phenylethyl). The result shows sharp contrast to the d-π interaction with an η^2-binding mode existed in $\mathbf{2}^{\mathbf{R}}$. Such a d-π interaction has been shown to affect stability of the copper(I) complex in CH_2Cl_2. Oxygenation of copper(I) complex $\mathbf{4}^{\mathbf{Phe}}$ supported by $^{H}Pym2^{Phe}$ produces a bis(μ-oxo)dicopper(III) complex, also being in sharp contrast to the case of the copper(I) complex $\mathbf{2}^{\mathbf{R}}$ with ligand $^{H}Pye2^{H–Phe}$, which preferentially affords a (μ-η^2:η^2-peroxo)dicopper(II) complex in the reaction with O_2. Furthermore, copper(I) complexes $\mathbf{3}^{\mathbf{Phe}}$ and $\mathbf{3}^{\mathbf{Phe–Ph}}$ supported by $^{Me}Pym2^{Phe}$ and $^{Me}Pym2^{Phe–Ph}$, respectively, possessing the methyl substituents at 6-position of $^{H}Pym2^{R}$ also exhibit a distorted trigonal pyramidal structure involving a similar η^1 d-π interaction. Strength of the d-π interaction in $\mathbf{3}^{\mathbf{Phe}}$ and $\mathbf{3}^{\mathbf{Phe–Ph}}$ is weaker than that of the d-π interaction with an η^2-binding mode in $\mathbf{2}^{\mathbf{H–Phe}}$ but stronger than that of the η^1 d-π interaction in $\mathbf{4}^{\mathbf{Phe}}$. Redox potential of copper(I) is also affected by the supporting ligand; $^{H}Pym2^{Phe}$ with the highest donor ability among the ligands gave the lowest $E_{1/2}$ value of the copper(I) complex, while $^{H}Pye2^{H–Phe}$ with the lowest donor ability showed the highest $E_{1/2}$ value. This was reflected in the copper(I)-dioxygen reactivity, where the reaction rate of copper(I) complex toward O_2 dramatically increases in the order of $\mathbf{1}^{\mathbf{R}} < \mathbf{2}^{\mathbf{R}} < \mathbf{3}^{\mathbf{R}} < \mathbf{4}^{\mathbf{R}}$. Structure of the resulting Cu_2/O_2 intermediate was also altered by the supporting ligand. Namely, oxygenation of copper(I) complex $\mathbf{3}^{\mathbf{R}}$ at a low temperature gave a (μ-η^2:η^2-peroxo)dicopper(II) complex as in the case of $\mathbf{2}^{\mathbf{H–Phe}}$, but its O–O bond is relatively weakened as compared to the peroxo complex derived from $\mathbf{2}^{\mathbf{H–Phe}}$, and a small amount of a bis(μ-oxo)dicopper(III) complex co-existed. These results can be attributed to the higher electron-donor ability of $^{Me}Pym2^{R}$ as compared to $^{H}Pye2^{H–Phe}$. On the other hand, the fact that $\mathbf{4}^{\mathbf{Phe}}$ mainly afforded a bis(μ-oxo)dicopper(III) complex suggests that the electron-donor ability of $^{Me}Pym2^{R}$ is not high enough to support the higher oxidation state of copper(III) of the bis(μ-oxo) complex.

Introduction

Great success has been brought about in copper/dioxygen chemistry using a variety of bis[2-(2-pyridyl)ethyl]amine-based tridentate ligands.[1-5] Karlin and his coworkers have first

developed a series of dinuclear copper(I) complexes supported by the dinucleating ligands containing two bis[2-(2-pyridyl)ethyl]amine tridentate metal-binging units, and succeeded in mimicking the structures and functions of the active sites of hemocyanin and tyrosinase (*reversible O_2–binding* and *aromatic ligand hydroxylation*).[6,7] Such pioneering works attracted many researchers in the related area to open the new field of copper/dioxygen bioinorganic chemistry.[8-10] The contribution of Itoh and his coworkers in this field is the finding of quantitative *aliphatic ligand hydroxylation* with a mononuclear copper complex of ligand $^{H}Pye2^{H–Phe}$ (*N*,*N*-bis[2-(2-pyridiyl)ethyl]phenylethylamine, R = -CH_2CH_2Ph; Chart 1).[11] Mechanistic studies have suggested that a bis(μ-oxo)dicopper(III) intermediate (**B** in Chart 2), formed from the peroxo complex (**A**) by the O–O bond homolysis, is the actual reactive intermediate for the aliphatic C–H bond activation.[12,13] Réglier *et al* have recently investigated a closely related system.[14-16]

Chart 1

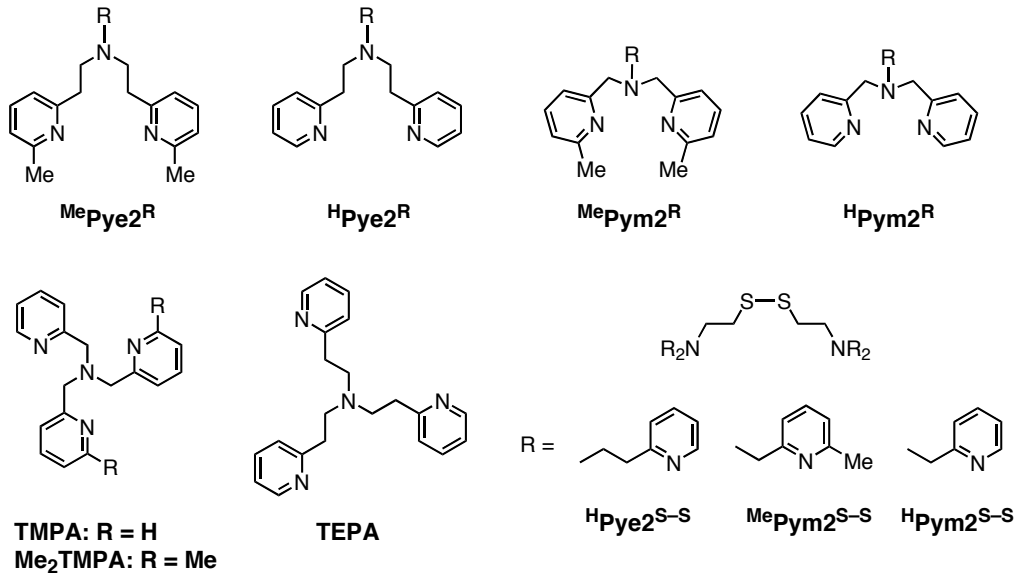

Structure and reactivity of copper complexes have been demonstrated to be altered significantly by introducing a small change in the supporting ligands. One of the most remarkable examples is found in a copper/dioxygen chemistry with the TMPA [tris(2-pyridylmethyl)amine] ligand system (Chart 1). The copper(I) complex of TMPA itself afforded a (μ-1,2-peroxo)dicopper(II) complex (**C** in Chart 2) in the reaction with O_2 at a low temperature,[17] whereas introduction of 6-methyl group into two of the three pyridine nuclei of the ligand (Me_2TMPA: bis(6-methyl-2-pyridylmethyl)(2-pyridylmethyl)amine, Chart 1) resulted in formation of a bis(μ-oxo)dicopper(III) complex (**B**) under similar experimental

conditions.[18] In this case, a small perturbation in the ligand triggers a drastic change in the oxidation state of metal (Cu^{II} *vs*. Cu^{III}) and oxygen (peroxo *vs*. oxo). Such a drastic change of the structure of copper complexes induced by the 6-methyl substituent has also been found in copper(I)/disulfide system, where ligand $^{Me}Pym2^{S-S}$ (Chart 1) affords a disulfide-dicopper(I) complex (type **E** in Chart 2) while reductive cleavage of the S–S bond of the ligand occurs to give a bis(μ-thiolato)dicopper(II) complex (type **F** in Chart 2) in the case of ligand $^{H}Pym2^{S-S}$ (Chart 1).[19] Such prominent effects of the 6-methyl substituent of the pyridyl ligands have also been observed in the related iron chemistry.[20-24]

Chart 2

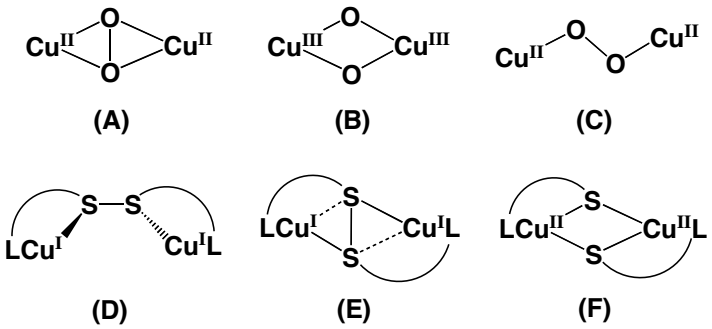

Effects of the alkyl linker chain in the tetradentate ligand system [methylene in TMPA *vs*. ethylene in TEPA: tris(2-pyridylethyl)amine, Chart 1] have also been investigated to demonstrate that the longer ethylene linker of TEPA can adapt its cuprous complex to a tetrahedral geometry, stabilizing the Cu(I) state of the complex.[25,26] Thus, the copper(I) complex of TEPA does not react with O_2, being in sharp contrast to the high reactivity of the copper(I) complex of TMPA.[17] In the copper(I)/disulfide case as well, ligand $^{H}Pye2^{S-S}$ (Chart 1) with the ethylene linker between the tertiary amine nitrogen and the pyridine nucleus affords a different type of disulfide-dicopper(I) complex (type **D** in Chart 2).[19]

In this chapter, ligand substituent effects on the structures and reactivities of copper(I) complexes supported by a series of pyridylalkylamine tridentate ligands such as bis[2-(6-methyl-2-pyridyl)ethyl]amine ($^{Me}Pye2^{R}$), bis[2-(2-pyridyl)ethyl]amine ($^{H}Pye2^{R}$), bis(6-methyl-2-pyridylmethyl)amine ($^{Me}Pym2^{R}$), and bis(2-pyridylmethyl)amine ($^{H}Pym2^{R}$) (Chart 1) have been systematically examined in order to clarify the ligand effects on copper/dioxygen chemistry.

Experimental Section

General. All chemicals used in this study except the ligands and the copper(I) complexes were commercial products of the highest available purity and were further purified by the standard methods, if necessary.[27] 6-Methyl-2-vinylpyridine was kindly supplied by Koei Chemical Co. Ltd, and was purified by fractional distillation. FT-IR spectra were recorded with a Shimadzu FTIR-8200PC or a Horiba FT-200 spectrophotometer. UV-vis spectra were measured using a Hewlett Packard HP8453 diode array spectrophotometer with a Unisoku thermostated cell holder designed for low temperature measurements (USP-203) or a Shimazdu diode array spectrometer Multispec-1500 equipped with the same cell holder. ESR spectra were recorded on a JEOL JES-FE2XG spectrometer at –150 ˚C. Mass spectra were recorded with a JEOL JMS–700T Tandem MS station or a PE SCIEX API 150EX (for ESI-MS). ESI-TOF/MS spectra were measured with a Micromass LCT spectrometer. NMR spectra were recorded on a JEOL FT-NMR Lambda 300WB, a JEOL FT-NMR GX-400, or a Bruker Advance 600 spectrometer. ^{1}H-NMR spectra were referenced to the residual proton resonance of the solvent and ^{13}C-NMR spectra to the solvent resonance (CD_2Cl_2: ^{1}H, δ = 5.32,^{13}C, δ = 53.8). Complete peak assignments in the ^{1}H- and ^{13}C-NMR spectra of the ligands and the copper(I) complexes have been accomplished by employing 2D-NMR techniques (COSY, NOESY, HMQC, and HMBC).

Electrochemical Measurements. The cyclic voltammetry (CV) measurements were performed on an ALS–630A electrochemical analyzer in anhydrous CH_2Cl_2 containing 0.1 M NBu_4ClO_4 as supporting electrolyte. The Pt working electrodes were polished with a polishing alumina suspension and rinsed with CH_2Cl_2 before use. The counter electrode was a Pt wire. Silver pseudo reference electrode was used, and the potentials were determined using the ferrocene/ferricenium (Fc/Fc^{+}) couple as a reference. All electrochemical measurements were carried out at 25 °C under an atmospheric pressure of Ar in a glove box (Miwa Co. Ltd.).

Synthesis of Ligands.

***N,N*-Bis[2-(6-methyl-2-pyridyl)ethyl]-2-phenylethylamine (^{Me}Pye2^{Phe}; Phe = -CH_2CH_2Ph).** This ligand was prepared by the reaction of 2-phenylethylamine (0.96 g, 7.9 mmol) and 6-methyl-2-vinylpyridine (1.90 g, 16.0 mmol) in refluxing methanol (40 mL) containing acetic acid (0.95 g, 16.0 mmol) for 10 days, and purified by column chromatography (SiO_2). Pale brown oil (6.3 % yield); ^{1}H-NMR (300 MHz, $CDCl_3$) δ 2.52 (6

H, s, -CH_3), 2.67–2.83 (4 H, m, -CH_2CH_2-), 2.85–3.00 (8 H, m, -CH_2CH_2-), 6.83 (2 H, d, J = 7.5 Hz, $H_{Py\text{-}3}$ or $H_{Py\text{-}5}$), 6.95 (2 H, d, J = 7.5 Hz, $H_{Py\text{-}3}$ or $H_{Py\text{-}5}$), 7.10–7.27 (5 H, m, C_6H_5), 7.42 (2 H, t, J = 7.5 Hz, $H_{Py\text{-}4}$).

***N*,*N*-Bis[2-(2-pyridyl)ethyl]-2-(4-methyloxyphenyl)ethylamine (^{H}Pye2$^{OMe–Phe}$; OMe-Phe = -$CH_2CH_2C_6H_4$-*p*-OMe).** This ligand was prepared by the reaction of 2-(4-methoxyphenyl)ethylamine (3.0 g, 20 mmol) and 2-vinylpyridine (10.5 g, 100 mmol) in refluxing methanol (50 mL) containing acetic acid (6.0 g, 100 mmol) for 10 days, and purified by column chromatography (SiO_2). Pale brown oil (54.3 % yield); FAB-HRMS (pos.) m/z = 362.227 ($[M + 1]^+$); ^{1}H-NMR (600 MHz, CD_2Cl_2) δ 2.65 (2 H, dd, J = 10.0 and 7.1 Hz, NCH_2CH_2Ar), 2.76 (2 H, dd, J = 10.0 and 7.1 Hz, NCH_2CH_2Ar), 2.89 (4 H, dd, J = 8.0 and 5.4 Hz, NCH_2CH_2Py), 2.97 (4 H, dd, J = 8.0 and 5.4 Hz, NCH_2CH_2Py), 3.77 (3 H, s, -OCH_3), 6.80 (2 H, dt, J = 8.7 and 2.1 Hz, $H_{Ar\text{-}3}$ and $H_{Ar\text{-}3'}$), 7.05 (2 H, d, J = 7.7 and 2.1 Hz, $H_{Ar\text{-}2}$ and $H_{Ar\text{-}2'}$), 7.06 (2 H, d, J = 7.7 Hz, $H_{Py\text{-}3}$), 7.09 (2 H, ddd, J = 7.7, 4.9, and 1.0 Hz, $H_{Py\text{-}5}$), 7.55 (2 H, td, J = 7.7 and 1.8 Hz, $H_{Py\text{-}4}$), 8.50 (2 H, ddd, J = 4.9, 1.8, and 1.0 Hz, $H_{Py\text{-}6}$); ^{13}C-NMR (600 MHz, CD_2Cl_2) 33.25 (NCH_2CH_2Ar), 36.47 (NCH_2CH_2Py), 54.26 (NCH_2CH_2Py), 55.53 (OCH_3), 56.53 (NCH_2CH_2Ar), 113.98 ($C_{Ar\text{-}3}$), 121.27 ($C_{Py\text{-}5}$), 123.63 ($C_{Py\text{-}3}$), 130.03 ($C_{Ar\text{-}2}$), 133.36 ($C_{Ar\text{-}1}$), 136.28 ($C_{Py\text{-}4}$), 149.50 ($C_{Py\text{-}6}$), 158.30 ($C_{Ar\text{-}4}$), 161.37 ppm ($C_{Py\text{-}2}$).

***N*,*N*-Bis[2-(2-pyridyl)ethyl]-2-(4-methylphenyl)ethylamine (^{H}Pye2$^{Me–Phe}$; Me-Phe = -$CH_2CH_2C_6H_4$-*p*-Me).** This ligand was prepared by the same procedure reported previously by Itoh and his coworkers.[12] ^{1}H-NMR (600 MHz, CD_2Cl_2) δ 2.30 (3 H, s, CH_3), 2.67 (2 H, dd, J = 8.5 and 5.3 Hz, NCH_2CH_2Ar), 2.77 (2 H, dd, J = 8.5 and 5.3 Hz, NCH_2CH_2Ar), 2.89 (4 H, dd, J = 8.1 and 5.4 Hz, NCH_2CH_2Py), 2.97 (4 H, dd, J = 8.1 and 5.4 Hz, NCH_2CH_2Py), 7.02 (2 H, d, J = 7.9 Hz, $H_{Ar\text{-}2}$ and $H_{Ar\text{-}2'}$), 7.05 (2 H, d, J = 7.5 Hz, $H_{Py\text{-}3}$), 7.07 (2 H, d, J = 7.9 Hz, $H_{Ar\text{-}3}$ and $H_{Ar\text{-}3'}$), 7.09 (2 H, ddd, J = 7.7, 4.9, and 1.0 Hz, $H_{Py\text{-}5}$), 7.54 (2 H, td, J = 7.7 and 1.9 Hz, $H_{Py\text{-}4}$), 8.49 (2 H, ddd, J = 4.9, 1.9, and 1.0 Hz, $H_{Py\text{-}6}$); ^{13}C-NMR (600 MHz, CD_2Cl_2) 21.07 (OCH_3), 33.68 (NCH_2CH_2Ar), 36.46 (NCH_2CH_2Py), 54.26 (NCH_2CH_2Py), 56.44 (NCH_2CH_2Ar), 121.28 ($C_{Py\text{-}5}$), 123.65 ($C_{Py\text{-}3}$), 129.02 ($C_{Ar\text{-}2}$), 129.24 ($C_{Ar\text{-}3}$), 135.63 ($C_{Ar\text{-}4}$), 136.30 ($C_{Py\text{-}4}$), 138.21 ($C_{Ar\text{-}1}$), 149.51 ($C_{Py\text{-}6}$), 161.37 ppm ($C_{Py\text{-}2}$).

***N*,*N*-Bis[2-(2-pyridyl)ethyl]-2-phenylethylamine (^{H}Pye2$^{H–Phe}$; H-Phe = -CH_2CH_2Ph).** This ligand was also prepared by the same procedure reported previously by Itoh and his coworkers.[12] ^{1}H-NMR (600 MHz, CD_2Cl_2) δ 2.71 (2 H, dd, J = 10.3 and 6.8 Hz, NCH_2CH_2Ph), 2.80 (2 H, dd, J = 10.3 and 6.8 Hz, NCH_2CH_2Ph), 2.89 (4 H, dd, J = 8.1 and 5.6 Hz, NCH_2CH_2Py), 2.97 (4 H, dd, J = 8.1 and 5.6 Hz, NCH_2CH_2Py), 7.06 (2 H, d, J = 7.7 Hz, $H_{Py\text{-}3}$),

7.10 (2 H, ddd, J = 7.5, 4.9, and 0.9 Hz, $H_{Py\text{-}5}$), 7.14 (2 H, d, J = 7.0 Hz, $H_{Ph\text{-}2}$ and $H_{Ph\text{-}2'}$), 7.17 (1 H, t, J = 7.3 Hz, $H_{Ph\text{-}4}$), 7.25 (2 H, t, J = 7.2 Hz, 2 H; $H_{Ph\text{-}3}$ and $H_{Ph\text{-}3'}$), 7.55 (2 H, td, J = 7.5 and 1.8 Hz, $H_{Py\text{-}4}$), 8.49 (2 H, ddd, J = 4.9, 1.8, and 0.9 Hz, $H_{Py\text{-}6}$); ^{13}C-NMR (600 MHz, CD_2Cl_2) 34.12 ($NCH_2\mathit{C}H_2Ph$), 36.30 ($NCH_2\mathit{C}H_2Py$), 54.22 ($N\mathit{C}H_2CH_2Py$), 56.33 ($N\mathit{C}H_2CH_2Ph$), 121.34 ($C_{Py\text{-}5}$), 123.70 ($C_{Py\text{-}3}$), 126.12 ($C_{Ph\text{-}4}$), 128.57 ($C_{Ph\text{-}3}$) 129.18 ($C_{Ph\text{-}2}$), 136.41 ($C_{Py\text{-}4}$), 141.37 ($C_{Ph\text{-}1}$), 149.46 ($C_{Py\text{-}6}$), 161.27 ppm ($C_{Py\text{-}2}$).

***N*,*N*-Bis[2-(2-pyridyl)ethyl]-2-(4-chlorophenyl)ethylamine (^{H}Pye2$^{Cl–Phe}$; Cl-Phe = -$CH_2CH_2C_6H_4$-*p*-Cl).** This ligand was also prepared by the same procedure reported previously by Itoh and his coworkers.[12] ^{1}H-NMR (600 MHz, CD_2Cl_2) δ 2.66 (2 H, dd, J = 7.8 and 5.6 Hz, $NCH_2C\mathit{H}_2Ar$), 2.76 (2 H, dd, J = 7.8 and 5.6 Hz, $NC\mathit{H}_2CH_2Ar$), 2.85 (4 H, dd, J = 7.9 and 6.6 Hz, $NCH_2C\mathit{H}_2Py$), 2.95 (4 H, dd, J = 7.9 and 6.6 Hz, $NC\mathit{H}_2CH_2Py$), 7.00 (2 H, d, J = 7.8 Hz, $H_{Py\text{-}3}$), 7.03 (2 H, d, J = 8.4 Hz, $H_{Ar\text{-}2}$ and $H_{Ar\text{-}2'}$), 7.09 (2 H, ddd, J = 7.6, 4.9, and 1.0 Hz, $H_{Py\text{-}5}$), 7.20 (2 H, d, J = 8.4 Hz, $H_{Ar\text{-}3}$ and $H_{Ar\text{-}3'}$), 7.53 (2 H, td, J = 7.6 and 1.9 Hz, $H_{Py\text{-}4}$), 8.49 (2 H, ddd, J = 4.9, 1.9, and 1.0 Hz, $H_{Py\text{-}6}$); ^{13}C-NMR (600 MHz, CD_2Cl_2) 33.55 ($NCH_2\mathit{C}H_2Ar$), 36.44 ($NCH_2\mathit{C}H_2Py$), 54.20 ($N\mathit{C}H_2CH_2Py$), 56.06 ($N\mathit{C}H_2CH_2Ar$), 121.30 ($C_{Py\text{-}5}$), 123.66 ($C_{Py\text{-}3}$), 128.51 ($C_{Ar\text{-}3}$), 130.67 ($C_{Ar\text{-}2}$), 131.66 ($C_{Ar\text{-}4}$), 136.29 ($C_{Py\text{-}4}$), 140.11 ($C_{Ar\text{-}1}$), 149.52 ($C_{Py\text{-}6}$), 161.29 ppm ($C_{Py\text{-}2}$).

***N*,*N*-Bis[2-(2-pyridyl)ethyl]-2-(4-nitrophenyl)ethylamine (^{H}Pye2$^{NO_2–Phe}$; NO_2-Phe = -$CH_2CH_2C_6H_4$-*p*-NO_2).** This ligand was also prepared by the same procedure reported previously by Itoh and his coworkers.[12] ^{1}H-NMR (600 MHz, CD_2Cl_2) δ 2.76–2.82 (4 H, m, $NC\mathit{H}_2C\mathit{H}_2Ar$), 2.84 (4 H, dd, J = 7.7 and 6.8 Hz, $NCH_2C\mathit{H}_2Py$), 2.96 (4 H, dd, J = 7.7 and 6.8 Hz, $NC\mathit{H}_2CH_2Py$), 7.00 (2 H, d, J = 7.7 Hz, $H_{Py\text{-}3}$), 7.09 (2 H, ddd, J = 8.7, 4.9, and 0.9 Hz, $H_{Py\text{-}5}$), 7.21 (2 H, d, J = 8.7 Hz, $H_{Ar\text{-}2}$ and $H_{Ar\text{-}2'}$), 7.53 (2 H, td, J = 7.7 and 1.8 Hz, $H_{Py\text{-}4}$), 8.03 (2 H, d, J = 8.7 Hz, $H_{Ar\text{-}3}$ and $H_{Ar\text{-}3'}$), 8.48 (2 H, ddd, J = 4.9, 1.8, and 0.9 Hz, $H_{Py\text{-}6}$); ^{13}C-NMR (600 MHz, CD_2Cl_2) 34.13 ($NCH_2\mathit{C}H_2Ar$), 36.37 ($NCH_2\mathit{C}H_2Py$), 54.07 ($N\mathit{C}H_2CH_2Py$), 55.50 ($N\mathit{C}H_2CH_2Ar$), 121.36 ($C_{Py\text{-}5}$), 123.57 ($C_{Ar\text{-}3}$), 123.64 ($C_{Py\text{-}3}$), 130.09 ($C_{Ar\text{-}2}$), 136.32 ($C_{Py\text{-}4}$), 146.71 ($C_{Ar\text{-}4}$), 149.67 ($C_{Ar\text{-}1}$), 149.54 ($C_{Py\text{-}6}$), 161.15 ppm ($C_{Py\text{-}2}$).

***N*,*N*-Bis[2-(2-pyridyl)ethyl]-2-methyl-2-phenylethylamine (^{H}Pye2$^{Phe–Me}$; Phe-Me = -$CH_2CH(Me)Ph$).** This ligand was prepared by the same precedure described above for the synthesis of ^{H}Pye2$^{OMe–Phe}$ using 2-methyl-2-phenylethylamine instead of 2-(4-methoxyphenyl)ethylamine. Pale brown oil; ^{1}H-NMR (600 MHz, CD_2Cl_2) δ 1.15 (3 H, d, J = 6.9 Hz, $NCH_2CH(C\mathit{H}_3)Ph$), 2.61 (1 H, dd, J = 12.8 and 8.0 Hz, $NC\mathit{H}_2CH(CH_3)Ph$), 2.71 (1 H, dd, J = 12.8 and 8.0 Hz, $NC\mathit{H}_2CH(CH_3)Ph$), 2.82–2.98 (7 H, m, $NCH_2C\mathit{H}(CH_3)Ph$,

NCH_2CH_2Py, NCH_2CH_2Py, and NCH_2CH_2Py), 7.00 (2 H, d, J = 7.8 Hz, H_{Py-3}), 7.11 (2 H, ddd, J = 7.5, 6.0, and 0.9 Hz, H_{Py-5}), 7.16 (2 H, d, J = 7.5 Hz, H_{Ph-2} and $H_{Ph-2'}$), 7.19 (1 H, t, J = 7.5 Hz, H_{Ph-4}), 7.28 (2 H, t, J = 7.5 Hz, H_{Ph-3} and $H_{Ph-3'}$), 7.54 (2 H, td, J = 7.7 and 1.9 Hz, H_{Py-4}), 8.52 (2 H, d, J = 4.2, Hz, H_{Py-6}); ^{13}C-NMR (600 MHz, CD_2Cl_2) 19.98 ($NCH_2CH(CH_3)Ph$), 36.08 (NCH_2CH_2Py), 38.79 ($NCH_2CH(CH_3)Ph$), 54.73 (NCH_2CH_2Py), 62.68 ($NCH_2CH(CH_3)Ph$), 121.33 (C_{Py-5}), 123.82 (C_{Py-3}), 126.22 (C_{Ph-4}), 127.72 (C_{Ph-2}), 128.53 (C_{Ph-3}), 136.46 (C_{Py-4}), 146.95 (C_{Ph-1}), 149.26 (C_{Py-6}), 161.28 ppm (C_{Py-2}).

***N*,*N*-Bis[2-(2-pyridyl)ethyl]-2,2-diphenylethylamine (^{H}Pye2$^{Phe–Ph}$; Phe-Ph = -CH_2CHPh_2).** Ligand ^{H}Pye2$^{Phe–Ph}$ has been reported in Chapter 1. ^{1}H-NMR (600 MHz, CD_2Cl_2) δ 2.81 (4 H, dd, J = 7.9 and 6.8 Hz, NCH_2CH_2Py), 2.97 (4 H, dd, J =7.9 and 6.8 Hz, NCH_2CH_2Py), 3.20 (2 H, d, J = 7.7 Hz, NCH_2CHPh_2), 4.15 (1 H, t, J = 7.7 Hz, NCH_2CHPh_2), 6.87 (2 H, d, J = 7.8 Hz, H_{Py-3}), 7.08 (2 H, ddd, J = 7.4, 4.9, and 1.1 Hz, H_{Py-5}), 7.18 (2 H, tt, J = 7.8 and 1.3 Hz, H_{Ph-4}), 7.21 (4 H, dd, J = 7.1 and 1.3 Hz, H_{Ph-2} and $H_{Ph-2'}$), 7.26 (4 H, td, J = 7.3 and 1.9 Hz, H_{Ph-3} and $H_{Ph-3'}$), 7.49 (2 H, ddd, J = 7.8, 7.4, and 1.8 Hz, H_{Py-4}), 8.50 (2 H, ddd, J = 4.9, 1.8, and 0.8 Hz, H_{Py-6}); ^{13}C-NMR (600 MHz, CD_2Cl_2) 35.95 (NCH_2CH_2Py), 50.17 (NCH_2CHPh_2), 54.49 (NCH_2CH_2Py), 60.19 (NCH_2CHPh_2), 121.24 (C_{Py-5}), 123.67 (C_{Py-3}), 126.45 (C_{Ph-4}), 128.62 (C_{Ph-3}), 128.63 (C_{Ph-2}), 136.27 (C_{Py-4}), 144.53 (C_{Ph-1}), 149.45 (C_{Py-6}), 161.28 ppm (C_{Py-2}).

***N*,*N*-Bis(6-methyl-2-pyridylmethyl)-2-phenylethylamine (^{Me}Pym2^{Phe}; Phe = -CH_2CH_2Ph).** Acetic acid (1.20 g, 20 mmol) was added to a methanol solution (200 mL) containing 2-phenylethylamine (1.21 g, 10 mmol) and 6-methyl-2-pyridinecarboxaldehyde (2.42 g, 20 mmol), and the solution was stirred for 1 h at room temperature. $NaBH_3CN$ (1.26 g, 20 mmol) was then added slowly to the solution, and the mixture was stirred for 3 days at room temperature. The reaction was quenched (pH = 1) by adding conc. HCl and the solvent was removed by evaporation. To the resulting material was added 15 % NaOH aqueous solution (100 mL), and the organic materials were extracted by $CHCl_3$ (50 mL x 3). After drying over anhydrous K_2CO_3, evaporation of the solvent gave a brown residue, from which ligand ^{Me}Pym2^{Phe} was isolated as a yellow oily material by SiO_2 column chromatography. Yield: 2.9 g (88 %). ^{1}H-NMR (600 Hz, CD_2Cl_2) δ 2.49 (6 H, s, -CH_3), 2.77 (2 H, dd, J = 8.0 and 6.9 Hz, -NCH_2CH_2Ph), 2.85 (2 H, dd, J = 8.0 and 6.9 Hz, -NCH_2CH_2Ph), 3.81 (4 H, s, -NCH_2Py), 6.99 (2 H, d, J = 7.6 Hz, H_{Py-5}), 7.12 (2 H, d, J = 7.5 Hz, H_{Ph-2} and H_{Ph-6}), 7.17 (1 H, t, J = 7.5 Hz, H_{Ph-4}), 7.20 (2 H, d, J = 7.6 Hz, H_{Py-3}), 7.24 (2 H, t, J = 7.5 Hz, H_{Ph-3} and H_{Ph-5}), 7.48 (2 H, t, J = 7.6 Hz, H_{Py-4}); ^{13}C-NMR (600 Hz, CD_2Cl_2) 24.53 (-Me), 33.86 (-NCH_2CH_2Ph),

56.45 (-N*C*H$_2$CH$_2$Ph), 60.76 (-N*C*H$_2$Py), 119.87 (C$_{Py-3}$), 121.44 (C$_{Py-5}$), 126.15 (C$_{Ph-4}$), 128.51 (C$_{Ph-3}$ and C$_{Ph-5}$), 129.28 (C$_{Ph-2}$ and C$_{Ph-6}$), 136.75 (C$_{Py-4}$), 141.22 (C$_{Ph-1}$), 157.86 (C$_{Py-6}$), 159.74 ppm (C$_{Py-2}$); FAB-MS (pos.) *m*/*z* = 332.19 ([L + H]$^+$).

***N*,*N*-Bis(6-methyl-2-pyridylmethyl)-2,2-diphenylethylamine (^{Me}Pym2$^{Phe–Ph}$; Phe-Ph = -CH$_2$CHPh$_2$).** This ligand was prepared by the same procedure described above for the synthesis of ^{Me}Pym2^{Phe} using 2,2-diphenylethylamine instead of 2-phenylethylamine. Yield: 37 %. ^{1}H-NMR (600 Hz, CD_2Cl_2) δ 2.50 (6 H, s, -CH$_3$), 3.18 (2 H, d, *J* = 7.8 Hz, -NC*H*$_2$CHPh$_2$), 3.80 (4 H, s, -NC*H*$_2$Py), 4.36 (1 H, t, *J* = 7.8 Hz, -NCH$_2$C*H*Ph$_2$), 6.89 (2 H, d, *J* = 7.6 Hz, H$_{Py-3}$), 6.99 (2 H, d, *J* = 7.6 Hz, H$_{Py-5}$), 7.12 (4 H, d, *J* = 7.2 Hz, H$_{Ph-2}$ and H$_{Ph-6}$), 7.19 (2 H, t, *J* = 7.2 Hz, H$_{Ph-4}$), 7.25 (4 H, t, *J* = 7.6 Hz, H$_{Ph-3}$ and H$_{Ph-5}$), 7.40 (2 H, t, *J* = 7.6 Hz, H$_{Py-4}$); ^{13}C-NMR (600 Hz, CD_2Cl_2) 24.54 (-Me), 49.84 (-NCH$_2$*C*HPh$_2$), 59.84 (-N*C*H$_2$CHPh$_2$), 61.06 (-N*C*H$_2$Py), 120.26 (C$_{Py-3}$), 121.46 (C$_{Py-5}$), 126.54 (C$_{Ph-4}$), 128.58 (C$_{Ph-3}$ and C$_{Ph-5}$), 128.75 (C$_{Ph-2}$ and C$_{Ph-6}$), 136.66 (C$_{Py-4}$), 144.16 (C$_{Ph-1}$), 157.71 (C$_{Py-6}$), 159.37 ppm (C$_{Py-2}$); FAB-MS (pos.) *m*/*z* = 408.2 ([L + H]$^+$).

***N*,*N*-Bis(6-methyl-2-pyridylmethyl)benzylamine (^{Me}Pym2^{Bn}; Bn = -CH$_2$Ph).** This ligand was prepared by the same procedure described above for the synthesis of ^{Me}Pym2^{Phe} using benzylamine instead of 2-phenylethylamine. Yield: 42 %. ^{1}H-NMR (400 MHz, $CDCl_3$) δ 2.51 (6 H, s, -CH$_3$), 3.68 (2 H, s, -C*H*$_2$Ph), 3.78 (4 H, s, -C*H*$_2$Py), 6.99 (2 H, d, *J* = 7.5 Hz, H$_{Py-5}$), 7.19–7.33 (3 H, m, H$_{Ph}$), 7.42 (2 H, d, *J* = 7.5 Hz, H$_{Py-3}$), 7.45 (2 H, d, *J* = 8.1 Hz, H$_{Ph}$), 7.55 (2 H, t, *J* = 7.5 Hz, H$_{Py-4}$); Anal. Calcd for $C_{21}H_{23}N_3$: C, 79.46; H, 7.30; N, 13.24. Found: C, 79.49; H, 7.37; N, 13.13; FAB-MS (pos.) *m*/*z* = 318 ([L + H]$^+$). FT-IR (KBr) 1591 and 1578 cm^{-1} (C=C, aromatic).

***N*,*N*-Bis(2-pyridylmethyl)-2-phenylethylamine (^{H}Pym2^{Phe}; Phe = -CH$_2$CH$_2$Ph).** This ligand was prepared by the same procedure described above for the synthesis of ^{Me}Pym2^{Phe} using 2-pyridine-carboxaldehyde instead of 6-methyl-2-pyridinecarboxaldehyde. Yield: 70 %. ^{1}H-NMR (400 Hz, $CDCl_3$) δ 2.78–2.88 (4 H, m, NC*H*$_2$C*H*$_2$Ph), 3.89 (4 H, s, NC*H*$_2$Py), 7.08–7.24 (7 H, m, Ph and Py$_{H-5}$), 7.38 (2 H, d, *J* = 7.7 Hz, Py$_{H-3}$), 7.59 (2 H, dt, *J* = 1.8 and 7.7 Hz, Py$_{H-4}$), 8.52 (2 H, d, *J* = 4.0 Hz, Py$_{H-6}$); FAB-HRMS (pos.) *m*/*z* = 304.1813, calcd for $C_{20}H_{22}N_3$ = 304.1814.

Synthesis of Copper(I) Complexes.

In this chapter, the copper(I) complexes supported by ligand ^{Me}Pye2^R, ^{H}Pye2^R, ^{Me}Pym2^R, and ^{H}Pym2^R are denoted as **1**^{R}, **2**^{R}, **3**^{R}, and **4**^{R}, respectively.

[Cu^I(^{Me}Pye2^{Phe})•CH$_3$CN]ClO$_4$ (1^{Phe}•CH$_3$CN). Ligand ^{Me}Pye2^{Phe} (126.1 mg, 0.35 mmol)

was treated with $[Cu^{I}(CH_3CN)_4]ClO_4$ (112.3 mg, 0.35 mmol) in CH_2Cl_2 (5 mL) under Ar atmosphere. After stirring for 30 min at room temperature, insoluble material was removed by filtration. Addition of ether (100 mL) to the filtrate gave a pale yellow powder that was precipitated by standing the mixture for several minutes. The supernatant was then removed by decantation, and the remained pale yellow solid was dissolved in CH_3CN (5 mL). Addition of ether (100 mL) to the filtrate gave a pale yellow powder that was precipitated by standing the mixture for several minutes. The supernatant was then removed by decantation, and the remained pale yellow solid was washed with ether three times, and dried (41 % yield). All procedures were done in a glove box ($[O_2] < 0.1$ ppm). ^{1}H-NMR (600 MHz, acetone-d_6) δ 2.04 (3 H, s, bound CH_3CN), 2.73–2.80 (4 H, m, -CH_2-CH_2-Ph), 2.90 (6 H, s, -CH_3), 3.20 (4H, br, -C$H_2$$CH_2$Py or -$CH_2CH_2$Py), 3.31 (4 H, t, -C$H_2$$CH_2$Py or -$CH_2CH_2$Py), 7.06–7.21 (5 H, m, aromatic H), 7.47 (2 H, t, J = 7.7 Hz, $H_{Py\text{-}3}$ or $H_{Py\text{-}5}$), 7.54 (2 H, d, J = 7.7 Hz, $H_{Py\text{-}3}$ or $H_{Py\text{-}5}$), 7.97 (2 H, t, J = 7.7 Hz, $H_{Py\text{-}4}$); FT-IR (KBr): 1105, 1086, and 625 cm^{-1} (ClO_4^-); FAB-MS (pos.), m/z = 422.28 ($[M]^+$); Anal. for $[Cu^{I}(^{Me}Pye2^{Phe})\bullet CH_3CN]ClO_4$. Calcd for $C_{26}H_{32}O_4N_4CuCl$: C, 55.41; H, 5.72; N, 9.94. Found: C, 55.28; H, 5.66; N, 9.67.

$[Cu^{I}(^{H}Pye2^{OMe–Phe})]ClO_4$ ($2^{OMe–Phe}$). Ligand $^{H}Pye2^{OMe–Phe}$ (108.4 mg, 0.3 mmol) was treated with $[Cu^{I}(CH_3CN)_4]ClO_4$ (96.1 mg, 0.3 mmol) in CH_2Cl_2 (5 mL) under Ar atmosphere. After stirring for 30 min at room temperature, insoluble material was removed by filtration. Addition of ether (100 mL) to the filtrate gave a pale yellow powder that was precipitated by standing the mixture for several minutes. The supernatant was then removed by decantation, and the remained pale yellow solid was washed with ether three times, and dried (68 % yield). All procedures were done in a glove box (DBO-1KP, Miwa Co. Ltd.), ($[O_2] < 0.1$ ppm). ^{1}H-NMR (600 MHz, CD_2Cl_2) δ 2.73 (2 H, br m, NCH_2CH_2Ar), 2.80–3.30 (10 H, br m, NCH_2CH_2Ar, NCH_2CH_2Py, and NCH_2CH_2Py), 3.77 (3 H, s, -OCH_3), 6.89 (2 H, d, J = 8.4 Hz, $H_{Ar\text{-}3}$ and $H_{Ar\text{-}3'}$), 7.11 (2 H, d, J = 8.4 Hz, $H_{Ar\text{-}2}$ and $H_{Ar\text{-}2'}$), 7.37, (4 H, br, $H_{Py\text{-}3}$ and $H_{Py\text{-}5}$), 7.82 (2 H, br t, J = 7.0 Hz, $H_{Py\text{-}4}$), 8.19 (2 H, br, $H_{Py\text{-}6}$); ^{13}C-NMR (600 MHz, CD_2Cl_2) 32.49 (NCH_2CH_2Ar), 34.04 (NCH_2CH_2Py), 54.56 (NCH_2CH_2Py), 55.88 (OCH_3), 56.28 (NCH_2CH_2Ar), 114.54 ($C_{Ar\text{-}3}$), 123.59 ($C_{Py\text{-}5}$), 125.18 ($C_{Ar\text{-}2}$), 126.64 ($C_{Py\text{-}3}$), 126.29 ($C_{Ar\text{-}1}$), 138.86 ($C_{Py\text{-}4}$), 150.13 ($C_{Py\text{-}6}$), 159.33 ($C_{Ar\text{-}4}$), 160.43 ppm ($C_{Py\text{-}2}$); FT-IR (KBr) 1247 and 1028 (–OCH_3) 1115, 1089, and 625 cm^{-1} (ClO_4^-); ESI-MS (pos.) m/z = 424.0 ($[M]^+$); Anal. for $[Cu^{I}(^{H}Pye2^{OMe–Phe})]ClO_4$. Calcd for $C_{23}H_{27}O_5N_3CuCl$: C, 52.67; H, 5.19; N 8.01. Found: C, 52.38; H, 5.23; N 7.95.

$[Cu^{I}(^{H}Pye2^{Me–Phe})]ClO_4$ ($2^{Me–Phe}$). This compound was prepared in a similar manner as for

the synthesis of **2$^{OMe–Phe}$** by treating ligand ^{H}Pye2$^{Me–Phe}$ (103.6 mg, 0.3 mmol) and $[Cu^{I}(CH_3CN)_4]ClO_4$ (96.1 mg, 0.3 mmol) in 56 % yield. All procedures were done in a glove box ($[O_2]$ < 0.1 ppm). ^{1}H-NMR (600 MHz, CD_2Cl_2) δ 2.32 (3 H, s, CH_3), 2.76 (2 H, t, J = 6.0 Hz, NCH_2CH_2Ar), 3.15 (2 H, t, J = 6.0 Hz, NCH_2CH_2Ar), 2.80–3.20 (8 H, br m, NCH_2CH_2Py and NCH_2CH_2Py), 7.08 (2 H, d, J = 7.8 Hz, H_{Ar-2} and $H_{Ar-2'}$), 7.18 (2 H, d, J = 7.8 Hz, H_{Ar-3} and $H_{Ar-3'}$), 7.32 (2 H, td, J = 7.8, and 1.1 Hz, H_{Py-5}), 7.33 (2 H, d, J = 7.8 Hz, H_{Py-3}), 7.80 (2 H, td, J = 7.8 and 1.8 Hz, H_{Py-4}), 8.10 (2 H, dt, J = 7.8 and 1.8 Hz, H_{Py-6}); ^{13}C-NMR (600 MHz, CD_2Cl_2) 21.12 (CH_3), 32.86 (NCH_2CH_2Ar), 32.98 (NCH_2CH_2Py), 54.55 (NCH_2CH_2Py), 56.38 (NCH_2CH_2Ar), 123.43 (C_{Ar-2}), 123.48 (C_{Py-5}), 126.18 (C_{Py-3}), 129.89 (C_{Ar-3}), 131.75 (C_{Ar-1}), 137.36 (C_{Ar-4}), 138.84 (C_{Py-4}), 150.10 (C_{Py-6}), 160.31 ppm (C_{Py-2}); FT-IR (KBr): 1112, 1089, and 625 cm^{-1} (ClO_4^-); ESI-MS (pos.) m/z = 407.9 ($[M]^+$); Anal. for $[Cu^{I}(^{H}Pye2^{Me–Phe})]ClO_4 \bullet 0.5H_2O$. Calcd for $C_{23}H_{28}O_{4.5}N_3CuCl$: C, 54.38; H, 5.45; N, 8.12. Found: C, 53.61; H, 5.42; N, 8.00.

$[Cu^{I}(^{H}Pye2^{H–Phe})]ClO_4$ (2$^{H–Phe}$). Synthetic procedure as well as mass and elemental analyses of this compound have been reported previously.[13] The NMR data taken by a Bruker Avance 600 spectrometer in CD_2Cl_2 are as follows. ^{1}H-NMR (600 MHz, CD_2Cl_2) δ 2.82 (2 H, t, J = 6.1 Hz, NCH_2CH_2Ph), 3.18 (2 H, t, J = 6.1 Hz, NCH_2CH_2Ph), 2.80–3.20 (8 H, br m, NCH_2CH_2Py and NCH_2CH_2Py), 7.18 (2 H, d, J = 7.5 Hz, H_{Ph-2} and $H_{Ph-2'}$), 7.30 (2 H, m, H_{Py-5}), 7.31 (1 H, t, J = 7.5 Hz, H_{Ph-4}), 7.33 (2 H, d, J = 7.8 Hz, H_{Py-3}), 7.38 (2 H, t, J = 7.5 Hz, H_{Ph-3} and $H_{Ph-3'}$), 7.79 (2 H, t, J = 7.8 and 1.8 Hz, H_{Py-4}), 8.08 (2 H, d, J = 4.1 Hz, H_{Py-6}); ^{13}C-NMR (600 MHz, CD_2Cl_2) 31.95 (NCH_2CH_2Ph), 34.03 (NCH_2CH_2Py), 54.54 (NCH_2CH_2Py), 56.02 (NCH_2CH_2Ph), 123.37 (C_{Py-3}), 123.57 (C_{Ph-2}), 127.40 (C_{Py-5}), 127.42 (C_{Ph-4}), 129.34 (C_{Ph-3}), 138.90 (C_{Py-4}), 134.71 (C_{Ph-1}), 150.23 (C_{Py-6}), 160.30 ppm (C_{Py-2}).

$[Cu^{I}(^{H}Pye2^{Cl–Phe})]ClO_4$ (2$^{Cl–Phe}$). This compound was prepared in a similar manner as for the synthesis of **2$^{OMe–Phe}$** by treating ligand ^{H}Pye2$^{Cl–Phe}$ (109.8 mg, 0.3 mmol) and $[Cu^{I}(CH_3CN)_4]ClO_4$ (96.1 mg, 0.3 mmol) in 59 % yield. All procedures were done in a glove box ($[O_2]$ < 0.1 ppm). ^{1}H-NMR (600 MHz, CD_2Cl_2) δ 2.77 (2 H, t, J = 6.2 Hz, NCH_2CH_2Ar), 2.90–3.20 (10 H, br m, NCH_2CH_2Ar, NCH_2CH_2Py, and NCH_2CH_2Py), 7.11 (2 H, d, J = 8.1 Hz, H_{Ar-2} and $H_{Ar-2'}$), 7.30 (2 H, d, J = 8.1 Hz, H_{Ar-3} and $H_{Ar-3'}$), 7.35–7.40 (4 H, m, H_{Py-3} and H_{Py-5}), 7.84 (2 H, t, J = 7.5 Hz, H_{Py-4}), 8.22 (2 H, br, H_{Py-6}); ^{13}C-NMR (600 MHz, CD_2Cl_2) 32.53 (NCH_2CH_2Ar), 34.35 (NCH_2CH_2Py), 54.68 (NCH_2CH_2Py), 56.27 (NCH_2CH_2Ar), 123.71 (C_{Py-5}), 126.31 (C_{Ar-2}), 126.37 (C_{Py-3}), 129.14 (C_{Ar-3}), 133.12 (C_{Ar-4}), 134.60 (C_{Ar-1}), 139.23 (C_{Py-4}), 150.36 (C_{Py-6}), 160.44 ppm (C_{Py-2}); FT-IR (KBr) 1121, 1089, and 625 cm^{-1} (ClO_4^-); ESI-MS (pos.) m/z = 428.0 ($[M]^+$); Anal. for $[Cu^{I}(^{H}Pye2^{Cl–Phe})]ClO_4$. Calcd for

$C_{22}H_{24}O_4N_3CuCl_2$: C, 49.96; H, 4.57; N, 7.94. Found: C, 49.92; H, 4.77; N, 7.61.

$[Cu^{I}(^{H}Pye2^{NO_2–Phe})]ClO_4$ ($2^{NO_2–Phe}$). This compound was prepared in a similar manner as for the synthesis of **$2^{OMe–Phe}$** by treating ligand $^{H}Pye2^{NO_2–Phe}$ (112.9 mg, 0.3 mmol) and $[Cu^{I}(CH_3CN)_4]ClO_4$ (96.1 mg, 0.3 mmol) in 68 % yield. All procedures were done in a glove box ($[O_2]$ < 0.1 ppm). ^{1}H-NMR (600 MHz, CD_2Cl_2) δ 2.86 (2 H, t, J = 7.0 Hz, NCH_2CH_2Ar), 3.05–3.15 (8 H, br, NCH_2CH_2Py), 3.07 (2 H, t, J = 7.0 Hz, NCH_2CH_2Ar), 7.33 (2 H, d, J = 8.6 Hz, H_{Ar-2} and $H_{Ar-2'}$), 7.38 (2 H, ddd, J = 7.8, 5.4, and 1.2 Hz, H_{Py-5}), 7.41 (2 H, d, J = 7.8 Hz, H_{Py-3}), 7.87 (2 H, td, J = 7.8 and 1.8 Hz, H_{Py-4}), 8.11 (2 H, d, J = 8.6 Hz, H_{Ar-3} and $H_{Ar-3'}$), 8.37 (2 H, ddd, J = 5.4, 1.8, and 0.8 Hz, H_{Py-6}); ^{13}C-NMR (600 MHz, CD_2Cl_2) 32.88 (NCH_2CH_2Ar), 34.83 (NCH_2CH_2Py), 55.04 (NCH_2CH_2Py), 56.83 (NCH_2CH_2Ar), 123.86 (C_{Py-5}), 123.91 (C_{Ar-3}), 126.35 (C_{Py-3}), 127.12 (C_{Ar-2}), 139.53 (C_{Py-4}), 144.49 (C_{Ar-4}), 147.18 (C_{Ar-1}), 150.63 (C_{Py-6}), 160.58 ppm (C_{Py-2}); FT-IR (KBr) 1514 and 1345 (–NO_2) 1113, 1089, and 625 cm^{-1} (ClO_4^-); ESI-MS (pos.) m/z = 439.0 ($[M]^+$); Anal. for $[Cu^{I}(^{H}Pye2^{NO_2–Phe})]ClO_4$•0.5$H_2O$. Calcd for $C_{22}H_{25}O_{6.5}N_4CuCl$: C, 48.18; H, 4.59; N, 10.22. Found: C, 48.41; H, 4.50; N, 10.07.

$[Cu^{I}(^{H}Pye2^{Phe–Me})]ClO_4$ ($2^{Phe–Me}$). This compound was prepared in a similar manner described above using ligand $^{H}Pye2^{Phe–Me}$ (172.7 mg, 0.5 mmol) and $[Cu^{I}(CH_3CN)_4]ClO_4$ (160.1 mg, 0.5 mmol) in 52 % yield. All procedures were done in a glove box ($[O_2]$ < 0.1 ppm). ^{1}H-NMR (600 MHz, CD_2Cl_2) δ 1.20 (3 H, d, J = 6.9 Hz, $NCH_2CH(CH_3)Ph$), 2.63 (1 H, dd, J = 12.9 and 4.2 Hz, $NCH_2CH(CH_3)Ph$), 2.75 (1 H, br, NCH_2CH_2Py), 2.80 (1 H, br, NCH_2CH_2Py), 2.85 (1 H, br, NCH_2CH_2Py), 2.93 (1 H, br, NCH_2CH_2Py), 2.95 (1 H, br, NCH_2CH_2Py), 2.98 (1 H, m, $NCH_2CH(CH_3)Ph$), 3.13 (1 H, br t, J = 12.0 Hz, NCH_2CH_2Py), 3.23 (1 H, br t, J = 14.6 Hz, NCH_2CH_2Py), 3.30 (1 H, br t, J = 11.7 Hz, NCH_2CH_2Py), 3.44 (1 H, t, J = 12.9 Hz, $NCH_2CH(CH_3)Ph$), 7.18 (2 H, d, J = 7.6 Hz, H_{Ph-2} and $H_{Ph-2'}$), 7.21 (1 H, br, H_{Py-5}), 7.31 (1 H, br, H_{Py-3}), 7.33 (1 H, t, J = 7.6 Hz, H_{Ph-4}), 7.36 (1 H, br, H_{Py-5}), 7.37 (1 H, br, H_{Py-3}), 7.39 (2 H, t, J = 7.6 Hz, H_{Ph-3} and $H_{Ph-3'}$), 7.76 (1 H, br, H_{Py-4}), 7.80 (1 H, br, H_{Py-4}), 7.94 (1 H, br, H_{Py-6}), 8.04 (1 H, br, H_{Py-6}); ^{13}C-NMR (600 MHz, CD_2Cl_2) 20.93 ($NCH_2CH(CH_3)Ph$), 33.63 (NCH_2CH_2Py), 33.98 (NCH_2CH_2Py), 38.96 ($NCH_2CH(CH_3)Ph$), 55.33 (NCH_2CH_2Py), 62.45 ($NCH_2CH(CH_3)Ph$), 121.24 (C_{Ph-2}), 123.37 (C_{Py-5}), 123.66 ($C_{Py-5'}$), 126.04 (C_{Py-3}), 126.25 ($C_{Py-3'}$), 127.61 (C_{Ph-4}), 129.45 (C_{Ph-3}), 138.81 (C_{Ph-1}), 138.96 (C_{Py-4}), 149.87 (C_{Py-6}), 150.28 ($C_{Py-6'}$), 160.27 ppm (C_{Py-2}); FT-IR (KBr): 1121, 1089, and 625 cm^{-1} (ClO_4^-); FAB-MS (pos.), m/z = 408.28 ($[M]^+$); Anal. for $[Cu^{I}(^{H}Pye2^{Phe–Me})]ClO_4$. Calcd for $C_{23}H_{27}O_4N_3CuCl$: C, 54.33; H, 5.35; N, 8.26. Found: C, 54.24; H, 5.30; N, 8.27.

$[Cu^{I}(^{H}Pye2^{Phe–Ph})]ClO_4$ ($2^{Phe–Ph}$). This compound was prepared in a similar manner as for

the synthesis of **2**$^{\mathbf{OMe–Phe}}$ by treating ligand ^{H}Pye2$^{Phe–Ph}$ (203.8 mg, 0.5 mmol) and [Cu^{I}(CH$_3$CN)$_4$]ClO$_4$ (160.1 mg, 0.5 mmol) in 67 % yield. All procedures were done in a glove box ([O$_2$] < 0.1 ppm). ^{1}H-NMR (600 MHz, CD$_2$Cl$_2$) δ 2.90 (2 H, br, NC*H*$_2$CH$_2$Py), 3.08 (2 H, br, NCH$_2$C*H*$_2$Py), 3.15 (4 H, br, NCH$_2$C*H*$_2$Py and NC*H*$_2$CH$_2$Py), 3.38 (2 H, d, J = 8.6 Hz, NC*H*$_2$CHPh$_2$), 4.20 (1 H, t, J = 8.6 Hz, NCH$_2$C*H*Ph$_2$), 7.23 (2 H, br, H$_{Ph-4}$), 7.29 (2 H, m, H$_{Py-5}$), 7.32 (4 H, m, H$_{Ph-2}$ and H$_{Ph-2'}$), 7.35 (4 H, br, H$_{Ph-3}$ and H$_{Ph-3'}$), 7.37 (2 H, m, H$_{Py-3}$), 7.81 (2 H, td, J = 7.8 and 1.8 Hz, H$_{Py-4}$), 7.95 (2 H, ddd, J = 5.3, 0.9, and 0.6 Hz, H$_{Py-6}$); ^{13}C-NMR (600 MHz, CD$_2$Cl$_2$) 33.80 (NCH$_2$*C*H$_2$Py), 49.41 (NCH$_2$*C*HPh$_2$), 54.79 (N*C*H$_2$CH$_2$Py), 60.44 (N*C*H$_2$CHPh$_2$), 123.64 (C$_{Py-5}$), 124.71 (C$_{Ph-2}$), 126.30 (C$_{Py-3}$), 127.79 (C$_{Ph-4}$), 129.53 (C$_{Ph-3}$), 138.27 (C$_{Ph-1}$), 138.98 (C$_{Py-4}$), 150.13 (C$_{Py-6}$), 160.27 ppm (C$_{Py-2}$); FT-IR (KBr) 1115, 1089, and 625 cm^{-1} (ClO$_4^-$); FAB-MS (pos.) m/z = 470.1 ([M]$^+$); Anal. for [Cu^{I}(^{H}Pye2$^{Phe–Ph}$)]ClO$_4$. Calcd for C$_{28}$H$_{29}$O$_4$N$_3$CuCl: C, 58.94; H, 5.12; N, 7.36. Found: C, 58.68; H, 5.04; N, 7.29.

[Cu^{I}(^{Me}Pym2^{Phe})]ClO$_4$ (3^{Phe}). Ligand ^{Me}Pym2^{Phe} (99.4 mg, 0.3 mmol) was treated with [Cu^{I}(CH$_3$CN)$_4$]ClO$_4$ (96.1 mg, 0.3 mmol) in CH$_2$Cl$_2$ (5 mL) under Ar atmosphere (in a glove box). After stirring for 30 min at room temperature, insoluble materials were removed by filtration. Addition of ether (100 mL) to the filtrate gave a white powder that was precipitated by standing the mixture for several minutes. The supernatant was then removed by decantation, and the remained pale brown solid was washed with ether three times, and dried. Yield: 114 mg (77 %). All procedures were done in a glove box (DBO-1KP, Miwa Co. Ltd.) ([O$_2$] < 0.1 ppm). ^{1}H-NMR (600 MHz, CD$_2$Cl$_2$) δ 2.56 (6 H, s, -CH$_3$), 2.83 (2 H, t, J = 6.2 Hz, -NCH$_2$C*H*$_2$Ph), 3.13 (2 H, d, J = 6.2 Hz, -NC*H*$_2$CH$_2$Ph), 3.88 (2 H, d, J = 16.0 Hz, -NC*H*HPy), 4.20 (2 H, d, J = 16.0 Hz, -NCH*H*Py), 6.95 (2 H, d, J = 7.3 Hz, H$_{Ph–2}$ and H$_{Ph–6}$), 7.24 (2 H, d, J = 7.7 Hz, H$_{Py-3}$), 7.28 (2 H, d, J = 7.7 Hz, H$_{Py-5}$), 7.33 (2 H, t, J = 7.3 Hz, H$_{Ph–3}$ and H$_{Ph–5}$), 7.43 (1 H, t, J = 7.3 Hz, H$_{Ph–4}$), 7.75 (2 H, t, J = 7.7 Hz, H$_{Py-4}$); ^{13}C-NMR (600 Hz, CD$_2$Cl$_2$) 27.36 (-Me), 33.94 (-NCH$_2$*C*H$_2$Ph), 56.27 (-N*C*H$_2$CH$_2$Ph), 59.70 (-N*C*H$_2$Py), 121.80 (C$_{Py-3}$), 122.61 (C$_{Ph-2}$ and C$_{Ph-6}$), 124.59 (C$_{Py-5}$), 127.80 (C$_{Ph-3}$ and C$_{Ph-5}$), 128.29 (C$_{Ph-4}$), 138.12 (C$_{Ph-1}$), 139.27 (C$_{Py-4}$), 157.26 (C$_{Py-2}$), 157.94 ppm (C$_{Py-6}$); FT-IR (KBr) 1109, 1090 and 625 cm^{-1} (ClO$_4^-$); ESI-MS (pos.) m/z = 394.4 ([M]$^+$); Anal. Calcd for C$_{22}$H$_{26}$O$_{4.5}$N$_3$CuCl: C, 52.48; H, 5.21; N, 8.35. Found: C, 52.85; H, 5.05; N, 8.46.

[Cu^{I}(^{Me}Pym2$^{Phe–Ph}$)]ClO$_4$ (3$^{Phe–Ph}$). This compound was prepared in a manner similar to the synthesis of complex **3**$^{\mathbf{Phe}}$ using ligand ^{Me}Pym2$^{Phe–Ph}$ (103.6 mg, 0.3 mmol) instead of ^{Me}Pym2^{Phe}. Yield 139 mg (81 %). ^{1}H-NMR (600 Hz, CD$_2$Cl$_2$) δ 2.58 (6 H, s, -CH$_3$), 3.46 (2 H, dd, J = 8.5 Hz, -NC*H*$_2$CHPh$_2$), 4.05 (2 H, d, J = 16.2 Hz, -NC*H*HPy), 4.14 (1 H, t, J = 8.5 Hz,

-NCH_2CHPh_2), 4.36 (2 H, d, J = 16.2 Hz, -NCH*H*Py), 7.00 (4 H, dd, J = 6.3 and 1.1 Hz, $H_{Ph\text{-}2}$ and $H_{Ph\text{-}6}$), 7.26–7.34 (10 H, m, $H_{Ph\text{-}3}$, $H_{Ph\text{-}4}$, $H_{Ph\text{-}5}$, $H_{Py\text{-}3}$ and $H_{Py\text{-}5}$), 7.81 (t, J = 7.7 Hz, $H_{Py\text{-}4}$); ^{13}C-NMR (600 Hz, CD_2Cl_2) 27.61 (-Me), 49.87 (-NCH_2CHPh_2), 60.95 (-NCH_2CHPh_2), 61.20 (-NCH_2Py), 121.85 ($C_{Py\text{-}5}$), 124.73 ($C_{Py\text{-}3}$), 125.50 ($C_{Ph\text{-}2}$ and $C_{Ph\text{-}6}$), 128.49 ($C_{Ph\text{-}4}$), 128.64 ($C_{Ph\text{-}3}$ and $C_{Ph\text{-}5}$), 139.57 ($C_{Py\text{-}4}$), 140.81 ($C_{Ph\text{-}1}$), 157.77 ($C_{Py\text{-}2}$) 158.01 ppm ($C_{Py\text{-}6}$); FT-IR (KBr) 1097 and 623 cm^{-1} (ClO_4^-); ESI-MS (pos.) m/z = 470.3 ([M]$^+$); Anal. Calcd for $C_{28}H_{30}O_{4.5}N_3CuCl$: C, 58.03; H, 5.22; N, 7.25. Found: C, 58.30; H, 5.09; N, 7.46.

[Cu^{I}(^{Me}Pym2^{Bn})(CH$_3$CN)]PF$_6$ (3^{Bn}•MeCN). Treatment of ligand ^{Me}Pym2^{Bn} (0.314 g, 0.99 mmol) and [Cu^{I}(CH$_3$CN)$_4$](ClO$_4$) (0.327 g, 1.00 mmol) in ethanol (20 mL) under anaerobic conditions (in a Schlenk flask) gave a yellow solution, to which an aqueous solution (10 mL) of NH_4PF_6 (0.489 g, 3.00 mmol) was added. The precipitated pale yellow materials were dissolved into the solution again by heating, and the solution was kept standing at room temperature to give yellow crystals. Yield: 0.413 g (72.8 %). ^{1}H-NMR (400 MHz, acetone-d_6) δ 2.40 (3 H, s, CH_3CN), 2.81 (6 H, s, -CH_3), 3.81 (2 H, d (br), J = 14.9 Hz, -NC*H*HPy), 4.03 (2 H, s, -CH_2Ph), 4.14 (2 H, d (br), J = 14.9 Hz, -NCH*H*Py), 7.27–7.36 (5 H, m, H_{Ph} and $H_{Py\text{-}3}$), 7.40 (2 H, d, J = 7.8 Hz, H_{Ph}), 7.48 (2 H, m, $H_{Py\text{-}5}$), 7.81 (2H, t, J = 7.7 Hz, $H_{Py\text{-}4}$); FT-IR (KBr) 1603 (C=C, aromatic), 1578, 839 and 557 cm^{-1} (PF_6^-); Anal. Calcd for $C_{23}H_{26}N_4CuPF_6$: C, 48.72; H, 4.62; N, 9.88. Found: C, 48.62; H, 4.64; N, 9.89. [Cu^{I}(^{Me}Pym2^{Bn})(CH$_3$CN)]ClO$_4$ was prepared similarly but without the salt exchange reaction with NH_4PF_6. Yield: 82 %. FT-IR (KBr) 1603 (C=C, aromatic), 1576, 1086, 794 and 623 cm^{-1} (ClO_4^-); FAB-MS (pos.) m/z = 380 ([M]$^+$); Anal. Calcd for $C_{23}H_{26}N_4O_4CuCl$: C, 52.97; H, 5.03; N, 10.74. Found: C, 52.64; H, 4.99; N, 10.77.

[Cu^{I}(^{Me}Pym2^{Bn})(CO)]PF$_6$ (3^{Bn}•CO). Treatment of [Cu^{I}(^{Me}Pym2^{Bn})(CH$_3$CN)]PF$_6$ (1.14 g, 2.01 mmol) in ethanol (4 mL) under CO atmosphere over night gave white powder which was collected by filtration. Yield: 1.04 g (93.0 %). ^{1}H-NMR (400 MHz, acetone-d_6): δ 2.85 (6 H, s, -CH_3), 3.99 (2 H, d, J = 15.9 Hz, -C*H*HPy), 4.31 (2 H, s, -CH_2Ph), 4.47 (2 H, d, J = 15.9 Hz, -CH*H*Py), 7.31 ~ 7.40 (5 H, m, H_{Ph} and $H_{Py\text{-}3}$), 7.49 (2 H, d, J = 7.8 Hz, H_{Ph}), 7.54 (2 H, m, $H_{Py\text{-}5}$), 7.90 (2 H, t, J = 7.7 Hz, $H_{Py\text{-}4}$); FT-IR (KBr) 2088 and 2100 (C≡O), 1606 (C=C, aromatic), 1578, 841 and 557 cm^{-1} (PF_6^-); Anal. Calcd for $C_{22}H_{23}N_3OCuPF_6$: C, 47.70; H, 4.19; N, 7.59. Found: C, 47.75; H, 4.16; N, 7.60. Single crystals of the copper(I) complex with ClO_4^- counter anion, [Cu^{I}(^{Me}Pym2^{Bn})(CO)]ClO$_4$, was obtained by the same treatment of [Cu^{I}(^{Me}Pym2^{Bn})(CH$_3$CN)]ClO$_4$ with CO in a 81 % yield. FT-IR (KBr) 2096 and 2085 (CO), 1606 (C=C, aromatic), 1578, 1091, 791 and 623 cm^{-1} (ClO_4^-). Anal. Calcd for

$C_{22}H_{23}N_3O_5CuCl$: C, 51.97; H, 4.56; N, 8.26. Found: C, 51.73; H, 4.52; N, 8.43.

$[Cu^{I}(^{Me}Pym2^{Bn})]PF_6$ (3^{Bn}). This complex was prepared by removing CO from $[Cu^{I}(^{Me}Pym2^{Bn})(CO)]PF_6$. Thus, a methanol solution of the CO-complex was heated on hot water bath (75 °C) for 10 min, and then the solvent was removed under reduced pressure to give yellow powder of $\mathbf{3^{Bn}}$. ^{1}H-NMR (400 MHz, acetone-d_6) δ 2.83 (6 H, s, -CH_3), 3.97 (2 H, s, -CH_2Ph), 3.8–4.3 (4 H, br s, -CH_2Py), 7.25–7.37 (7 H, m, H_{Ph} and $H_{Py\text{-}3}$), 7.45 (2 H, d, J = 7.7 Hz, $H_{Py\text{-}5}$), 7.86 (2 H, t, J = 7.7 Hz, $H_{Py\text{-}4}$); FT-IR (KBr) 1610 (C=C, aromatic), 1577, 849 and 557 cm^{-1} (PF_6^-); EI-MS (in CH_2Cl_2) m/z = 380.1 ([M]$^+$). Satisfactory result of elemental analysis could not be obtained due to instability of the complex.

$[Cu^{I}(^{H}Pym2^{Phe})]ClO_4$ (4^{Phe}). Ligand $^{H}Pym2^{Phe}$ (91.0 mg, 0.3 mmol) was treated with $[Cu^{I}(CH_3CN)_4]ClO_4$ (96.0 mg, 0.3 mmol) in acetone (5 mL) under Ar atmosphere in a glovebox. After stirring for 5 min at room temperature, insoluble material was removed by filtration. Addition of ether (100 mL) to the filtrate gave a pale brown powder that was precipitated by standing the mixture for several minutes. The supernatant was then removed by decantation, and the remained pale brown solid was washed with ether three times and dried to give complex **1** in 90 %. A single crystals suitable for X-ray analysis were obtained by vapor diffusion of ether into an acetone solution of $\mathbf{4^{Phe}}$; FT-IR (KBr) 1107, 1090, and 625 cm^{-1} (ClO_4^-); ESI-MS (pos.) m/z = 366.3 ([M]$^+$); Anal. Calcd for $C_{20}H_{21}O_4N_3CuCl$: C, 51.51; H, 4.54; N, 9.01. Found: C, 51.29; H, 4.49; N, 8.94.

Caution! The perchlorate salts in this study are all potentially explosive and should be handled with care.

X–ray Structure Determination. The single crystal was mounted on a CryoLoop (Hamptom Research Co.) or a glass-fiber. Data of X–ray diffraction were collected by a Rigaku RAXIS–RAPID imaging plate two–dimensional area detector using a graphite–monochromated Mo$K\alpha$ radiation (λ = 0.71070 Å) to 2θ max of 55.0 ° or a Cu$K\alpha$ radiation (λ = 1.54186 Å) to 2θ max of 136.6 °. All the crystallographic calculations except for $\mathbf{2^{H–Phe}}$, $\mathbf{3^{Bn}}$**•MeCN**, and $\mathbf{3^{Bn}}$**•CO** were performed by using Crystal Structure software package of the Rigaku Corporation and Molecular Structure Corporation [Crystal Structure: Crystal Structure Analysis Package version 2.0, Rigaku Corp. and Molecular Structure Corp. (2001)].

The crystallographic calculation of $\mathbf{2^{H–Phe}}$ was performed by using the teXsan crystallographic software package of Molecular Structure Corporation (1999). The crystal structures except for $[Cu^{I}(^{H}Pye2^{H–Phe})]ClO_4$ were solved by the direct methods and refined by the full–matrix least squares using SIR-92. All non–hydrogen atoms and hydrogen atoms were

refined anisotropically and isotropically, respectively. In the case of $\mathbf{2}^{\mathbf{H-Phe}}$, the crystal structure was solved by the direct methods and refined by the full–matrix least squares using SHELX-97. All non–hydrogen atoms of $\mathbf{2}^{\mathbf{H-Phe}}$ were refined anisotropically, but the hydrogen atoms were not refined.

Data collection of copper(I) complexes $\mathbf{3}^{\mathbf{Bn}}$**•MeCN** and $\mathbf{3}^{\mathbf{Bn}}$**•CO** were carried out on a Rigaku *R*-axis IV imaging plate area detector with graphite monochromated Mo$K\alpha$ radiation (λ = 0.71070 Å). A single crystal was mounted on the tip of a glass rod. The structures were solved by a direct method (SHELX-86 for $\mathbf{3}^{\mathbf{Bn}}$**•MeCN** and SIR92 for $\mathbf{3}^{\mathbf{Bn}}$**•CO**) and expanded using a Fourier technique. The structures were refined by a full-matrix least-squares method by using teXsan crystallographic software package (Molecular Structure Corporation). Non-hydrogen atoms were refined with anisotropic displacement parameters. Hydrogen atoms were positioned at calculated positions (0.95 Å). They were included, but not refined, in the final least-squares cycles.

Kinetic Measurements. The oxygenation reactions of the copper(I) complexes except for $\mathbf{4}^{\mathbf{Phe}}$ were carried out in a 1 mm or a 1 cm path length UV-vis cell that was held in a Unisoku thermostated cell holder USP-203 (a desired temperature can be fixed within ± 0.5 °C). After the deaerated solution of the copper(I) complex in the cell was kept at a desired temperature for several minutes, dry dioxygen gas was continuously supplied by gentle bubbling from a thin needle. Formation of the dicopper-dioxgen complex was monitored by following an increase in the characteristic absorption of the dicopper-dioxgen complex. The reactions obeyed second-order kinetics and the second-order rate constants (k_{obs}) were obtained as the slopes of linear lines of the second-order plots, $(A - A_0)/\{(A_\infty - A)[\mathrm{Cu}]_0\}$ *vs*. time, where A_0 and A_∞ are the initial and final absorption and $[\mathrm{Cu}]_0$ is the initial concentration of copper(I) complexes.

The oxygenation reaction of copper(I) complex $\mathbf{4}^{\mathbf{Phe}}$ were performed using a multi-scan stopped-flow spectrophotometer (RSP-1000, Unisoku Co., Ltd.) in acetone at –94 °C. Decomposition process of the oxygenated intermediate was followed separately by using a Hewlett Packard 8453 photo diode array spectrophotometer with a Unisoku thermostated cell holder designed for low temperature measurements (USP-203, a desired temperature can be fixed within ± 0.5 °C).

Product Analysis.

Degradation of Copper(I) Complex $\mathbf{4}^{\mathbf{Phe}}$ in $\mathbf{CH_2Cl_2}$. Ligand $^{H}\mathrm{Pym2}^{Phe}$ (91.0 mg, 0.3 mmol) was treated with $[\mathrm{Cu^I(CH_3CN)_4}]\mathrm{ClO_4}$ (96.0 mg, 0.3 mmol) in $\mathrm{CH_2Cl_2}$ (5 mL) under

anaerobic conditions (Ar), and the mixture was stirred for 3 days at room temperature in a glovebox. In the course of the reaction, the color of solution gradually changed from pale yellow to dark blue, and insoluble materials gradually precipitated. After removing the insoluble material by filtration, addition of ether (100 mL) to the filtrate gave a blue powder material that was precipitated by standing the mixture for several minutes. The supernatant was then removed by decantation, and the remained blue solid was washed with ether three times and dried under air to give $[Cu^{II}(^{H}Pym2^{Phe})(Cl)]ClO_4$ (**5**^{Phe}) in 88 %. A single crystal of **5**^{Phe} suitable for X-ray analysis was obtained by vapor diffusion of ether into an acetonitrile solution of the complex; FT-IR (KBr) 1092, and 621 cm^{-1} (ClO_4^-); FAB-MS (pos.) m/z = 401.1 ($[M]^+$); Anal. Calcd for $C_{20}H_{21}O_4N_3CuCl_2$: C, 47.87; H, 4.22; N, 8.37. Found: C, 47.86; H, 4.16; N, 8.30.

Ligand Hydroxylation of Copper(I) Complex 4^{Phe} with O_2. $[Cu^{I}(^{H}Pym2^{Phe})]ClO_4$ (18.6 mg, 0.04 mmol) was dissolved into deaerated CH_2Cl_2 (5 mL) under anaerobic conditions, and the solution was then exposed to O_2 gas and stirred for 2 h at –80 ˚C. A mixture of organic materials was obtained after an ordinary work-up treatment of the reaction mixture with an NH_4OH aq and following extraction by CH_2Cl_2. Yield of the hydroxylation product was determined as 18 % based on the copper(I) starting material by using an integral ratio in the ^{1}H-NMR spectrum between the methine proton (-C*H*OH-) at δ 4.82 of the hydroxylation product and the pyridine protons at the 6-position ($Py_{H\text{-}6}$, δ 8.56) both from $^{H}Pym2^{Phe}$-OH and $^{H}Pym2^{Phe}$. ($Py_{H\text{-}6}$ of $^{H}Pym2^{Phe}$-OH and $^{H}Pym2^{Phe}$ are overlapped); (-C*H*OH-) : ($Py_{H\text{-}6}$) = 0.18 : 2.00. The hydroxylated product $^{H}Pym2^{Phe}$-OH was isolated by an alumina column chromatographic treatment on the mixture of organic material (eluent: hexane–Et_2O); ^{1}H-NMR (300 Hz, $CDCl_3$) δ 2.79 (1H, dd, J = 13.5 and 10.0 Hz, NC*H*$_2$CH(OH)Ph), 2.98 (1H, dd, J = 13.5 and 2.7 Hz, NC*H*$_2$CH(OH)Ph), 3.95 (2H, d, J = 15.0 Hz, 2 x NCH*H*Py), 4.09 (2H, d, J = 15.0 Hz, 2 x NC*H*HPy), 4.82 (1H, dd, J = 10.0 and 2.7 Hz, NCH$_2$C*H*(OH)Ph), 7.15–7.35 (9H, m, Ph, $Py_{H\text{-}3}$, and $Py_{H\text{-}5}$), 7.61 (2H, td, J = 7.7 and 1.8 Hz, $Py_{H\text{-}4}$), 8.58 (2 H, ddd, J = 4.8, 1.8 and 0.9 Hz, $Py_{H\text{-}6}$); ESI–MS (pos.) m/z = 320.3 ($[M + 1]^+$).

Manometory. The O_2-uptake measurement was carried out on the reaction of $[Cu^{I}(^{H}Pym2^{Phe})]ClO_4$ (20.9 mg. 0.05 mmol) in CH_2Cl_2 (5 mL) at –80 ˚C. The volume of O_2 consumed during the oxygenation reaction of the copper(I) complex was determined to be 0.7 mL as a difference of the O_2 consumption between Cu/O_2 intermediate formation and blank solution without the reactants under exactly the same conditions using a manometer designed for the small-scale reaction. Thus, the stoichiometry of Cu : O_2 was calculated to be 2:1 (±

0.03).

Theoretical Calculations. Density functional calculations were performed on a COMPAQ DS20E computer using the Amsterdam Density Functional (ADF) program version 1999.02 developed by Baerends *et al*.[28,29] The electronic configurations of the molecular systems were described by an uncontracted triple-ζ Slater-type orbital basis set (ADF basis set V) with a single polarization function used for each atom. Core orbitals were frozen through 1s (C, O, N), 2p (Cl), and 3p (Cu). The calculations were performed using the local exchange-correlation potential by Vosko *et al*.[30] and the nonlocal gradient corrections by Becke[31] and Perdew[32,33] during the geometry optimizations. First-order scalar relativistic correlations were added to the total energy. Final geometries and energetics were optimized by using the algorithm of Versluis and Ziegler[34] provided in the ADF package and were considered converged when the changes in bond lengths between subsequent iterations fell below 0.01 Å.

Visible Resonance Raman Measurements. The 514.5 nm line of an Ar^+ laser (Model GLG3200, NEC) was used as the exciting source. Visible resonance Raman scattering was detected with a liquid nitrogen cooled CCD detector (Model LN/CCD-1340 x 400PB, Princeton Instruments) attached to a 1 m single polychromator (Model MC-100DG, Ritsu Oyo Kogaku). The slit width and slit height were set to be 150 μm and 20 mm, respectively. The spectral slit width is 5.7 cm^{-1}. A wavenumber per one channel is 0.69 cm^{-1}. The laser power used was 10 mW at the sample point. All measurements were carried out with a spinning cell (1000 rpm) at –80 ~ –100 ˚C. Raman shifts were calibrated with indene and acetone, and accuracy of the peak positions of the Raman lines was ±1 cm^{-1}.

Results and Discussion

In this chapter, the copper(I) complexes are numbered as follows: $\mathbf{1^R}$ for the $^{Me}Pye2^R$-complexes, $\mathbf{2^R}$ for the $^{H}Pye2^R$-complexes, $\mathbf{3^R}$ for the $^{Me}Pym2^R$-complexes and $\mathbf{4^R}$ for the $^{H}Pym2^R$-complexes. This order is related to the order of the electron-donor ability of pyridine nitrogen; $^{Me}Pye2^R$ < $^{H}Pye2^R$ < $^{Me}Pym2^R$ < $^{H}Pym2^R$. However, the results and discussions are presented in the order of $\mathbf{2^R \rightarrow 1^R \rightarrow 4^R \rightarrow 3^R}$ for reasons of convenience.

1. Copper(I) Complexes 2^R of Bis[2-(2-pyridyl)ethyl]amine Tridentate Ligands ($^{H}Pye2^R$).

Synthesis of Ligands and Copper(I) Complexes. Ligands $^{H}Pye2^{R}$ (Chart 3) were prepared by Michael addition of 2-phenylethylamine derivatives to 2-vinylpyridine in refluxing methanol under acidic conditions. The copper(I) complexes ($\mathbf{2^{R}}$) were obtained by treating the ligand with an equimolar amount of $[Cu^{I}(CH_3CN)_4](ClO_4)$ in CH_2Cl_2 under anaerobic conditions (in a glove box).

Chart 3

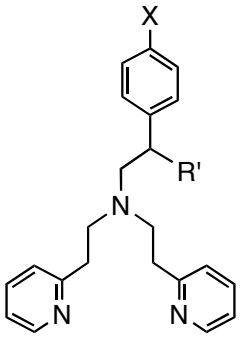

Ligand	R'	X
$^{H}Pye2^{H–Phe}$	H	H
$^{H}Pye2^{OMe–Phe}$	H	OMe
$^{H}Pye2^{Me–Phe}$	H	Me
$^{H}Pye2^{Cl–Phe}$	H	Cl
$^{H}Pye2^{NO_2–Phe}$	H	NO_2
$^{H}Pye2^{Phe–Me}$	Me	H
$^{H}Pye2^{Phe–Ph}$	Ph	H

Structural Characterization of $\mathbf{2^{R}}$. Crystal structures of $[Cu^{I}(^{H}Pye2^{X–Phe})]ClO_4$ ($\mathbf{2^{X–Phe}}$, X = H, Me, OMe, Cl, and NO_2), $[Cu^{I}(^{H}Pye2^{Phe–Me})]ClO_4$ ($\mathbf{2^{Phe–Me}}$), and $[Cu^{I}(^{H}Pye2^{Phe–Ph})ClO_4$ ($\mathbf{2^{Phe–Ph}}$) have been determined as shown in Figure 1. The crystallographic data of $\mathbf{2^{X–Phe}}$, $\mathbf{2^{Phe–Me}}$, and $\mathbf{2^{Phe–Ph}}$ are presented in Table 1, and their selected bond lengths around the copper ion are summarized in Table 2. It is noteworthy that there are ten crystallographically independent molecules in the unit cell of $\mathbf{2^{H–Phe}}$, making it as an unusually long rectangular parallelepiped structure (a = 15.695(2) Å, b = 78.34(1) Å, c = 17.389(4) Å), while other complexes consist of normal unit cell involving one or two crystallographically independent molecules (Table 1).

All the cuprous complexes exhibit a similar type of copper(I)-arene interaction in crystals, where the phenyl ring of the ligand sidearm is positioned just above the cuprous ion to make a coordinative interaction in a η^2-fashion (see Figure 1). Thus, the cuprous ion in each complex adapts to a distorted tetrahedral geometry consisted of the three nitrogen atoms (one N_{Am} and two N_{Py}) and the C_1–C_2 moiety of the ligand sidearm. The η^2-bonding interaction is, however, significantly unsymmetrical, and the Cu–C_1 bond lengths are always longer than that of Cu–C_2 (Table 2).[35-41,42] Apparently, the Cu–C distances in the copper(I)-arene interaction largely alter depending on the *p*-substituents (X) of the ligands, although the Cu–N distances are rather constant in the series ($d_{Cu–N(Am)}$ = 2.115 ± 0.024 Å; $d_{Cu–N(py)}$ = 1.990 ± 0.023 Å) (Table 2). Namely, the Cu–C_2 bond lengths of $\mathbf{2^{H–Phe}}$, $\mathbf{2^{Me–Phe}}$, $\mathbf{2^{OMe–Phe}}$, $\mathbf{2^{Phe–Me}}$, and $\mathbf{2^{Phe–Ph}}$ (2.172 ~

2.211 Å) are shorter than those of $\mathbf{2}^{\mathbf{Cl–Phe}}$ and $\mathbf{2}^{\mathbf{NO_2–Phe}}$ (2.476 and 2.388 Å), while the Cu–C_1 distances in $\mathbf{2}^{\mathbf{OMe–Phe}}$, $\mathbf{2}^{\mathbf{Cl–Phe}}$, and $\mathbf{2}^{\mathbf{NO_2–Phe}}$ (2.514 ~ 2.656 Å) are elongated as compared to those of $\mathbf{2}^{\mathbf{H–Phe}}$, $\mathbf{2}^{\mathbf{Me–Phe}}$, $\mathbf{2}^{\mathbf{Phe–Me}}$, and $\mathbf{2}^{\mathbf{Phe–Ph}}$ (2.309 ~ 2.359 Å). Thus, the difference in bond length between Cu–C_1 and Cu–C_2 becomes significantly large in $\mathbf{2}^{\mathbf{OMe–Phe}}$ as compared to that of the others. Crystal packing forces may be a factor influencing the Cu–C bond lengths in the crystal. However, such an effect is relatively small, if any, since the differences in Cu–C_1 and Cu–C_2 bond lengths among the ten crystallographically independent molecules of $\mathbf{2}^{\mathbf{H–Phe}}$ in the unit cell are relatively small (Cu–C_1 = 2.326 ± 0.069 Å, Cu–C_2 = 2.213 ± 0.035 Å). Thus, it can be concluded that the differences in the Cu–C bond lengths are mainly attributable to the difference in strength of the copper(I)-arene interaction. This issue is further examined in the following experiments.

C–C bond lengths of the phenyl rings of the copper(I)-arene complexes are listed in Table 3 where the corresponding values of another phenyl group without the copper(I)-arene interaction in $\mathbf{2}^{\mathbf{Phe–Ph}}$ are also included. Overall, the copper(I)-arene interaction causes little effect on the structure of the aromatic ring of the complexes.

The features of the copper(I)-arene interaction found in the crystal structures are well reproduced by the optimized structures obtained by the DFT calculations (see Experimental Section).[43] Figure 2 shows the calculated structures of copper(I)-arene complexes together with the Cu–C_1 and Cu–C_2 bond lengths. The calculated Cu–C_2 bond lengths are always shorter than those of Cu–C_1, and the average Cu–C lengths [$1/2(d_{Cu–C1} + d_{Cu–C2})$] of $\mathbf{2}^{\mathbf{H–Phe}}$ and $\mathbf{2}^{\mathbf{Me–Phe}}$ are shorter than those of $\mathbf{2}^{\mathbf{OMe–Phe}}$, $\mathbf{2}^{\mathbf{Cl–Phe}}$, and $\mathbf{2}^{\mathbf{NO_2–Phe}}$ as observed in the crystal structures in Figure 1. The larger difference in bond length between Cu–C_1 and Cu–C_2 in $\mathbf{2}^{\mathbf{OMe–Phe}}$ is also reproduced by the DFT calculation, though the calculated Cu–C_2 bond lengths of $\mathbf{2}^{\mathbf{Cl–Phe}}$ and $\mathbf{2}^{\mathbf{NO_2–Phe}}$ are relatively shorter than those in the crystal structures (Table 2). The interaction between the d_{z^2} orbital of Cu^I and the π orbital of the benzene ring is clearly seen at the HOMO-5 level of $\mathbf{2}^{\mathbf{H–Phe}}$ and $\mathbf{2}^{\mathbf{Me–Phe}}$ as shown in Figure 3, where the Cu-C_2 interaction is much more apparent as compared with the Cu–C_1 interaction.

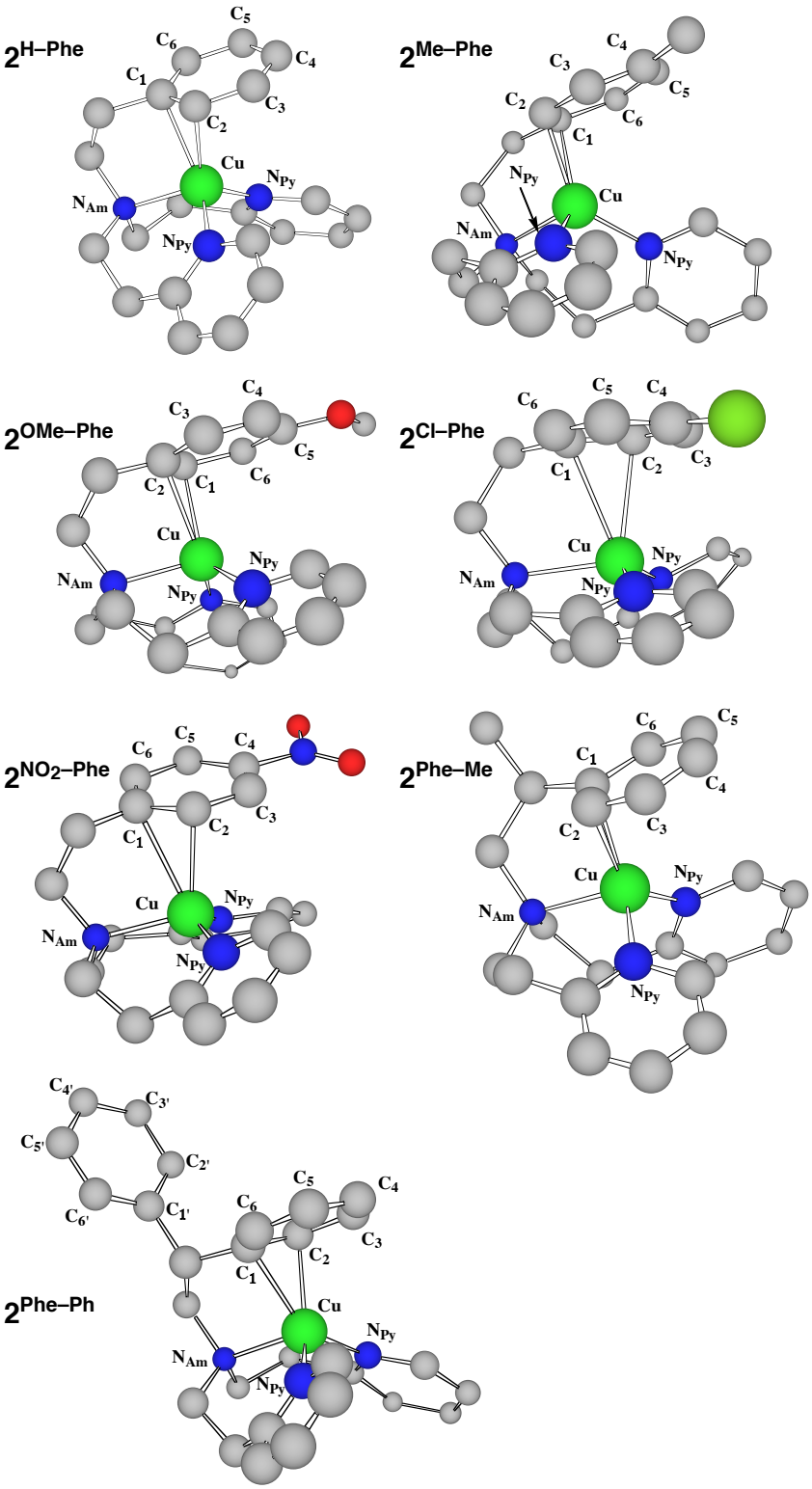

Figure 1. Chem 3D views of the crystal structures of $\mathbf{2}^{\mathbf{X–Phe}}$ (X = OMe, Me, H, Cl, and NO_2), $\mathbf{2}^{\mathbf{Phe–Me}}$, and $\mathbf{2}^{\mathbf{Phe–Ph}}$. The counter anions and hydrogen atoms are omitted for clarity.

Table 1. Summary of X-ray Crystallographic Data of the Copper(I) Complexes $\mathbf{2^R}$.

	$[Cu^I(^{H}\mathbf{Pye2}^{H–Phe})]ClO_4$ ($\mathbf{2}^{H–Phe}$)	$[Cu^I(^{H}\mathbf{Pye2}^{Me–Phe})]ClO_4$ ($\mathbf{2}^{Me–Phe}$)	$[Cu^I(^{H}\mathbf{Pye2}^{OMe–Phe})]ClO_4$ ($\mathbf{2}^{OMe–Phe}$)
empirical formula	$C_{22}H_{25}N_3O_3ClCu$	$C_{23}H_{27}N_3O_4ClCu$	$C_{23}H_{27}N_3O_5ClCu$
formula weight	494.46	508.49	524.48
crystal system	monoclinic	orthorhombic	monoclinic
space group	$P2_1/a$ (#14)	$Pna2_1$ (#33)	$P2_1/n$ (#14)
a, Å	15.695(2)	33.879(1)	9.9597(2)
b, Å	78.34(1)	10.9386(4)	17.1256(5)
c, Å	17.389(4)	11.9705(5)	13.3791(3)
β, deg	90.73(2)	90	102.674(1)
V, Å^3	21380(6)	4436.1(2)	2226.41(8)
Z	40	8	4
F(000)	10240.00	2112.00	1088.00
D_{calc}, g/cm^3	1.536	1.523	1.565
T, °C	–180	–115	–115
crystal size, mm	0.25 x 0.15 x 0.07	0.20 x 0.20 x 0.10	0.20 x 0.30 x 0.10
μ (MoKα or CuKα), cm^{-1}	28.89	11.41	11.43
diffractometer	Rigaku RAXIS-RAPID	Rigaku RAXIS-RAPID	Rigaku RAXIS-RAPID
radiation	CuKα (1.54186 Å)	MoKα (0.71069 Å)	MoKα (0.71069 Å)
$2\theta_{max}$, deg	136.5	55.0	55.0
no. of reflns measd	231838	39027	20743
no. of reflns obsd	36884 [$I > -3.00\sigma(I)$, 2θ< 136.51°]	5073 [$I > 0.01\sigma(I)$]	4179 [$I > 1.0\sigma(I)$]
no. of variables	2791	632	326
R [a]	0.058	0.032	0.027
R_w [b]	0.141	0.076	0.039
GOF	1.12	0.98	0.89

[a] $R = \Sigma||F_o| - |F_c||/\Sigma|F_o|$. [b] $R_w=\{\Sigma w(|F_o| - |F_c|)^2/\Sigma wF_o^2\}^{1/2}$; $w = 1/\sigma^2(|F_o|)$.

Table 1. Summary of X-ray Crystallographic Data of the Copper(I) Complexes $\mathbf{2}^{\mathbf{R}}$ (continuted).

	$[Cu^{I}(^{H}\mathbf{Pye2}^{Cl-Phe})]ClO_4$ ($\mathbf{2}^{Cl-Phe}$)	$[Cu^{I}(^{H}\mathbf{Pye2}^{NO_2-Phe})]ClO_4$ ($\mathbf{2}^{NO_2-Phe}$)
empirical formula	$C_{22}H_{24}N_3O_4Cl_2Cu$	$C_{22}H_{24}N_4O_6ClCu$
formula weight	528.90	539.46
crystal system	monoclinic	monoclinic
space group	$P2_1/n$ (#14)	$P2_1$ (#4)
a, Å	12.6164(8)	12.6536(4)
b, Å	12.9552(9)	12.9535(5)
c, Å	15.007(1)	14.8924(6)
β, deg	111.821(2)	112.4000(5)
V, Å^3	2277.1(3)	2256.8(1)
Z	4	4
$F(000)$	1088.00	1112.00
D_{calc}, g/cm^3	1.543	1.588
T, °C	–115	–115
crystal size, mm	0.20 x 0.20 x 0.10	0.20 x 0.20 x 0.10
μ (MoKα), cm^{-1}	12.28	11.41
diffractometer	Rigaku RAXIS-RAPID	Rigaku RAXIS-RAPID
radiation	MoKα (0.71069 Å)	MoKα (0.71069 Å)
$2\theta_{max}$, deg	55.0	55.0
no. of reflns measd	20670	21756
no. of reflns obsd	3303 [$I > 0.5\sigma(I)$]	5205 [$I > 0.01\sigma(I)$]
no. of variables	314	662
R [a]	0.079	0.0327
R_w [b]	0.103	0.049
GOF	1.34	0.96

[a] $R = \Sigma||F_o| - |F_c||/\Sigma|F_o|$. [b] $R_w = \{\Sigma w(|F_o| - |F_c|)^2/\Sigma wF_o^2\}^{1/2}$; $w = 1/\sigma^2(|F_o|)$.

Table 1. Summary of X-ray Crystallographic Data of the Copper(I) Complexes $\mathbf{2}^{\mathbf{R}}$ (continuted).

	$[Cu^{I}(^{H}\mathbf{Pye2}^{\mathbf{Phe-Me}})]ClO_4$ ($\mathbf{2}^{\mathbf{Phe-Me}}$)	$[Cu^{I}(^{H}\mathbf{Pye2}^{\mathbf{Phe-Ph}})]ClO_4$ ($\mathbf{2}^{\mathbf{Phe-Ph}}$)
empirical formula	$C_{23}H_{27}N_3O_4ClCu$	$C_{28}H_{29}N_3O_4ClCu$
formula weight	508.49	570.55
crystal system	triclinic	monoclinic
space group	P-1 (#2)	$P2_1/n$ (#14)
a, Å	15.621(2)	8.6219(5)
b, Å	17.202(2)	17.4195(9)
c, Å	8.2593(9)	17.0987(8)
α, deg	92.232(6)	
β, deg	90.706(4)	95.844(2)
χ, deg	87.545(4)	
V, Å^3	2215.6(4)	2554.7(2)
Z	4	4
F(000)	1056.00	1184.00
D_{calc}, g/cm^3	1.524	1.483
T, °C	–100	–115
crystal size, mm	0.20 x 0.20 x 0.20	0.20 x 0.20 x 0.10
μ (MoKα), cm^{-1}	11.42	10.00
diffractometer	Rigaku RAXIS-RAPID	Rigaku RAXIS-RAPID
radiation	MoKα (0.71069 Å)	MoKα (0.71069 Å)
$2\theta_{max}$, deg	55.0	54.9
no. of reflns measd	13360	23207
no. of reflns obsd	6018 [$I > 3.0\sigma(I)$]	4156 [$I > 1.0\sigma(I)$]
no. of variables	638	364
R [a]	0.046	0.041
R_w [b]	0.072	0.076
GOF	0.89	0.82

[a] $R = \Sigma||F_o| - |F_c||/\Sigma|F_o|$. [b] $R_w = \{\Sigma w(|F_o| - |F_c|)^2/\Sigma wF_o^2\}^{1/2}$; $w = 1/\sigma^2(|F_o|)$.

Table 2. Selected Bond Lengths (Å) around the Copper Ion of the $\mathbf{2}^{\mathbf{R}}$.[a]

Complex	Cu–N_{Am}	Cu–N_{Py}	Cu–C_1	Cu–C_2
$\mathbf{2}^{\mathbf{H–Phe}}$	2.089	2.006	2.336	2.211
$\mathbf{2}^{\mathbf{Me–Phe}}$	2.114	2.013	2.359	2.207
$\mathbf{2}^{\mathbf{OMe–Phe}}$	2.098	1.992	2.514	2.195
$\mathbf{2}^{\mathbf{Cl–Phe}}$	2.137	1.972	2.656	2.476
$\mathbf{2}^{\mathbf{NO_2–Phe}}$	2.115	1.967	2.597	2.388
$\mathbf{2}^{\mathbf{Phe–Me}}$	2.113	2.001	2.309	2.220
$\mathbf{2}^{\mathbf{Phe–Ph}}$	2.131	2.002	2.347	2.172

[a] Average values are presented in case more than two crystallographically independent molecules exist in the unit cell.

Table 3. Selected Bond Lengths (Å) of the Phenyl Ring of the $\mathbf{2}^{\mathbf{R}}$.[a]

Complex	C_1–C_2	C_2– C_3	C_3– C_4	C_4– C_5	C_5– C_6	C_6– C_1
$\mathbf{2}^{\mathbf{H–Phe}}$	1.403	1.388	1.386	1.379	1.387	1.413
$\mathbf{2}^{\mathbf{Me–Phe}}$	1.412	1.380	1.405	1.385	1.399	1.422
$\mathbf{2}^{\mathbf{OMe–Phe}}$	1.398	1.408	1.389	1.395	1.375	1.409
$\mathbf{2}^{\mathbf{Cl–Phe}}$	1.361	1.361	1.412	1.342	1.372	1.391
$\mathbf{2}^{\mathbf{NO_2–Phe}}$	1.403	1.381	1.396	1.377	1.402	1.402
$\mathbf{2}^{\mathbf{Phe–Me}}$	1.369	1.395	1.368	1.406	1.394	1.397
$\mathbf{2}^{\mathbf{Phe–Ph}}$	1.420	1.402	1.370	1.396	1.390	1.409
$\mathbf{2}^{\mathbf{Phe–Ph}}$ [b]	1.406	1.385	1.384	1.397	1.401	1.382

[a] Average values are presented in case plural crystallographically independent molecules exist in the unit cell. Atomic numbers of the phenyl ring of copper(I) complexes are indicated in Figure 1. [b] Bond lengths of another phenyl ring which does not interact with the cuprous ion in $\mathbf{2}^{\mathbf{Phe–Ph}}$.

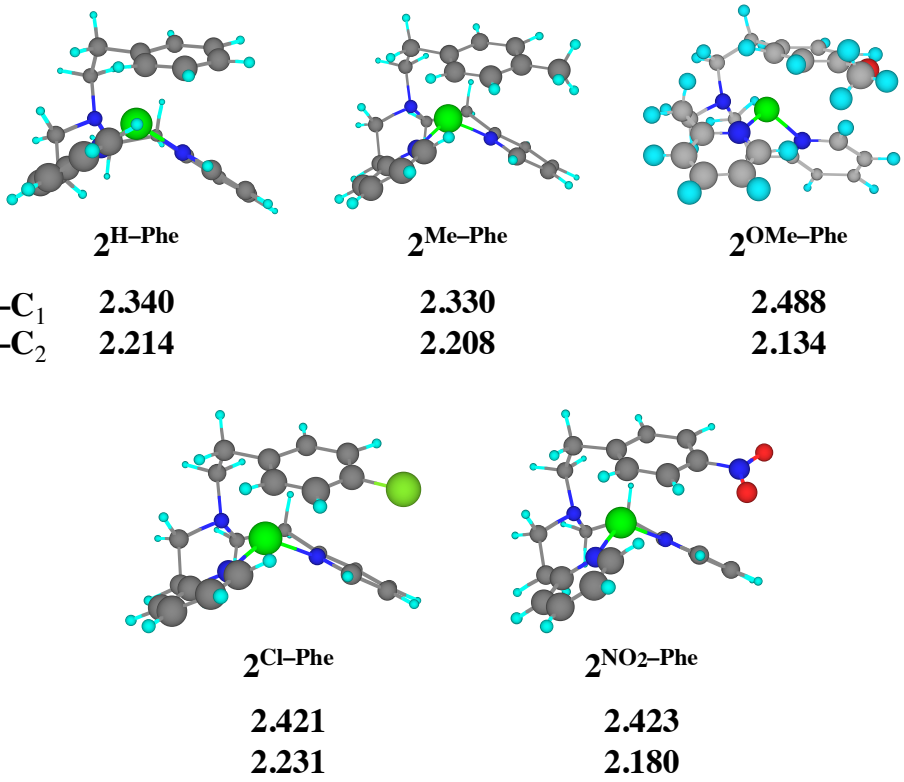

Figure 2. Optimized structures of $\mathbf{2}^{\mathbf{X\text{–}Phe}}$ (X = H, Me, OMe, Cl, and NO_2) obtained by the DFT calculation with the Cu–C distances in the d-π interaction.

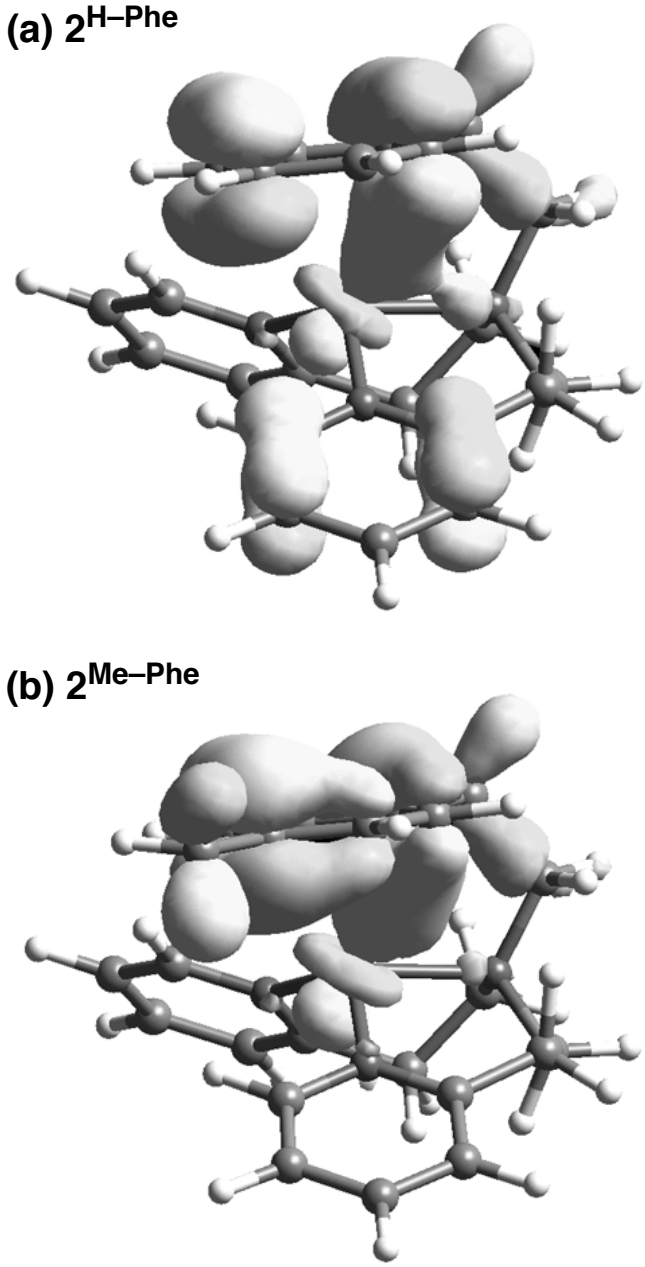

Figure 3. d-π Orbital interaction of (a) **2**$^{\mathbf{H–Phe}}$ and (b) **2**$^{\mathbf{Me–Phe}}$, obtained by the DFT calculation at the HOMO–5 level.

Physicochemical Properties of $\mathbf{2^R}$ in Solution. In the UV-vis spectra, the copper(I) complexes $\mathbf{2^R}$ exhibit a characteristic absorption band around 290 nm (ε = 7000 ~ 11000 M^{-1} cm^{-1}) (Table 4). This absorption band can be assigned to the metal-to-phenyl charge transfer (MLCT) as suggested for Cu^I–η^2-indolyl complex by Shimazaki *et al* (308 nm, ε = 18000 M^{-1} cm^{-1}).[41] In fact, the absorption band around 290 nm disappeared, when CH_3CN was added into the CH_2Cl_2 solution of the complex. This assignment is supported by the ^{13}C-NMR chemical shifts of the aromatic carbons of the ligand sidearm of $\mathbf{2^{Me–Phe}}$ in CD_2Cl_2, which are moved to the similar positions to those of the free ligand by the addition of CD_3CN as shown in Table 5. Further studies are required for detailed discussion about the MLCT transitions.

Table 4. UV-vis and Thermodynamic Data for the Titration of the Copper(I) Complexes $\mathbf{2^R}$ with CH_3CN in CH_2Cl_2.

Complex	λ_{max}, nm	ε, M^{-1} cm^{-1}	K_{as}, M^{-1} [a]	ΔH^o, kJ mol^{-1}	ΔS^o, J K^{-1} mol^{-1}
$\mathbf{2^{H–Phe}}$	290	8820	6.4 ± 0.1	–12.4 ± 1.6	–33.6 ± 6.6
$\mathbf{2^{Me–Phe}}$	294	7000	8.6 ± 0.1	–13.2 ± 0.9	–34.7 ± 3.6
$\mathbf{2^{OMe–Phe}}$	297	8520	12.2 ± 0.1	–15.6 ± 2.4	–41.5 ± 9.5
$\mathbf{2^{Cl–Phe}}$	288	8190	30.3 ± 0.2	–18.2 ± 1.9	–43.8 ± 7.6
$\mathbf{2^{NO_2–Phe}}$	287	— [b]	91.7 ± 2.0	–20.6 ± 0.5	–43.7 ± 2.0
$\mathbf{2^{Phe–Me}}$	290	9700	0.21 ± 0.001	–9.7 ± 0.8	–51.5 ± 3.3
$\mathbf{2^{Phe–Ph}}$	289	11000	0.10 ± 0.002	–7.3 ± 0.3	–47.5 ± 1.4

[a] At –20 °C. [b] The ε value could not be determined accurately due to overlap with the strong absorption band of the nitro group in the ligand.

In Figure 4 is shown the spectral change in the titration of $\mathbf{2^{Me–Phe}}$ by CH_3CN in CH_2Cl_2 at –20 °C as a typical example. Disappearance of the absorption band at around 290 nm may be due to ligand exchange reaction between the aromatic ring and the added CH_3CN (Scheme 1) as demonstrated in the Cu^I-η^2-indolyl system.[41] Then the association constant of CH_3CN to the copper(I) complex, K_{as} = $[Cu^IL•CH_3CN]/[Cu^IL][CH_3CN]$, has been determined as 8.6 ± 0.1 M^{-1} by analyzing the absorption change as indicated in the inset of Figure 4, and the K_{as} values at –20 °C for all other complexes have been determined by the same treatment as listed in Table 4. In addition, thermodynamic parameters, ΔH^0 and ΔS^0, for the binding of CH_3CN to the copper(I) center have been determined from the temperature dependence of K_{as} according to the equation: $\ln K_{as} = -\Delta H^0/(RT) + \Delta S^0/R$ (Table 4 and Figure 5).

Scheme 1

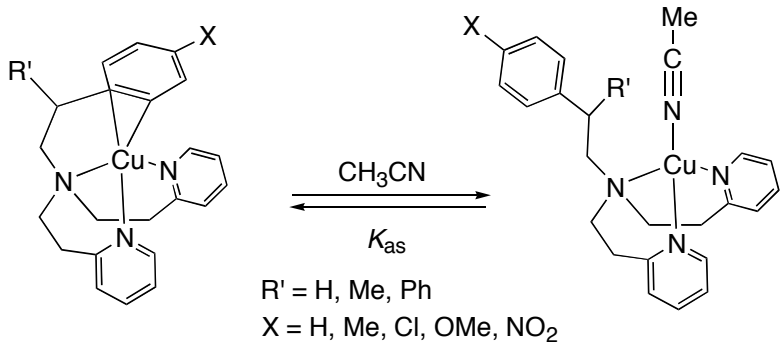

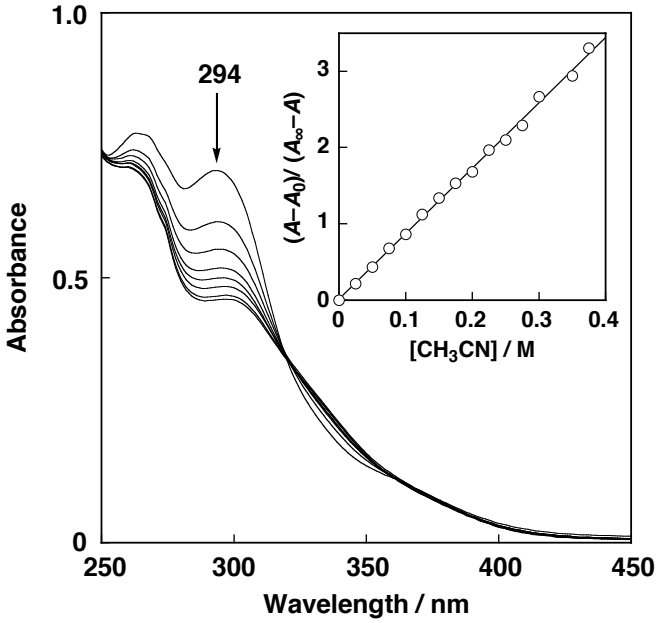

Figure 4. Spectral change for the titration of $\mathbf{2}^{\mathbf{Me–Phe}}$ (1.0×10^{-4} M) with CH_3CN at –20 ˚C in CH_2Cl_2. Inset: plot of $(A–A_0)/(A_\infty–A)$ *vs*. [CH_3CN] based on the absorption change at 294 nm.

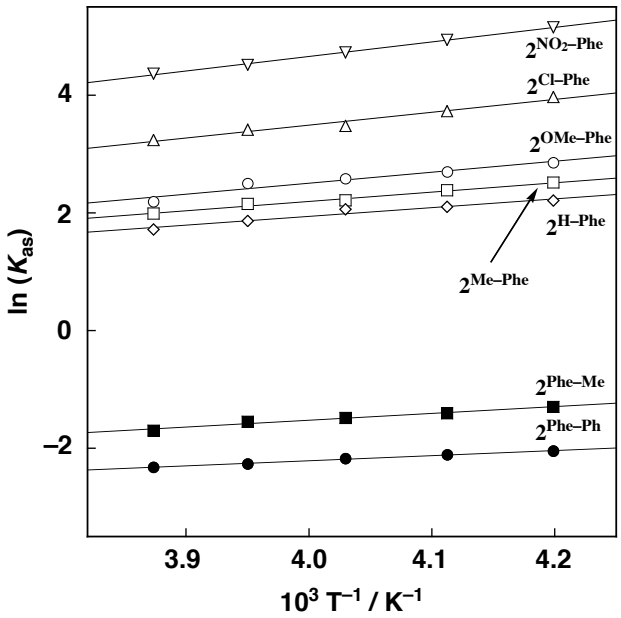

Figure 5. Plots of lnK_{as} *vs*. T^{-1} for the titration of the copper(I) complexes $\mathbf{2}^{\mathbf{R}}$ with CH_3CN in CH_2Cl_2.

Strength of the CH_3CN-binding (K_{as}) can be evaluated by the ΔH^0 term which reflects difference in the binding energy between CH_3CN and the phenyl ring to the copper(I) ion. Since the Cu–MeCN bond strength may be virtually the same in the CH_3CN complex (right species in Scheme 1) irrespective of the type of X, the difference in ΔH^0 may directly reflect the energy difference in the copper(I)-arene interaction in the d-π complexes (left species in Scheme 1), where the smaller the $-\Delta H^0$ value, the stronger is the copper(I)-arene interaction. Apparently, the copper(I)-arene interaction is stronger in $\mathbf{2}^{\mathbf{H–Phe}}$ and $\mathbf{2}^{\mathbf{Me–Phe}}$, thus smaller in K_{as}, while *p*-substituents, OMe, Cl, and NO_2, weaken the copper(I)-arene interaction in the series of $\mathbf{2}^{\mathbf{X–Phe}}$. There is a compensating effect between ΔH^0 and ΔS^0. On the other hand, the methyl and phenyl groups at the benzylic position in $\mathbf{2}^{\mathbf{Phe–Me}}$ and $\mathbf{2}^{\mathbf{Phe–Ph}}$ results in the smaller $-\Delta H^0$ value and the larger $-\Delta S^0$ value. In the case of $\mathbf{2}^{\mathbf{Phe–Me}}$ and $\mathbf{2}^{\mathbf{Phe–Ph}}$, there is probably sterical crowding due to the close proximity of R' (Me and Ph) and the coordinated CH_3CN, which leads to the weaker binding. Thus, the K_{as} values of $\mathbf{2}^{\mathbf{Phe–Me}}$ and $\mathbf{2}^{\mathbf{Phe–Ph}}$ become significantly smaller as compared to those of $\mathbf{2}^{\mathbf{X–Phe}}$. Then, the maximum energy difference reaches 13.3 kJ mol^{-1} between $\mathbf{2}^{\mathbf{Phe–Ph}}$ and $\mathbf{2}^{\mathbf{NO_2–Phe}}$.

^{1}H- and ^{13}C-NMR studies have provided further insight into the copper(I)-arene interaction in solution. Assignment of all signals in the ^{1}H- and ^{13}C-NMR spectra have been accomplished by employing 2D-NMR techniques such as COSY, NOESY, HMQC, and

HMBC as summarized in Experimental Section. The aromatic regions of the ^{1}H- and ^{13}C-NMR of $\mathbf{2}^{\mathbf{Me-Phe}}$ in CD_2Cl_2 at 25 °C are shown in Figure 6 as typical examples. Apparently, the two ^{1}H and ^{13}C nuclei of the *ortho*- (2- and 6-) and *meta*- (3- and 5-) positions of the phenyl group of the ligand sidearm appear to be magnetically equivalent. If the copper(I)-arene interaction in solution was fixed at the C_1–C_2 moiety as seen in the crystal structure, the ^{1}H and ^{13}C nuclei at the 2- and 3-positions would provide different peaks from those of ^{1}H and ^{13}C at the 6- and 5-positions, respectively. Thus, the phenyl group is possibly swinging above the cuprous ion as illustrated in Scheme 2, when the *ortho*- (2- and 6-) and *meta*- (3- and 5-) positions of the phenyl group become equivalent. The ^{1}H- and ^{13}C-NMR signals of the aromatic rings did not change at all even at –80 °C, suggesting that the energy barrier for the aromatic-swinging above the copper(I) ion is very low.

Scheme 2

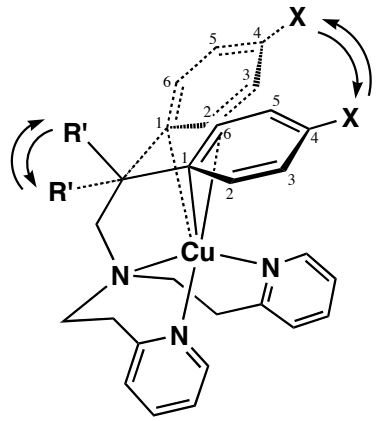

In Table 5 are summarized the ^{13}C-NMR data of the aromatic groups of the free ligands and the corresponding copper(I) complexes. The copper(I)-arene interaction induces up-field shifts of the ^{13}C signals bound to the copper(I) ion [C_1 and C_2 (C_6)], while other ^{13}C signals of C_3 (C_5) and C_4 exhibit down-field shifts with one exception at C_4 in $^{H}Pye2^{NO_2-Phe}$. The up-field shift at C_1 and C_2 (C_6) can be attributed to the electron-donating effect by the copper(I) ion through the d-π interaction. In this case as well, the electron-withdrawing substituents of $\mathbf{2}^{\mathbf{Cl-Phe}}$ and $\mathbf{2}^{\mathbf{NO_2-Phe}}$ resulted in the smaller up-field shift values as compared to the others, being consistent with their weaker copper(I)-arene interaction.

The copper(I)-arene interaction has also been examined by using cyclic voltammetry in CH_2Cl_2. The copper(I) complexes exhibit a reversible or quasi-reversible redox couple due to the one-electron oxidation-reduction of the copper center. A typical example of the cyclic voltammogram is shown in Figure 7, and the redox potentials ($E_{1/2}$ *vs*. Fc/Fc^{+}) of all the

copper(I) complexes are listed in Table 6. In this case, the $E_{1/2}$ values may reflect an inductive effect of the arene substituents. Namely, the more electron donating the substituent is, the more positive is the $E_{1/2}$ value in the series of $\mathbf{2}^{\mathbf{X-Phe}}$.

Table 5. The ^{13}C-NMR Data of the Aromatic Group in the Free Ligands ^{H}Pye2^{R} and the Copper(I) Complexes 2^{R}.[a]

		C_1	C_2 (C_6)	C_3 (C_5)	C_4
^{H}Pye2^{H-Phe}	δ_{ligand} [b]	141.37	129.18	128.57	126.12
	$\delta_{complex}$ [c]	134.71	123.57	129.34	127.42
	$\Delta\delta$ [d]	–6.66	–5.61	0.77	1.30
^{H}Pye2^{Me-Phe}	δ_{ligand} [b]	138.21	129.02	129.24	135.63
	$\delta_{complex}$ [c]	131.75	123.43	129.89	137.36
	$\Delta\delta$ [d]	–6.46	–5.59	0.65	1.73
	$\delta_{complex}$ [e]	136.61	127.20	129.62	135.08
^{H}Pye2$^{OMe-Phe}$	δ_{ligand} [b]	133.36	130.03	113.98	158.30
	$\delta_{complex}$ [c]	126.29	125.18	114.54	159.33
	$\Delta\delta$ [d]	–7.07	–4.85	0.56	1.03
^{H}Pye2^{Cl-Phe}	δ_{ligand} [b]	140.11	130.67	128.51	131.66
	$\delta_{complex}$ [c]	134.60	126.31	129.14	133.12
	$\Delta\delta$ [d]	–5.51	–4.36	0.63	1.46
^{H}Pye2$^{NO_2-Phe}$	δ_{ligand} [b]	149.67	130.09	123.57	146.71
	$\delta_{complex}$ [c]	147.18	127.12	123.91	144.49
	$\Delta\delta$ [d]	–2.49	–2.97	0.34	–2.22
^{H}Pye2^{Phe-Me}	δ_{ligand} [b]	146.95	127.72	128.53	126.22
	$\delta_{complex}$ [c]	138.81	121.24	129.45	127.61
	$\Delta\delta$ [d]	–8.14	–6.48	0.92	1.39
^{H}Pye2^{Phe-Ph}	δ_{ligand} [b]	144.53	128.63	128.62	126.45
	$\delta_{complex}$ [c]	138.27	124.71	129.53	127.79
	$\Delta\delta$ [d]	–6.26	–3.92	0.91	1.34

[a] In CD_2Cl_2. [b] Chemical shift of the free ligand. [c] Chemical shift of the copper(I) complex. [d] $\Delta\delta = (\delta_{complex} - \delta_{ligand})$. [e] Chemical shifts of the aromatic carbons of the ligand sidearm of $[Cu^{I}(^{H}Pye2^{Me-Phe})]ClO_4$ (0.025 M) measured in CD_2Cl_2 containing CD_3CN (1.43 M) at 25 °C. Under this condition, 18 % of the copper(I) complex keeps the d-π interaction.

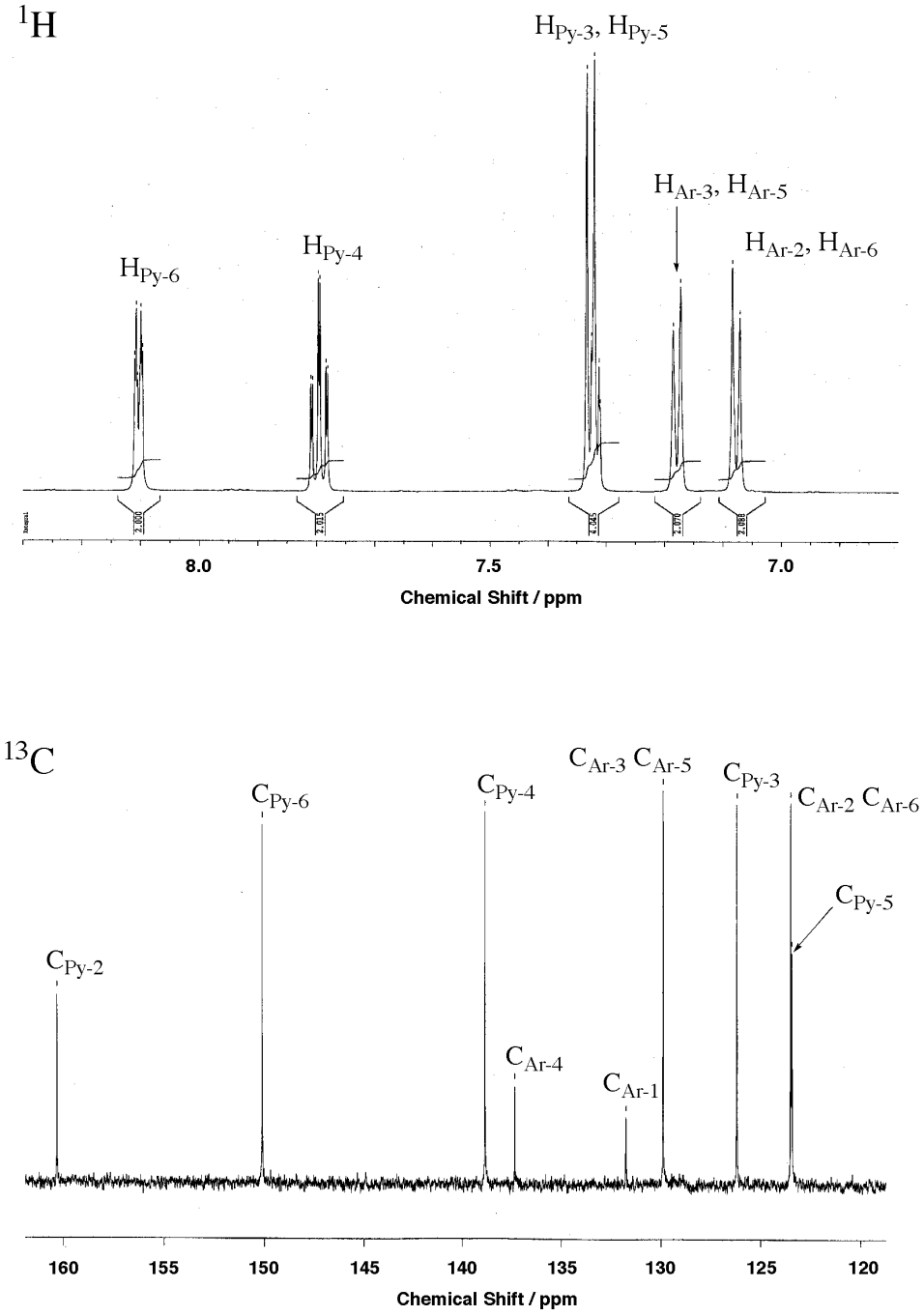

Figure 6. ^{1}H- and ^{13}C-NMR (aromatic region) of $\mathbf{2}^{\mathbf{Me-Phe}}$ in CD_2Cl_2.

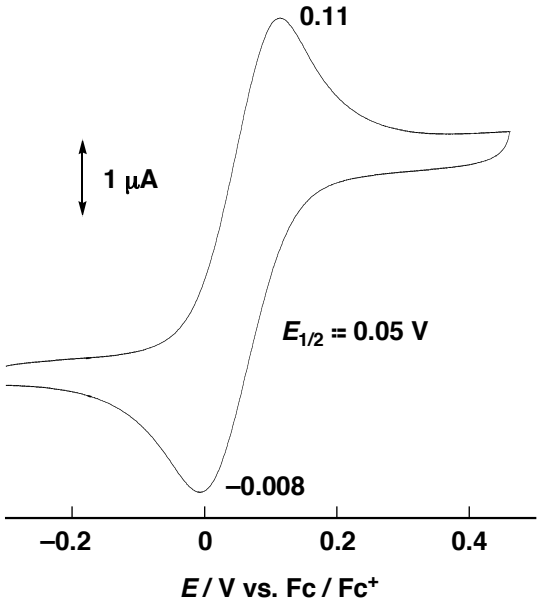

Figure 7. Cyclic voltammogram of $[Cu^{I}(^{H}Pye2^{Me–Phe})]ClO_4$ (**2**$^{Me–Phe}$, 2.0 x 10^{-3} M) in CH_2Cl_2 containing 0.1 M TBAP; working electrode Pt, counter electrode Pt, pseudo-reference electrode Ag wire, scan rate 10 mV/s.

Table 6. Electrochemical Data from Cyclic Voltammetry Experiment ($E_{1/2}$ and ΔE)[a] and the Second-order Rate Constants (k_{obs}) for the Formation of (μ-η^2:η^2–Peroxo)dicopper(II) Complex (**A**).[b]

Complex	$E_{1/2}$, V *vs.* Fc/Fc$^+$	ΔE, V	k_{obs}, M^{-1} s^{-1}
2$^{H–Phe}$	0.07	0.53	0.28 ± 0.001
2$^{Me–Phe}$	0.05	0.12	0.70 ± 0.005
2$^{OMe–Phe}$	0.05	0.18	1.96 ± 0.01
2$^{Cl–Phe}$	–0.01	0.24	1.51 ± 0.006
2$^{NO_2–Phe}$	–0.03	0.15	5.21 ± 0.03
2$^{Phe–Me}$	0.16	0.17	— [c]
2$^{Phe–Ph}$	0.15	0.34	— [c]

[a] The electrochemical measurements were performed using CH_2Cl_2 containing 0.1 M tetrabutylammonium perchlorate (TBAP) at a scan rate of 10 ~ 50 mV s^{-1} at 25 °C. [b] At –80 °C in CH_2Cl_2. [c] Very slow.

Reactivity of 2^{R} toward Dioxygen. Copper(I) complex $\mathbf{2}^{\mathbf{H–Phe}}$ has been shown to react with O_2 at a low temperature to give a (μ-η^2:η^2-peroxo)dicopper(II) complex **A**, the model compound of the active oxygen intermediate of hemocyanin, tyrosinase, and catechol oxidase (Scheme 3)[44] by Itoh and his coworkers.[12]

Scheme 3

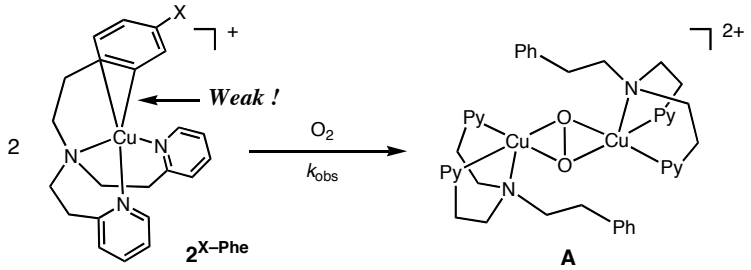

Oxygenation reactions of other copper(I) complexes $\mathbf{2}^{\mathbf{X–Phe}}$ (X = Me, OMe, Cl, and NO_2) were examined under the same experimental conditions (at –80 °C in CH_2Cl_2). The copper(I) complexes $\mathbf{2}^{\mathbf{X–Phe}}$ reacted with O_2 to give an oxygenated intermediate which was ESR-silent and gave essentially the same absorption spectrum as that of the (μ-η^2:η^2-peroxo)dicopper(II) complex derived from $\mathbf{2}^{\mathbf{H–Phe}}$ (λ_{max} = 364 nm).[21] These features are strong evidences for the formation of (μ-η^2:η^2-peroxo)dicopper(II) complex (**A**) in all the cases. Interestingly, however, the formation rate (k_{obs}) of the peroxo intermediate was significantly different depending on the *p*-substituent (X) of ^{H}Pye2$^{X–Phe}$, and the copper(I) complexes $\mathbf{2}^{\mathbf{Phe–Me}}$ and $\mathbf{2}^{\mathbf{Phe–Ph}}$ exhibited virtually no reactivity toward O_2 under the same experimental conditions (Scheme 3 and Table 6). Thus, the reactivity of the copper(I) complexes toward O_2 is significantly altered by the ligand substituents R' and X (see Scheme 3). More importantly, tendency of the formation rates (k_{obs}) of the peroxo intermediate **A** is very close to that of K_{as}. Namely, the stronger the copper(I)-arene interaction, the lower is the dioxygen reactivity of $\mathbf{2}^{\mathbf{X–Phe}}$. Thus, it is concluded that the interaction of O_2 and Cu^{I} is significantly affected by the *p*-substituents X and the benzylic substituents R' through the copper(I)-arene interaction.

2. Copper(I) Complex 1^{R} of Bis[2-(6-methyl-2-pyridyl)ethyl]amine Tridentate Ligand (^{Me}Pye2^{Phe}).

In the previous section, the substituted effects in the bis[2-(2-pyridyl)ethyl]amine tridentate ligand system (^{H}Pye2^{R}) have been examined in detail. In this section, effects of the methyl substituent on the 6-position of pyridine nucleus have been examined.

Synthesis of Ligands and Copper(I) Complexes. Ligand ^{Me}Pye2^{Phe} (Phe = -CH_2CH_2Ph: Chart 4) was prepared by Michael addition of 2-phenylethylamine to 6-methyl-2-vinylpyridine in refluxing methanol under acidic conditions. The copper(I) complex of ^{Me}Pye2^{Phe} was obtained by treating the ligand with an equimolar amount of $[Cu^{I}(CH_3CN)_4](ClO_4)$ in CH_2Cl_2 under anaerobic conditions (in a glove box).

Chart 4

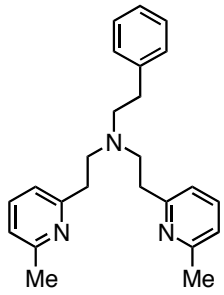

^{Me}Pye2^{Phe}

Crystal Structure of 1^{Phe}•CH_3CN. Crystal structure of the copper(I) complex $\mathbf{1}^{Phe}$•CH_3CN of ligand ^{Me}Pye2^{Phe} has been determined by X-ray crystallographic analysis as shown in Figure 8. The crystallographic data and the selected bond length and angles are summarized in Table 7 and Table 8, respectively.

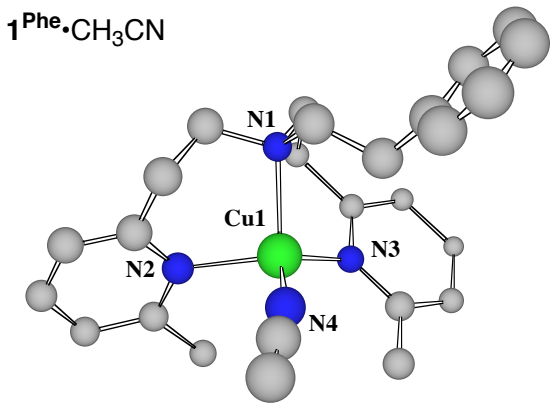

Figure 8. Chem 3D view of the crystal structure of $\mathbf{1}^{Phe}$•CH_3CN. The counter anions and hydrogen atoms are omitted for clarity.

Table 7. Summary of X-ray Crystallographic Data of $\mathbf{1}^{\mathbf{Phe}}\bullet CH_3CN$

	Complex $\mathbf{1}^{\mathbf{Phe}}\bullet CH_3CN$
empirical formula	$C_{26}H_{32}N_4O_4ClCu$
formula weight	563.56
crystal system	triclinic
space group	P1 (#1)
a, Å	11.956(1)
b, Å	12.073(1)
c, Å	10.379(1)
α, deg	106.494(2)
β, deg	106.108(5)
χ, deg	99.266(3)
V, Å^3	1332.5(2)
Z	2
F(000)	588.00
D_{calc}, g/cm^3	1.405
T, °C	–115
crystal size, mm	0.30 x 0.30 x 0.20
μ (MoKα), cm^{-1}	9.58
diffractometer	Rigaku RAXIS-RAPID
radiation	MoKα (0.71069 Å)
$2\theta_{max}$, deg	55.0
no. of reflns measd	9468
no. of reflns obsd	4862 [$I > 1.5\sigma(I)$]
no. of variables	714
R^a	0.042
$R_w{}^b$	0.064
GOF	0.84

[a] $R = \Sigma||F_o| - |F_c||/\Sigma|F_o|$. [b] $R_w=\{\Sigma w(|F_o| - |F_c|)^2/\Sigma wF_o{}^2\}^{1/2}$.

Table 8. Selected Bond Lengths (Å) and Angles (deg) of $\mathbf{1}^{\mathbf{Phe}}$•$CH_3CN$

Complex $\mathbf{1}^{\mathbf{Phe}}$•$CH_3CN$			
Molecular 1		Molecular 2	
Cu(1)–N(1)	2.216(7)	Cu(2)–N(5)	2.152(6)
Cu(1)–N(2)	2.054(6)	Cu(2)–N(6)	1.996(7)
Cu(1)–N(3)	2.009(7)	Cu(2)–N(7)	2.133(6)
Cu(1)–N(4)	1.930(8)	Cu(2)–N(8)	2.005(6)
N(1)–Cu(1)–N(2)	98.3(3)	N(5)–Cu(2)–N(6)	98.3(3)
N(1)–Cu(1)–N(3)	96.3(2)	N(5)–Cu(2)–N(7)	96.9(3)
N(2)–Cu(1)–N(3)	122.0(3)	N(6)–Cu(2)–N(7)	123.3(3)
N(1)–Cu(1)–N(4)	113.7(3)	N(5)–Cu(2)–N(8)	114.3(3)
N(2)–Cu(1)–N(4)	122.4(3)	N(6)–Cu(2)–N(8)	124.8(3)
N(3)–Cu(1)–N(4)	101.4(3)	N(7)–Cu(2)–N(8)	96.6(3)

The unit cell of $[Cu^{I}(^{Me}Pye2^{Phe})(CH_3CN)](ClO_4)$ ($\mathbf{1}^{\mathbf{Phe}}$•$CH_3CN$) consists of two crystallographically independent Cu^{I}-complex ions including two *N*-bound acetonitrile molecules and two ClO_4^- ions. The cuprous ion in $\mathbf{1}^{\mathbf{Phe}}$•$CH_3CN$ has a distorted tetrahedral geometry with a N_4 donor set, one from the bound CH_3CN and the others from the tridentate ligand $^{Me}Pye2^{Phe}$ (Figure 8). Although bond distances and angles between the two molecules (molecular 1 and molecular 2) are slightly different each other, structural parameters (Cu–N distances and N–Cu–N angles) of $\mathbf{1}^{\mathbf{Phe}}$•$CH_3CN$ are fairly similar to those of the reported dinuclear Cu^{I} complex, $[Cu^{I}_2(N4PY2)(CH_3CN)_2](ClO_4)_2$ ($\mathbf{2}^{\mathbf{N4}}$•CH_3CN), where each copper ion has a pseudotetrahedral geometry supported by the bis[2-(2-pyridyl)ethyl]amine ($^{H}Pye2$) unit and one molecule of CH_3CN (Cu–N distances: 1.945–2.151 Å, N–Cu–N angles: 98.1–122.8 °) (Scheme 4).[45] Thus, the 6–methyl group of the pyridine nucleus of $^{Me}Pye2^{Phe}$ induces little effect on the structure of the *four-coordinate* copper(I) complex.

On the other hand, Karlin and his coworkers have also reported nearly T-shaped *three-coordinate* copper(I) complex $\mathbf{2}^{\mathbf{Bn}}$ supported by *N*,*N*-bis[2-(2-pyridyl)ethyl]benzylamine (Scheme 5),[46] where the Cu–N_{Py} distances are significantly shorter (1.873, 1.893 Å) than those in $\mathbf{1}^{\mathbf{Phe}}$•$CH_3CN$ and $\mathbf{2}^{\mathbf{N4}}$•CH_3CN. This is probably due to the steric effect of the 6–methyl group in $^{Me}Pye2^{Phe}$, which prohibits formation of such a three-coordinate copper(I) complex having

the shorter Cu–N_{Py} distance. It has previously been demonstrated that the donor ability of the pyridine nucleus carrying the 6–methyl group is diminished due to the steric repulsion between the methyl group and metal ion.[20,47] Thus, only the *four-coordinate* tetrahedral geometry with the longer Cu–N distance is available in the ^{Me}Pye2^{Phe} ligand system. Consequently, removal of the bound CH_3CN from **1**^{Phe}•CH_3CN becomes difficult. This point will be discussed later in more detail.

Scheme 4

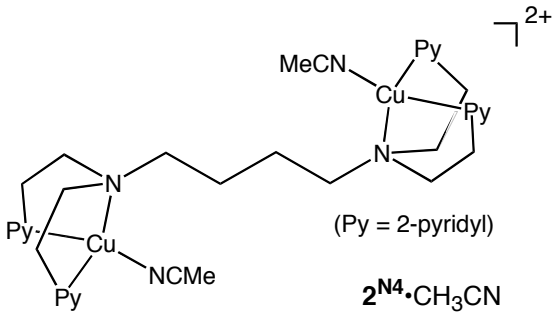

2^{N4}•CH_3CN

Scheme 5

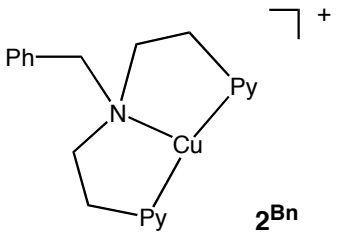

2^{Bn}

Physicochemical Properties and Reactivity of 1^{Phe}•CH_3CN in Solution. In contrast to the fact that complexes **2**^{R} supported by ligands ^{H}Pye2^{R} exhibit a characteristic absorption band around 300 nm due to metal-to-ligand charge transfer (MLCT) band (Table 4), complex **1**^{Phe}•CH_3CN does not show such an absorption band in CH_2Cl_2. Thus, it can be said that the coordination of CH_3CN in **1**^{Phe}•CH_3CN is rather strong to prevent the Cu^{I}–phenyl (d-π) interaction. In addition, ^{1}H-NMR study of **1**^{Phe}•CH_3CN shows the peak of CH_3CN bound to cupric ion (δ = 2.04, see Experimental Section) in acetone-d_6, indicating that the tetrahedral geometry of **1**^{Phe} involving CH_3CN molecule retains in solution as well as in crystal structure.

Complex **1**^{Phe}•CH_3CN exhibited a reversible redox couple at 0.30 V *vs*. Fc/Fc^{+} (ferrocene/ferrocenium) in CH_2Cl_2. The good reversibility of the cyclic voltammetry indicates

that the coordination of CH_3CN in $\mathbf{1}^{Phe}$•CH_3CN is maintained during the electrochemical redox process. In other words, the coordination of CH_3CN in $\mathbf{1}^{Phe}$•CH_3CN is strong enough to keep the four-coordinate copper ion as discussed above. The higher redox potential of $\mathbf{1}^{Phe}$•CH_3CN (0.30 V *vs*. Fc/Fc^+) as compared with those of $\mathbf{2}^{R}$ supported by $^{H}Pye2^{R}$ (–0.03 ~ 0.15 V *vs*. Fc/Fc^+; see Table 6) can be attributed to the bound CH_3CN, which stabilizes the copper(I) state of the complex. The 6–methyl group in $^{Me}Pye2^{Phe}$ may also result in increase of $E_{1/2}$, since Tanaka and his coworkers have demonstrated that introduction of the 6–methyl group induces a positive shift of $E_{1/2}$ of the copper(II) complexes of TMPA ligands.[47]

In constrast to the case of $\mathbf{2}^{X–Phe}$ which affords a (μ-η^2:η^2-peroxo)dicopper(II) complex in the oxygenation reaction (Scheme 3), $\mathbf{1}^{Phe}$•CH_3CN does not react with O_2 at all. (Scheme 6) The high oxidation potential of $\mathbf{1}^{Phe}$•CH_3CN (0.30 V *vs*. Fc/Fc^+) as compared with $\mathbf{2}^{X–Phe}$ (–0.03 ~ 0.15 V *vs*. Fc/Fc^+; see Table 6) is certainly an important factor for the stability toward dioxygen. The strong binding of CH_3CN to Cu^I in $\mathbf{1}^{Phe}$•CH_3CN may also prohibit the initial coordination of O_2 to the metal center. Thus, the 6-methyl substituent in $^{Me}Pye2^{Phe}$ has been found to induce large effect not only on the structure but also on the redox reactivity of the copper(I) complex.

Scheme 6

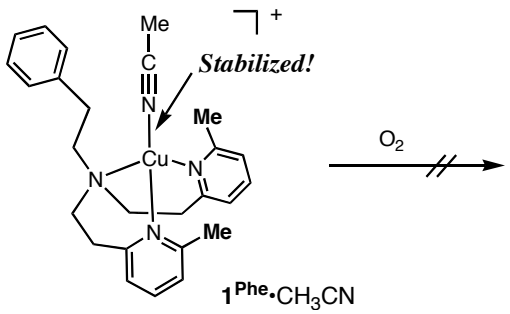

3. Copper(I) Complex $\mathbf{4}^{Phe}$ of Bis(2-pyridylmethyl)amine Tridentate Ligand (^{H}Pym2^{Phe}).

In the previous sections, the substituent effects in the bis[2-(2-pyridyl)ethyl]amine tridentate ligand system have been extensively studied. In this section, structure, physicochemical properties, and reactivities of the copper(I) complexes in the bis(2-pyridylmethyl)amine tridetate ligand system have been explored.

Synthesis of Ligand and Copper(I) Complex. Ligand $^{H}Pym2^{Phe}$ (Chart 5) was was

prepared by the reductive coupling between 2-phenylethylamine and 2 equiv of 2-pyridinecarboxaldehyde in the presence of $NaBH_3CN$ as the reductant in methanol. The copper(I) complex of $^{H}Pym2^{Phe}$ was obtained by treating the ligand with an equimolar amount of $[Cu^{I}(CH_3CN)_4](ClO_4)$ in acetone under anaerobic conditions (in a glove box).

Chart 5

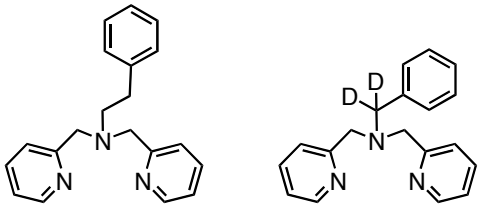

$^{H}Pym2^{Phe}$ $^{H}Pym2^{Bn}$

Characterization of the Copper(I) Complex of $^{H}Pym2^{Phe}$. In contrast to a large number of studies on the structure and reactivity of the copper(I) complexes supported by a series of bis[2-(2-pyridyl)ethyl]amine tridentate ligands ($^{H}Pye2^{R}$, Chart 3),[1,48] little is known about the chemistry of copper(I) complexes of the (2-pyridylmethyl)amine tridentate ligands $^{H}Pym2^{R}$ (Chart 5). This may be due in part to instability of the copper(I) complexes of $^{H}Pym2^{R}$ in solution. In fact, treatment of ligand $^{H}Pym2^{Bn}$ [R = Bn (benzyl; $-CD_2Ph$)] with $[Cu^{I}(CH_3CN)_4]X$ ($X = ClO_4^-, PF_6^-$) in CH_2Cl_2 readily resulted in a color change of the solution from pale yellow to dark blue (within a couple of minutes) even under anaerobic conditions, and a copper(II) complex, $[Cu^{II}(^{H}Pym2^{Bn})(Cl)]X$, was obtained from the final reaction mixture.[49,50] Such an instability of the copper(I) complex of $^{H}Pym2^{Bn}$ was significantly suppressed when the ligand sidearm R was replaced from benzyl (Bn) to phenethyl (Phe; $-CH_2CH_2Ph$). This has been attributed to the existence of a copper(I)-arene interaction in the $^{H}Pym2^{Phe}$-complex as described below.

The crystal structure of copper(I) complex of $^{H}Pym2^{Phe}$ (**4**^{Phe}) is shown in Figure 9, and the crystallographic data and the selected bond distances and angles are summarized in Tables 9 and 10, respectively. There are two crystallographically independent molecules (designated as molecule 1 and molecule 2 in Table 10) in the unit cell of complex **4**^{Phe}. As clearly seen in Figure 9, compound **4**^{Phe} exhibits a distinct d-π interaction between the cuprous ion and the phenyl ring of the ligand sidearm (R = Phe). The copper center has a trigonal pyramidal geometry consisted of the two pyridine nitrogen atoms (N_{Py}) and one of the carbon atoms at the ortho position (C_{ortho}) of the phenyl ring occupying the trigonal basal plane and the tertiary

amine nitrogen atom (N_{am}) as the axial ligand. Deviation of the copper(I) ion from the basal plane is only 0.1021 Å in molecule 1 and 0.1037 Å in molecule 2. The distance between Cu and C_{ortho} (2.186 and 2.163 Å for molecule 1 and molecule 2, respectively) is much shorter than that between Cu and N_{am} (2.242 and 2.229 Å), and the Cu–C_{ortho} distance is also much shorter than those of Cu–C_{sub} [Cu(1)–C(15): 2.63 Å in molecule 1 and Cu(2)–C(35): 2.60 Å in molecule 2] and Cu–C_{meta} [Cu(1)–C(17): 2.50 Å in molecule 1 and Cu(2)–C(37): 2.53 Å in molecule 2]. Thus, the copper(I)-arene interaction in $\mathbf{4}^{\mathbf{Phe}}$ can be described as an η^1-binding. Although several examples of the copper(I)-arene interaction with the η^2-binding mode have been reported so far (see Figure 1),[35-41,51,52] this is the first example of the copper(I)-arene interaction with η^1-binding mode. Thus, the binding mode of the d-π interaction changes from η^2 to η^1 by changing the alkyl linker chain length from ethylene to methylene in the (2-pyridyl)alkylamine tridentate ligand system. The difference in the binding mode (η^1 vs η^2) between these two systems could be attributed in part to the difference in the electron-donor ability of pyridine as discussed below.

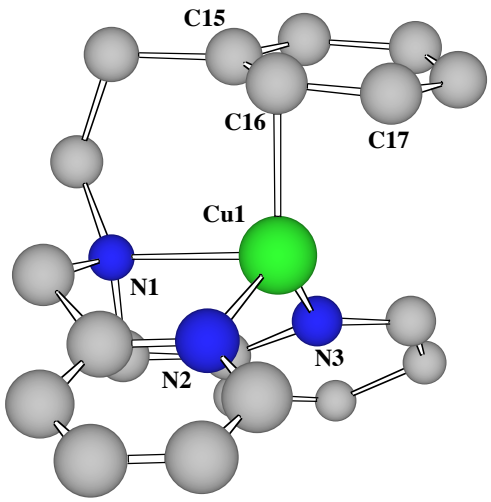

Figure 9. Chem 3D view of the crystal structure of $[Cu^{I}(^{H}Pym2^{Phe})]ClO_4$ ($\mathbf{4}^{\mathbf{Phe}}$). The counter anion and hydrogen atoms are omitted for clarity.

Table 9. Summary of the X-ray Crystallographic Data for Complexes **4**^{Phe} and **5**^{Phe}.

	4^{Phe}	**5**^{Phe}
empirical formula	$C_{20}H_{21}N_3CuClO_4$	$C_{20}H_{21}N_3CuCl_2O_4$
formula weight	466.40	501.86
crystal system	triclinic	monoclinic
space group	P–1 (#2)	$P2_1/n$ (#14)
a, Å	7.287(8)	9.8824(2)
b, Å	11.54(1)	15.2501(4)
c, Å	23.58(2)	14.1688(2)
α, deg	90.48(5)	90
β, deg	92.01(4)	91.298(1)
χ, deg	92.12(3)	90
V, Å^3	1980.2(3)	2134.80(8)
Z	4	4
$F(000)$	960.00	1028.00
D_{calc}, g/cm^3	1.564	1.561
T, °C	–120	–120
crystal size, mm	0.40 x 0.40 x 0.10	0.20 x 0.20 x 0.20
μ (MoKα), cm^{-1}	12.70	13.05
diffractometer	Rigaku RAXIS-RAPID	Rigaku RAXIS-RAPID
$2\theta_{max}$, deg	55.0	54.7
no. of reflns measd	12173	20143
no. of reflns obsd	6196 ([$I > 0.01\sigma(I)$])	3345 [$I > 3.00\sigma(I)$]
no. of variables	566	292
R [a]	0.093	0.033
R_w [b]	0.095	0.041
GOF	0.98	0.90

[a] $R = \Sigma||F_o| - |F_c||/\Sigma|F_o|$. [b] $R_w = \{\Sigma w(|F_o| - |F_c|)^2/\Sigma wF_o^2\}^{1/2}$.

Table 10. Selected Bond Lengths (Å) and Angles (deg) of Complexes **4**^{Phe} and **5**^{Phe}.

Complex 4^{Phe}			
Molecular 1		**Molecular 2**	
Cu(1)–N(1)	2.242(5)	Cu(2)–N(4)	2.229(5)
Cu(1)–N(2)	2.009(5)	Cu(2)–N(5)	1.994(5)
Cu(1)–N(3)	2.017(5)	Cu(2)–N(6)	2.073(5)
Cu(1)–C(16)	2.186(6)	Cu(2)–C(36)	2.163(6)
N(1)–Cu(1)–N(2)	83.7(2)	N(4)–Cu(2)–N(5)	81.1(2)
N(1)–Cu(1)–N(3)	81.8(2)	N(4)–Cu(2)–N(6)	82.2(2)
N(2)–Cu(1)–N(3)	122.2(2)	N(5)–Cu(2)–N(6)	123.5(2)
N(1)–Cu(1)–C(16)	96.5(2)	N(4)–Cu(2)–C(36)	98.9(2)
N(2)–Cu(1)–C(16)	111.6(3)	N(5)–Cu(2)–C(36)	122.9(2)
N(3)–Cu(1)–C(16)	125.5(2)	N(6)–Cu(2)–C(36)	112.9(2)
Complex 5^{Phe}			
Cu(1)–Cl(1)	2.276(1)	Cu(1)–N(1)	2.068(2)
Cu(1)–N(2)	1.982(2)	Cu(1)–N(3)	1.996(2)
Cu(1)–O(3)	2.7495(9)		
Cl(1)–Cu(1)–N(1)	178.46(7)	Cl(1)–Cu(1)–N(2)	97.67(7)
N(1)–Cu(1)–N(2)	82.76(9)	Cl(1)–Cu(1)–N(3)	98.08(7)
N(1)–Cu(1)–N(3)	81.47(9)	N(2)–Cu(1)–N(3)	164.22(9)

In CH_2Cl_2, the copper(I) complex **4**^{Phe} exhibits an absorption band around 290 nm (shoulder), which can be assigned to the metal-to-ligand charge transfer transition (MLCT) in the d-π interaction as previously reported for the other copper(I)-arene complexes (see Table 4).[41] When CH_3CN was added into the CH_2Cl_2 solution of complex **4**^{Phe}, the shoulder band around 290 nm gradually disappeared (Figure 10). This may be due to the ligand exchange reaction between the aromatic ring of the ligand sidearm and the added CH_3CN as in the case of ^{H}Pye2^{R} system (Scheme 1). The association constant of CH_3CN to the copper(I) complex,

K_{as} = [$Cu^{I}L$•CH_3CN]/[$Cu^{I}L$][CH_3CN], was then determined as 3360 ± 17 M^{-1} at –20 °C in CH_2Cl_2 by analyzing the spectral change of the titration (the inset of Figure 10). The K_{as} value of complex $\mathbf{4}^{\mathbf{Phe}}$ is significantly larger than that of the copper(I) complex $\mathbf{2}^{\mathbf{H-Phe}}$ (6.4 M^{-1} from Table 4). Thus, the acetonitrile binding is much stronger in $\mathbf{4}^{\mathbf{Phe}}$ than in $\mathbf{2}^{\mathbf{H-Phe}}$. This, on the other hand, indicates that the η^1-binding interaction in $\mathbf{4}^{\mathbf{Phe}}$ is much weaker than the η^2-binding interaction in $\mathbf{2}^{\mathbf{H-Phe}}$.[53]

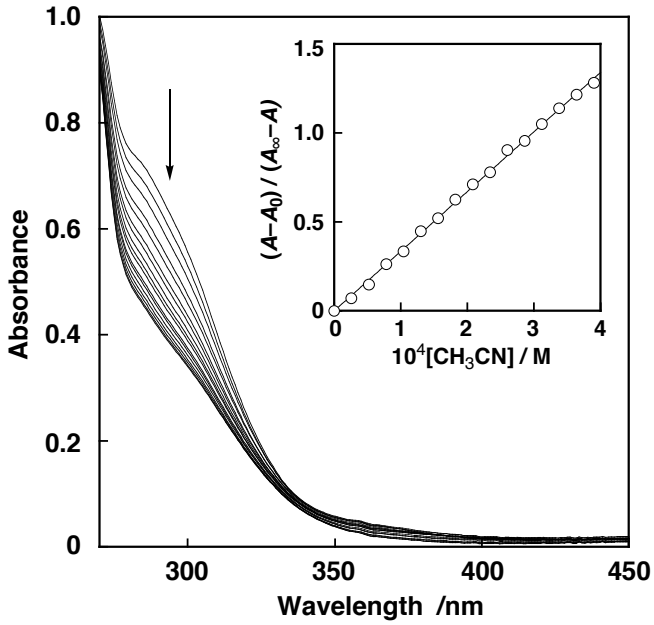

Figure 10. Spectral change for the titration of [Cu^{I}(^{H}Pym2^{Phe})]ClO_4 ($\mathbf{4}^{\mathbf{Phe}}$) (1.0 x 10^{-4} M) with CH_3CN in CH_2Cl_2 at –20 °C. Inset: plot of $(A–A_0)/(A_\infty–A)$ *vs*. [CH_3CN] based on the absorption change at 290 nm.

In the cyclic voltametric measurement in CH_2Cl_2, complex $\mathbf{4}^{\mathbf{Phe}}$ exhibits a quasi-reversible redox couple at $E_{1/2}$ = –0.20 V *vs*. Fc/Fc^+ due to the one-electron redox reaction of the copper center.[54] This value is lower than the redox potential of copper(I) complex $\mathbf{2}^{\mathbf{H-Phe}}$ (0.07 V from Table 6). The negative shift of $E_{1/2}$ in the 2-pyridylmethylamine ligand system (^{H}Pym) as compared to the 2-(2-pyridyl)ethylamine ligand (^{H}Pye) clearly indicates that the pyridine donor ability of the former ligand (^{H}Pym2^{Phe}) is higher than that of the later one (^{H}Pye2^{H-Phe}). The higher donor ability of the 2-pyridylmethylamine ligand (^{H}Pym) can be simply attributed to the chelate ring size effect, which is normally in the order of 5-member ring > 6-member ring.[25] Thus, it can be said that the tridentate ligand with stronger donor ability (^{H}Pym2^{Phe}) affords the weaker d-π interaction with the η^1-binding mode, whereas

the tridentate ligands with weaker donor ability (^{H}Pye2$^{H–Phe}$) tend to provide the stronger d-π interaction with the η^2-binding mode. Steric effects induced by the different chelate-ring size between ^{H}Pym2^{Phe} (5-member ring) and ^{H}Pye2$^{H–Phe}$ (6-member ring) might also be an important factor controlling the binding mode of d-π interaction (η^1 vs η^2) though.

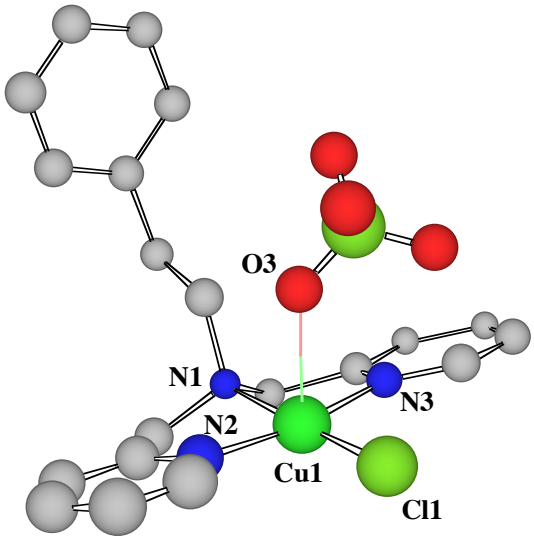

Figure 11. Chem 3D view of the crystal structure of [Cu^{II}(^{H}Pym2^{Phe})Cl]ClO$_4$ (**5**^{Phe}). The hydrogen atoms are omitted for clarity.

As described above, stability of the copper(I) complexes of ^{H}Pym2^{R} was significantly enhanced when the alkyl substituent R was replaced from benzyl (Bn) to phenylethyl (Phe). Nonetheless, complex **4**^{Phe} decomposed very slowly to give a copper(II) complex [Cu^{II}(^{H}Pym2^{Phe})(Cl)]ClO$_4$ (**5**^{Phe}) in a 88 % yield.[50] Crystal structure of complex **5**^{Phe} is shown in Figure 11, and the crystallographic data and the selected bond distances and angles are presented in Tables 9 and 10, respectively. The copper(II) ion has a square planar geometry consisted of the N_3Cl donor set, where there is no d-π interaction between the cupric ion and the phenyl ring of Phe, but the perchlorate anion weakly coordinates to the copper(II) ion from the axial direction [Cu(1)–O(3): 2.75 Å]. Deviation of the copper ion from the least square plane consisted of the N_3Cl donor set is only 0.0219 Å.

Copper(I)-Dioxygen Reactivity of Complex 4^{Phe}. Reaction of [Cu^{I}(^{H}Pym2^{Phe})]ClO$_4$ (**4**^{Phe}) and dioxygen at –94 °C in acetone gave an unstable intermediate exhibiting an absorption band at 385 nm (ε = ~8000 M^{-1} cm^{-1}) (Figure 12). The time course of the absorption change can be fitted by second-order kinetics, and the second-order rate constant

(k_{obs}) was obtained from the slope of the liner line of the second-order plot shown in the inset of Figure 12. The second-order dependence on the intermediate has also been confirmed by the result that the second-order rate constants (k_{obs}) obtained at various initial concentrations of $\mathbf{4}^{\mathbf{Phe}}$ were inversely proportional to the initial concentration of $\mathbf{4}^{\mathbf{Phe}}$ as expected from the equation of the second-order plot: $(A_0 - A)/\{(A - A_\infty)[\mathbf{4}^{\mathbf{Phe}}]_0\} = k_{obs}t$. The second-order kinetics clearly indicates that two molecules of the copper complex are involved in the rate-determining step (rds) of the intermediate formation process. It has been presumed that the bimolecular reaction between a mononuclear (superoxo)copper(II) complex, generated by the reaction of $\mathbf{4}^{\mathbf{Phe}}$ and O_2, and another molecule of copper(I) complex $\mathbf{4}^{\mathbf{Phe}}$ is the rate-determining step.[12] Thus, the 385 nm-intermediate of the oxygenation reaction is a dicopper complex involving an oxygen atom bridge(s). In fact, stoichiometry of the reaction was Cu : O_2 = 2 : 1 (± 0.03) (determined by manometry), and the solution of oxygenated intermediate was ESR-silent.

Judging from the accumulated experimental data in copper(I)/dioxygen chemistry,[1,48,55,56] the above results strongly indicate that the dicopper complex is a bis(μ-oxo)dicopper(III) complex (**B**, see Chart 2). The λ_{max} value (385 nm) of the dicopper complex is very close to that of Suzuki's bis(μ-oxo)dicopper(III) complex supported by Me_2-TPA ligand [bis(6-methyl-2-pyridylmethyl)(2-pyridylmethyl)amine] (λ_{max} = 378 nm),[18] but is different from that of the (μ-η^2:η^2-peroxo)dicopper(II) complex (**A**) generated from copper(I) complex $\mathbf{2}^{\mathbf{H-Phe}}$ (λ_{max} = 362 nm).[57] Moreover, the oxygenated dicopper complex exhibits no distinct LMCT band around 530 nm that should appear if the dicopper complex were a (μ-η^2:η^2-peroxo)dicopper(II) complex (**A**).[58] Unfortunately, however, instability of the oxygenated intermediate has precluded us to obtain the resonance Raman data.

The bis(μ-oxo)dicopper(III) complex supported by $^{H}Pym2^{Phe}$ was not stable and decomposed even at the low temperature to cause aliphatic ligand hydroxylation at the benzylic position of the phenethyl sidearm (~18 % yield based on the copper(I) starting material; the maximum yield is 50 %).[59] The decomposition rates were determined from the decay of the absorption band at 385 nm due to the bis(μ-oxo) complex at various temperatures. The decomposition reaction obeys first-order kinetics, and $\ln(k_{obs}/T)$ is plotted against T^{-1} to give an Eyring plot (Figure 13), from which the activation parameters have been determined as $\Delta H^{\ddagger}$= 6.3 ± 0.3 kcal mol^{-1} and $\Delta S^{\ddagger}$= –34.0 ± 1.5 cal K^{-1} mol^{-1}. The $\Delta H^{\ddagger}$ value is relatively similar to that of the aliphatic ligand hydroxylation in the bis(μ-oxo)dicopper(III) complex supported by the didentate ligand ($^{H}Pye1^{Phe,Et}$:

N-ethyl-*N*-[2-(2-pyridyl)ethyl]-2-phenylethylamine) ($\Delta H^{\ddagger}$= 9.3 ± 0.1 kcal mol^{-1}), while the $\Delta S^{\ddagger}$ value is negatively lager than that of the ^{H}Pye1^{Phe,Et} system ($\Delta S^{\ddagger}$= –17.3 ± 0.4 cal K^{-1} mol^{-1}),[13] suggesting that the transition state is more highly ordered in the present reaction system as compared to that in the didentate ligand system.

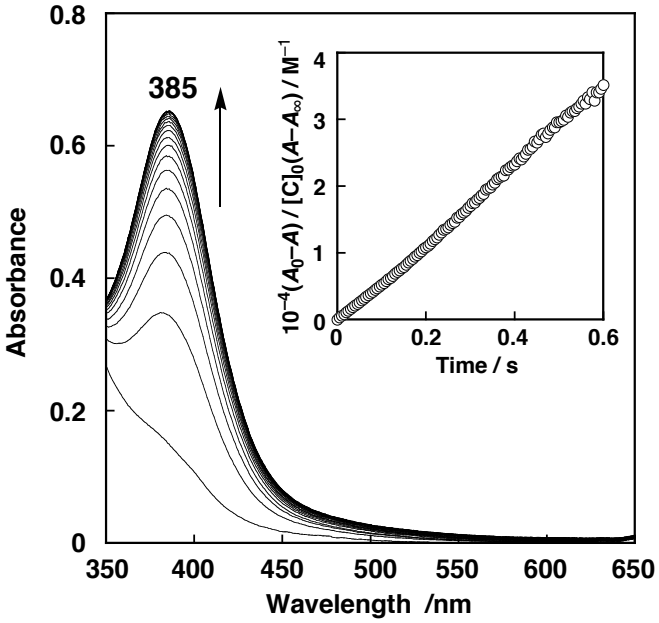

Figure 12. Spectral change observed upon introduction of O_2 gas into an acetone solution of **4**^{Phe} (2.0 x 10^{-4} M) at –94 °C. Inset: second-order plot based on the absorption change at 385 nm.

Consequently, the changing of the ethylene linker (-CH_2CH_2-) of ^{H}Pye2$^{H–Phe}$ to the methylene linker (-CH_2-) to give ^{H}Pym2^{Phe} resulted in a drastic change in the structure of oxygenated dicopper intermediate; (μ-η^2:η^2-peroxo)dicopper(II) complex (**A**) *vs.* bis(μ-oxo)dicopper(III) complex (**B**) (Chart 2). In other words, ^{H}Pym2^{Phe} ligand induces the O–O bond cleavage of a μ-peroxo dicopper(II) complex (**A**) to give the bis(μ-oxo)dicopper(III) complex (**B**) as the oxygenation product. Furthermore, the formation rate constant (k_{obs} = 5.9 x 10^4 M^{-1} s^{-1} at –94 °C in acetone) of the bis(μ-oxo)dicopper(III) complex of ^{H}Pym2^{Phe} is significantly larger than that of the (μ-η^2:η^2-peroxo)dicopper(II) complex of ^{H}Pye2$^{H–Phe}$ (1.21 M^{-1} s^{-1}) under the same experimental conditions. These results can be explained by taking account of the difference in electron-donor ability of the pyridine nitrogen in the tridentate ligand systems as discussed above. Namely, the ^{H}Pym2^{Phe} ligand with the stronger donor ability can support the higher oxidation state of copper(III) of the

bis(μ-oxo) complex (**B**), but the ^{H}Pye2$^{H–Phe}$ with the lower donor ability can only support the (μ-η^2:η^2-peroxo)dicopper(II) complex (**A**). This conclusion is consistent with the lower oxidation potential of the copper(I) complex of ^{H}Pym2^{Phe} (–0.20 V *vs*. Fc/Fc$^+$) as compared to that of the copper(I) complex of ^{H}Pye2$^{H–Phe}$ (0.08 V *vs*. Fc/Fc$^+$).

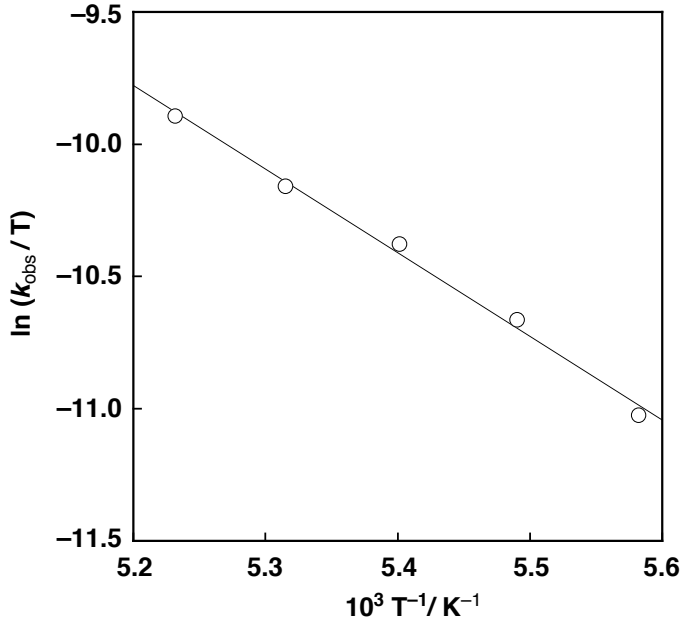

Figure 13. Eyring plot for the ligand hydroxylation of $[Cu^{III}_2(^{H}Pym2^{Phe})_2(\mu\text{-}O)_2](ClO_4)_2$.

4. Copper(I) Complexes 3^{R} of Bis(6-methyl-2-pyridylmethyl)amine Tridentate Ligands (^{Me}Pym2^{R}).

In the last section of this chapter, effects of 6-methyl pyridine have been also investigated in the bis(2-pyridylmethyl)amine tridentate ligand system.

Synthesis and Characterization of Copper(I) Complexes 3^{R}. The tridentate ligands [^{Me}Pym2^{R}; R = -CH_2Ph (Bn), -CH_2CH_2Ph (Phe) and -CH_2CHPh_2 (Phe–Ph)] (Chart 6) were prepared by reductive coupling of the corresponding amines (RNH_2) and 2 equiv of 6-methyl-2-pyridinecarboxaldehyde in the presence of $NaBH_3CN$ as the reductant. Treatment of the ligand with an equimolar amount of $[Cu^{I}(CH_3CN)_4]ClO_4$ under anaerobic conditions (Ar) gave the corresponding copper(I) complexes **3^{R}** as ClO_4^- salts. In the case of **3^{Bn}**, single

crystals of the CH_3CN-containing complex, **3^{Bn}•CH_3CN**, were obtained as a PF_6^- salt which was prepared by the salt exchange reaction of the ClO_4^--complex with NH_4PF_6. **3^{Bn}•CH_3CN** can be easily converted into air-stable carbonyl complex **3^{Bn}•CO** by treating it with CO gas. Furthermore, the CO ligand in **3^{Bn}•CO** can be easily removed by heating it at 75 °C for 10 min to give complex **3^{Bn}** without any external ligand. Crystal structures of $[Cu^I(^{Me}Pym2^{Phe})]ClO_4$ (**3^{Phe}**), $[Cu^I(^{Me}Pym2^{Phe-Ph})]ClO_4$ (**3^{Phe-Ph}**), $[Cu^I(^{Me}Pym2^{Bn})(CH_3CN)]PF_6$ (**3^{Bn}•CH_3CN**) and $[Cu^I(^{Me}Pym2^{Bn})(CO)]ClO_4$ (**3^{Bn}•CO**) have been determined by X-ray crystallographic analysis as shown in Figure 14. The crystallographic data of the complexes are presented in Table 11, and their selected bond lengths and angles around the copper ion are summarized in Table 12.

Chart 6

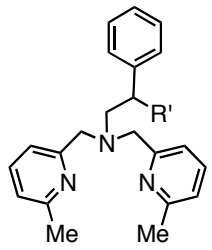

$^{Me}Pym2^{R}$

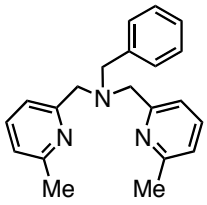

$^{Me}Pym2^{Bn}$

$^{Me}Pym2^{Phe}$: R' = H
$^{Me}Pym2^{Phe-Ph}$; R' = Ph

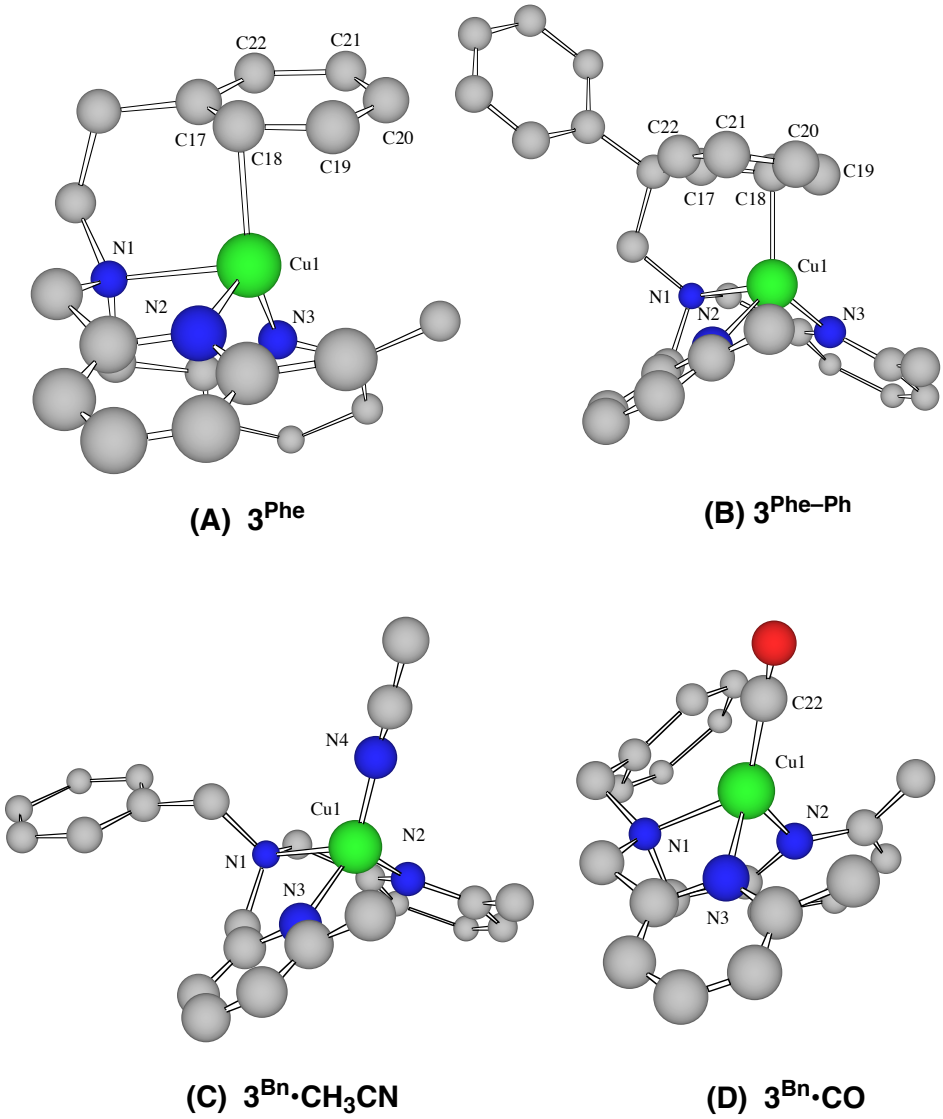

Figure 14. Chem 3D views of the crystal structures of (A) $[Cu^{I}(^{Me}Pym2^{Phe})]ClO_4$ (**3^{Phe}**), (B) $[Cu^{I}(^{Me}Pym2^{PhePh})]ClO_4$ (**$3^{Phe–Ph}$**), (C) $[Cu^{I}(^{Me}Pym2^{Bn})(CH_3CN)]PF_6$ (**3^{Bn}•CH_3CN**), and (D) $[Cu^{I}(^{Me}Pym2^{Bn})(CO)]ClO_4$ (**3^{Bn}•CO**). The counter anions and hydrogen atoms are omitted for clarity.

Table 11. Summary of the X-ray Crystallographic Data for Complexes **3^{Phe}**, **3$^{Phe–Ph}$**, **3^{Bn}•CH$_3$CN**, and **3^{Bn}•CO**

	3^{Phe}	**3$^{Phe–Ph}$**
empirical formula	$C_{22}H_{25}N_3CuClO_4$	$C_{28}H_{29}N_3CuClO_4$
formula weight	494.46	570.55
crystal system	monoclinic	triclinic
space group	$P2_1/n$ (#14)	P1 (#1)
a, Å	11.7088(3)	7.715(4)
b, Å	14.6661(5)	8.887(6)
c, Å	12.4843(4)	9.361(6)
α, deg		83.77(3)
β, deg	93.147(1)	88.29(2)
χ, deg		75.93(3)
V, Å^3	2140.6(1)	618.9(6)
Z	4	1
F(000)	1024.00	296.00
D_{calc}, g/cm^3	1.534	1.531
T, °C	–115	–115
crystal size, mm	0.20 x 0.20 x 0.10	0.40 x 0.10 x 0.10
μ (MoKα), cm^{-1}	11.80	10.32
diffractometer	Rigaku RAXIS-RAPID	Rigaku RAXIS-RAPID
radiation	MoKα (0.71069 Å)	MoKα (0.71075 Å)
$2\theta_{max}$, deg	54.9	55.0
no. of reflns measd	20832	5544
no. of reflns obsd	3743 [$I > 3.0\sigma(I)$]	2647 [$I > 0.1\sigma(I)$]
no. of variables	306	364
R [a]	0.031	0.046
R_w [b]	0.043	0.050
GOF	0.88	0.86

[a] $R = \Sigma||F_o| - |F_c||/\Sigma|F_o|$. [b] $R_w=\{\Sigma w(|F_o| - |F_c|)^2/\Sigma wF_o^2\}^{1/2}$.

Table 11. Summary of the X-ray Crystallographic Data for Complexes **3^{Phe}**, **3$^{Phe–Ph}$**, **3^{Bn}•CH$_3$CN**, and **3^{Bn}•CO** (continued)

	3^{Bn}•CH$_3$CN	**3^{Bn}•CO**
empirical formula	$C_{23}H_{26}N_4CuPF_6$	$C_{22}H_{23}N_3O_5CuCl$
formula weight	567.00	508.44
crystal system	monoclinic	triclinic
space group	$P2_1/c$	P-1
a, Å	14.380(2)	11.159(2)
b, Å	7.196(2)	17.147(2)
c, Å	25.291(4)	12.387(2)
α, deg		88.88(1)
β, deg	99.58(1)	109.24(1)
χ, deg		91.35(1)
V, Å^3	2580.6(9)	2237.1(6)
Z	4	4
F(000)	1160.00	1048.00
D_{calc}, g/cm^3	1.459	1.510
T, °C	22	–120
crystal size, mm	0.30 x 0.25 x 0.15	0.40 x 0.25 x 0.25
μ (MoKα), cm^{-1}	9.70	11.35
diffractometer	Rigaku *R*-axis IV	Rigaku *R*-axis IV
radiation	MoKα (λ = 0.71070 Å)	MoKα (λ = 0.71070 Å)
$2\theta_{max}$, deg	51.4	51.6
no. of reflns measd	4365	7193
no. of reflns obsd	3616 [$I > 3.0\sigma(I)$]	6582 [$I > 3.0\sigma(I)$]
no. of variables	317	577
R [a]	0.087	0.044
R_w [b]	0.132	0.073
GOF	1.91	1.39

[a] $R = \Sigma||F_o| - |F_c||/\Sigma|F_o|$. [b] $R_w = \{\Sigma w(|F_o| - |F_c|)^2/\Sigma wF_o^2\}^{1/2}$.

Table 12. Selected Bond Lengths (Å) and Angles (deg) of Complexes $\mathbf{3^{Phe}}$, $\mathbf{3^{Phe–Ph}}$, $\mathbf{3^{Bn}•CH_3CN}$, and $\mathbf{3^{Bn}•CO}$

		Complex $\mathbf{3^{Phe}}$	
Cu(1)–N(1)	2.201(2)	Cu(1)–N(2)	2.056(2)
Cu(1)–N(3)	2.008(2)	Cu(1)–C(17)	2.629
Cu(1)–C(18)	2.148(3)	Cu(1)–C(19)	2.499(3)
C(17)–C(18)	1.415(4)	C(18)–C(19)	1.402(4)
C(19)–C(20)	1.392(4)	C(20)–C(21)	1.391(4)
C(21)–C(22)	1.373(4)	C(17)–C(22)	1.403(4)
N(1)–Cu(1)–N(2)	81.68(8)	N(1)–Cu(1)–N(3)	84.33(8)
N(2)–Cu(1)–N(3)	116.25(9)	N(1)–Cu(1)–C(18)	96.3(1)
N(2)–Cu(1)–C(18)	103.75(9)	N(3)–Cu(1)–C(18)	139.57(9)
N(1)–Cu(1)–C(19)	129.61(9)	N(2)–Cu(1)–C(19)	111.35(9)
N(3)–Cu(1)–C(19)	124.81(9)	C(18)–Cu(1)–C(19)	34.1(1)
		Complex $\mathbf{3^{Phe–Ph}}$	
Cu(1)–N(1)	2.191(5)	Cu(1)–N(2)	1.970(4)
Cu(1)–N(3)	2.048(5)	Cu(1)–C(17)	2.639
Cu(1)–C(18)	2.165(5)	Cu(1)–C(19)	2.424(6)
C(17)–C(18)	1.385(8)	C(17)–C(22)	1.376(8)
C(18)–C(19)	1.401(8)	C(19)–C(20)	1.373(8)
C(20)–C(21)	1.365(8)	C(21)–C(22)	1.384(8)
N(1)–Cu(1)–N(2)	84.5(2)	N(1)–Cu(1)–N(3)	80.8(2)
N(2)–Cu(1)–N(3)	115.6(2)	N(1)–Cu(1)–C(18)	90.3(2)
N(2)–Cu(1)C(18)	132.0(2)	N(3)–Cu(1)–C(18)	110.6(2)
N(1)–Cu(1)C(19)	125.2(2)	N(2)–Cu(1)–C(19)	124.9(2)
N(3)–Cu(1)C(19)	114.5(2)	C(18)–Cu(1)–C(19)	35.0(2)

Table 12. Selected Bond Lengths (Å) and Angles (deg) of Complexes $\mathbf{3^{Phe}}$, $\mathbf{3^{Phe–Ph}}$, $\mathbf{3^{Bn}•CH_3CN}$, and $\mathbf{3^{Bn}•CO}$ (continued)

Complex $\mathbf{3^{Bn}•CH_3CN}$			
Cu(1)–N(1)	2.215(4)	Cu(1)–N(2)	2.050(5)
Cu(1)–N(3)	2.051(5)	Cu(1)–N(4)	1.918(6)
N(1)–Cu(1)–N(2)	80.3(2)	N(1)–Cu(1)–N(3)	82.1(2)
N(1)–Cu(1)–N(4)	119.1(2)	N(2)–Cu(1)–N(3)	115.1(2)
N(2)–Cu(1)–N(4)	120.8(2)	N(3)–Cu(1)–N(4)	122.4(2)
Complex $\mathbf{3^{Bn}•CO}$			
Molecular 1			
Cu(1)–N(1)	2.131(3)	Cu(1)–N(2)	2.042(2)
Cu(1)–N(3)	2.063(3)	Cu(1)–C(22)	1.806(3)
N(1)–Cu(1)–N(2)	83.73(9)	N(1)–Cu(1)–N(3)	80.51(10)
N(1)–Cu(1)–C(22)	127.7(1)	N(2)–Cu(1)–N(3)	105.22(9)
N(2)–Cu(1)–C(22)	129.0(1)	N(3)–Cu(1)–C(22)	117.6(1)
Molecular 2			
Cu(2)–N(4)	2.124(3)	Cu(2)–N(5)	2.054(3)
Cu(2)–N(6)	2.051(3)	Cu(2)–C(44)	1.800(3)
N(4)–Cu(2)–N(5)	83.68(10)	N(4)–Cu(2)–N(6)	80.6(1)
N(4)–Cu(2)–C(44)	129.0(1)	N(5)–Cu(2)–N(6)	108.0(1)
N(5)–Cu(2)–C(44)	121.8(1)	N(6)–Cu(1)–C(44)	122.2(1)

d-π Interaction in $\mathbf{3^R}$. Copper(I) complexes $\mathbf{3^{Phe}}$ and $\mathbf{3^{Phe–Ph}}$ involving -CH_2CH_2Ph (Phe) and -CH_2CHPh_2 (Phe–Ph) sidearm, respectively, exhibit a copper(I)-arene interaction in

crystals, where the phenyl ring of the ligand sidearm exists just above the cuprous ion as shown in Figure 14A and 14B, respectively. The cuprous ion of each complex adapts to a trigonal pyramidal geometry consisting of the two pyridine nitrogen atoms N(2) and N(3) and one of the *ortho*-carbon atoms of the phenyl ring C(18) occupying the trigonal basal plane and the tertiary alkyl amine nitrogen atom N(1) as the axial ligand. Deviation of the copper(I) ion from the basal plane is 0.076 Å and 0.163 Å in $\mathbf{3}^{\mathbf{Phe}}$ and $\mathbf{3}^{\mathbf{Phe–Ph}}$, respectively. It should be noted that the distances between Cu and C(18) (2.148 Å in $\mathbf{3}^{\mathbf{Phe}}$ and 2.165 Å in $\mathbf{3}^{\mathbf{Phe–Ph}}$) is much shorter than Cu–C(17) distances (2.629 Å in $\mathbf{3}^{\mathbf{Phe}}$ and 2.639 Å in $\mathbf{3}^{\mathbf{Phe–Ph}}$). Thus, the copper(I)-arene interaction in these complexes can be described as an η^1-binding interaction.

As already discussed in the previous section, copper(I) complexes $\mathbf{2}^{\mathbf{R}}$ (R = H–Phe, Phe–Me, and Phe–Ph: $-CH_2CH(X)Ph$ where X = H, Me, and Ph, respectively) supported by $^{H}Pye2^{R}$ with the longer ethylene linker exhibit a distorted tetrahedral geometry involving a d-π interaction with an η^2-binding mode, while complex $\mathbf{4}^{\mathbf{Phe}}$ with $^{H}Pym2^{Phe}$ shows a trigonal pyramidal structure involving a d-π interaction with an η^1-binding mode. (see Figures 1 and 9) Thus, the copper(I)-arene interaction in $\mathbf{3}^{\mathbf{R}}$ resembles that in complex $\mathbf{4}^{\mathbf{Phe}}$. In fact, the distances from the copper(I) ion to the aromatic carbon atom and to the ligand nitrogen atoms in $\mathbf{3}^{\mathbf{Phe}}$ and $\mathbf{3}^{\mathbf{Phe–Ph}}$ are similar to those in $\mathbf{4}^{\mathbf{Phe}}$.

In the UV-vis spectra, copper(I) complexes $\mathbf{3}^{\mathbf{Phe}}$ and $\mathbf{3}^{\mathbf{Phe–Ph}}$ exhibit a characteristic absorption band around 270 nm (Table 13), which has been tentatively assigned to an MLCT (metal-to-ligand charge transfer) band through the d-π interaction as in the case of other copper(I) complexes exhibiting a d-π interaction.[41] Relative strength of the d-π interaction can be evaluated by the competitive binding of CH_3CN to the cuprous ion (titration of $\mathbf{3}^{\mathbf{R}}$ by CH_3CN) in a non-polar solvent such as CH_2Cl_2. The MLCT band around 270 nm gradually decreased, when CH_3CN was added into a CH_2Cl_2 solution of $\mathbf{3}^{\mathbf{R}}$. In Figure 15 is shown the spectral change for the titration of complex $\mathbf{3}^{\mathbf{Phe}}$ by CH_3CN in CH_2Cl_2 at –20 °C as a typical example. Decrement of the absorption band around 270 nm may be due to the ligand exchange reaction between the phenyl ring of the d-π interaction and the added CH_3CN. The association constant of CH_3CN to the copper(I) ion of $\mathbf{3}^{\mathbf{Phe}}$, $K_{as} = [Cu^{I}L{\bullet}CH_3CN]/[Cu^{I}L][CH_3CN]$, was then determined as 622 ± 15 M^{-1} by analyzing the absorption change as indicated in the inset of Figure 15, and the K_{as} values for $\mathbf{3}^{\mathbf{Phe–Ph}}$ and $\mathbf{3}^{\mathbf{Bn}}$ were determined similarly as listed in Table 13, where the K_{as} values for $\mathbf{2}^{\mathbf{H–Phe}}$ and $\mathbf{4}^{\mathbf{Phe}}$ are also included for comparison.

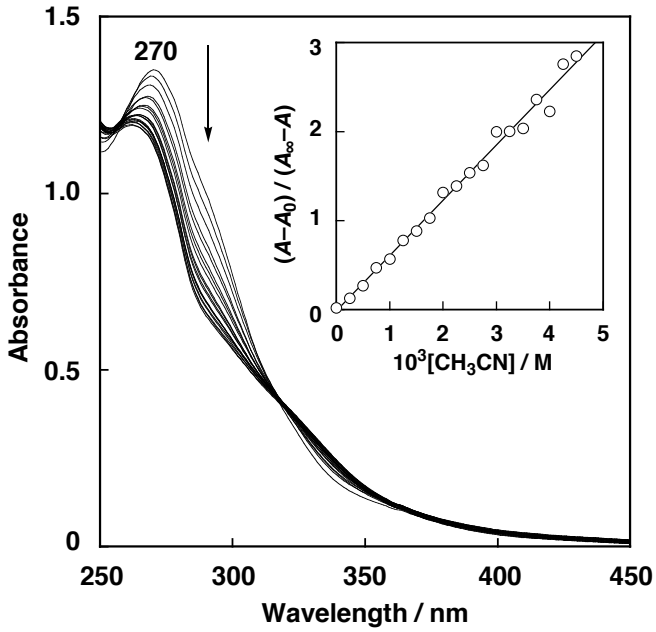

Figure 15. Spectral change in the titration of $\mathbf{3}^{\mathbf{Phe}}$ (1.0×10^{-4} M) with CH_3CN at –20 ˚C in CH_2Cl_2. at –20 ˚C. Inset: plot of $(A - A_0)/(A_\infty - A)$ *vs*. [CH_3CN] based on the absorption change at 270 nm.

Table 13. The UV-vis Data and the Equilibrium Constants K_{as} for the Titration of Copper(I) Complexes with CH_3CN in CH_2Cl_2[a]

Complex	λ_{max}, nm (ε, M^{-1} cm^{-1})	K_{as}, M^{-1}
$\mathbf{2}^{\mathbf{H–Phe}}$	290 (8820)	6.4 ± 0.1
$\mathbf{3}^{\mathbf{Phe}}$	270 (13500)	622 ± 15
$\mathbf{3}^{\mathbf{Phe–Ph}}$	270 (13100)	230 ± 6.0
$\mathbf{3}^{\mathbf{Bn}}$	285 [b] (20900)	4470 ± 330
$\mathbf{4}^{\mathbf{Phe}}$	290 (6010)	3360 ± 17

[a] At –20 °C. [b] Shoulder.

The K_{as} value may reflect the strength of the d-π interaction in the copper(I) complexes. Namely, the smaller the K_{as} value (thus, weaker the CH_3CN-binding), the stronger the d-π interaction as discussed in the previous sections. As clearly seen in Table 13, the K_{as} values of $\mathbf{3}^{\mathbf{Phe}}$ and $\mathbf{3}^{\mathbf{Phe–Ph}}$ are much larger than that of $\mathbf{2}^{\mathbf{H–Phe}}$ having the η^2-binding interaction, but are

smaller than that of $\mathbf{4}^{\mathbf{Phe}}$. Thus, the strength of d-π interaction decreases in the order of $\mathbf{2}^{\mathbf{H–Phe}} > \mathbf{3}^{\mathbf{R}} > \mathbf{4}^{\mathbf{Phe}}$ (the strength of d-π interaction in $\mathbf{3}^{\mathbf{Bn}}$ is discussed below). Although the theoretical aspects of the d-π interaction have yet to be addressed in detail, the order of strength of the d-π interaction seems to be corelated to the order of the electron-donor ability of ligand; $\mathbf{2}^{\mathbf{R}} < \mathbf{3}^{\mathbf{R}} < \mathbf{4}^{\mathbf{R}}$ (the order of electron-donor ability of pyridine is discussed below). Namely, the d-π interaction becomes stronger ($\mathbf{2}^{\mathbf{R}} > \mathbf{3}^{\mathbf{R}} > \mathbf{4}^{\mathbf{R}}$) as the electron donor ability of ligands becomes weaker ($\mathbf{2}^{\mathbf{R}} < \mathbf{3}^{\mathbf{R}} < \mathbf{4}^{\mathbf{R}}$). On the other hand, the meaningful difference in K_{as} between $\mathbf{3}^{\mathbf{Phe}}$ and $\mathbf{3}^{\mathbf{Phe–Ph}}$ can be attributed to a steric effect of the benzylic substituent (Ph) in $\mathbf{3}^{\mathbf{Phe–Ph}}$, which prohibit free rotation of the ligand sidearm, thus stabilizing the d-π interaction (see Scheme 3).

Copper(I) Complexes of $^{\mathbf{Me}}\mathbf{Pym2}^{\mathbf{Bn}}$. Crystal structures of $\mathbf{3}^{\mathbf{Bn}}\bullet\mathbf{CH_3CN}$ and $\mathbf{3}^{\mathbf{Bn}}\bullet\mathbf{CO}$ are shown in Figure 14C and 14D, respectively. Copper(I) complex $\mathbf{3}^{\mathbf{Bn}}\bullet\mathbf{CH_3CN}$ exhibits a distorted trigonal pyramidal structure with a N_4 donor set, where two pyridine nitrogen atoms N(2) and N(3) and acetonitrile nitrogen N(4) occupy the trigonal basal plane and tertiary amine nitrogen N(1) acts as an axial ligand. The axial ligand N(1), however, largely slips out of the ideal position of the apex of trigonal pyramidal geometry. Apparently, there is no interaction between the cuprous ion and the phenyl group of the ligand sidearm ($-CH_2Ph$) in $\mathbf{3}^{\mathbf{Bn}}\bullet\mathbf{CH_3CN}$.

The unit cell of copper(I) complex $\mathbf{3}^{\mathbf{Bn}}\bullet\mathbf{CO}$ consists of two crystallographically independent molecules. Both of the cuprous centers of $\mathbf{3}^{\mathbf{Bn}}\bullet\mathbf{CO}$ have also a distorted trigonal pyramidal (or a significantly distorted tetrahedral) geometry where CH_3CN ligand in $\mathbf{3}^{\mathbf{Bn}}\bullet\mathbf{CH_3CN}$ is replaced by CO molecule. In this complex as well, there is no d-π interaction between the metal center and the phenyl group of the benzyl substituent.

The CO ligand in $\mathbf{3}^{\mathbf{Bn}}\bullet\mathbf{CO}$ can be easily removed by heating it in methanol to give $\mathbf{3}^{\mathbf{Bn}}$ involving no external ligand. Although structural examination of $\mathbf{3}^{\mathbf{Bn}}$ has yet to be accomplished due to its instability in solution, complex $\mathbf{3}^{\mathbf{Bn}}$ exhibits a shoulder absorption band at 285 nm in CH_2Cl_2. This absorption band disappeared when acetonitrile was added into the solution of $\mathbf{3}^{\mathbf{Bn}}$, and the final spectrum of the titration was identical to that of $\mathbf{3}^{\mathbf{Bn}}\bullet\mathbf{CH_3CN}$ [λ_{max} = 313 nm (ε = 7700 M^{-1} cm^{-1})]. Thus, the 285 nm band of $\mathbf{3}^{\mathbf{Bn}}$ can be also attributed to a MLCT transition of a d-π interaction, although the binding mode of copper(I) to the phenyl group is not clear at present. As clearly seen in Table 13, the K_{as} value of $\mathbf{3}^{\mathbf{Bn}}$ is significantly larger than those of $\mathbf{3}^{\mathbf{R}}$ (R = Phe and Phe–Ph) and fairly close to that of $\mathbf{4}^{\mathbf{Phe}}$. This means that the d-π interaction in $\mathbf{3}^{\mathbf{Bn}}$ is much weaker than that in $\mathbf{3}^{\mathbf{Phe}}$ and $\mathbf{3}^{\mathbf{Phe–Ph}}$ and is comparable to that in $\mathbf{4}^{\mathbf{Phe}}$. The weaker interaction could be attributed to the shorter methylene linker between the

amine nitrogen atom and the phenyl ring of ligand sidearm. Namely, the methylene linker may be too short to construct a stable d-π interaction.

Redox Potential of the Copper(I) Complexes $\mathbf{3^R}$. Copper(I) complexes $\mathbf{3^{Phe}}$ and $\mathbf{3^{Phe–Ph}}$ exhibit a quasi-reversible redox couple due to one-electron oxidation-reduction of the copper center in CH_2Cl_2. The redox potentials ($E_{1/2}$ *vs*. Fc/Fc^+) of them are listed in Table 14 together with those of $\mathbf{1^{Phe}}$, $\mathbf{2^{H–Phe}}$ and $\mathbf{4^{Phe}}$. The redox behavior of $\mathbf{3^{Bn}}$ was not so simple probably due to instability of the complex under the present experimental conditions.

As clearly seen in Table 14, the $E_{1/2}$ values of $\mathbf{1^{Phe}}$, $\mathbf{2^{H–Phe}}$, $\mathbf{3^{Phe}}$, and $\mathbf{4^{Phe}}$ decrease in this order ($E_{1/2}$ = 0.30, 0.07 V, –0.06 V, and –0.20 V *vs*. Fc/Fc^+, respectively). The higher $E_{1/2}$ values of $\mathbf{1^{Phe}}$ and $\mathbf{2^{H–Phe}}$ have been attributed to the lower electron-donor ability of pyridine of pyridylethylamine ligands ($^{Me}Pye2^{Phe}$ and $^{H}Pye2^{Phe}$) as compared to that of other ligands, which can be simply attributed to the chelate ring size effect that is normally in the order of 6-member ring < 5-member ring.[25] Then, it becomes apparent that the 6-methyl groups in $\mathbf{1^{Phe}}$ and $\mathbf{3^{Phe}}$ somewhat reduce the electron donor ability of pyridine to cause the negative shift of $E_{1/2}$ as compared to that of $\mathbf{2^{H–Phe}}$ and $\mathbf{4^{Phe}}$, respectively. However, the electron-donor ability of pyridine in $\mathbf{3^{Phe}}$ is still higher than that in $\mathbf{2^{H–Phe}}$, making the order of $E_{1/2}$ as $\mathbf{1^{Phe}} > \mathbf{2^{Phe}} > \mathbf{3^{Phe}} > \mathbf{4^{Phe}}$. The fact that the $E_{1/2}$ value of $\mathbf{3^{Phe–Ph}}$ is somewhat higher than that of $\mathbf{3^{Phe}}$ suggests that the stronger d-π interaction stabilizes the lower oxidation state of copper(I) more than the copper(II) oxidation state. A similar trend was seen in the $\mathbf{2^R}$ system, where the $E_{1/2}$ value of $\mathbf{2^{Phe–Ph}}$ is higher than that of $\mathbf{2^{H–Phe}}$ ($\Delta E_{1/2}$ = 0.08 V; see Table 6).

Copper(I)-Dioxygen Reactivity. Ligand effects on the copper(I)-dioxygen reactivity were also examined. The copper(I) complexes of $^{H}Pye2$-type ligands ($\mathbf{2^R}$) mainly afford (μ-η^2:η^2-peroxo)dicopper(II) complex **A** in the reaction with O_2 at a low temperature (see Scheme 3), whereas the copper(I) complex of $^{H}Pym2^{R}$ ($\mathbf{4^R}$) predominantly affords bis(μ-oxo)dicopper(III) complex **B** in a similar reaction (Figure 12). Thus, it is curious to know what is obtained in the oxygenation reaction of $\mathbf{3^R}$.

Treatment of copper(I) complexes $\mathbf{3^{Phe}}$ with O_2 in anhydrous acetone at –80 °C readily afforded a brown color solution which exhibited an intense absorption band at 355 nm (ε = 18700 M^{-1} cm^{-1}) together with a relatively weak band at 511 nm (770 M^{-1} cm^{-1}) as shown in Figure 16. Similar spectra were obtained in the reaction of $\mathbf{3^{Phe–Ph}}$ and $\mathbf{3^{Bn}}$ under the same experimental conditions (see Table 14 and Figure 17). After a short lag phase (0 ~ 10 s), the reaction obeys second-order kinetics, and the second-order rate constant (k_{obs}) was obtained from the slope of the liner line of the second-order plot shown in the inset of Figure 16. The

second-order kinetics clearly indicates that two molecules of the copper complex are involved in the rate-determining step of the Cu_2/O_2 complex formation process. It can be presumed that the bimolecular reaction between a mononuclear (superoxo)copper(II) complex, generated by the reaction of $\mathbf{3^R}$ and O_2, and another molecule of copper(I) complex is the rate-determining step. The initial lag phase shown in Figure 16 may be due to the time required to attain the pre-equilibrium reaction between the copper(I) complex and O_2 to give the (superoxo)copper(II) intermediate.[13] From the dependence of the rate constants on the reaction temperature shown as Arrhenius plots in Figure 18 were obtained the activation enthalpy ($\Delta H^{\neq}$) of 5.8 ± 0.3 and 8.2 ± 0.3 kJ mol^{-1} and the activation entropy ($\Delta S^{\neq}$) of –140.1 ± 1.6 and –139.1 ± 1.5 J K^{-1} mol^{-1} for the oxygenation reaction of $\mathbf{3^{Phe}}$ and $\mathbf{3^{Phe–Ph}}$, respectively. The significantly large negative $\Delta S^{\neq}$ values are consistent with the proposed mechanism, where the bimolecular reaction between the monomeric (superoxo)copper(II) complex, $[Cu^{II}(^{Me}Pym2^{R})(O_2^{\bullet-})]^+$, and another Cu(I) starting compound is the rate determining step.[12]

Table 14. Redox Potentials ($E_{1/2}$)[a] of the Copper(I) Complexes, UV-vis and Resonance Raman Data of the Cu_2/O_2 Complexes, and the Second-order Rate Constants (k_{obs}) for the Formation of Cu_2/O_2 Complexes at –80 °C in Acetone.

		Cu_2/O_2 complex		
	$E_{1/2}$,	UV-vis	Raman	Formation Rate
Complex	V *vs*. Fc/Fc^{+} [a]	λ_{max}, nm (ε, M^{-1} cm^{-1})	$\nu_{O–O}$ ($\Delta\nu_{16O-18O}$)	k_{obs}, M^{-1} s^{-1}
$\mathbf{1^{Phe}}$•CH_3CN	0.30	NR	NR	NR
$\mathbf{2^{H–Phe}}$	0.07	362 (15400) ~520 (770)	746 (42)	4.1
$\mathbf{3^{Phe}}$	–0.06	355 (18700) 511 (770)	726 (36)	130.0
$\mathbf{3^{Phe–Ph}}$	0.01	356 (16700) ~505 (700)	716 (37)	33.6
$\mathbf{3^{Bn}}$	–	353 (23500) 529 (970)	714 (39)	29.2
$\mathbf{4^{Phe}}$	–0.20	385 (6540)	–	59000 [b]

[a] The electrochemical measurements were performed in CH_2Cl_2 containing 0.1 M tetrabutylammonium perchlorate (TBAP) at a scan rate of 10 ~ 50 mV s^{-1} at 25 ° C. [b] At –94 °C in acetone.

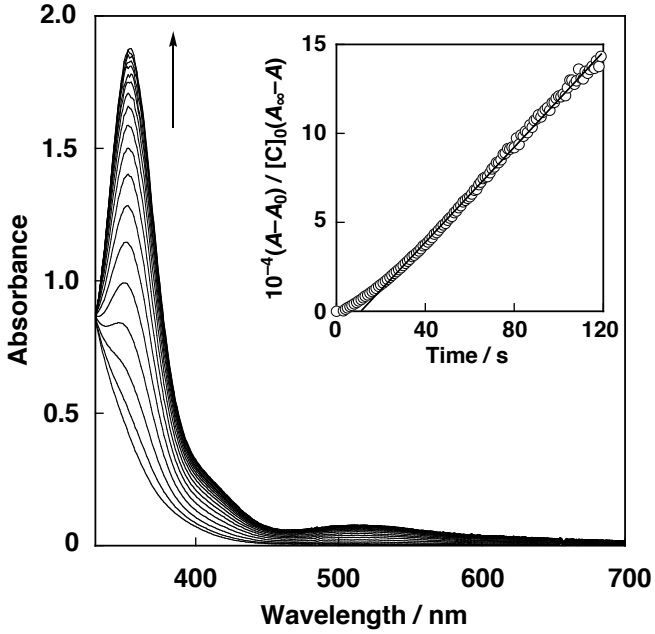

Figure 16. Spectral change observed upon introduction of O_2 gas into acetone solution of $\mathbf{3}^{\mathbf{Phe}}$ (2.0 x 10^{-4} M) at –80 °C. Inset: second-order plot based on the absorption change at 355 nm.

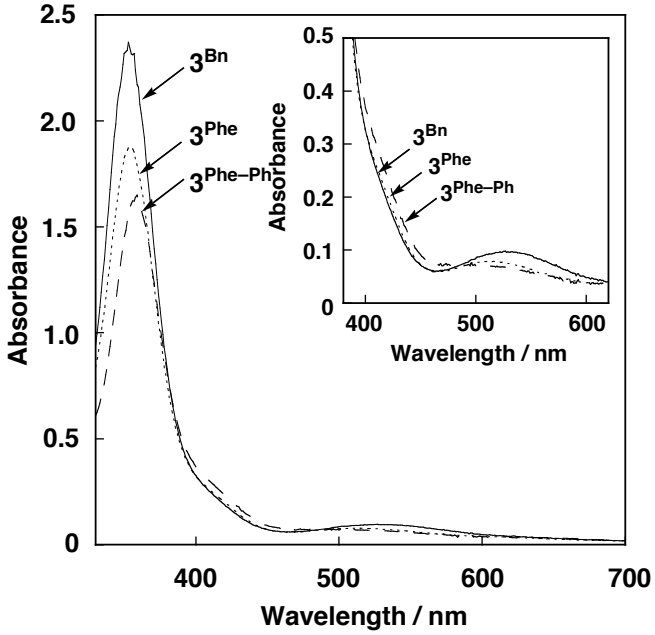

Figure 17. Absorption spectra of the oxygenated products of $\mathbf{3}^{\mathbf{Phe}}$, $\mathbf{3}^{\mathbf{Phe–Ph}}$ and $\mathbf{3}^{\mathbf{Bn}}$ in acetone at –80 °C. The initial concentration of $\mathbf{3}^{\mathbf{Phe}}$, $\mathbf{3}^{\mathbf{Phe–Ph}}$ and $\mathbf{3}^{\mathbf{Bn}}$ is 2.0 x 10^{-4} M.

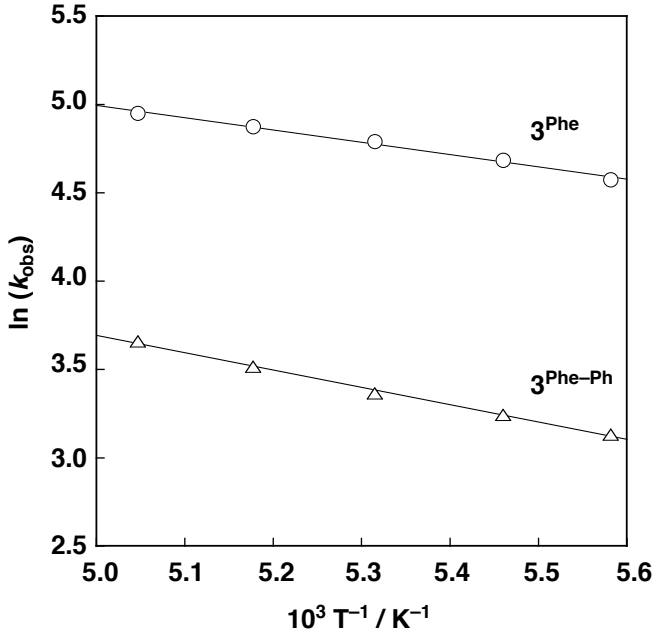

Figure 18. Arrhenius plots for the oxygenation reaction of $\mathbf{3}^{\mathbf{Phe}}$ (○) and $\mathbf{3}^{\mathbf{Phe–Ph}}$ (△).

In all the cases, frozen CH_2Cl_2 solution of the oxygenated product was ESR silent at –150 ˚C. The UV-vis features shown in Figure 17 as well as the ESR-silence strongly suggest that the oxygenated product is (μ-η^2:η^2-peroxo)dicopper(II) complex **A**. It should be noted, however, that intensity of the LMCT bands at ~355 and ~510 nm due to the side-on peroxo complex **A** is somewhat different among the three ligand systems ^{Me}Pym2^{R} (R = Bn, Phe and Phe–Ph, decreasing in this order) and the shoulder ~400 nm seems to grow up in going from ^{Me}Pym2^{Bn} to ^{Me}Pym2$^{Phe–Ph}$. The spectral feature around 400 nm can be attributed to co-existence of a bis(μ-oxo)dicopper(III) complex **B**. This was confirmed by the resonance Raman studies described below.

Figure 19 shows the resonance Raman spectra of the oxygenated product of $\mathbf{3}^{\mathbf{Bn}}$, $\mathbf{3}^{\mathbf{Phe}}$ and $\mathbf{3}^{\mathbf{Phe–Ph}}$ obtained with 514.5 nm excitation in acetone at –90 °C. In all the cases, a relatively intense Raman band at 714~726 cm^{-1} with an isotope shift of 36~39 cm^{-1} with $^{18}O_2$ was obtained. These Raman features have been ascribed to the O–O bond stretching vibration of the side-on peroxo ligand.[60] Thus, the data unambiguously support the formation of (μ-η^2:η^2-peroxo)dicopper(II) complex **A**. In addition, Cu–Cu stretching vibrations in the (μ-η^2:η^2-peroxo)dicopper(II) core were observed at 312 and 280 cm^{-1} for $\mathbf{3}^{\mathbf{Phe–Ph}}$ and 314 and 282 cm^{-1} for $\mathbf{3}^{\mathbf{Phe}}$ (data not shown in Figure 19), further confirming the formation of side-on

peroxo dicopper(II) complex **A**.[61,62] Notably, the frequency of the O–O bond stretching vibration of **A** supported by ^{Me}Pym2^{R} (714~726 cm^{-1}) is relatively lower than that of the ^{H}Pye2^{Phe}-complex (746 cm^{-1}, see Table 14). The results clearly suggest that the O–O bond in the ^{Me}Pym2^{R}-complexes is relatively weakened as compared to that in the ^{H}Pye2$^{H–Phe}$-complex. This could be also attributed to the higher electron-donor ability of pyridine in ^{Me}Pym2^{R} as compared to ^{H}Pye2^{R} as discussed below.

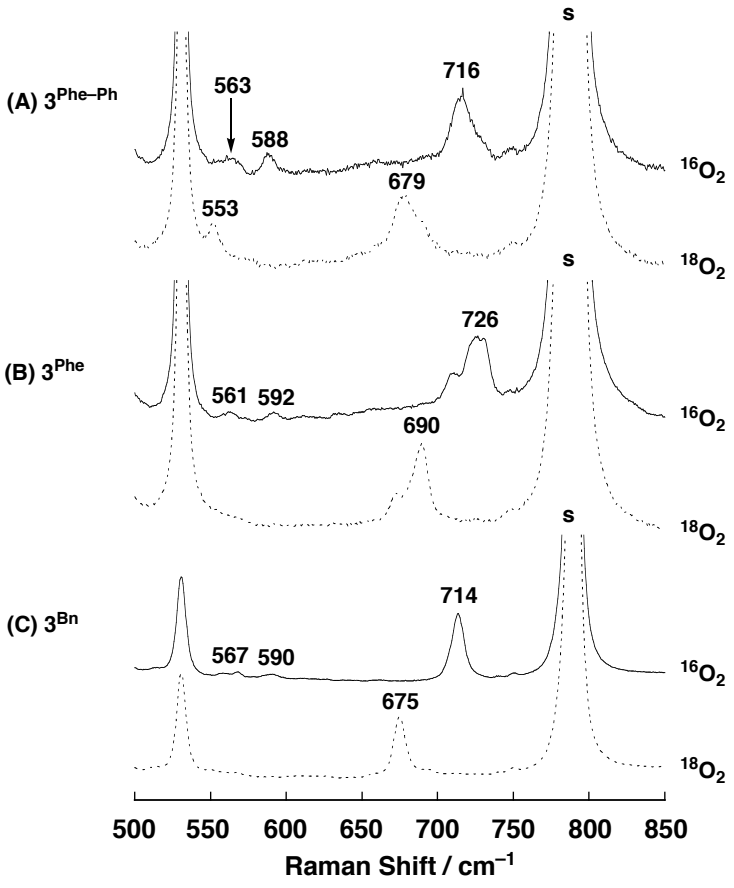

Figure 19. Resonance Raman spectra of the oxygenated products of (A) **3**$^{Phe–Ph}$, (B) **3**^{Phe} and (C) **3**^{Bn} obtained with 514.5 nm excitation in acetone at –90 °C. The mark 's' denotes the solvent peak.

As stated above, the UV-vis spectra (Figure 17) suggested co-existence of bis(μ-oxo)dicopper(III) complex **B** in solution. This was confirmed by the resonance Raman data. Namely, weak Raman bands due to bis(μ-oxo)dicopper(III) complex **B** were detected at 588 and 563 cm^{-1} (Fermi doublet) for **3**$^{Phe–Ph}$, 592 and 561 cm^{-1} for **3**^{Phe}, and 590 and 567 cm^{-1} for **3**^{Bn}. The Fermi doublet signals of **3**$^{Phe–Ph}$ in the $^{16}O_2$-derivative shift into one band at 553

cm^{-1}. Thus, the isotope shift was calculated to be 23 cm^{-1} by subtracting the frequency (553 cm^{-1}) of the $^{18}O_2$-derivative from the average frequency (578 cm^{-1}) of the $^{16}O_2$-derivative. These results are consistent with the well-established Raman data of the bis(μ-oxo)dicopper(III) complexes.[63] It is also apparent that the content of bis(μ-oxo)dicopper(III) complex **B** increases in going from $\mathbf{3}^{\mathbf{Bn}}$ to $\mathbf{3}^{\mathbf{Phe-Ph}}$. Thus, the Raman peaks of the $^{18}O_2$-derivatives derived from $\mathbf{3}^{\mathbf{Bn}}$ and $\mathbf{3}^{\mathbf{Phe}}$ were too weak to be detected (see Figure 19 (B) and (C)). These results are also consistent with the UV-vis data shown in Figure 17, where content of the bis(μ-oxo)dicopper(III) species somewhat increases in going from $\mathbf{3}^{\mathbf{Bn}}$ to $\mathbf{3}^{\mathbf{Phe-Ph}}$, although the reason for this phenomena is not clear at present.

Consequently, copper(I) complexes $\mathbf{3}^{\mathbf{R}}$ have been demonstrated to afford mainly the side-on peroxo dicopper(II) complex **A** in the reaction with O_2 at the low temperature. This clearly demonstrates that the introduction of 6-methyl group into the pyridylmethylamine tridentate ligand $^{H}Pym2^{R}$ to make $^{Me}Pym2^{R}$ resulted in a drastic change in the structure of Cu_2/O_2 complex from bis(μ-oxo)dicopper(III) **B** to (μ-η^2:η^2-peroxo)dicopper(II) **A**. The result can be explained by taking account of the decreased electron-donor ability of pyridine of $^{Me}Pym2^{R}$ due to the steric repulsion between the bound metal ion and the 6-methyl substituent as well as the case of $^{Me}Pye2^{R}$. Ligand $^{Me}Pym2^{R}$ with the lower donor ability may not be able to stabilize the higher oxidation state of copper(III) in **B**, thus providing the side-on peroxo complex **A** with the copper(II) oxidation state as the major product. Thus, the electronic effect of $^{Me}Pym2^{R}$ seems to be closer to that of $^{H}Pye2^{R}$; both ligands afford the (μ-η^2:η^2-peroxo)dicopper(II) complex **A**. Nonetheless, strength of the O–O bond of the side-on peroxo ligand in the $^{Me}Pym2^{R}$-complex is weakened as compared to the O–O bond strength of the $^{H}Pye2^{R}$-complex as evident from the lower ν_{O-O} value of the former (Table 14).

Reactivity difference in the Cu_2/O_2-formation process (rate constant k_{obs} in Table 14) evidences the ligand effects more clearly. Namely, $\mathbf{4}^{\mathbf{Phe}}$ supported by the ligand with the highest electron-donor ability reacted with O_2 more than 10^4-fold faster than $\mathbf{2}^{\mathbf{H-Phe}}$ with the ligand with the lowest electron-donor ability, whereas the reactivity of $\mathbf{3}^{\mathbf{R}}$ is just between them. In summary, the structure, physicochemical properties and reactivity of the copper(I) complexes supported by pyridylalkylamine tridentate ligands can be finely tuned not only by changing the alkyl linker chain length between pyridine nucleus and tertiary amine nitrogen but also by introducing methyl substituent at the 6-position of pyridine donor group. These results may provide significantly important informations about the ligand effects on the dioxygen-activation chemistry by copper(I) complexes.

Reference

(1) Kopf, M.-A.; Karlin, K. D., In *Biomimetic Oxidations Catalyzed by Transition Metal Complexes*; Meunier, B., Ed. Imperial College Press: London, 2000; pp 309-362.

(2) Karlin, K. D.; Zuberbühler, A. D., In *Bioinorganic Catalysis*, 2nd ed.; Reedijk, J.; Bouwman, E., Eds. Marcel Dekker: New York, 1999; pp 469-534.

(3) Karlin, K. D.; Kaderli, S.; Zuberbuhler, A. D. *Acc. Chem. Res.* **1997**, *30*, 139-147.

(4) Fox, S.; Karlin, K. D., In *Reactive Oxygen in Biochemistry*; Valentine, J. S.; Foote, C. S.; Greenberg, A.; Liebman, J. F., Eds. Chapman & Hall: Glasgow, 1995; pp 188-231.

(5) Schindler, S. *Eur. J. Inorg. Chem.* **2000**, 2311-2326.

(6) Karlin, K. D.; Haka, M. S.; Cruse, R. W.; Gultneh, Y. *J. Am. Chem. Soc.* **1985**, *107*, 5828-5829.

(7) Karlin, K. D.; Gultneh, Y.; Hutchinson, J. P.; Zubieta, J. *J. Am. Chem. Soc.* **1982**, *104*, 5240-5242.

(8) Kitajima, N.; Moro-oka, Y. *Chem. Rev.* **1994**, *94*, 737-757.

(9) Mirica, L. M.; Ottenwaelder, X.; Stack, T. D. P. *Chem. Rev.* **2004**, *104*, 1013-1045.

(10) Lewis, E. A.; Tolman, W. B. *Chem. Rev.* **2004**, *104*, 1047-1076.

(11) Itoh, S.; Kondo, T.; Komatsu, M.; Ohshiro, Y.; Li, C. M.; Kanehisa, N.; Kai, Y.; Fukuzumi, S. *J. Am. Chem. Soc.* **1995**, *117*, 4714-4715.

(12) Itoh, S.; Nakao, H.; Berreau, L. M.; Kondo, T.; Komatsu, M.; Fukuzumi, S. *J. Am. Chem. Soc.* **1998**, *120*, 2890-2899.

(13) Itoh, S.; Taki, M.; Nakao, H.; Holland, P. L.; Tolman, W. B.; Que, L.; Fukuzumi, S. *Angew. Chem. Int. Ed.* **2000**, *39*, 398-400.

(14) Blain, I.; Bruno, P.; Giorgi, M.; Lojou, E.; Lexa, D.; Réglier, M. *Eur. J. Inorg. Chem.* **1998**, 1297-1304.

(15) Blain, I.; Giorgi, M.; De Riggi, I.; Réglier, M. *Eur. J. Inorg. Chem.* **2000**, 393-398.

(16) Blain, I.; Giorgi, M.; De Riggi, I.; Réglier, M. *Eur. J. Inorg. Chem.* **2001**, 205-211.

(17) Jacobson, R. R.; Tyeklar, Z.; Farooq, A.; Karlin, K. D.; Liu, S.; Zubieta, J. *J. Am. Chem. Soc.* **1988**, *110*, 3690-3692.

(18) Hayashi, H.; Fujinami, S.; Nagatomo, S.; Ogo, S.; Suzuki, M.; Uehara, A.; Watanabe, Y.; Kitagawa, T. *J. Am. Chem. Soc.* **2000**, *122*, 2124-2125.

(19) Itoh, S.; Nagagawa, M.; Fukuzumi, S. *J. Am. Chem. Soc.* **2001**, *123*, 4087-4088.

(20) Zang, Y.; Elgren, T. E.; Dong, Y.; Que, J., L. *J. Am. Chem. Soc.* **1993**, *115*, 811-813.

(21) Que, J., L.; Dong, Y. *Acc. Chem. Res.* **1996**, *29*, 190-196.

(22) Zheng, H.; Zang, Y.; Dong, Y.; Young, J., V. G.; Que, J., L. *J. Am. Chem. Soc.* **1999**, *121*, 2226-2235.

(23) Chen, K.; Que, J., L. *Angew. Chem. Int. Ed.* **1999**, *38*, 2227-2229.

(24) Costas, M.; Tipton, A. K.; Chen, K.; Jo, D.-H.; Que, J., L. *J. Am. Chem. Soc.* **2001**, *123*, 6722-6723.

(25) Karlin, K. D.; Sherman, S. E. *Inorg. Chim. Acta* **1982**, *65*, L39-L40.

(26) Schatz, M.; Becker, M.; Thaler, F.; Hampel, F.; Schindler, S.; Jacobson, R. R.; Tyeklar, Z.; Murthy, N. N.; Ghosh, P.; Chen, Q.; Zubieta, J.; Karlin, K. D. *Inorg. Chem.* **2001**, *40*, 2312-2322.

(27) Armarego, W. L. F.; Perrin, D. D., *Purification of Laboratory Chemicals,* 4th ed.; Butterworth-Heinemann: Oxford, 1996.

(28) Baerends, E. J.; Ellis, D. E.; Ros, P. *Chem. Phys.* **1973**, *2*, 41-51.

(29) te Velde, B.; Baerends, E. J. *J. Comput. Phys.* **1992**, *99*, 84-98.

(30) Vosko, S. H.; Wilk, L.; Nusair, M. *Can. J. Phys.* **1980**, *58*, 1200-1211.

(31) Becke, A. *Phys. Rev. A* **1988**, *38*, 3098-3100.

(32) Perdew, J. P. *Phys. Rev. B* **1986**, *33*, 8822-8824.

(33) Perdew, J. P. *Phys. Rev. B* **1986**, *34*, 7406.

(34) Versluis, L.; Ziegler, T. *J. Chem. Phys.* **1988**, *88*, 322-328.

(35) Turner, R. W.; Amma, E. L. *J. Am. Che. Soc.* **1966**, *88*, 1877-1882.

(36) Dines, M. B.; Bird, P. H. *J. Chem. Soc., Chem. Commum* **1973**, 12.

(37) Schmidbaur, H.; Bublak, W.; Hiber, B.; Reber, G.; Müller, G. *Angew. Chem. Int. Ed. Engl.* **1986**, *25*, 1089-1090.

(38) Niemeyer, M. *Organometallics* **1998**, *17*, 4649-4656.

(39) Striejewske, W. S.; Conry, R. R. *Chem. Commun.* **1998**, 555-556.

(40) Conry, R. R.; Striejewske, W. S.; Tipton, A. A. *Inorg. Chem.* **1999**, *38*, 2833.

(41) Shimazaki, Y.; Yokoyama, H.; Yamauchi, O. *Angew. Chem. Int. Ed.* **1999**, *38*, 2401-2403.

(42) The Cu–C2 distances of the copper(I) complexes are comparable to the Cu–C distances of the known Cu^{I}–η^2-benzene complexes (2.09~2.30 Å)[35-37] and in the recently reported Cu^{I}–η^2-phenyl (2.07~2.30 Å)[38], Cu^{I}–η^2-naphthyl (2.13, 2.41 Å)[39,40] and Cu^{I}–η^2-indolyl (2.23, 2.27 Å)[41] complexes.

(43) Dargel, T. K.; Hertwig, R. H.; Koch, W. *Mol. Phys.* **1999**, *96*, 583-591.

(44) Kitajima, N.; Fujisawa, K.; Moro-oka, Y. *J. Am. Chem. Soc.* **1989**, *111*, 8975-8976.

(45) Karlin, K. D.; Haka, M. S.; Cruse, R. W.; Meyer, G. J.; Farooq, A.; Gultneh, Y.; Hayes, J. C.; Zubieta, J. *J. Am. Chem. Soc.* **1988**, *110*, 1196-1207.

(46) Blackburn, N. J.; Karlin, K. D.; Concannon, M.; Hayes, J. C.; Gultneh, Y.; Zubieta, J. *Chem. Commun.* **1984**, 939-940.

(47) Nagao, H.; Komeda, N.; Mukaida, M.; Suzuki, M.; Tanaka, K. *Inorg. Chem.* **1996**, *35*, 6809-6815.

(48) Itoh, S.; Fukuzumi, S. *Bull. Chem. Soc. Jpn.* **2002**, *75*, 2081-2095.

(49) e.g.) $[Cu^{II}(^{H}Pym2^{Bn})(Cl)]PF_6$: 63 % isolated yield; FT-IR (KBr) 850 cm^{-1} (PF_6^-); FAB-MS (pos.) m/z = 389.0 ($[M - PF_6]^+$); Anal. Calcd for $C_{19}H_{17}D_2N_3CuClPF_6$: C, 42.63; H+D, 3.95; N, 7.85. Found: C, 42.48; H+D, 3.85; N, 7.72.

(50) Formation of the copper(II)-chloride complex in CH_2Cl_2 can be attributed to a reductive dehalogenation reaction of the solvent by the copper(I) complex (*cf.* Jacobson, R. R.; Tyeklár, Z.; Karlin, K. D. *Inorg. Chim. Acta.* **1991**, *181*, 111-118). However, disproportionation reaction of $[Cu^{I}(^{H}Pym2^{Bn})]PF_6$ also took place to give to a mixture of copper(II) and copper(0) materials in the case of non-halogenated solvent such as acetone.

(51) Rodesiler, P. F.; Amma, E. L. *J. Chem. Soc., Chem. Commun* **1974**, 599-600.

(52) Pasquali, M.; Floriani, C.; Gaetani-Manfredotti, A. *Inorg. Chem.* **1980**, *19*, 1191-1197.

(53) Instability of complex $\mathbf{4}^{\mathbf{Phe}}$ in CH_2Cl_2 (gradual formation of the copper(II)-chloride complex $\mathbf{5}^{\mathbf{Phe}}$), however, precluded the detailed NMR studies on the (η^1-arene)copper(I) complex of $^{H}Pym2^{Phe}$

(54) The redox potential of $[Cu^{I}(^{H}Pym2^{Bn})]ClO_4$ (–0.22 V *vs.* Fc/Fc^+) is nearly the same to that of $[Cu^{I}(^{H}Pym2^{Phe})]ClO_4$ (complex $\mathbf{4}^{\mathbf{Phe}}$; –0.20 V). Thus, the different stability of the complex(I) complexes supported by $^{H}Pym2^{R}$ (R = Bn and Phe) may not be attributed to difference in the redox potential.

(55) Stack, T. D. P. *Dalton Trans.* **2003**, 1881-1889.

(56) Que, L.; Tolman, W. B. *Angew. Chem. Int. Ed.* **2002**, *41*, 1114-1137.

(57) Itoh, S.; Kumei, H.; Taki, M.; Nagatomo, S.; Kitagawa, T.; Fukuzumi, S. *J. Am. Chem. Soc.* **2001**, *123*, 6708-6709.

(58) The lower ε value (~8000 M^{-1} cm^{-1} at 385 nm) of the oxygenated intermediate is due to the instability of the copper(I) starting material in solution. Namely, the copper(I) complex was gradually converted into the copper(II) complex **3** during the preparation

of a copper(I) solution for the kinetic measurements.

(59) The low yield of ligand hydroxylation could also attributed to the instability of the copper(I) starting material.

(60) Baldwin, M. J.; Root, D. E.; Pate, J. E.; Fujisawa, K.; Kitajima, N.; Solomon, E. I. *J. Am. Chem. Soc.* **1992**, *114*, 10421-10431.

(61) Henson, M. J.; Mahadevan, V.; Stack, T. D. P.; Solomon, E. I. *Inorg. Chem.* **2001**, *40*, 5068-5069.

(62) In the reaction of $\mathbf{3^{Bn}}$, the Cu-Cu stretching vibration was not detected, the reason for which is not clear at present.

(63) Holland, P. L.; Cramer, C. J.; Wilkinson, E. C.; Mahapatra, S.; Rodgers, K. R.; Itoh, S.; Taki, M.; Fukuzumi, S.; Que, L. J.; Tolman, W. B. *J. Am. Chem. Soc.* **2000**, *122*, 792-802.

Chapter 3

Reactivities of Copper(I) Complexes toward Benzyl Halides

Abstract: The reaction of *p*-substituted benzyl halides (^{Y}BnX; X = Cl, Br, and I; Y = *p*-substituent: OMe, *t*-Bu, Me, H, F, Cl, and NO_2) and copper(I) complexes supported by a series of (2-pyridyl)alkylamine ligands has been investigated in order to shed light on the mechanism of copper(I) complex mediated carbon-halogen bond activation, including ligand effects on the redox reactivity of copper(I) complexes which are relevant to the chemistry. For both the tridentate ligand ^{H}Pym2^{Phe} [*N*,*N*-bis(2-pyridylmethyl)-2-phenylethylamine] and tetradentate ligand TMPA [tris(2-pyridylmethyl)amine] complexes, the C–C coupling reaction of benzyl halides proceeded smoothly to give corresponding 1,2-diphenylethane derivatives and copper(II)-halide complex products. Kinetic analysis revealed that the reaction obeys second-order kinetics both on the copper complex and the substrate; Rate = k[Cu]^2[^{Y}BnX]^2. A reaction mechanism involving a dinuclear copper(III)-halide organometallic intermediate is proposed, based on the kinetic results, including observed electronic effects of *p*-substituents (Hammett plot) and the rate-dependence on the BDE (bond dissociation energy) of the C–X bond, as well as the ligand effects.

Introduction

A large number of biomimetic transition-metal complexes supported by a wide variety of ligands have so far been developed to evaluate the active site structures and functions of many metalloenzymes.[1] For copper, a great deal of effort has been made especially in oxygen activation chemistry to provide profound insights into the catalytic mechanism of copper monooxygenases and copper oxidases.[2-4] Among the series of nitrogen donor ligands, (2-pyridyl)alkylamine ligands have played very important roles in exploring the structures and reactivities of copper-dioxygen intermediates.[2-6] Included are a series of tetradentate, tridentate, and didentate ligands developed by connecting (2-pyridyl)methyl ($PyCH_2$–; ^{H}Pym) and (2-pyridyl)ethyl ($PyCH_2CH_2$–; ^{H}Pye) groups to the nitrogen atom(s) of ammonia (NH_3) and alkylamines (RNH_2 and RR'NH). One of the most familiar *tetradentate* ligands is TMPA (also called TPA, Chart 1), which was adopted for the synthesis of (*trans*-μ-1,2-peroxo)dicopper(II)

complex **C**, the first structurally characterized copper-dioxygen complex (Chart 2).[7] It has been demonstrated that modifications of TMPA ligand by replacing one or two ^{H}Pym moiety to ^{H}Pye causes large effects on copper(I)-dioxygen reactivity.[8] For example, the copper(I) complex of TEPA (Chart 1), consisting of three ^{H}Pye groups, exhibits virtually no reactivity toward molecular oxygen.[9]

Chart 1

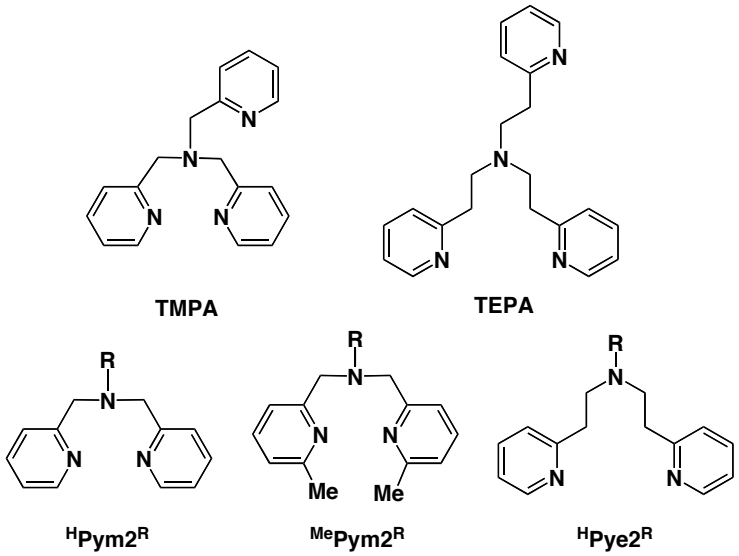

Chart 2

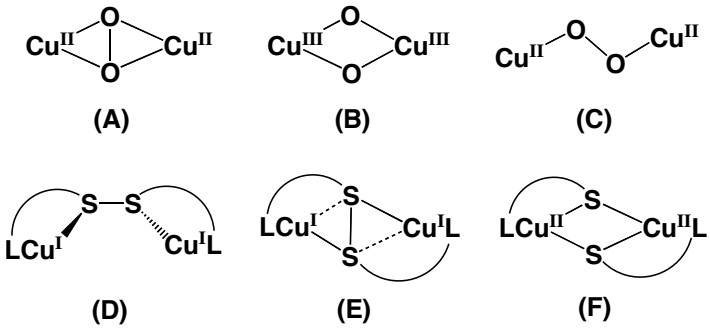

Bis[2-(2-pyridyl)ethyl]amine tridentate ligands (^{H}Pye2^{R}, Chart 1) have also been widely employed in copper(I)/dioxygen chemistry. In contrast to the case of TMPA *tetradentate* ligand, the *tridentate* ^{H}Pye2^{R} ligands with ethylene linker (^{H}Pye) predominantly afford a side-on peroxo dicopper(II) complex (**A**, Chart 2) in the reaction of the corresponding copper(I) complexes and dioxygen at a low temperature.[5,10-16] Furthermore, in chapter 2 it has been demonstrated that oxygenation of a copper(I) complex supported by the

[bis(2-pyridyl)methyl]amine tridentate ligand (^{H}Pym2^{R}) with shorter methylene linker (^{H}Pym) provided a bis(μ-oxo)dicopper(III) complex **B** instead of the peroxo complex **A** and the reactivity of copper(I) complexes is greatly affected by placement of a methyl group into the 6-position of a pyridine nucleus within chelating ligands.

The different reactivity of copper(I) complexes toward O_2 can mostly be attributed to the difference in electron-donor ability of pyridine as well as ligand denticity (tetradentate *vs*. tridentate). The electron-donor ability of pyridine is altered not only by changing the alkyl linker chain length (–CH_2– in Pym *vs*. –CH_2CH_2– in Pye) but also by introducing a methyl group at the 6-position as ^{Me}Pym2^{R} (Chart 1). Electron donor effects imparted by synthetically derived 4-pyridyl substituents also leads to measurable systematic variation in copper(I)-dioxygen chemistry with tridentate and tetradentate ligands.[15-18] Similar ligand effects have been found in the dicopper-disulfur complexes supported by a series of disulfide ligands LCH_2CH_2S–SCH_2CH_2L, where the redox state of copper as well as the Cu_2S_2 core structure is largely affected by the structure of metal binding site L (^{H}Pym2^{R}, ^{Me}Pym2^{R}, and ^{H}Pye2^{R}), providing dicopper(I)-disulfide complexes with different core structures, **D** and **E**, and the bis(μ-thiolato)dicopper(II) complex **F**, as shown in Chart 2.[19,20]

In this chapter, the C–C coupling reaction of benzyl halides by copper(I) complexes supported by the series of tridentate and tetradentate (2-pyridyl)alkylamine ligands shown in Chart 1 (Eq 1) has been investigated to clarify the effects of ligands on the reactivity of copper(I) complexes.

$$2\,LCu^{I} + 2\,{}^{Y}BnX \rightarrow 2\,LCu^{II}X + {}^{Y}Bn - {}^{Y}Bn \qquad (1)$$

The C–C coupling reaction of alkyl halides by alkaline and alkaline earth metals as well as several low-valent transition-metal ions are well known in synthetic organic chemistry.[21] Lithium organocuprates are popular copper reagents for such a C–C coupling reaction.[22] However, the reaction of alkyl halides with simple copper(I) complexes such as those with (2-pyridyl)alkylamine ligands is relatively rare. In this regard, Karlin and his coworkers reported that the copper(I) complex of TMPA (Chart 1) reacted efficiently with benzyl halide derivatives to give the corresponding C–C coupling dimer products and the corresponding copper(II)-halide complex as indicated in Eq 1.[23] Formation of such copper(II)-halide complexes has also been reported recently in the reactions of related copper(I) complexes in the presence of organohalides such as CH_2Cl_2 or $CHCl_3$ (see chapter 2).[7,24-26] However, mechanistic details of such C–C coupling reactions have yet to be elucidated.

The purpose of the present study is to obtain further insights into the effects of ligands on the redox chemistry of copper(I) complexes with respect to an understanding of the carbon-halogen bond activation mechanism by these ligand-copper(I) complexes. The results reported herein may also provide mechanistic insight into the initiation process for atom transfer radical polymerization (ATRP) of olefins mediated by alkyl halides and copper(I) complexes.[27,28]

Experimental Section

General. All chemicals used in this study, except the ligands and the copper(I) complexes, were commercial products of the highest available purity and were further purified by standard methods, if necessary.[29] The ligands and the copper(I) complexes were prepared according to reported methods (see chapter 2 in case of ligand $^{H}Pym2^{Phe}$ and the complex).[13,30,31] FT-IR spectra were recorded on a Shimadzu FTIR-8200PC and UV–visible spectra were taken on a Hewlett Packard 8453 photo diode array spectrophotometer equipped with a HP 89090A thermostated cell holder or a Unisoku cryostat cell holder USP-203. ^{1}H-NMR spectra were recorded on a JEOL FT-NMR Lambda 300WB or a JEOL FT-NMR GX-400 spectrometer. Mass spectra were recorded on a JEOL JMS-700T Tandem MS-station mass spectrometer. ESI-MS (electrospray ionization mass spectra) measurements were performed on a PE SCIEX API 150EX spectrometer. Cyclic voltammetry measurements were performed on an ALS 630 electrochemical analyzer in deaerated acetone containing 0.10 M NBu_4ClO_4 as supporting electrolyte. The Pt working electrodes (BAS) were polished with BAS polishing alumina suspension and rinsed with acetone before use. The counter electrode was a platinum wire. A silver pseudo reference electrode was employed, and electrochemical potentials were determined using the ferrocene/ferricenium (Fc/Fc^{+}) couple as a reference. All electrochemical measurements were carried out at 25 °C under an atmospheric pressure of Ar in a glovebox (DBO-1KP, Miwa Co. Ltd.).

Product Analysis. Typically, the copper(I) complex (0.02 mmol) was dissolved into deaerated acetone (5 mL) under anaerobic conditions. A benzyl halide (0.20 mmol) was then added to this solution, and the resulting mixture was stirred for 4 h at an appropriate temperature (see text). After removal of the solvent by evaporation, 15 % NH_4OH aqueous solution (10 mL) was added to the residue, and organic products were extracted by $CHCl_3$ (5 mL x 3). After drying over K_2CO_3, concentration of the solvent gave an organic materials, in

which formation of the C–C coupled dimer product was confirmed by comparing the ESI–MS and ^{1}H–NMR to those of the authentic sample. The yield of the C–C coupling product was determined by ^{1}H–NMR spectroscopy using $CHCl_2CHCl_2$ as an internal standard.

Kinetic Measurements. Typically, the reaction of benzyl halide (20–250 mM) and the copper(I) complex (2.0 mM) in acetone was followed by monitoring the increase of absorption in the visible region due to the d-d band of the copper(II)-halide product. The reaction obeyed a second-order rate law, and the second-order rate constants were determined from a standard plot of $(A_0 - A)/\{(A - A_\infty)[LCu]_0\}$ against time, as shown in the inset of Figure 1.

Results

Products and Kinetics. As in the case of TMPA ligand system reported by Karlin *et al*,[23] the reaction of copper(I) complex with short armed tridentate ligand, $[Cu^I(^HPym2^{Phe})]ClO_4$ (0.02 mmol) [$^HPym2^{Phe}$; (2-pyridyl)methylamine tridentate ligand with phenylethyl substituent (R = Phe; $–CH_2CH_2Ph$) see Chart 1] and benzyl chloride (^{H}BnCl) (0.2 mmol) proceeded smoothly in acetone at 50 °C to give the corresponding C–C coupling dimer, 1,2-diphenylethane, in a 67 % yield based on the copper(I) complex (the yield was corrected by doubling the isolated yield of the C–C coupling dimer since the molar ratio of the copper(I) complex and the dimer product is 2 : 1, see Eq 1). In this reaction, the copper(I) complex was quantitatively converted into the corresponding copper(II)-chloride complex, $[Cu^{II}(^HPym2^{Phe})Cl]ClO_4$ (see chapter 2).

Figure 1 shows spectral changes observed for the reaction, where a characteristic absorption band at 660 nm due to a ligand field transition of the copper(II)-chloride complex gradually increases as the reaction proceeds. Notably, the time course of the absorption change at 660 nm could be fitted by a second-order rate law equation even in the presence of a large excess of ^{H}BnCl (pseudo-first-order conditions), and the second-order rate constant (k_{obs}) was obtained from the slope of the line from the second-order plot (inset of Figure 1). This second-order dependence of this reaction has been confirmed by the result that the second-order rate constants (k_{obs}) obtained at various initial concentrations of $[Cu^I(^HPym2^{Phe})]ClO_4$ were inversely proportional to the initial concentration of $[Cu^I(^HPym2^{Phe})]ClO_4$, as expected from the equation for a second-order plot: $(A_0 - A)/\{(A - A_\infty)[Cu]_0\} = k_{obs}t$. Furthermore, the second-order rate constant (k_{obs}) also exhibited a second-order dependence on ^{H}BnCl concentration (Figure 2). Thus, the kinetic equation for the

reaction can be summarized as Rate = $k[Cu]^2[^{H}BnCl]^2$, where k is an apparent fourth-order rate constant.

Substituent Effects of the Substrates. The reaction of a series of *p*-substituted benzyl chlorides (^{Y}BnCl; Y = OMe, *t*-Bu, Me, H, F, Cl, and NO_2) and $[Cu^{I}(^{H}Pym2^{Phe})]ClO_4$ was also examined under the same experimental conditions (Table 1). In all cases, the corresponding C–C coupling dimer products were obtained in fairly good yields, and the reaction obeyed second-order kinetics with respect to both the copper complex and the substrate, thus also obeying the kinetic equation, Rate = $k[Cu]^2[^{R}BnCl]^2$. The apparent fourth-order rate constants were obtained in the same manner, and they are listed in Table 1. It is obvious that the reaction rate increases as the electron-withdrawing nature of the *p*-substituent (Y) increases, and the Hammett plot of log k *vs.* σ_p^- [32] gave a linear correlation with a positive slope ($\rho = 1.1$) as shown in Figure 3. Furthermore, the reactivity of benzyl halides (^{H}BnX) increases in the order of Cl < Br < I, and the rate constants exhibit a linear correlation with the bond dissociation energy (BDE)[33] of the carbon-halogen bond of the substrates, as demonstrated by the plot given in Figure 4. The electronic effects of the *p*-substituents as well as the effect of BDE on the reaction rates are discussed below.

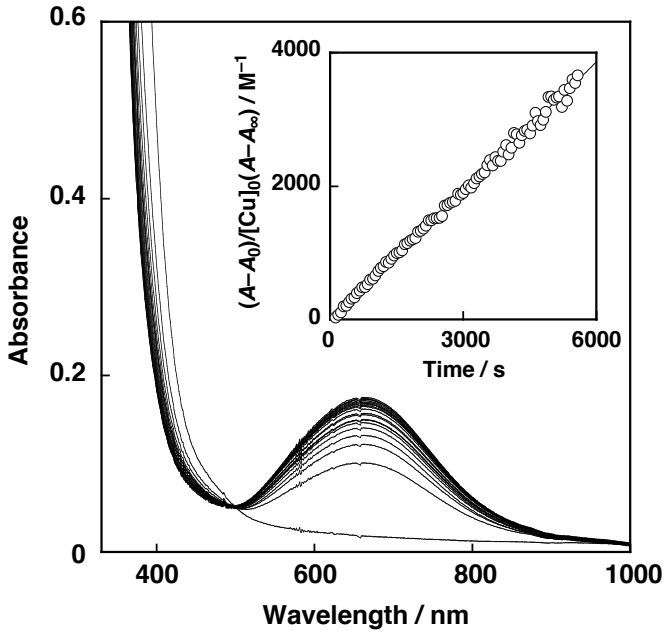

Figure 1. Spectral change of the reaction between $[Cu^{I}(^{H}Pym2^{Phe})]ClO_4$ (2.0×10^{-3} M) and benzyl chloride (0.084 M) in acetone at 50 °C. Inset: second-order plot based on the absorption change at 660 nm.

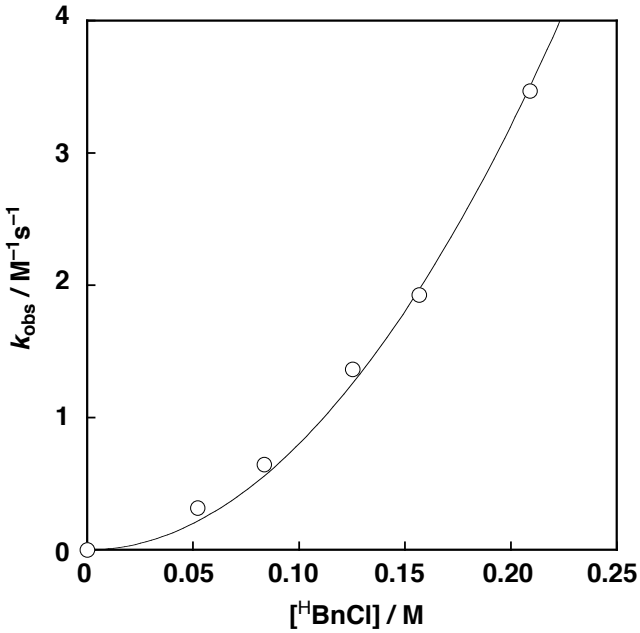

Figure 2. Plot of k_{obs} *vs*. [^{H}BnCl] for the reaction of benzyl chloride and [Cu^{I}(^{H}Pym2^{Phe})]ClO_4 in acetone at 50 °C.

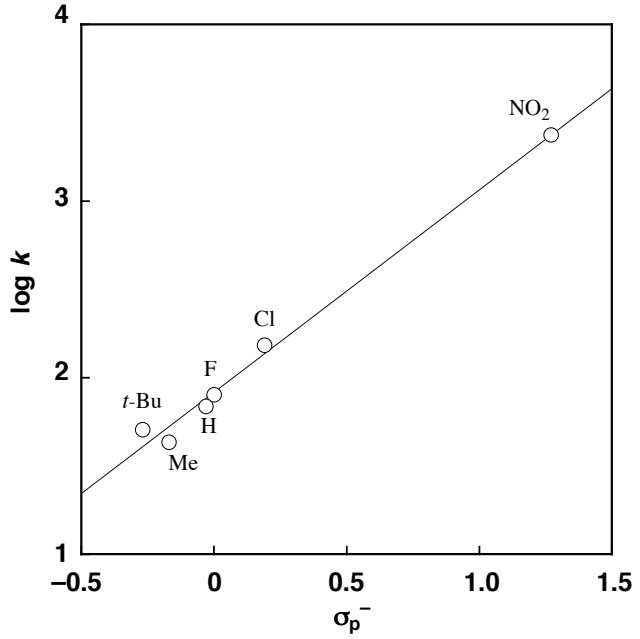

Figure 3. Hammett plot for the reaction of *p*-substituents benzyl chloride by [Cu^{I}(^{H}Pym2^{Phe})]ClO_4 in acetone at 50 °C.

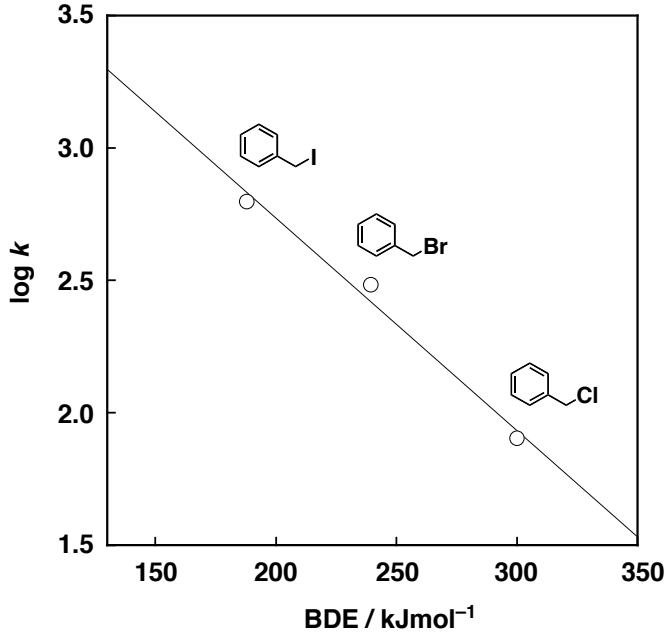

Figure 4. Plot of log *k vs*. BDE of the carbon-halogen bond of the substrates for the reaction of ^{H}BnX (X = Cl, Br, and I) and [Cu^{I}(^{H}Pym2^{Phe})]ClO$_4$ in acetone at 50 ˚C.

Ligand Effects. The reactivity of copper(I) complexes with other ligands shown in Chart 1 has also been examined in the reaction with ^{H}BnCl at 50 °C in acetone. Interestingly enough, the reaction of [Cu^{I}(TMPA)(CH$_3$CN)]ClO$_4$ was extremely fast (completed within a second at 50 °C), whereas the copper(I) complexes with ^{Me}Pym2^{Phe}, ^{H}Pye2^{Phe} (R = phenylethyl, see Chart 1), and TEPA exhibited virtually no reactivity. Thus, the supporting ligands caused dramatically different differential affects on the reactivity of copper(I) toward benzyl chloride.

Since the reaction of [Cu^{I}(TMPA)(CH$_3$CN)]ClO$_4$ and ^{H}BnCl was too fast to be followed at 50 °C, kinetic analysis of the reaction was performed at –80 ˚C. As in the case of [Cu^{I}(^{H}Pym2^{Phe})]ClO$_4$, the reaction obeyed second-order kinetics with respect to both the copper complex (Figure 5) and ^{H}BnCl (Figure 6). Yields of the dimer products and the apparent fourth-order rate constants for the reactions of a series of ^{Y}BnCl (Y = OMe, *t*-Bu, Me, H, F, Cl, and NO$_2$) are also listed in Table 1. In this case as well, the reaction rate increases as the electron-withdrawing nature of the *p*-substituents increases, and the Hammett plot of log *k* vs. σ_p^- [32] also gave a linear correlation with a positive slope of $\rho = 2.3$ (Figure 7). The similar kinetic behavior of the [Cu^{I}(TMPA)(CH$_3$CN)]ClO$_4$ and [Cu^{I}(^{H}Pym2^{Phe})]ClO$_4$ systems clearly suggests that the reaction mechanisms of both systems are essentially the same, even though

the reaction rates vary significantly.

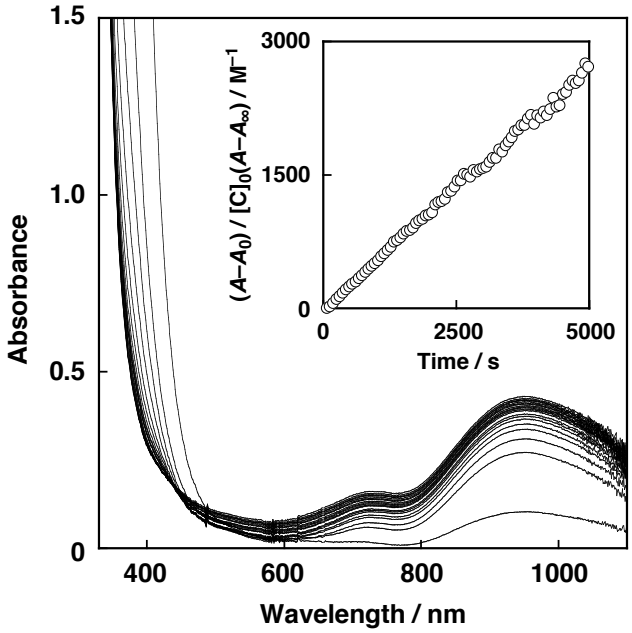

Figure 5. Spectral change of the reaction between $[Cu^{I}(TMPA)(CH_3CN)]ClO_4$ (2.0×10^{-3} M) and benzyl chloride (0.11 M) in acetone at –80 °C. Inset: second-order plot based on the absorption change at 950 nm.

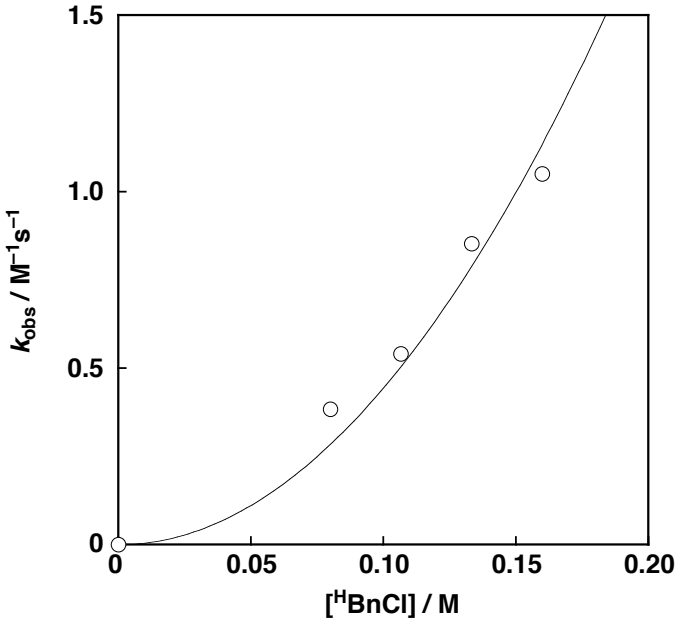

Figure 6. Plot of k_{obs} *vs*. [^{H}BnCl] for the reaction of ^{H}BnCl and $[Cu^{I}(TMPA)(CH_3CN)]ClO_4$ in acetone at –80 °C.

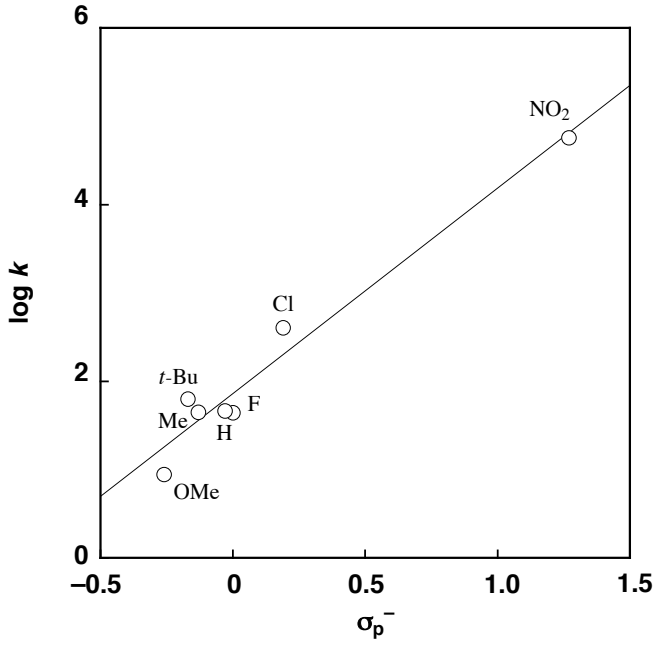

Figure 7. Hammett plot for the reactions of *p*-substituents benzyl chloride and [[Cu^{I}(TMPA)(CH_3CN)]ClO_4 in acetone at –80 ˚C.

Table 1. The Yields of C–C Coupling Dimer and the Apparent Fourth-Order Rate Constants *k* for the Reactions of *p*-Substituted Benzyl Chlorides (^{Y}BnCl) and [Cu^{I}(^{H}Pym2^{Phe})]ClO_4 or [Cu^{I}(TMPA)(CH_3CN)]ClO_4 in Acetone.

	[Cu^{I}(^{H}Pym2^{Phe})]ClO_4		[Cu^{I}(TMPA)(CH_3CN)]ClO_4	
p–Y	Yield / % [a]	*k* / $M^{-3}s^{-1}$ [a]	Yield / % [b]	*k* / $M^{-3}s^{-1}$ [c]
OMe	39	____ [d]	74	8.8 ± 0.2
t-Bu	77	51.4 ± 2.4	77	44.6 ± 2.0
Me	67	43.2 ± 2.6	89	65.5 ± 2.9
H	67	80.2 ± 1.5	94	44.4 ± 2.2
F	69	69.0 ± 2.5	93	46.4 ± 4.0
Cl	72	153 ± 3.0	95	404 ± 17
NO_2	74	2370 ± 66	97	57500 ± 930

[a] At 50°C. [b] At 20 ˚C. [c] At –80 ˚C. [d] Too slow to be determined.

Discussion

Based on the kinetic results described above, a mechanism for the C–C coupling reaction shown in Scheme 1 is proposed. Oxidative addition of the copper(I) complex to the C–X bond of substrate will afford a copper(III) organometallic intermediate **I**. Then, a bimolecular reaction of intermediate **I** takes place to give the C–C coupled dimer and the copper(II)-halide complex as products.

Scheme 1

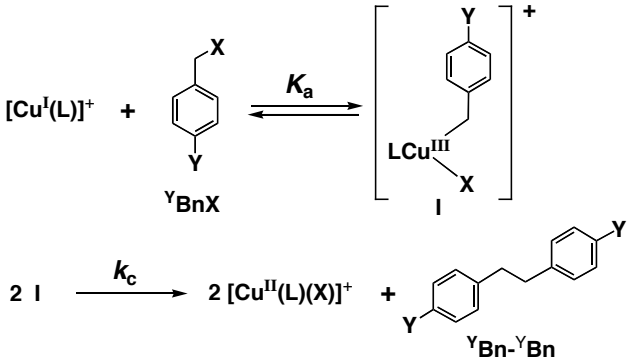

From this mechanism is derived the following kinetic equation (2),

$$\text{Rate} = \frac{k_c K_a^{\,2}[{}^{Y}\text{BnX}]^2[\text{Cu}]_T^{\,2}}{(1+K_a[{}^{Y}\text{BnX}])^2} \qquad (2)$$

Since the reaction is second-order with respect to both the copper complex (Figure 1) and the substrate (Figure 2), the $K_a[{}^{Y}\text{BnX}]$ term must be much smaller than unity ($K_a[{}^{Y}\text{BnX}] << 1$) under the present experimental conditions. As such, the kinetic equation can be simplified as Eq 3,

$$\text{Rate} = k_c K_a^{\,2}[{}^{Y}\text{BnX}]^2[\text{Cu}]_T^{\,2} \qquad (3)$$

where $k_c K_a^{\,2}$ corresponds to the apparent fourth-order rate constant k. Although the k_c and K_a processes could not be evaluated separately, the linear correlation between the rate constant and BDE (Figure 4) can be simply attributed to the oxidative addition process (K_a). Namely, the oxidative addition of copper(I) into the C–X bond of the substrates may be enhanced as the C–X bond becomes weaker.

With respect to the electronic effects of *p*-substituents (Y) of ^{Y}BnCl, the

electron-withdrawing substituents may stabilize the intermediate **I** since its benzylic carbon has a carboanionic (δ^-) character. Thus, the formation of intermediate **I** (K_a process) would be accelerated by the electron-withdrawing substituents, being consistent with the positive slope of the Hammett plot (Figure 3 and Figure 7). On the other hand, the C–C coupling process (k_c) may be more like a radical character in nature (the transition state of the C–C coupling reaction is discussed below). Thus, *p*-substituent effects on the k_c process might be smaller than those for the K_a process.

Inspection of the oxidation potential and dioxygen reactivity of the copper(I) complexes gave ones a clue to understand the remarkable effects of the supporting ligands in the present C-X bond activation chemistry (see Table 2). With regard to the oxidation potential (E_{ox}; i.e., the measure of the Cu^I/Cu^{II} redox couple) of the copper(I) complexes, significant differences exist, with values ranging from –430 mV to +120 mV *vs*. Fc/Fc^+ (Table 2). Apparently, the copper(I) complexes with large negative E_{ox} values, $[Cu^I(TMPA)(CH_3CN)]ClO_4$ and $[Cu^I(^{H}Pym2^{Phe})]ClO_4$, react with benzyl halides, whereas the copper(I) complexes with the higher E_{ox} value do not. The lower oxidation potentials of $[Cu^I(TMPA)(CH_3CN)]ClO_4$ and $[Cu^I(^{H}Pym2^{Phe})]ClO_4$ indicate that their higher oxidation states (Cu^{II} and Cu^{III}) are more stabilized than those of the others, due to the overall stronger donating ability of the ligands (TMPA and $^{H}Pym2^{Phe}$).[34] Thus, the observed reactivity of $[Cu^I(TMPA)(CH_3CN)]ClO_4$ and $[Cu^I(^{H}Pym2^{Phe})]ClO_4$ toward ^{Y}BnX can be attributed in part to ligand stabilization of the copper(III)-intermediate **I**, enhancing its formation process (K_a process in Scheme 1). In other words, the ligands with lower donor ability such as $^{Me}Pym2^{Phe}$, $^{H}Pye2^{Phe}$, and TEPA would unlikely support such a high oxidation state proposed for intermediate **I**, resulting in no reactivity toward ^{Y}BnX. In support of this notion, the reactivity of $[Cu^I(TMPA)(CH_3CN)]ClO_4$ and $[Cu^I(^{H}Pym2^{Phe})]ClO_4$ towards O_2 (which involves a redox process) is significantly greater (in rate) than that of the other complexes (compare the k_{obs} values in Table 2), and $[Cu^I(^{H}Pym2^{Phe})]ClO_4$ provides the high-valent bis(μ-oxo)dicopper(III) complex **B** in contrast to the case of $[Cu^I(^{Me}Pym2^{Phe})]ClO_4$ and $[Cu^I(^{H}Pye2^{Phe})]ClO_4$ which produce the side-on peroxo dicopper(II) complex **A** (the difference in structure of the Cu_2O_2 complex derived from $[Cu^I(TMPA)(CH_3CN)]ClO_4$ from those of the others can be attributed to the difference in ligand denticity).[2]

Although no direct evidence concerning an intermediate or nature of the transition state associated with the k_c process is available, ones' knowledge that a bis(μ-oxo)dicopper(III) complex **B** forms with the tridentate ligand $^{H}Pym2^{Phe}$ lets ones propose a transition state for the

C–C coupling reaction as shown in Scheme 2. The second-order dependence both on the copper complex and the substrate indicate that intermediate **I** (Scheme 1) should collapse together, where halogen ions (X) may act as the bridging ligands to connect the two copper ions. The Cu_2X_2 core structure resembles the Cu_2O_2 core structure in bis(μ-oxo)dicopper(III) complex **B**, and halides are well known bridging ligands.[35] Although the copper ion is drawn as 6-coordinated in Scheme 2, the coordination number of copper could be five. In such a case, one of the pyridine nuclei of $^{H}Pym2^{Phe}$ is detached from the copper center.

Table 2. Oxidation Potential (E_{ox}) and O_2-Reactivity (Structure of the Cu_2O_2-Complex Formed and Its Formation Rate Constant) of the Copper(I) Complexes.

Ligand	E_{ox} / V *vs.* Fc/Fc^{+} [a]	Cu_2O_2-Complex	O_2-reactivity k_{obs} / $M^{-1}s^{-1}$
TMPA	–0.43 (–0.06)	**C** [b]	(1.0 ± 0.2) x 10^{5} [c]
$^{H}Pym2^{Phe}$	–0.30 (+0.07)	**B** [d]	(5.9 ± 0.02) x 10^{4} [d, e]
$^{Me}Pym2^{Phe}$	–0.040 (+0.33)	**A** [f]	70 ± 0.4 [f, g]
$^{H}Pye2^{Phe}$	0 (+0.37)	**A**	[h]2.0 ± 0.1 [h, i]
TEPA	+0.12 (+0.49)	—	NR [j]

[a] In acetone containing 0.1 M tetrabutylammonium perchlorate (TBAP), scan rate: 50 ~ 100 mV s^{-1} at 25 °C. E_{ox} values *vs.* SCE are shown in parenthesis. [b] Ref 7. [c] At –90 °C in THF; Ref 22. [d] Ref 17. [e] At –94 °C in acetone. [f] Ref 19. [g] At –94 °C in acetone. [h] Ref 13. [i] At –80 °C in THF. [j] Ref 9.

Scheme 2

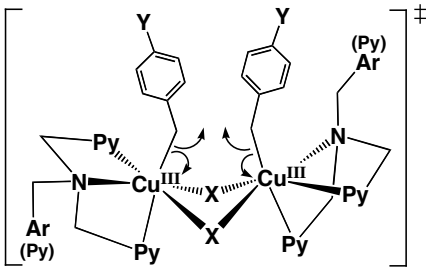

In the case of the tetradentate TMPA ligand system, at least one pyridine donor should be free from metal-coordination (Ar = Py in the TMPA system). In fact, one of the pyridine donors in the starting copper(I) complex $[Cu^{I}(TMPA)(CH_3CN)]ClO_4$ does not coordinate to the metal ion.[7,31] Then, the extremely high reactivity of the TMPA tetradentate ligand system

can be interpreted as follows. The uncoordinated Py group may attack the copper center from the back side of Cu–C bond, which induces the Cu–C bond cleavage to enhance the C–C bond formation (a so-called push effect). Thus, the presence of the ligand TMPA accelerates not only the K_a process by stabilizing the high-valent copper(III) oxidation state of intermediate **I** but also the k_c process by enhancing the Cu–C bond breaking. In support of TMPA at least transiently supporting a copper(III) oxidation state, it is noted that a bis(μ-oxo)dicopper(III) complex is supported by a 6-methyl substituted TMPA ligand.[36] It is for these reasons that it is suggested why the copper(I) complex of TMPA exhibits such a high reactivity in the C–X cleavage and C–C bond formation reactions.

In atom transfer radical polymerization (ATRP) of olefins mediated by alkyl halides (RX) and copper(I) complexes (Cu^IL; L = ligand), the initiation process involves a reaction of RX and Cu^IL, generating an alkyl radical species $R^\bullet$, which adds to the olefin to initiate the radical chain polymerization reaction. It has been proposed that the initiation process involves electron-transfer from Cu^IL to RX, producing a radical anion intermediate $RX^{\bullet-}$ from which the organic radical $R^\bullet$ is generated by homolytic cleavage of the carbon-halogen bond of $RX^{\bullet-}$. Eventual formation of the free organic radical $R^\bullet$ has been well documented by several lines of experimental evidence.[27,28]

In the present C–C coupling reaction, however, a similar electron-transfer initiated reaction between the copper(I) complex and ^{Y}BnX is unlikely, since this process would be energetically unfavorable; the reduction peak potential of ^{Y}BnX (*cf.* ^{H}BnCl: –2.24 V *vs*. SCE; ^{H}BnBr: –1.74 V *vs*. SCE, scan rate 0.1 V s^{-1} in CH_3CN)[37] is significantly negative as compared to the oxidation potential of the copper(I) complexes ($[Cu^I(TMPA)(CH_3CN)]ClO_4$: –0.06 V *vs*. SCE; $[Cu^I(^HPym2^{Phe})]ClO_4$: +0.07 V *vs*. SCE, see Table 2). If such an electron-transfer occurred, it should be the rate-determining process. However, the second-order dependence both on the copper(I) complex and the substrate is inconsistent with this mechanism, since this should obey first-order kinetics with respect to both the copper(I) complex and the substrate. Namely, once the rate-determining electron-transfer occurred, the ^{Y}Bn$^\bullet$ alkyl radical generated would rapidly collapse to give the C–C coupling dimer product. Thus, in order to explain the kinetic data observed for the present RX reductive coupling chemistry, there must be an association between the copper complex and the substrate such as intermediate **I**, which undergoes a bimolecular reaction to give the final products (Scheme 1). Further studies are being undertaken to obtain information concerning intermediate **I**.

References

(1) Gavrilova, A. L.; Bosnich, B. *Chem. Rev.* **2004**, *104*, 349-383.

(2) Mirica, L. M.; Ottenwaelder, X.; Stack, T. D. P. *Chem. Rev.* **2004**, *104*, 1013-1045.

(3) Lewis, E. A.; Tolman, W. B. *Chem. Rev.* **2004**, *104*, 1047-1076.

(4) Kim, E.; Chufán, E. E.; Kamaraj, K.; Karlin, K. D. *Chem. Rev.* **2004**, *104*, 1077-1133.

(5) Itoh, S.; Fukuzumi, S. *Bull. Chem. Soc. Jpn.* **2002**, *75*, 2081-2095.

(6) Schindler, S. *Eur. J. Inorg. Chem.* **2000**, 2311-2326.

(7) Tyeklár, Z.; Jacobson, R. R.; Wei, N.; Murthy, N. N.; Zubieta, J.; Karlin, K. D. *J. Am. Chem. Soc.* **1993**, *115*, 2677-2689.

(8) Schatz, M.; Becker, M.; Thaler, F.; Hampel, F.; Schindler, S.; Jacobson, R. R.; Tyeklár, Z.; Murthy, N. N.; Ghosh, P.; Chen, Q.; Zubieta, J.; Karlin, K. D. *Inorg. Chem.* **2001**, *40*, 2312-2322.

(9) Karlin, K. D.; Hayes, J. C.; Juen, S.; Hutchinson, J. P.; Zubieta, J. *Inorg. Chem.* **1982**, *21*, 4106-4108.

(10) Karlin, K. D.; Kaderli, S.; Zuberbühler, A. D. *Acc. Chem. Res.* **1997**, *30*, 139-147.

(11) Pidcock, E.; Obias, H. V.; Abe, M.; Liang, H.-C.; Karlin, K. D.; Solomon, E. I. *J. Am. Chem. Soc.* **1999**, *121*, 1299-1308.

(12) Pidcock, E.; Obias, H. V.; Zhang, C. X.; Karlin, K. D.; Solomon, E. I. *J. Am. Chem. Soc.* **1998**, *120*, 7841-7847.

(13) Itoh, S.; Nakao, H.; Berreau, L. M.; Kondo, T.; Komatsu, M.; Fukuzumi, S. *J. Am. Chem. Soc.* **1998**, *120*, 2890-2899.

(14) Liang, H.-C.; Karlin, K. D.; Dyson, R.; Kaderli, S.; Jung, B.; Zuberbühler, A. D. *Inorg. Chem.* **2000**, *39*, 5884-5894.

(15) Henson, M. J.; Vance, M. A.; Zhang, C. X.; Liang, H.-C.; Karlin, K. D.; Solomon, E. I. *J. Am. Chem. Soc.* **2003**, *125*, 5186-5192.

(16) Zhang, C. X.; Liang, H.-C.; Kim, E.-i.; Shearer, J.; Helton, M. E.; Kim, E.; Kaderli, S.; Incarvito, C. D.; Zuberbuhler, A. D.; Rheingold, A. L.; Karlin, K. D. *J. Am. Chem. Soc.* **2003**, *125*, 634-635.

(17) Shearer, J.; Zhang, C. X.; Hatcher, L. Q.; Karlin, K. D. *J. Am. Chem. Soc.* **2003**, *125*, 12670-12671.

(18) Zhang, C. X.; Kaderli, S.; Costas, M.; Kim, E.-i.; Neuhold, Y. M.; Karlin, K. D.; Zuberbühler, A. D. *Inorg. Chem.* **2003**, *42*, 1807-1824.

(19) Itoh, S.; Nagagawa, M.; Fukuzumi, S. *J. Am. Chem. Soc.* **2001**, *123*, 4087-4088.

(20) Ueno, Y.; Tachi, Y.; Itoh, S. *J. Am. Chem. Soc.* **2002**, *124*, 12428-12429.

(21) Smith, M. B.; March, J., *March's advanced organic chemistry: reactions, mechanisms, and structure*, 5th ed.; Wiley: New York, 2000; p 537.

(22) Collman, J. P.; Hegedus, L. S.; Norton, J. R.; Finke, R. G., Eds. *Principles and Applications of Organotransition Metal Chemistry*, 2nd ed.; University Science Books: Mill Valley, 1987; p 682.

(23) Jacobson, R. R.; Tyeklár, Z.; Karlin, K. D. *Inorg. Chim. Acta* **1991**, *181*, 111-118.

(24) Komiyama, K.; Furutachi, H.; Nagatomo, S.; Hashimoto, A.; Hayashi, H.; Fujinami, S.; Suzuki, M.; Kitagawa, T. *Bull. Chem. Soc. Jpn* **2004**, *77*, 59-72.

(25) Wei, N.; Murthy, N. N.; Chen, Q.; Zubieta, J.; Karlin, K. D. *Inorg. Chem.* **1994**, *33*, 1953-1965.

(26) Lucchese, B.; Humphreys, K. J.; Lee, D.-H.; Incarvito, C. D.; Sommer, R. D.; Rheingold, A. L.; Karlin, K. D. *Inorg. Chem.* **2004**, *43*, 5987-5998.

(27) Patten, T. E.; Matyjaszewski, K. *Acc. Chem. Res.* **1999**, *32*, 895-903.

(28) Matyjaszewski, K.; Xia, J. H. *Chem. Rev.* **2001**, *101*, 2921-2990.

(29) Armarego, W. L. F.; Perrin, D. D., *Purification of Laboratory Chemicals*, 4th ed.; Butterworth-Heinemann: Oxford, 1996.

(30) Karlin, K. D.; Sherman, S. E. *Inorg. Chim. Acta* **1982**, *65*, L39-L40.

(31) Jacobson, R. R.; Tyeklár, Z.; Farooq, A.; Karlin, K. D.; Liu, S.; Zubieta, J. *J. Am. Chem. Soc.* **1988**, *110*, 3690-3692.

(32) Hansch, C.; Leo, A.; Taft, R. W. *Chem. Rev.* **1991**, *91*, 165-195.

(33) Verevkin, S. P.; Krasnykh, E. L.; Wright, J. S. *Phys. Chem. Chem. Phys.* **2003**, *5*, 2605-2611.

(34) Stabilization of the higher oxidation state of intermediate **I** could also be attributed to the coordination/geometry/denticity overall effects of the ligands.

(35) Hathaway, B. J., In *Comprehensive Coordination Chemistry*; Wilkinson, G., Ed. Pergamon: New York, 1987; pp 533-774.

(36) Mizuno, M.; Hayashi, H.; Fujinami, S.; Furutachi, H.; Nagatomo, S.; Otake, S.; Uozumi, K.; Suzuki, M.; Kitagawa, T. *Inorg. Chem.* **2003**, *42*, 8534-8544.

(37) Andrieux, C. P.; Legorande, A.; Savéant, J. M. *J. Am. Chem. Soc.* **1992**, *114*, 6892-6904.

Chapter 4

Reactivities of Dicopper–Dioxygen (Cu_2/O_2), and Dicopper–Disulfide (Cu_2/S_2) Complexes toward Phenol Derivatives

Abstract: Reactivities of dicopper–dioxygen (Cu_2/O_2), and dicopper–disulfide (Cu_2/S_2) complexes toward external phenol derivatives have been systematically investigated in detail. Oxidation of neutral phenols (ArOH) by the (μ-η^2:η^2-peroxo)dicopper(II) complex (**A**) and the bis(μ-oxo)dicopper(III) complex (**B**) supported by the 2-(2-pyridyl)ethylamine tridentate and didentate ligands, $^{H}Pye2^{Bz-d2}$ and $^{H}Pye1^{Bz-d2,Et}$, respectively, have been carried out in order to get insight into the phenolic O–H bond activation mechanism by metal-oxo species. In both cases (**A** and **B**), the C–C coupling dimer was obtained as a solely isolable product in ~50 % yield base on the dicopper-dioxygen (Cu_2/O_2) complexes, suggesting that both **A** and **B** act as electron transfer oxidants for the phenol oxidation. The rate-dependence in the oxidation of phenols by the Cu_2/O_2 complexes on the one-electron oxidation potentials of the phenol substrates as well as the kinetic deuterium isotope effects obtained using ArOD have indicated that the reaction involves a proton-coupled electron transfer (PCET) mechanism. These results are in sharp contrast to the case of hydrogen atom transfer reactions to cumylperoxyl radical (**C**). Thus, the results unambiguously confirmed that the oxidation of phenols by the Cu_2O_2 complex proceeds via the PCET mechanism rather than the HAT mechanism involved in the cumylperoxyl radical system. The reactivity difference between **A** and **B** has also been discussed by taking account of the existed fast equilibrium between **A** and **B**. On the other hand, a novel C–S bond formation reaction has been also found to take place, when a lithium phenolate derivative was treated with a disulfide-bridged dicopper(I) complex or a bis(μ-thiolato)dicopper(II) complex under very mild conditions. The reaction has been suggested to proceed via a disulfide-bridged (μ-phenoxo)dicopper(I) complex as the common reaction intermediate. Copper(II) complexes of the modified ligands containing a thioether group (products of the C–S bond formation reaction) have been isolated and structurally characterized by X-ray analysis as model compounds of the active site of galactose oxidase. Mechanism of the C–S bond formation reaction is also discussed in relation to the biosynthetic mechanism of the organic cofactor Tyr-Cys of galactose oxidase.

Introduction

Conversion of a phenol to a phenoxyl radical is an important process in a variety of biological systems. Particular attention has recently focused on the catalytic roles of phenoxyl radical intermediates in ribonucleotide reductases, cytochrome *c* oxidase, prostaglandin H synthase, and photosystem II.[1] The phenoxyl radicals in those systems are derived from the active site tyrosines via the oxidation with transition-metal oxo species in the respective enzymes. Thus, the mechanism of phenoxyl radical formation in the reaction with transition-metal oxo complexes is also an important subject in bioinorganic chemistry. For the formation of a phenoxyl radical species from a neutral phenol, there are two possible reaction pathways; direct hydrogen atom transfer (HAT) and proton-coupled electron transfer (PCET). Mechanistic arguments concerning the net hydrogen atom transfer reaction (HAT *vs*. PCET) is one of the most important and fundamental issues in several biological and industrial processes involving O–H and C–H bond activation.[1-4]

In this chapter, the auther and his coworkers describe the first systematic study on the oxidation of neutral phenols (ArOH) by the (μ-η^2:η^2-peroxo)dicopper(II) complex (**A**) and the bis(μ-oxo)dicopper(III) complex (**B**) (Chart 1) supported by 2-(2-pyridyl)ethylamine tridentate and didentate ligands ^{H}Pye2$^{Bz\text{-}d2}$ and ^{H}Pye1$^{Bz\text{-}d2,Et}$, respectively [(R = -CD_2Ph) see Chart 2].[5,6] Comparison of the rate-dependences in the oxidation of phenols by the Cu_2/O_2 complexes on the one-electron oxidation potentials of the phenol substrates (E^0_{ox}) provides profound insights into the mechanistic basis of the phenol-oxidation as well as the electron-transfer oxidation ability of the Cu_2/O_2 complexes. The reactivity of phenols for hydrogen atom transfer reaction using cumylperoxyl radical (**C**) as the hydrogen acceptor have been also examined. The rates of hydrogen atom transfer from phenols to cumylperoxyl radical were determined directly by monitoring the decay of cumylperoxyl radical by ESR. Direct comparison of the rate-dependence on E^0_{ox} of phenols between the Cu_2/O_2 system and the cumylperoxyl radical system provided a quantitative basis to compare the PCET mechanism and the HAT mechanism.

Chart 1

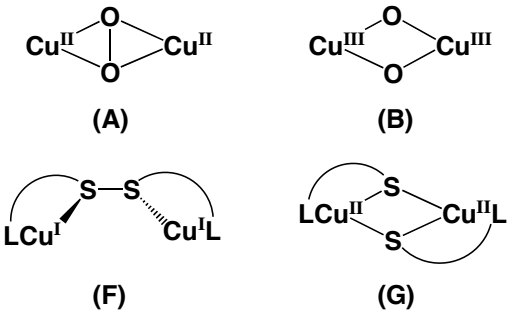

Chart 2

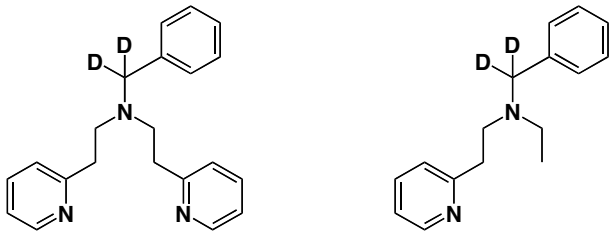

In addition, copper-sulfur complexes have also attracted considerable interest in connection with the structures and functions of copper reaction centers in biological electron-transfer systems as well as copper-dioxygen complexes.[7-9] Among the series of copper-sulfur complexes, dinuclear copper complexes bridged by sulfur atoms have been given much recent attention in relation to the bis(μ-thiolato)dicopper core, $Cu(RS)_2Cu$, of the Cu_A sites of cytochrome *c* oxidase (C*c*O) and nitrous oxide reductase (N_2OR).[10-13] To replicate such an interesting $Cu(RS)_2Cu$ core structure, Tolman's group and Itoh's group have developed the bis(μ-thiolato)dicopper complexes of both the $Cu^{1.5+}$-$Cu^{1.5+}$ (mix-valent) and Cu^{2+}-Cu^{2+} oxidation states.[14-17] Itoh and his coworkers have further demonstrated that the bis(μ-thiolato)dicopper(II) complex (**F**) can be reversibly converted to the corresponding disulfide-bridged dicopper(I) complex (**G**) by treating the former with an external ligand such as Cl^- (see Chart 1).[17] Such a clean isomerization between the bis(μ-thiolato)dicopper(II) complex and the disulfide-dicopper(I) complex provides important insights into the mechanism of ubiquitous redox interconversion between thiolates and disulfides ($2\ RS^- \leftrightarrows RS\text{-}SR + 2\ e^-$).

Chart 3

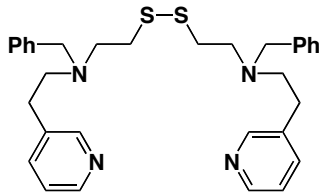

^{H}Pye1$^{Bn,S–S}$

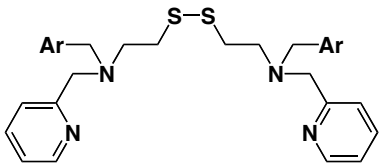

^{H}Pym1$^{Xyl,S–S}$

The isomerization between the bis(μ-thiolato)dicopper(II) complex and the disulfide-dicopper(I) complex is also worthy to be investigated, since it is an isoelectronic process of the interconversion between (μ-peroxo)dicopper(II) (**A**) complex and bis(μ-oxo)dicopper(III) complex (**B**), which has recently attracted a great deal of attention as a possible dioxygen activation mechanism by copper monooxygenases.[18-20] Thus, recent efforts in copper biomimetic chemistry have also been directed to the development of (μ-disulfido)dicopper(II) complexes with both the end-on (μ-η^1:η^1) and side-on (μ-η^2:η^2) binding modes as the sulfur versions of the corresponding (μ-peroxo)dicopper(II) complexes.[21-23] In contrast to the extensive studies on the reactivity of dicopper-dioxygen complexes,[19] however, little is known about the reactivity of dicopper-disulfur complexes toward external substrates.

In this chapter, the author and his coworkers have also investigated the reaction of disulfide-bridged dicopper(I) complex (**F**) supported by ligand ^{H}Pye1$^{Bn,S–S}$ and bis(μ-thiolato)dicopper(II) complex (**G**) generated by using ligand ^{H}Pym1$^{Xyl,S–S}$ (see Chart 1 and Chart 3)[17,24] with a lithium phenolate derivative to find a novel C–S bond formation. The reaction is of particular interest, since the process is related to the biogenetic pathway of the novel organic cofactor Tyr-Cys of galactose oxidase (see, Figure 1).[25] In addition, the reaction can be regarded as a sulfur version of the tyrosinase model reaction; the hydroxylation (C–O bond formation) of phenolates by the (μ-η^2:η^2-peroxo)dicopper(II) complex,[5] although the binding mode of bridging ligands and the oxidation state of copper are different between the peroxo and disulfide systems.

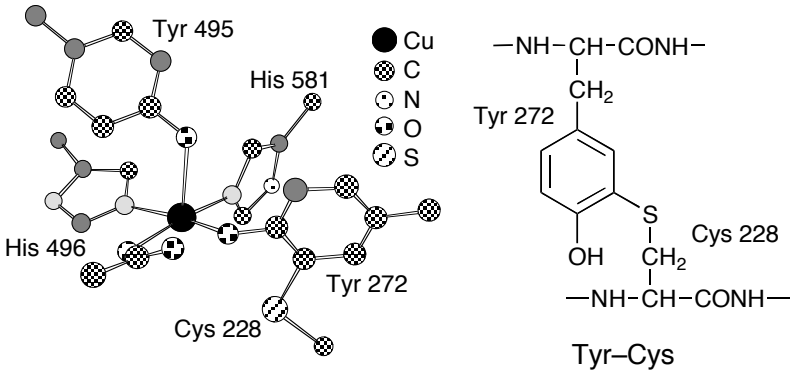

Figure 1. The active site structure (left) and the organic cofactor (right) of galactose oxidase.[25]

Experimental Section

General. All chemicals used in this study, except the ligands, deuterated *p*-substituted phenols, and the copper(I) complexes, were commercial products of the highest available purity and were further purified by the standard methods, if necessary.[26] Synthetic procedures of the ligands, the dicopper-dioxygen complexes, and the dicopper-disulfide complexes as well as the lithium phenolates were reported previously.[5,17,24] The deuterated phenols (*p*-X-C_6H_4OD) were prepared by the reaction of the lithium phenolates with acetic acid-d_1 CH_3COOD (98 %, Aldrich), and the purity of the product was confirmed by ^{1}H-NMR and MS. FT-IR spectra were recorded with a Shimadzu FTIR-8200PC. UV-vis spectra were measured using a Hewlett Packard HP8453 diode array spectrophotometer with a Unisoku cryostat cell holder USP-203. Mass spectra were recorded with a JEOL JMS–700T Tandem MS station and the GC-MS analyses were carried out by using a Shimadzu GCMS–QP2000 gas chromatograph mass spectrometer. ESI-MS (electrospray ionization mass spectra) measurements were performed on a PE SCIEX API 150EX spectrometer. ^{1}H- and ^{13}C-NMR spectra were recorded on a JEOL FT-NMR Lambda 300WB or a JEOL FT-NMR GX-400 spectrometer. ESR measurements were performed on a JEOL X-band spectrometer (JES-ME-LX).

Product Analysis of the Reaction of Cu_2O_2 Complexes and Phenols. The (μ-η^2:η^2-peroxo)dicopper(II) complex and the bis(μ-oxo)dicopper(III) complex supported by ^{H}Pye2$^{Bz\text{-}d2}$ and ^{H}Pye1$^{Bz\text{-}d2,Et}$, respectively, were generated in situ by treating the corresponding copper(I) complex [Cu^{I}(L)]PF_6 (0.04 mmol) with O_2 gas at –80 °C in anhydrous acetone (50 mL) for 10~20 min. Excess O_2 was then removed by bubbling Ar gas into the solution for 10

min. A cold solution (–80 °C) of phenol (0.08 mmol) in 5 mL of anhydrous acetone was added into the solution by cannulation and the mixture was stirred for overnight at this temperature using an EYELA low-temp pairstirrer PSL-1800. The reaction was quenched by adding 0.4 M $HClO_4$ (5 mL) at –80 °C, and then the mixture was warmed up to room temperature. After evaporation of the solvent, the remaining residue was extracted by ethyl acetate (5 mL x 3), and the combined ethyl acetate solution was dried over $MgSO_4$. After removal of $MgSO_4$ by filtration, concentration of the solvent gave an organic material. Formation of the C–C coupling dimer products was confirmed by GC-MS and ^{1}H-NMR, and the yields were determined by ^{1}H-NMR using CH_2ClCH_2Cl as an internal reference.

Product Analysis of the Reaction of Cu_2S_2 Complexes and Lithium Phenolates.

^{H}Pym1$^{Xyl,S–ArOH}$. To a CH_2Cl_2 or CH_3CN solution (30 mL) containing $[Cu^{II}_2(^{H}Pym1^{Xyl,S–S})'_2](ClO_4)_2$ (86.9 mg, 0.1 mmol) was added lithium 2,4-di-*tert*-butylphenolate (21.2 mg, 0.1 mmol) with stirring. After the solution was stirred for overnight at room temperature, 25 % NH_4OH aqueous solution (5 mL) was added and the solvent was removed by evaporation. To the resulting material was added 25 % NH_4OH aqueous solution (10 mL), and organic products were extracted by $CHCl_3$ (5 mL x 3). After drying over anhydrous K_2CO_3, evaporation of the solvent gave a brown material, from which $^{H}Pym1^{Xyl,S–ArOH}$ was isolated in 68 % (in the case of using CH_2Cl_2), 84 % (in the case of using CH_3CN) as a brown oily material by silica gel column chromatography (eluent: $CHCl_3$); ^{1}H-NMR (CD_2Cl_2, 400 MHz) δ 1.26 (9 H, s, ^{t}Bu), 1.39 (9 H, s, ^{t}Bu), 2.33 (3 H, s, Xyl-C*H*$_3$), 2.70 (2 H, t, J = 6.3 Hz, -N-CH$_2$-C*H*$_2$-S-), 2.88 (2 H, t, J = 6.3 Hz, -N-C*H*$_2$-CH$_2$-S-), 3.64 (2 H, s, -N-C*H*$_2$-Xyl), 3.76 (2 H, s, -N-C*H*$_2$-Py), 7.06 (1 H, d, J = 6.4 Hz, H_{Xyl-2}), 7.14–7.21 (4 H, m, $H_{Xyl-4,5,6}$ and H_{Py-5}), 7.29 (1 H, d, J = 2.4 Hz, H_{ArO-5}), 7.33 (1 H, d, J = 2.4 Hz, H_{ArO-3}), 7.45 (1 H, d, J = 8.0 Hz, H_{Py-3}), 7.64 (2 H, td, J = 8.0 and 2.0 Hz, Py_{H-4}), 8.16 (1 H, br, -O*H*), 8.49 (1 H, d, J = 4.8 Hz, H_{Py-6}); FAB-HRMS (pos.) m/z = 477.2938, calcd for $C_{30}H_{41}N_2OS$ = 477.2939.

^{H}Pye1$^{Bn,S–ArOH}$. Product analysis of this product was performed in the same manner as the case of $^{H}Pym1^{Xyl,S–ArOH}$ using $[Cu^{I}_2(^{H}Pye1^{Bn,S–S})](ClO_4)_2$ (86.9 mg, 0.1 mmol) instead of $[Cu^{II}_2(^{H}Pym1^{Xyl,S})'_2](ClO_4)_2$ as a brown oily material in 74 % (in the case of using CH_2Cl_2), 90 % (in the case of using CH_3CN); ^{1}H-NMR (CD_2Cl_2, 400 MHz) δ 1.27 (9 H, s, ^{t}Bu), 1.39 (9 H, s, ^{t}Bu), 2.68 (2 H, t, J = 6.1 Hz, -N-CH$_2$-C*H*$_2$-S-), 2.82–2.95 (6 H, m, -N-C*H*$_2$-CH$_2$-S- and -N-C*H*$_2$-C*H*$_2$-Py), 3.72 (2 H, s, -N-C*H*$_2$-Ph), 7.03–7.09 (2 H, m, $H_{Py-3,5}$) 7.23–7.32 (5 H, m, Ph), 7.35 (1 H, br, H_{ArO-5}), 7.37 (1 H, d, J = 2.2 Hz, H_{ArO-3}), 7.54 (1 H, t, J = 5.8 Hz, H_{Py-4}), 8.44 (1 H, d, J = 4.6 Hz, H_{Py-6}), 8.67 (1 H, br, -O*H*); FAB-HRMS (pos.) m/z = 477.2943, calcd for

$C_{30}H_{41}N_2OS$ = 477.2939.

Syntheses of Copper(II) Complexes.

[Cu^{II}(^{H}Pym1$^{Xyl,S-ArO}$)NO_3]. Ligand ^{H}Pym1$^{Xyl,S-ArOH}$ (63.9 mg, 0.13 mmol) was treated with $Cu^{II}(NO_3)_2$•$3H_2O$ (24.1 mg, 0.1 mmol) in acetone (5 mL). After stirring for 1 h at room temperature, the solvent was removed by evaporation. The remained pale green powder was washed with *n*-hexane (3 mL x 3) and collected in 99% yield (59.4 mg). Single crystals were obtained for the X-ray analysis by liquid-liquid phase diffusion of *n*-hexane into an acetone : *n*-hexane = 1 : 1 solution of complex; FT-IR (KBr) 1279 and 1475 cm^{-1} (NO_3^-); FAB-MS (pos.) *m/z* = 538.2 ([M – NO_3]$^+$); Anal. Calcd for $C_{30}H_{40}N_3SCuO_{4.5}$: C, 59.04; H, 6.61; N, 6.89. Found: C, 59.17; H, 6.47; N, 6.94.

[Cu^{II}(^{H}Pye1$^{Bn,S-ArO}$)NO_3]. Ligand ^{H}Pye1$^{Bn,S-ArOH}$ (63.9 mg, 0.13 mmol) was treated with $Cu^{II}(NO_3)_2$•$3H_2O$ (24.1 mg, 0.1 mmol) in acetone (5 mL). After stirring for 1 h at room temperature, the solution was poured into ether (100 mL) to provide the blue precipitate, which was collected by filtration. The precipitate was washed with ether and dried in vacuo. (59.4 mg; 99% yield). Single crystals were obtained for the X-ray analysis by vapor diffusion of ether into an acetone solution of the complex. FT-IR (KBr) 1279 and 1475 cm^{-1} (NO_3^-); FAB-MS (pos.) *m/z* = 538.2 ([M – NO_3]$^+$); Anal. Calcd for $C_{30}H_{40}N_3SCuO_{4.5}$: C, 59.04; H, 6.61; N, 6.89. Found: C, 59.20; H, 6.47; N, 6.98.

Electrochemical Measurements. Cyclic voltammetry measurements were performed on an ALS 630 electrochemical analyzer in deaerated acetone containing 0.10 M NBu_4ClO_4 as supporting electrolyte. The Pt working electrodes (BAS) were polished with BAS polishing alumina suspension and rinsed with acetone before use. The counter electrode was a platinum wire. A silver pseudo reference electrode was employed, and electrochemical potentials were determined using the ferrocene/ferricenium (Fc/Fc^+) couple as a reference. All electrochemical measurements were carried out at 25 °C under an atmospheric pressure of Ar in a glovebox (DBO-1KP, Miwa Co. Ltd.).

The second harmonic ac voltammetry (SHACV) was employed to determine the one-electron oxidation potentials (E^0_{ox}) of phenols. The SHACV measurements were performed using an ALS-630A electrochemical analyzer in deaerated CH_3CN containing 0.10 M $Bu_4N^+PF_6^-$ as a supporting electrolyte. The platinum working electrode was polished with alumina suspension and rinsed with CH_3CN before use. The counter electrode was a platinum wire. The measured potentials were recorded with respect to an $Ag/AgNO_3$ (0.01 M) reference electrode. The E^0_{ox} values (*vs*. $Ag/AgNO_3$) were converted to those *vs*. SCE by addition of

0.29 V. All electrochemical measurement were carried out at 25 ˚C under an atmospheric pressure of Ar in a glove box (Miwa Co. Ltd.)

Kinetic Measurements of the Reaction of Cu_2O_2 Complexes and Phenols by UV-vis. The copper-dioxygen complexes (**A** and **B**) were generated in situ by the reaction of the Cu^I complexes (0.15 mM) and dry O_2 gas in acetone at –80 °C (introduced by gentle bubbling for a few minutes) in a UV-vis cell (1 cm path length), which was held in a Unisoku thermostated cell holder designed for the low temperature experiments (fixed within ± 0.5 ˚C). After formation of the dicopper-dioxygen complexes, excess O_2 was removed by bubbling Ar into the solution for 5 min. Then, the reaction was initiated by adding an excess amount of the substrate into the solution, and the pseudo-first-order rate constants (k_{obs}) were determined by following the decrease in the absorption due to the dicopper-oxygen complexes.

Kinetic Measurements of the Reaction of Cumylperoxyl Radical and Phenols by ESR. Typically, photoirradiation of an oxygen-saturated propionitrile solution containing di-*t*-butyl peroxide (1.0 M) and cumene (1.0 M) with a 1000 W Mercury lamp resulted in formation of cumylperoxyl radical (g = 2.0156) which could be detected at –80°C. The g value was calibrated by using an Mn^{2+} marker. Upon cutting off the light, the decay of the ESR intensity was recorded with time. The decay rate was accelerated by the presence of ArOH (1.0 x 10^{-2} M). Rates of hydrogen atom transfer from ArOH to cumylperoxyl radical were monitored by measuring the decay of ESR signal in the presence of various concentrations of ArOH in acetone at –80°C. Pseudo-first-order rate constants were determined by a least-squares curve fit using a microcomputer. The first-order plots of $\ln(I - I_\infty)$ vs time (I and I_∞ are the ESR intensity at time t and the final intensity, respectively) were linear for three or more half-lives with the correlation coefficient, $r > 0.99$.

X-ray Structure Determination. The single crystals of $[Cu^{II}(^{H}Pym1^{Xyl,S-ArO})NO_3]$ and $[Cu^{II}(^{H}Pye1^{Bn,S-ArO})NO_3]$ were mounted on a CryoLoop (Hamptom Research Co.) or a glass-fiber. Data of X-ray diffraction were collected by a Rigaku RAXIS-RAPID imaging plate two-dimensional area detector using graphite-monochromated Mo$K\alpha$ radiation (λ = 0.71069 Å) to 2 θ_{max} of 55 °. All the crystallographic calculations were performed by using Crystal Structure software package of the Molecular Structure Corporation [Crystal Structure: Crystal Structure Analysis Package version 3.0, Molecular Structure Corp. and Rigaku Corp. (2001)]. The crystal structures were solved by the direct methods and refined by the full-matrix least squares using SIR92. All non-hydrogen atoms and hydrogen atoms were refined anisotropically and isotropically, respectively. Summary of the X-ray crystallographic

data and selected bond lengths and angles are given in Tables 2 and 3.

Results and Discussion

In chapter 2, it has been demonstrated that the reaction of the copper(I) complexes supported by the pyridylalkylamine ligands and dioxygen afforded (μ-η^2:η^2-peroxo)dicopper(II) complex and/or bis(μ-oxo)dicopper(III) complex (**A** and **B** in Chart 1, respectively) depending on the structure of the supporting ligands. In chapter 3, the effects of pyridylalkylamine ligands on the reactivity of copper(I) complexes toward alkyl halides have been also explored in detail. In this chapter, reactivity of the dicopper-dioxygen complexes (**A** and **B**) generated by using the pyridyl alkylamine ligands toward external substrate such as phenol derivatives are investigated. In addition, reactivity of the disulfide-dicopper(I) and bis(μ-thiolato)dicopper(II) complexes (**F** and **G**) which can be regarded as the sufur versions of the dicopper-dioxygen complexes, toward phenol derivatives are also examined.

1. Reactivity of Dicopper–Dioxygen (Cu_2/O_2) Complexes toward Phenols.

Oxidation of Phenols by the (μ-η^2:η^2-Peroxo)dicopper(II) Complex (A). The (μ-η^2:η^2-peroxo)dicopper(II) complex (**A**) was generated by the reaction of the copper(I) complex of ^{H}Pye2^{Bz-d2} (Chart 2) with dioxygen at –80 °C in acetone as previously reported.[5] Treatment of 4-substituted phenols such as *p*-$MeOC_6H_4OH$ (**1**), *p*-$Bu^tC_6H_4OH$ (**5**), and *p*-ClC_6H_4OH (**10**) (for the numbering of phenol substrates, see Table 1) with the peroxo complex **A** (0.02 mmol) at –80 °C under anaerobic conditions gave the corresponding C–C coupling dimer in 42 %, 38 %, and 32 % yields, respectively, based on the peroxo complex **A**. The lower yields for **5** and **10** can be attributed to their lower reactivity toward the peroxo complex **A**. Namely, the oxidation of **5** and **10** by **A** competes with the self-decomposition of **A**. Then, the nearly 50 % yield of the dimer product based on **A** suggests that the (μ-η^2:η^2-peroxo)dicopper(II) complex formally acts as an one-electron oxidant for ArOH producing an equimolar amount of $ArO^{\bullet}$ (0.02 mmol), which spontaneously dimerizes to give the C–C coupling product in nearly 50 % yield (0.01 mmol) based on **A**.[27]

The reaction was followed by UV-vis spectrum by monitoring a decrease in absorbance at 364 nm due to the (μ-η^2:η^2-peroxo)dicopper(II) complex (**A**) (Figure 2). The reaction obeyed first-order kinetics in the presence of an excess amount of the substrate (see inset of Figure 2), and the pseudo-first-order rate constant k_{obs} was proportional to the substrate

concentration as demonstrated in Figure 3, from which the second-order rate constant k^{A}_{2} was obtained as the slope. These kinetic behaviors indicate that the reaction between the neutral phenol and peroxo complex **A** is a simple bimolecular process in contrast to the case of oxygenation reaction of the lithium phenolate by **A**, where a Michaelis-Menten type saturation dependence of the rate on the substrate concentration was observed.[5] The second-order rate constants k^{A}_{2} for the oxidation of variously substituted phenols by **A** were determined similarly, and are listed in Table 1 together with the E^{0}_{ox} values of the phenols determined using the second-harmonic ac voltammetry (SHACV) (Figure 4).[28]

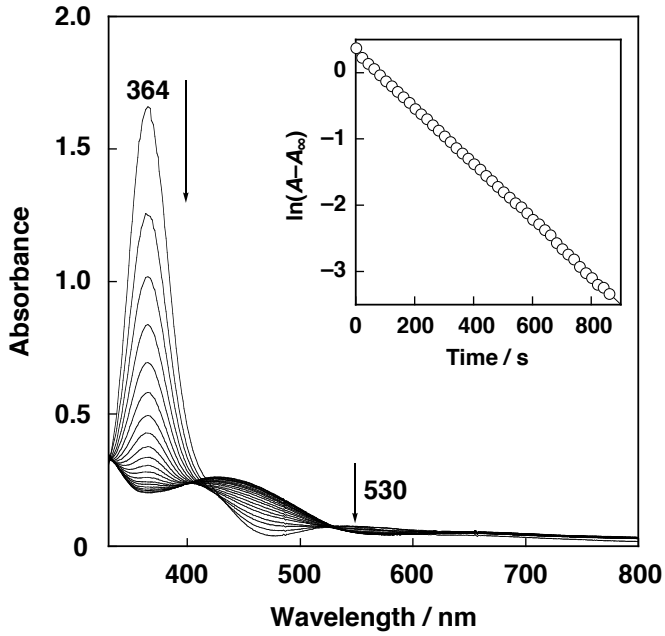

Figure 2. Spectral change for the reaction of 4-*tert*-butylphenol (20 x 10^{-3} M) and $[Cu^{II}_{2}(^{H}Pye2^{Bz-d2})_{2}(\mu\text{-}O_{2})]^{2+}$ (**A**) (7.5 x 10^{-5} M) in acetone at –80 °C. Interval: 60 s. Inset: pseudo-first-order plot based on the absorption change at 364 nm.

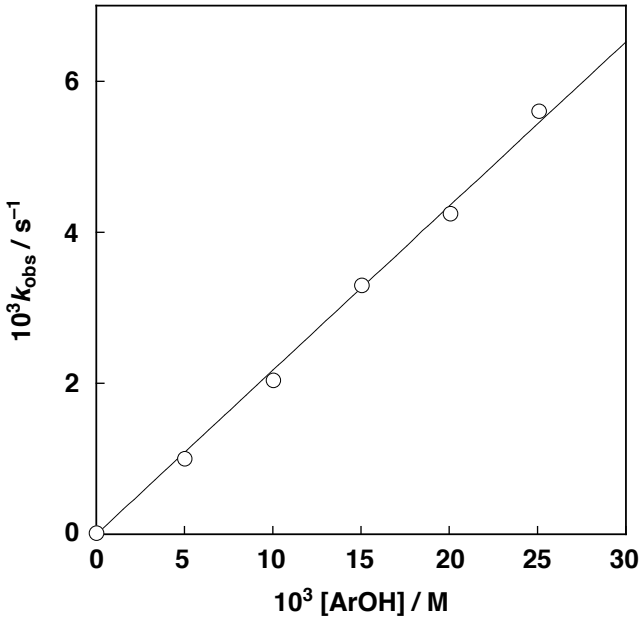

Figure 3. Plot of k_{obs} against the substrate concentration for the reaction between 4-*tert*-butylphenol and $[Cu^{II}_2(^{H}Pye2^{Bz-d2})_2(\mu\text{-}O_2)]^{2+}$ (**A**) in acetone at –80 °C.

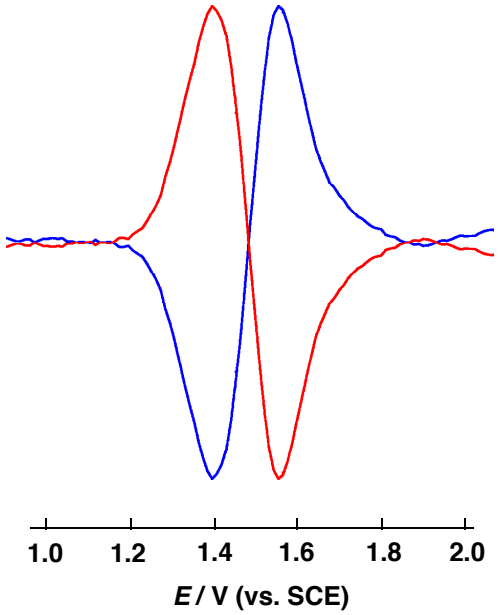

Figure 4. SHACV of 4-*tert*-butylphenol (5.0×10^{-3} M) in CH_3CN containing 0.1 M NBu_4PF_6 at 25 °C; working electrode Pt, counter electrode Pt wire, reference electrode Ag/ 0.01 M $AgNO_3$, sweep rate 10 mVs^{-1}, ac amplitude 25 mV, ac frequency 100 Hz, and phase shift 5 / 185°.

Table 1. Oxidation Potential (E^0_{ox}) of ArOH and the Rate Constants for the C–C Coupling Reactions of ArOH by the (μ-η^2:η^2-Peroxo)dicopper(II) Complex (**A**), the Bis(μ-oxo)dicopper(III) Complex (**B**), and Cumylperoxyl Radical (**C**).

	ArOH	E^0_{ox} / V [a] (vs. SCE)	k_2 / M^{-1} s^{-1}		
			A [b]	B [c]	C
1	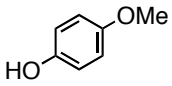	1.43	16.6	—— [d]	70
2	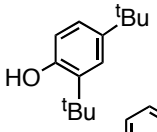	1.46	3.84	—— [d]	28
3	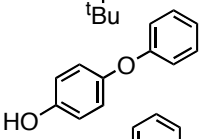	1.49	1.51	41.4	8.6
4	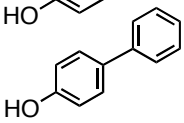	1.52	0.36	15.1	8.3
5	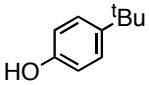	1.52	0.22	13.1	9.0
6	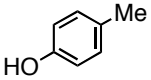	1.54	0.17	7.5	11
7	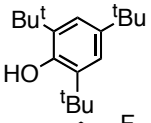	1.58	0.015	0.47	61
8	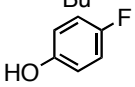	1.61	0.0077	0.30	—— [e]
9	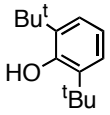	1.62	0.0040	0.18	17
10	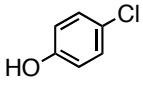	1.63	0.0026	0.10	—— [e]

[a] Determined by SHACV in CH_3CN at 25 °C. [b] $[Cu^{II}_2(^{H}Pye2^{Bz\text{-}d2})_2(\mu\text{-}O_2)]^{2+}$ (7.5×10^{-5} M) in acetone at –80 °C. [c] $[Cu^{III}_2(^{H}Pye1^{Bz\text{-}d2,Et})_2(\mu\text{-}O)_2]^{2+}$ (7.5×10^{-5} M) in acetone at –80 °C. [d] Too fast to be determined. [e] Too slow to be determined.

The k^{A}_{2} values of the phenols increase with increasing the driving force of electron transfer from phenols to **A**, *i.e.*, with decreasing the E^{0}_{ox} values. According to the Marcus theory of electron transfer, a plot of $(RT/F)\ln k$ *vs*. the free energy change of electron transfer (ΔG^{0}_{et}), which is given by ($E^{0}_{ox} - E^{0}_{red}$), should be linear with a slope of –0.5, provided that the driving force of electron transfer ($-\Delta G^{0}_{et}$) is much smaller than the reorganization energy of electron transfer (λ).[29] Plot of $(RT/F)\ln k^{A}_{2}$ *vs*. E^{0}_{ox} for the one-electron oxidation of phenols by **A** affords good linear correlations as expected for electron transfer reactions (part A in Figure 5). However, the slope (–0.72) is significantly more negative than –0.5.

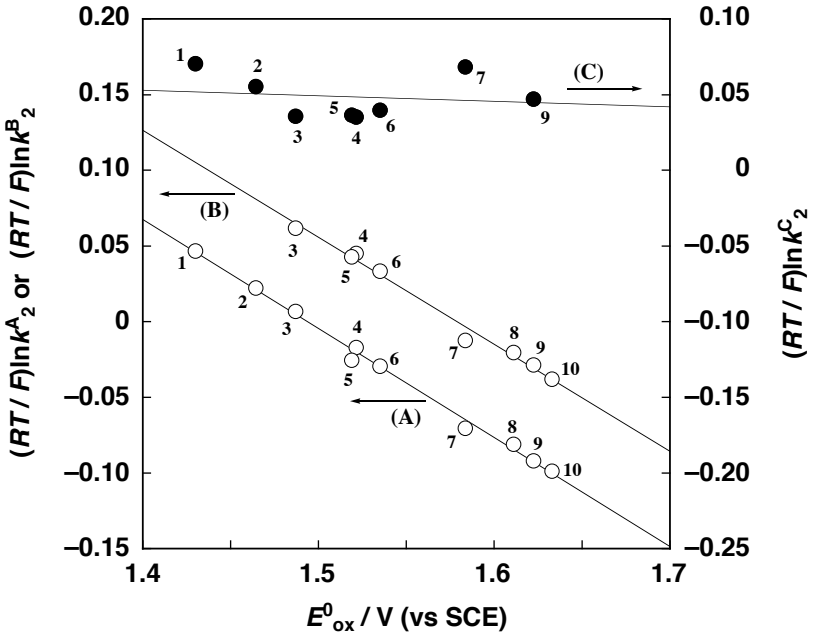

Figure 5. Plots of $(RT/F)\ln(k_2)$ against the oxidation potential (E^{0}_{OX}) of ArOH for the reactions of ArOH with (μ-η^2:η^2-peroxo)dicopper(II) complex (**A**), bis(μ-oxo)dicopper(III) complex (**B**) and cumylperoxyl radical (**C**) in acetone at –80 °C.

The electron transfer from ArOH to **A** may be followed by proton transfer from the resulting cation radical intermediate $ArOH^{\bullet+}$ to an intermediate **D** $[Cu_2/O_2]^{+}$ to generate a phenoxyl radical species $ArO^{\bullet}$ and the product complex **E** $[Cu_2/O(OH)]^{2+}$ (Scheme 1). [30] For the intermediates **D**, a (μ-oxo)(μ-oxyl radical)dicopper(II) or a bis(μ-oxo)dicopper(II,III) form can be drawn. The phenoxyl radical species $ArO^{\bullet}$ thus produced readily coupled to give the C–C coupling dimer product in ~50 % based on **A** as experimentally observed.[31]

Scheme 1

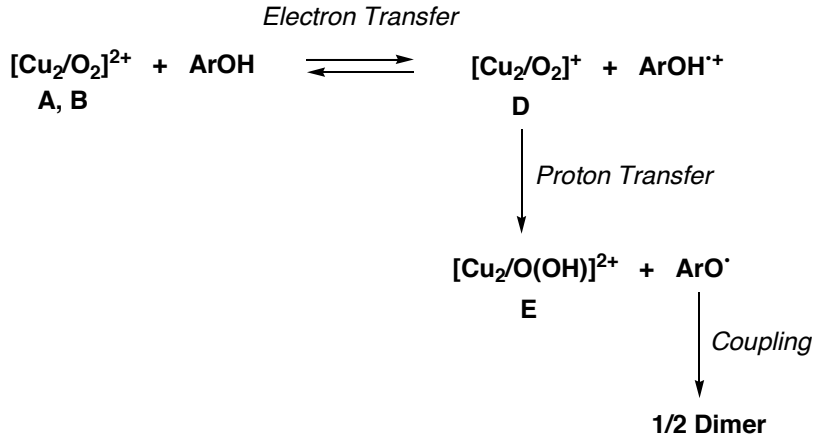

If electron transfer from phenols to the peroxo complex **A** is the rate-determining, followed by the fast proton transfer, the slope of the Marcus plot in Figure 5 (part A) should be the normal value of –0.5, when the electron transfer is exergonic (the free energy change of electron transfer is negative).[29] On the other hand, if the proton transfer is the rate-determining, the electron transfer is in equilibrium and thereby the slope should be –1.0, when the free energy of electron transfer is normally endergonic (the free energy of electron transfer is positive).[29] If the rates of electron transfer and proton transfer are comparable and thereby coupled to each other, a value between –0.5 and –1.0 would be obtained.[32-34,35] Thus, the slope of –0.72 observed in Figure 5 (part A) indicates that the electron transfer from phenols to **A** is endergonic and coupled with the proton transfer (PCET mechanism) as illustrated in Scheme 1.

Kinetic deuterium isotope effects on the second-order rate constants k^{A}_{2} ($k^{A}_{2(H)}/k^{A}_{2(D)}$) were determined as 1.32 for phenol **1** [*p*-$MeOC_6H_4OH(D)$], 1.23 for phenol **3** [*p*-$PhOC_6H_4OH(D)$], 1.56 for phenol **5** [*p*-$Bu^tC_6H_4OH(D)$], and 1.21 for phenol **10** [*p*-$ClC_6H_4OH(D)$]. Existence of the distinct kinetic deuterium isotope effects (1.21 ~ 1.56) clearly indicates that the proton transfer is involved in the rate-determining step. These values are, however, significantly small as compared to the kinetic deuterium isotope effects observed in the hydrogen atom transfer reaction (HAT) from toluene and dihydroanthracene to permanganate (k_H/k_D = 6 ± 1 and 3.0 ± 0.6, respectively),[36] but are nearly the same to that reported for the proton-coupled electron transfer reaction (PCET) between guanine and $Ru(bpy)_3^{3+}$ (k_H/k_D = 1.4).[33] These results strongly support the PCET mechanism for the oxidation of phenols by the peroxo complex **A**. Recent DFT studies by Mayer and coworkers

have suggested that PCET mechanism is more likely than the HAT mechanism for the oxidation of a phenol to a phenoxyl radical species.[37]

Oxidation of Phenols by the Bis(*μ*-oxo)dicopper(III) Complex (B). Oxidation of phenols by the bis(*μ*-oxo)dicopper(III) complex **B** was also examined under the same experimental conditions (at –80 °C in acetone, anaerobic). The bis(*μ*-oxo)dicopper(III) complex was generated by the reaction of the copper(I) complex of the didentate ligand ^{H}Pye1$^{Bz\text{-}d2,Et}$ and O_2. In this case as well, the oxidation product was the corresponding C–C coupling dimers as reported previously,[38] and the yields were determined as 45 %, 42 %, and 37 % for the dimer products from *p*-$MeOC_6H_4OH$ (**1**), *p*-$Bu^tC_6H_4OH$ (**5**), and *p*-ClC_6H_4OH (**10**), respectively. In this case as well, the lower yield of **10** can be attributed to the lower reactivity of **10** toward the bis(*μ*-oxo) complex **B**. Thus, nearly the same yields around 50 % of the dimer products also suggest that the bis(*μ*-oxo)dicopper(III) complex **B** also acts as a one-electron oxidant for the phenol oxidation.[42]

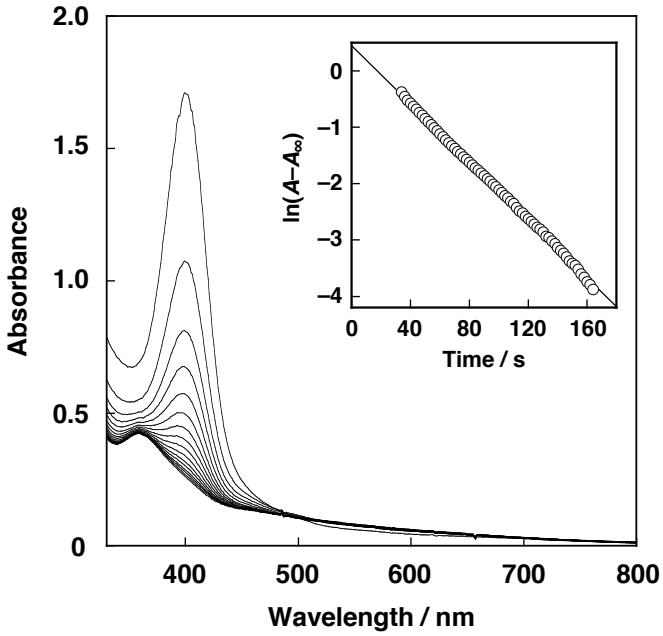

Figure 6. Spectral change for the reaction of 4-*tert*-butylphenol (1.8×10^{-3} M) and $[Cu^{III}_2(^{H}Pye1^{Bz\text{–}d2,Et})_2(\mu\text{-}O)_2]^{2+}$ (**B**) (7.5×10^{-5} M) in acetone at –80 °C. Interval: 10 s. Inset: pseudo-first-order plot based on the absorption change at 400 nm.

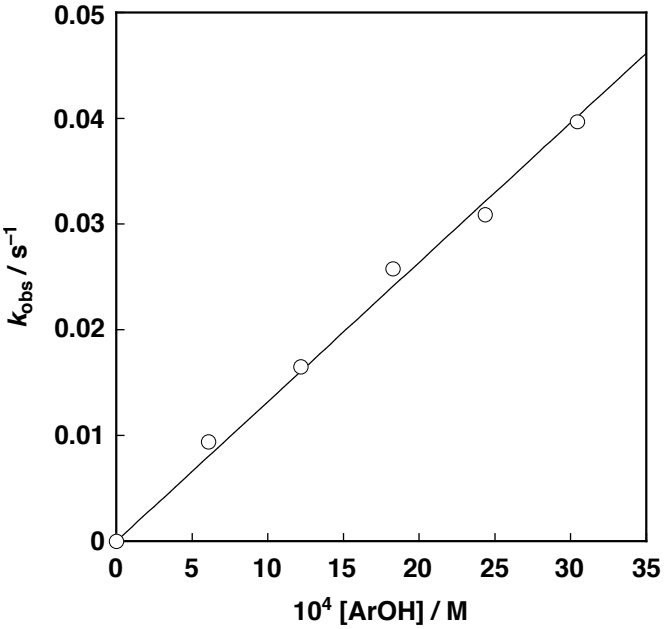

Figure 7. Plot of k_{obs} against the substrate concentration for the reaction of 4-*tert*-butylphenol and $[Cu^{III}_2(^{H}Pye1^{Bz\text{-}d2,Et})_2(\mu\text{-}O)_2]^{2+}$ (**B**) in acetone at –80 °C.

The second-order rate constants k^{B}_2 have been determined by the same kinetic treatment (first-order dependence both on **B** and the substrate, Figures 6 and 7). Plot of $(RT/F)\ln k^{B}_2$ *vs.* E^{0}_{ox} for the one-electron oxidation of phenols by **B** in Figure 5 (part B) also gives a good linear correlation with virtually the same slope (–0.71) as in the case of **A** (–0.72) in Figure 5 (part A). Kinetic deuterium isotope effects ($k^{B}_{2(H)}/k^{B}_{2(D)}$) have also been determined as 1.22 for phenol **3** [*p*-$PhOC_6H_4OH(D)$], 1.48 for phenol **5** [*p*-$Bu^tC_6H_4OH(D)$], and 1.23 for phenol **10** [*p*-$ClC_6H_4OH(D)$]. These results indicate that electron transfer from phenols to **B** is also coupled with the subsequent proton transfer (PCET mechanism) as the case of **A** (Scheme 1).[39]

Oxidation of Phenols by Cumylperoxyl Radical (C). Cumylperoxyl radical has recently been demonstrated to act as a hydrogen atom acceptor in the reaction with *N*,*N*-dimethylanilines, where a one-step hydrogen atom transfer (HAT) mechanism has been confirmed.[40] Thus, the reaction of the same series of phenols with cumylperoxyl radical has also been examined in acetone at –80 °C with use of ESR. Photoirradiation of an oxygen saturated acetone solution containing di-*t*-butylperoxide and cumene with a 1000 W Mercury lamp results in formation of the Cumylperoxyl radical **C** which was readily detected by ESR as shown in Figure 8. The ESR spectrum consists of a single isotropic signal with the *g* value of 2.0156 showing no detectable hyperfine structure in agreement with the ESR features of

cumylperoxyl radical.[41, 42]

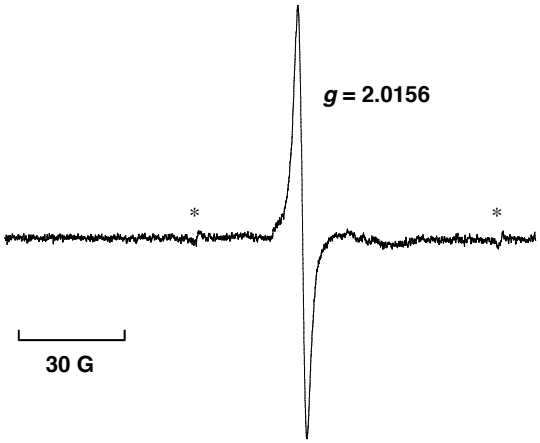

Figure 8. ESR spectrum of cumylperoxyl radical (**C**) in acetone at –80 °C generated in the photoirradiation of an oxygen-saturated acetone solution containing di-*tert*-butylperoxide (0.1 M) and cumene (0.1 M). The asterisk (*) denotes the Mn^{II} maker.

Scheme 2

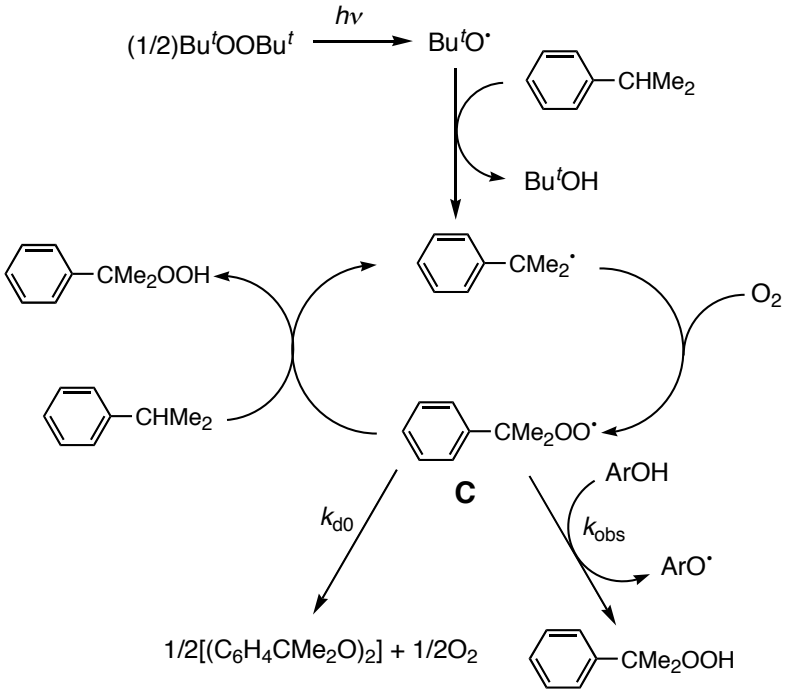

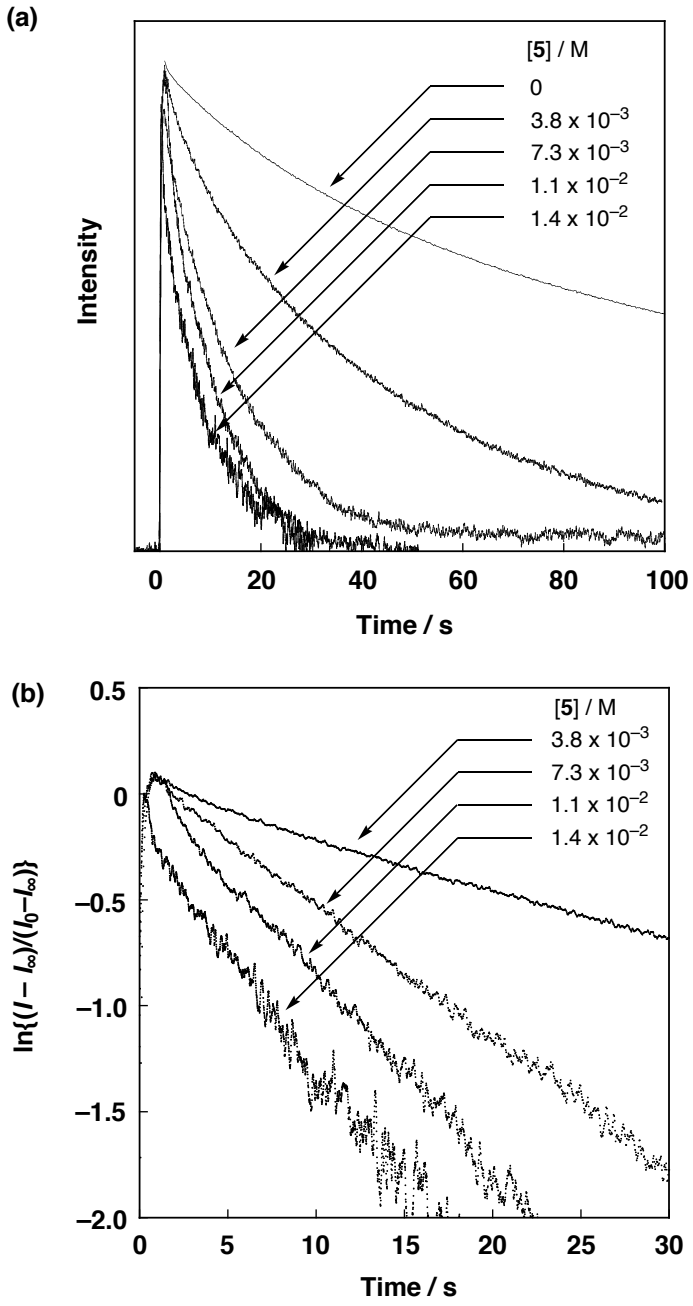

Figure 9. (a) Time dependence of the ESR signal intensity of cumylperoxyl radical (**C**) in the presence of **5** in O_2-saturated acetone at –80 °C. (b) First-order plots.

The cumylperoxyl radical (**C**) is formed via a radical chain process shown in Scheme 2.[43-47] The photoirradiation of Bu^{t}OOBu^t results in the homolytic cleavage of the O–O bond to produce Bu^{t}O$^\bullet$,[48-54] which abstracts a hydrogen atom from cumene to give cumyl radical, followed by the facile addition of oxygen to give **C**. The cumylperoxyl radical (**C**) can also

abstract a hydrogen atom from cumene in the propagation step to yield cumene hydroperoxide, accompanied by regeneration of cumyl radical (Scheme 2).[42,55] In the termination step, cumylperoxyl radicals decay by a bimolecular reaction to yield the corresponding peroxide and oxygen (Scheme 2).[42,55] When the light is cut off, the ESR signal intensity decays obeying second-order kinetics due to the bimolecular reaction in Scheme 3 ([**5**] = 0 M in Figure 9a).[56]

In the presence of ArOH, the decay rate of **C** after cutting off the light becomes much faster than that in the absence of ArOH as shown in Figure 9a. The decay rate in the presence of ArOH obeys pseudo-first-order kinetics rather than second-order kinetics as shown in Figure 9b. Thus, the decay of the ESR signal due to **C** in the presence of ArOH is ascribed to the hydrogen atom transfer from ArOH to **C** (Scheme 2). The pseudo-first-order rate constants (k_{obs}) increase linearly with an increase in [ArOH] as shown in Figure 10. The rate constants (k^C_2) of intermolecular hydrogen atom transfer from a series of ArOH to **C** are determined from the slope of linear plots (Figure 10) and the determined k^C_2 values are listed in Table 1.

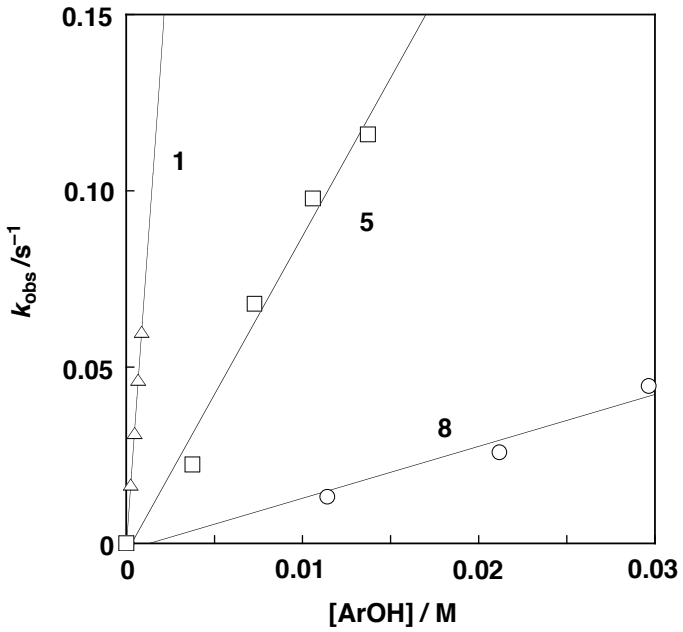

Figure 10. Plots of k_{obs} vs [ArOH] for hydrogen transfer from ArOH (1, 5, and 8) to cumylperoxyl radical (**C**) in O_2-saturated acetone at –80 °C.

Plot of $(RT/F)\ln k^C_2$ *vs.* E^0_{ox} for the net-hydrogen atom transfer from ArOH to cumylperoxyl radical is shown in Figure 5 (part C), where the k^C_2 values are rather constant irrespective of the E^0_{ox} values. The small rate-dependence of k^C_2 on E^0_{ox} is similar to the case of

the HAT reaction with *N*,*N*-dimethylanilines,[40] but shows sharp contrast with the case of the one-electron oxidation of ArOH by the Cu_2/O_2 complexes in Figure 5 (parts A and B). The contrasting results in Figure 5 (parts A and B *vs*. part C) confirm that the electron transfer step is definitely involved in the oxidation of phenols by (μ-η^2:η^2-peroxo)dicopper(II) complex (**A**) and the bis(μ-oxo)dicopper(III) complex (**B**).

Reactive Cu_2/O_2 Species in the Phenol-Oxidation. So far, oxidation reactions of phenols by the (μ-η^2:η^2-peroxo)dicopper(II) complex (**A**) and the bis(μ-oxo)dicopper(III) complex (**B**) have been investigated to demonstrate that the yield of C–C coupling dimer and the dependence of k_2 on E^0_{ox} (Figure 5) as well as the kinetic deuterium isotope effect ($k_{2(H)}/k_{2(D)}$) were nearly the same between the two systems. The only difference was found in the rate constants, k^A_2 *vs*. k^B_2, for the same substrate; the k^B_2 values are about two-order of magnitude larger than the k^A_2 values (Table 1). These differences in the rate constants could be attributed to the difference in the intrinsic reactivity between the peroxo complex **A** and the bis(μ-oxo) complex **B** for the oxidation of ArOH. In such a case, the one-electron reduction potential (E^0_{red}) of **B** may be ~0.1 V higher than the E^0_{red} value of **A** judging from the two parallel relations in Figure 5.

There is, however, another possibility that the bis(μ-oxo) complex **B** is the real active species in both cases, and the rate difference between the two systems is attributed to the difference in absolute concentration of **B**. Namely, in the tridentate ligand system $^{H}Pye2^{Bz-d2}$, the peroxo complex **A** is the major species and the bis(μ-oxo) complex **B** exists as a minor component in the rapid equilibrium between them. In such a case, the observed rate constant is given as $k^B_2K/(1 + K)$, where K is an equilibrium constant between **A** and **B** in the tridentate ligand system. Then, the K value is estimated as 0.017 ~ 0.037, given that the k^B_2 value in the tridentate ligand system $^{H}Pye2^{Bz-d2}$ is the same to the k^B_2 value in the didentate ligand system $^{H}Pye1^{Bz-d2,Et}$. This is consistent with the previous report that the bis(μ-oxo)dicopper(III) complex coexists as a minor product when the (μ-η^2:η^2-peroxo)dicopper(II) complex is prepared using 2-(2-pyridyl)ethylamine tridentate ligands $(PyCH_2CH_2)_2NR$.[57,58]

If the peroxo complex **A** was a real active species for PCET-oxidation of neutral phenols, the reaction of **A** with lithium phenolate would proceed *via* an outer sphere electron transfer mechanism, since the phenolate has a much more negative oxidation potential than the corresponding neutral phenol. In such a case, the oxidation product of lithium phenolate by the peroxo complex **A** should also be the phenoxyl radical which is eventually converted into the dimer product. This is, however, inconsistent with the previous data demonstrating that the

oxygenation of phenolate by the peroxo complex **A** proceeds via the electrophilic aromatic substitution mechanism in an association complex to give the catechols, but not the dimer. Thus, the bis(μ-oxo)dicopper(III) complex (**B**) may be the real active species in both the tridentate and didentate ligand systems and the reduction potential of (μ-η^2:η^2-peroxo)dicopper(II) complex (**A**) may be much more negative than that of **B**. This may be the reason why tyrosinase employs the (μ-η^2:η^2-peroxo)dicopper(II) intermediate to accomplish the aromatic oxygenation reaction of phenols. In other words, formation of a phenoxyl radical species by the reaction of a phenol substrate with the bis(μ-oxo)dicopper(III) intermediate may be prevented in the enzymatic system by keeping the Cu–Cu distance about 3.5 Å, which can only accommodate the (μ-η^2:η^2-peroxo)dicopper(II) intermediate.[59]

2. Reactivity of Disulfide-Bridged Dicopper(I) (Cu_2/S_2) Complexes toward a Phenolate.

Structural Equilibrium Between Cu_2S_2 Complexes. As stated in Introduction, the bis(μ-thiolato)dicopper(II) complex **G** can be easily converted to the corresponding disulfide-bridged dicopper(I) complex **F** when it is treated with external ligand such as chloride ion in non-polar solvent such as CH_2Cl_2.[17] Here it has also been found that the equilibrium position between **G** and **F** is largely affected by the solvent used as shown in Figure 11. Namely, the bis(μ-thiolato)dicopper(II) complex **G** exists as a major component in CH_2Cl_2, while replacement of the solvent to acetone significantly decreases the ratio of **G** (judging from the intensity of the LMCT band at 813 nm of **G**,[17] **G** : **F** = 64 : 36 in acetone). Furthermore, **G** was completely converted into **F**, when **G** was dissolved into CH_3CN (Figure 11). Titration of complex **G** with CH_3CN was performed in CH_2Cl_2 at 25 ˚C (Figure 12). The association constant of CH_3CN to **G** producing **F**, defined by $K_{as} = (A - A_0)/(A \bullet [CH_3CN]^2)$, was determined as 24.6 M^{-2}. The thermodynamic parameters for the CH_3CN-binding were also determined as $\Delta H^0 = -73.8 \pm 7.9$ kJmol^{-1} and $\Delta S^0 = -221 \pm 27$ JK^{-1}mol^{-1} from the temperature dependence of K_{as} according to the equation of $\ln K_{as} = -\Delta H^0/RT + \Delta S^0/R$ (Figure 13). Thus, the stronger the coordination ability of solvent, the more favorable the disulfide-bridged dicopper(I) complex (**F**) formation. Coordination of the solvent molecule may stabilize the tetrahedral geometry of copper to induce the formation of disulfide-dicopper(I) complex **F**.[17]

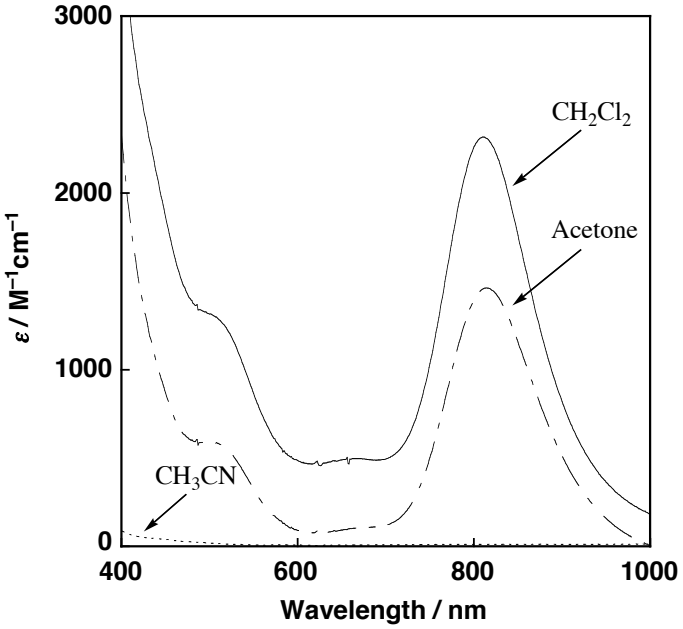

Figure 11. UV-vis spectra of complex **G** prepared by using $^{H}Pym1^{Xyl,S-S}$ (2.0 x 10^{-4} M) in CH_2Cl_2, acetone, and CH_3CN at 20 °C.

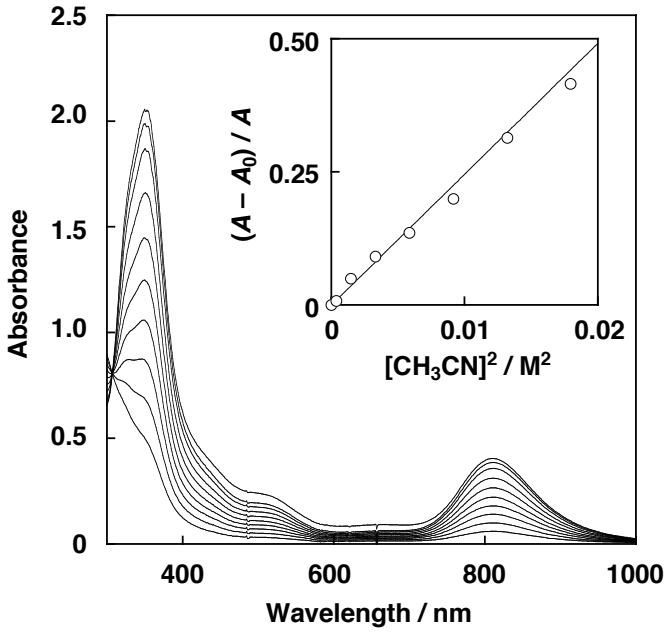

Figure 12. Spectral change for the titration of complex **G** (2.0 x 10^{-4} M) with CH_3CN at 25 °C in CH_2Cl_2. Inset: plot of $(A - A_0) / A$ versus $[CH_3CN]^2$ based on the absorption change at 813 nm.

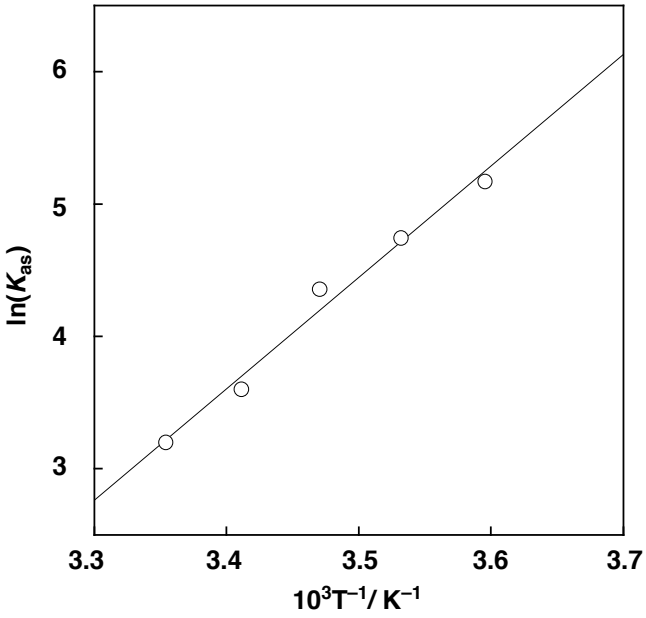

Figure 13. Van't Hoff plot for the titration of **G** (2.0 x 10^{-4}) with CH_3CN in CH_2Cl_2.

Reactivity of Dicopper-Disulfide Complexes toward Phenolates. The reactivity of complexes **F** and **G** toward an external substrate was examined. Addition of lithium 2,4-di-*tert*-butylphenolate to a CH_2Cl_2 solution of complex **G** also resulted in disappearance of the LMCT band due to **G**, suggesting that the similar isomerization of **G** to a disulfide-dicopper(I) complex occurred. In this case, stoichiometry of the phenolate to **G** was 1 : 1 (phenolate : Cu = 1 : 2). Thus, the primary product of the phenolate-titration may be a disulfide-bridged (μ-phenoxo)dicopper(I) complex **H** as indicated in Scheme 3. In this case, further reaction took place at a prolonged reaction time to induce the C–S bond formation reaction (Scheme 3). After the workup treatment of the reaction mixture in a preparative scale, ligand $^{H}Pym1^{Xyl,S-ArOH}$ was isolated in a 68 % yield based on the starting dicopper complex **G** (See Experimantal Section).

The same C–S bond formation reaction took place, when the disulfide-bridged dicopper(I) complex **F** supported by $^{H}Pye1^{Bn,S-S}$ was treated with the lithium phenolate under the same experimental conditions to give the modified ligand $^{H}Pye1^{Bn,S-ArOH}$ in a 74 % yield. These results clearly suggest that the C–S bond formation proceeds through a disulfide-bridged (μ-phenoxo)dicopper(I) complex **H** as the common reaction intermediate. In fact, the yields of $^{H}Pye1^{Bn,S-ArOH}$ and $^{H}Pym1^{Xyl,S-ArOH}$ increased to 90 % and 84 %, respectively, when the reactions were carried out in CH_3CN, that is the solvent favoring the disulfide

complex formation as described above. On the other hand, no reaction took place, when the ligand itself (without copper) was treated with lithium phenolate under the same experimental conditions.

Scheme 3

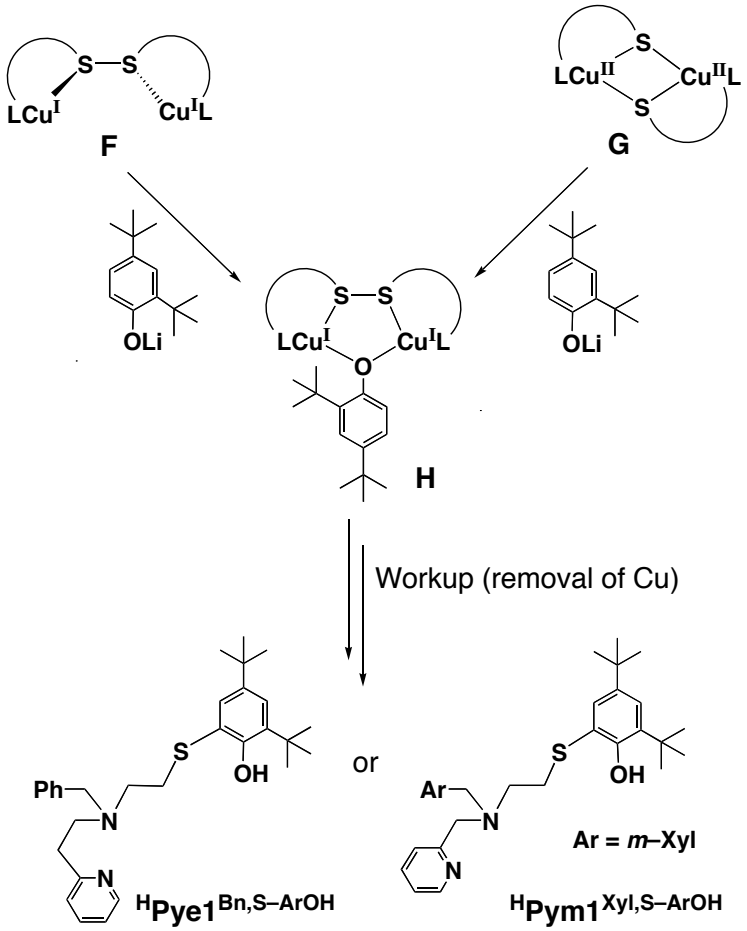

Although the structures of modified ligands ^{H}Pye1$^{Bn,S–ArOH}$ and ^{H}Pym1$^{Xyl,S–ArOH}$ were well supported by the ^{1}H-NMR and MS analyses, the C–S bond formation was definitely confirmed by the X-ray crystallographic analysis of the copper(II) complexes prepared by treating $Cu(NO_3)_2•3H_2O$ and the isolated ^{H}Pye1$^{Bn,S–ArOH}$ and ^{H}Pym1$^{Xyl,S–ArOH}$ ligands, respectively (See Experimantal Section). The crystal structures of [Cu^{II}(^{H}Pye1$^{Bn,S–ArO}$)]NO_3 and [Cu^{II}(^{H}Pym1$^{Xyl,S–ArO}$)]NO_3 are shown in Figure 14, and the crystallographic data and the selected bond lengths and angles are summarized in Tables 2 and 3, respectively. As clearly shown in Figure 14, there exists a thioether bond between the sulfur atom of the ligand and the α-position of the phenolate. Each cupric ion exhibits a significantly distorted five-coordinate

trigonal bipyramidal geometry (τ = 0.52 for the $[Cu^{II}(^{H}Pye1^{Bn,S-ArO})]NO_3$ and τ = 0.64 for the $[Cu^{II}(^{H}Pym1^{Xyl,S-ArO})]NO_3$), where the basal plane is consisted of sulfur atom S(1), tertiary amine nitrogen N(1), and one of the oxygen atoms of the nitrate anion O(2), and the axial positions are occupied by pyridine nitrogen N(2) and phenolate oxygen O(1). The copper(II) complexes of the modified ligands can be regarded as model compounds of the active site of galactose oxidase, since $^{H}Pye1^{Bn,S-ArOH}$ and $^{H}Pym1^{Xyl,S-ArOH}$ involve the 2-alkylthiophenol skeleton existed in the organic cofactor Tyr-Cys of the enzyme (Figure 1).

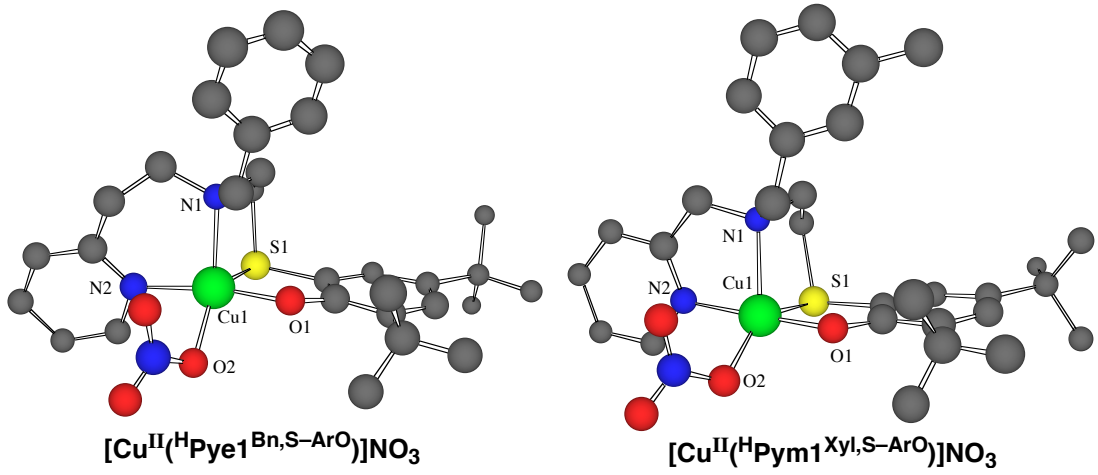

Figure 14. Chem 3D views of the crystal structures of the $[Cu^{II}(^{H}Pye1^{Bn,S-ArO})]NO_3$ and the $[Cu^{II}(^{H}Pym1^{Xyl,S-ArO})]NO_3$. The hydrogen atoms are omitted for clarity.

Although mechanistic details of the C–S bond formation reaction have yet to be clarified, there may be two possible reaction pathways from intermediate **H** (Scheme 4). Path (a) is an ionic mechanism where heterolytic cleavage of the S–S bond occurs to induce an electrophilic attack of the generated cationic sulfur to the α-position of phenolate to give intermediate **I**, which may readily rearrange to product **K** (aromatization). This mechanism is analogous to the electrophilic aromatic substitution mechanism of the tyrosinase reaction, where aromatic hydroxylation (C–O bond formation) of phenolates occurs in the reaction with the (μ-η^2:η^2-peroxo)dicopper(II) complex.[5] Another possibility is a homolytic cleavage of the S–S bond in **H** [path (b)]. In this case, electron-transfer from the bound phenolate to one of the generated thiyl radicals may occur to give phenoxyl-thiyl diradical intermediate **J**, from which radical coupling between the α-carbon and the thiyl radical centers occurs to give intermediate

I. This mechanism resembles the proposed mechanism of post-translational modification of galactose oxidase.[60] Detailed mechanistic studies as well as further characterization of the $Cu^{II}(^{H}Pye1^{Bn,S-ArO})]NO_3$ and $[Cu^{II}(^{H}Pym1^{Xyl,S-ArO})]NO_3$ are being undertaken in order to shed light on the enzymatic functions.

Scheme 4

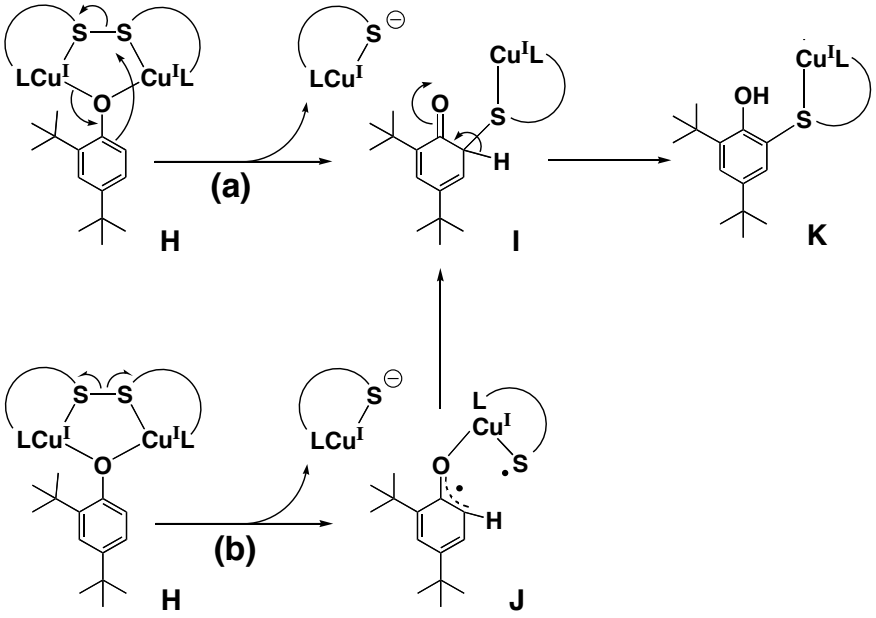

Table 2. Summary of X-ray Crystallographic Data

	$[Cu^{II}(^{H}Pye1^{Bn,S-ArO})]NO_3$	$[Cu^{II}(^{H}Pym1^{Xyl,S-ArO})]NO_3$
empirical formula	$C_{30}H_{39}N_3O_4SCu$	$C_{30}H_{39}N_3O_4SCu$
formula weight	601.26	601.26
crystal system	monoclinic	monoclinic
space group	$P2_1/a$ (#14)	$P2_1/a$ (#14)
a, Å	11.72(1)	11.227(2)
b, Å	13.80(1)	13.716(2)
c, Å	19.45(2)	19.488(2)
β, deg	103.95(3)	101.568(9)
V, Å^3	3055(4)	2940.1(8)
Z	4	4
F(000)	1268.00	1268.00
D_{calc}, g/cm^3	1.307	1.358
T, °C	–120	–114
crystal size, mm	0.30 x 0.30 x 0.10	0.15 x 0.20 x 0.05
μ (MoKα), cm^{-1}	8.21	8.53
diffractometer	Rigaku RAXIS-RAPID	Rigaku RAXIS-RAPID
radiation	MoKα (0.71069 Å)	MoKα (0.71069 Å)
$2\theta_{max}$, deg	54.9	55.0
no. of reflns measd	58498	28017
no. of reflns obsd	4368 [$I > 1.0\sigma(I)$]	4116 [$I > 1.0\sigma(I)$]
no. of variables	392	392
R^a	0.048	0.036
$R_w{}^b$	0.056	0.037
GOF	0.985	0.94

[a] $R = \Sigma||F_o| - |F_c||/\Sigma|F_o|$. [b] $R_w = \{\Sigma w(|F_o| - |F_c|)^2/\Sigma wF_o{}^2\}^{1/2}$.

Table 3. Selected Bond Lengths (Å) and Angles (deg)

$[Cu^{II}(^{H}Pye1^{Bn,S-ArO})]NO_3$

Cu(1)–S(1)	2.478(1)	Cu(1)–O(1)	1.889(2)
Cu(1)–O(2)	2.050(3)	Cu(1)–N(1)	2.175(4)
Cu(1)–N(2)	1.979(3)		
S(1)–Cu(1)–O(1)	84.24(8)	S(1)–Cu(1)–O(2)	133.20(9)
S(1)–Cu(1)–N(1)	87.16(8)	S(1)–Cu(1)–N(2)	95.15(9)
O(1)–Cu(1)–O(2)	87.3(1)	O(1)–Cu(1)–N(1)	94.7(1)
O(1)–Cu(1)–N(2)	170.9(1)	O(2)–Cu(1)–N(1)	139.5(1)
O(2)–Cu(1)–N(2)	86.6(1)	N(1)–Cu(1)–N(2)	94.3(1)

$[Cu^{II}(^{H}Pym1^{Xyl,S-ArO})]NO_3$

Cu(1)–S(1)	2.399(1)	Cu(1)–N(1)	2.217(3)
Cu(1)–N(2)	1.971(3)	Cu(1)–O(1)	1.884(2)
Cu(2)–O(2)	2.003(2)		
S(1)–Cu(1)–N(1)	88.29(8)	S(1)–Cu(1)–N(2)	92.43(9)
S(1)–Cu(1)–O(1)	86.58(8)	S(1)–Cu(1)–O(2)	139.87(8)
N(1)–Cu(1)–N(2)	81.9(1)	N(1)–Cu(1)–O(1)	96.7(1)
N(1)–Cu(1)–O(2)	131.8(1)	N(2)–Cu(1)–O(1)	178.3(1)
N(2)–Cu(1)–O(2)	91.2(1)	O(1)–Cu(1)–O(2)	90.4(1)

Reference

(1) Stubbe, J.; van der Donk, W. A. *Chem. Rev.* **1998**, *98*, 705-762.

(2) Mayer, J. M. *Acc. Chem. Rev.* **1998**, *31*, 441-450.

(3) Roth, J. P.; Yoder, J. C.; Won, T.-J.; Mayer, J. M. *Science* **2001**, *294*, 2524-2526.

(4) Cukier, R. I.; Nocera, D. G. *Annu. Rev. Phys. Chem.* **1998**, *49*, 337-369.

(5) Itoh, S.; Kumei, H.; Taki, M.; Nagatomo, S.; Kitagawa, T.; Fukuzumi, S. *J. Am. Chem. Soc.* **2001**, *123*, 6708-6709.

(6) Taki, M.; Itoh, S.; Fukuzumi, S. *J. Am. Chem. Soc.* **2001**, *123*, 6203-6204.

(7) Solomon, E. I.; Szilagyi, R. K.; George, S. D.; Basumallick, L. *Chem. Rev.* **2004**, *104*,

419-458.

(8) Rorabacher, D. B. *Chem. Rev.* **2004**, *104*, 651-697.

(9) Henkel, G.; Krebs, B. *Chem. Rev.* **2004**, *104*, 801-824.

(10) Tsukihara, T.; Aoyama, H.; Yamashita, E.; Tomizaki, T.; Yamaguchi, H.; Shinzawa-Itoh, K.; Nakashima, R.; Yaono, R.; Yoshikawa, S. *Science* **1995**, *269*, 1069-1074.

(11) Iwata, S.; Ostermeier, C.; Ludwig, B.; Michel, H. *Nature* **1995**, *376*, 660-669.

(12) Wilmanns, M.; Lappalainen, P.; Kelly, M.; Saver-Eriksson, E.; Saraste, M. *Proc. Natl. Acad. Sci. U.S.A.* **1995**, *92*, 11955-11959.

(13) Charnock, J. M.; Dreusch, A.; Korner, H.; Neese, F.; Nelson, J.; Kannt, A.; Michel, H.; Garner, C. D.; Kroneck, P. M., H.; Zumft, W. G. *Eur. J. Biochem.* **2000**, *267*, 1368-1381.

(14) Houser, R. P.; Halfen, J. A.; Young, V. G.; Blackburn, N. J.; Tolman, W. B. *J. Am. Chem. Soc.* **1995**, *117*, 10745-10746.

(15) Houser, R. P.; Young, V. G.; Tolman, W. B. *J. Am. Chem. Soc.* **1996**, *118*, 2101-2102.

(16) Itoh, S.; Nagagawa, M.; Fukuzumi, S. *J. Am. Chem. Soc.* **2001**, *123*, 4087-4088.

(17) Ueno, Y.; Tachi, Y.; Itoh, S. *J. Am. Chem. Soc.* **2002**, *124*, 12428-12429.

(18) Mirica, L. M.; Ottenwaelder, X.; Stack, T. D. P. *Chem. Rev.* **2004**, *104*, 1013-1045.

(19) Lewis, E. A.; Tolman, W. B. *Chem. Rev.* **2004**, *104*, 1047-1076.

(20) Itoh, S.; Fukuzumi, S. *Bull. Chem. Soc. Jpn.* **2002**, *75*, 2081-2095.

(21) Helton, M. E.; Chen, P.; Paul, P. P.; Tyeklar, Z.; Sommer, R. D.; Zakharov, L. N.; Rheingold, A. L.; Solomon, E. I.; Karlin, K. D. *J. Am. Chem. Soc.* **2003**, *125*, 1160-1161.

(22) Fujisawa, K.; Moro-oka, Y.; Kitajima, N. *J. Chem. Soc., Chem. Commun.* **1994**, 623-624.

(23) Brown, E. C.; Aboelella, N. W.; Reynolds, A. M.; Aullón, G.; Alvarez, S.; Tolman, W. B. *Inorg. Chem.* **2004**, *43*, 3335-3337.

(24) Osako, T.; Ueno, Y.; Tachi, Y.; Itoh, S. *Inorg. Chem.* **2003**, *42*, 8087-8097.

(25) Ito, N.; Phillips, S. E. V.; Stevens, C.; Ogel, Z. B.; McPherson, M. J.; Keen, J. N.; Yadav, K. D. S.; Knowles, P. F. *Nature* **1991**, *350*, 87-90.

(26) Armarego, W. L. F.; Perrin, D. D., *Purification of Laboratory Chemicals*. 4th ed.; Butterworth-Heinemann: Oxford, 1996.

(27) The phenol-oxidation reactions by the Cu_2/O_2 complexes were carried out under

anaerobic conditions (an excess amount of O_2 was removed by bubbling Ar gas after the generation of Cu_2/O_2 complexes) at –80 °C for several hours, and the reaction mixtures were quenched at this temperature (–80 °C) by adding $HClO_4$ (see, Experimental Section). In all the cases examined, the dimer products of phenols were obtained as solely isolable products in less than 50 % yields, but neither the corresponding catechols nor the quinone products were obtained from the final reaction mixtures. Thus, the Cu_2/O_2 complexes act as one-electron oxidants rather than two-electron oxidants, when the reduced Cu_2/O_2 complexes produced in the oxidation of phenol may have no ability to further oxidize the phenol. However, the reactivity of the reduced Cu_2/O_2 complexes has yet to be clarified.

(28) The SHACV has been demonstrated to provide a superior approach to directly evaluating the one-electron redox potentials in the presence of a follow-up chemical reaction, relative to the better-known dc and fundamental harmonic ac methods. See: Patz, M.; Mayr, H.; Maruta, J.; Fukuzumi, S. *Angew. Chem., Int. Ed. Engl.* **1995**, *34*, 1225-1227.

(29) Marcus, R. A.; Sutin, N. *Biochim. Biophys. Acta* **1985**, *811*, 265-322.

(30) The intermediate **E** $[Cu_2/O(OH)]^{2+}$ might have a structure of (μ-oxo)(μ-hydroxo)dicopper(II,III) or (μ-oxyl radical)(μ-hydroxo)dicopper(II,II). Thus **E** must be ESR active. However, the ESR spectrum of the final reaction mixture was essentially ESR silent with a little contamination of a copper(II) signal ($g_{//}$ = 2.074, $g_{\perp}$ = 2.059, $A_{//}$ = 149 G). Thus, the intermediate **E** might be further converted into a diamagnetic species such as a tetranuclear copper complex. Further characterization of the product complex has been unsuccessful due to its instability at higher temperature.

(31) In the case of 2,4,6-tri-tert-butylphenol, formation of the corresponding phenoxyl radical ($ArO^{\bullet}$, λ_{max} = 400, 630 nm) was confirmed by the UV-vis spectrum. For spectral data of $ArO^{\bullet}$, see: Forrester, A. R.; Hay, J. M.; Thomson, R. H.; "*Organic Chemistry of Stable Free Radicals*"; Academic: New York, 1968; pp 1-80.

(32) Goto, Y.; Watanabe, Y.; Fukuzumi, S.; Jones, J. P.; Dinnocenzo, J. P. *J. Am. Chem. Soc.* **1998**, *120*, 10762-10763.

(33) Weatherly, S. C.; Yang, I. V.; Thorp, H. H. *J. Am. Chem. Soc.* **2001**, *123*, 1236-1237.

(34) Ram, M. S.; Hupp, J. T. *J. Phys. Chem.* **1990**, *94*, 2378-2380.

(35) The precise dependence expected would be a curved plot with a limiting slope of –0.5 at low driving forces and a limiting slope of –1.0 at high driving forces. The range of

driving forces investigated here likely does not allow this dependence to be resolved, resulting in a linear plot with an overall slope of –0.72.

(36) Gardner, K. A.; Kuehnert, L. L.; Mayer, J. M. *Inorg. Chem.* **1997**, *36*, 2069-2078.

(37) Mayer, J. M.; Hrovat, D. A.; Thomas, J. L.; Borden, W. T. *J. Am. Chem. Soc.* **2002**, *124*, 11142-11147.

(38) Mahadevan, V.; DuBois, J. L.; Hedman, B.; Hodgson, K. O.; Stack, T. D. P. *J. Am. Chem. Soc.* **1999**, *121*, 5583-5584.

(39) Tolman and his coworkers have demonstrated an important role of hydrogen bonding interaction between the oxygen atom of bis(μ-oxo)dicopper(III) core and a hydrogen atom being activated in the aliphatic ligand hydroxylation reaction; Mahapatra, S.; Halfen, J. A.; Wilkinson, E. C.; Pan, G.; Wang, X.; Young, V. G. Jr.; Cramer, C. J.; Que, L. Jr.; Tolman, W. B. *J. Am. Chem. Soc.* **1996**, *118*, 11555-11574. Such a hydrogen bonding interaction between the oxo group of **B** and phenols may also play an important role to accelerate the electron-transfer step.

(40) Fukuzumi, S.; Shimoosako, K.; Suenobu, T.; Watanabe, Y. *J. Am. Chem. Soc.* **2003**, *125*, 9074-9082.

(41) Bersohn, M.; Thomas, J. R. *J. Am. Chem. Soc.* **1964**, *86*, 959.

(42) Fukuzumi, S.; Ono, Y. *J. Chem. Soc., Perkin Trans. 2.* **1977**, 622-625.

(43) Sheldon, R. A., In *The Activation of Dioxygen and Homogeneous Catalytic Oxidation*; Barton, D. H. R.; Martell, A. E.; Sawyer, D. T., Eds. Plenum: New York and London, 1933; pp 9-30.

(44) Parshall, G. W.; Ittel, S. D. *Homogeneous Catalysis*, 2nd ed.; Wiley: New York, 1992; Chapter 10.

(45) Sheldon, R. A.; Kochi, J. K. *Adv. Catal.* **1976**, *25*, 272-413.

(46) Shilov, A. E., Ed. *Activation of Saturated Hydrocarbons by Transition Metal Complexes*; D. Reidel Publishing Co.: Dordrecht, The Netherlands, 1984; Chapter 4.

(47) Bottcher, A.; Birnbaum, E. R.; Day, M. W.; Gray, H. B.; Grinstaff, M. W.; Labinger, J. A. *J. Mol. Catal.* **1997**, *117*, 229-242.

(48) Kochi, J. K., *Free Radicals in Solution*; J Wiley & Sons: New York, 1957.

(49) Kochi, J. K.; Krusic, P. J.; Eaton, D. R. *J. Am. Chem. Soc.* **1969**, *91*, 1877-1879.

(50) Krusic, P. J.; Kochi, J. K. *J. Am. Chem. Soc.* **1968**, *90*, 7155-7157.

(51) Kochi, J. K.; Krusic, P. J. *J. Am. Chem. Soc.* **1969**, *91*, 3938-3940.

(52) Kochi, J. K.; Krusic, P. J. J. *J. Am. Chem. Soc.* **1969**, *91*, 3942-3944.

(53) Kochi, J. K.; Krusic, P. J. *J. Am. Chem. Soc.* **1969**, *91*, 3944-3946.

(54) Howard, J. A.; Furimsky, E. *Can. J. Chem.* **1974**, *52*, 555-556.

(55) Fukuzumi, S.; Ono, Y. *J. Chem. Soc., Perkin Trans. 2.* **1977**, 784-788.

(56) Howard, J. A. *Adv. Free-Radical Chem.* **1972**, *4*, 49-173.

(57) Pidcock, E.; DeBeer, S.; Obias, H. V.; Hedman, B.; Hodgson, K. O.; Karlin, K. D.; Solomon, E. I. *J. Am. Chem. Soc.* **1999**, *121*, 1870-1878.

(58) The equilibrium position between **A** and **B** has been suggested to be largely dependent on the size of the alkyl group R in the tridentate ligand $(PyCH_2CH_2)_2NR$.[20] When R is a small substituent such as methyl, the content of **B** becomes larger (~20 %),[71] (but the population of **B** in the equilibrium becomes significantly smaller when R is larger such as benzyl and phenethyl; (Itoh, S.; Nakao, H.; Berreau, L. M.; Kondo, T.; Komatsu, M.; Fukuzumi, S. *J. Am. Chem. Soc.* **1998**, *120*, 2890-2899).

(59) The bis(μ-oxo)dicopper(III) complex requires much shorter Cu–Cu distance (~2.8 Å).[16]

(60) Rogers, M. S.; Baron, A. J.; McPherson, M. J.; Knowles, P. F.; Dooley, D. M. *J. Am. Chem. Soc.* **2000**, *122*, 990–991.

Concluding Remarks

This thesis describes control of the structures, physicochemical properties, and reactivities of copper complexes by a series of pyridylalkylamine ligands. Particular attention has been focused on the ligand effects on the reactivities of copper(I) complexes toward dioxygen and benzyl halides. Reaction of copper(II) complexes and H_2O_2 as well as oxidation mechanism of phenols by dicopper-dioxygen complexes supported by 2-(2-pyridyl)ethylamine ligands and a novel C–S bond formation reaction between a phenolate and disulfide-dicopper complexes have been also investigated in detail to provide profound insights into the reactivities of Cu(II), Cu_2O_2, and Cu_2S_2 complexes supported by the pyridylalkylamine ligands. The results and findings in this work are summarized as follows.

1. The first detection of a mononuclear (η^2-peroxo)copper(II) complexes has been successfully accomplished in reaction of the copper(II) complexes suppored by 2-(2-pyridyl)ethylamine ligands and H_2O_2 by using a low-temperature stopped-flow technique. These results provide important information about the reactive intermediates involved in the mononuclear copper oxidases and copper oxygenases.

2. Systematic structural changing of the series of the pyridylalkylamine ligands leads to drastic changes not only in the structure and reactivity of the copper(I) complexes but also in the structure of derived dicopper-dioxygen species. In addtion, d-π interaction in copper(I) complexes has been quantitatively evaluated, and its effects on the copper(I)-dioxygen reactivity have also been clarified in detail. These results suggest that such effects may exist in the enzymatic system to dictate the fine tuning of the copper(I)-dioxygen reactivity.

3. The C–C coupling reaction of benzyl halides by copper(I) complexes with pyridylmethylamine tridentate and tetradentate ligands ($^{H}Pym2^{Phe}$ and TMPA, respectively) proceeded smoothly to give the corresponding 1,2-diphenylethane derivatives and copper(II)-halide complex products. The reaction mechanism involving a dinuclear copper(III)-halide organometallic intermediate is proposed from the kinetic results. The results may provide mechanistic insights into the initiation process for atom

transfer radical polymerization (ATRP) of olefins mediated by alkyl halides and copper(I) complexes.

4. It has been found that oxidation of neutral phenols by (μ-η^2:η^2-peroxo)dicopper(II) and bis(μ-oxo)dicopper(III) complexes proceeds via a proton-coupled electron transfer (PCET) mechanism rather than a direct hydrogen atom transfer (HAT) mechanism. In addition, the direct comparison of reaction rates between Cu_2O_2 complexes has indicated that the bis(μ-oxo)dicopper(III) complex acts as the real active species in the oxidation of neutral phenols. These results may give important insights into the hydrogen atom abstraction mechanism from tyrosine by metal-oxo species in several biological systems. In addition, a novel C–S bond formation reaction has been found to take place, when a lithium phenolate derivative was treated with a disulfide-bridged dicopper(I) complex or a bis(μ-thiolato)dicopper(II) complex under very mild conditions. Copper(II) complexes of the modified ligands containing a thioether group as model compounds of the active site of galactose oxidase have been obtained from the C–S bond formation reaction. These results provide mechanistic insights into the post-translational modification of the organic cofactor of galactose oxidase as well as the reactivities of Cu_2S_2 complexes.

List of Publications

The content of thesis is composed of the following papers.

Original Paper:

1. Modulation of Coordination Chemistry in Copper(I) Complexes Supported by Bis[2-(2-pyridyl)ethyl]amine-Based Tridentate Ligands
   Takao Osako, Yoshimitsu Tachi, Masayasu Taki, Shunichi Fukuzumi, and Shinobu Itoh
   Inorg. Chem., **40** (26), 6604-6609 (2001).

2. Low-temperature Stopped-flow Studies on the Reactions of Copper(II) Complexes and H_2O_2. The First Detection of a Mononuclear Copper(II)-peroxo Intermediate
   Takao Osako, Shigenori Nagatomo, Yoshimitsu Tachi, Teizo Kitagawa, and Shinobu Itoh
   Angew. Chem., **114** (22), 4501-4504 (2002); *Angew. Chem. Int. Ed.*, **41** (22), 4325-4328 (2002).

3. Oxidation Mechanism of Phenols by Dicopper–Dioxygen (Cu_2/O_2) Complexes
   Takao Osako, Kei Ohkubo, Masayasu Taki, Yoshimitsu Tachi, Shunichi Fukuzumi, and Shinobu Itoh
   J. Am. Chem. Soc., **125** (36), 11027-11033 (2003).

4. Structures and Redox Reactivities of Copper Complexes of (2-Pyridyl)alkylamine Ligands. Effects of the Alkyl Linker Chain Length
   Takao Osako, Yoshiki Ueno, Yoshimitsu Tachi, and Shinobu Itoh
   Inorg. Chem., **42** (24), 8087-8097 (2003).

5. Quantitative Evaluation of d–π Interaction in Copper(I) Complexes and Control of Copper(I)–Dioxygen Reactivity
   Takao Osako, Yoshimitsu Tachi, Matsumi Doe, Motoo Shiro, Kei Ohkubo, Shunichi Fukuzumi, and Shinobu Itoh
   Chem. Eur. J., **10** (1), 237-246 (2004).

6. Dinuclear copper-dioxygen intermediates supported by polyamine ligands
   Shinichi Teramae, Takao Osako, Shigenori Nagatomo, Teizo Kitagawa, Shunichi Fukuzumi, and Shinobu Itoh
   J. Inorg. Biochem., **10** (1), 746-757 (2004).

7. Model complexes of the active site of galactose oxidase. Effects of the metal ion binding sites
   Masayasu Taki, Haruna Hattori, Takao Osako, Shigenori Nagatomo, Motoo Shiro, Teizo Kitagawa, and Shinobu Itoh
   Inorg. Chim. Acta, **357** (11), 3369-3381 (2004).

8. C-S Bond Formation Reaction between Phenolate and Disulfide-bridged Dicopper(I) Complexes
   Takao Osako, Yoshiki Ueno, Yoshimitsu Tachi, and Shinobu Itoh
   Inorg. Chem., **43** (21), 6516-6518 (2004).

9. Carbon-Halogen Bond Activation Mechanism by Copper(I) Complexes of (2-Pyridyl)alkylamine Ligands
   Takao Osako, Kenneth D. Karlin, and Shinobu Itoh
   Inorg. Chem., in press. (2005).

Acknowledgments

The author would like to express his gratitude to Professor Shinobu Itoh for his kind guidance, invaluable suggestions and continuous encouragement throughout this study.

The author expresses his heartily thanks to Dr. Masayasu Taki for their useful suggestions.

The author is deeply grateful to Professor Shunichi Fukuzumi, Dr. Kei Ohkubo and the members of Fukuzumi's Laboratory (Osaka University) for their useful suggestions, the DFT-caluculation and ESR measurement.

The author is much grateful to Professor Masatatsu Suzuki and his coworkers (Kanazawa University) and Professor Kenneth D. Karlin (John Hopkins University) for their useful suggestions.

The author also thanks Professor Teizo Kitagawa and coworkers, especially Dr. Shigenori Nagatomo and Dr. Takehiko Tosha, of Okazaki Institute for Molecular Science for their help in trying to obtain the resonance Raman spectra and Dr. Motoo Shiro (Rigaku Agency) for X-ray measurement.

The author thanks the members of Analytical Center of Osaka City University, especially Ms. Matsumi Doe for the 2–D NMR measurements.

Thanks are also given to Dr. Yoshimitsu Tachi and all members of Bio Chemical Reaction Laboratory at Department of Chemistry, Graduate School of Science, Osaka City University for valuable suggestions and kindly friendship.

This thesis work is financially supported by Research Fellowships of Japan Society for the Promotion of Science (JSPS) for the Young Scientists.

Finally, the author acknowledges continuous encouragement and assistant given by his father, Kousei Osako, his mother, Yuriko Osako, and his friends.

Takao Osako
Department of Chemistry
Graduate School of Science
Osaka City University

Osaka, Japan
January, 2005